Water stable isotopes in Alpine ice cores as proxies for temperature and atmospheric circulation

Inauguraldissertation

der Philosophisch-naturwissenschaftlichen Fakultät

der Universität Bern

vorgelegt von

Isabella Mariani

aus Italien

Leiterin der Arbeit:

Prof. Dr. M. Schwikowski

Departement für Chemie und Biochemie der Universität Bern

Von der Philosophisch – naturwissenschaftlichen Fakultät angenommen.

Der Dekan:

Bern, 16. Dezember 2013   Prof. Dr. S. Decurtins

Summary

Water stable isotope ratios and net snow accumulation in ice cores are commonly interpreted as temperature or precipitation proxies. However, only in a few cases a direct calibration with instrumental data has been attempted. Taking advantage of the dense network of observations in the European Alpine region, in this PhD study the relationship of the annually and seasonally resolved proxy data from two highly-resolved ice cores was rigorously tested, comparing the proxies with local temperature and precipitation. The analysis focused on the most recent decades, where the highest amount and quality of meteorological data are available and the ice core dating uncertainty is minimal. The two ice cores were from the Fiescherhorn glacier in the Northern Alps (3900 m a.s.l.) and Grenzgletscher in the Southern Alps (4200 m a.s.l.). Due to the orographic barrier, the two flanks of the Alpine chain are affected by distinct patterns of precipitation. The different location of the two glaciers therefore offered a unique opportunity to test if such a specific setting is reflected in the proxy data.

On a seasonal scale a high fraction of $\delta^{18}O$ variability was explained by the seasonal cycle of temperature (~60% for the ice cores, ~70% for the nearby stations of the Global Network of Isotopes in Precipitation, GNIP). When the seasonality was removed, the correlations decreased for all sites indicating that factors other than temperature such as changing moisture sources and/or precipitation regimes affected the isotopic signal on this timescale. Post-depositional phenomena may additionally have modified the ice core data. On an annual scale the high variability of precipitation, especially at high-altitude sites, might considerably bias the isotopic signal toward the season with more precipitation. The annual $\delta^{18}O$/temperature relationship was significant at the Fiescherhorn, whereas for Grenzgletscher this was the case only when weighting the temperature with precipitation. The fact that at Grenzgletscher the annual mean of $\delta^{18}O$ is only representative for temperature during precipitation was attributed to a strong interannual variability of precipitation distribution. For such a glacier site, only a precipitation weighted temperature can be reconstructed. In both cases the fraction of interannual temperature variability explained was ~20%, comparable to the values obtained from the GNIP stations data. Even for glacier sites in close proximity (only 60 km) within the same mountain range, distinct local precipitation patterns can result in variations how the temperature proxy signal is preserved. Thus, a careful individual calibration of the local $\delta^{18}O$/T relation is essential for every ice core site. Consistent with previous studies, an altitude effect for the $\delta^{18}O$ of -0.17‰/100 m was observed, considering an extended elevation range i.e., combining data of the two ice core sites and four GNIP stations.

Net accumulation on the glacier was significantly correlated with precipitation for Grenzgletscher during the entire period of investigation, whereas for Fiescherhorn this was the case only for the less recent period (1961-1977). Local phenomena, probably related to wind, seem to partly disturb the Fiescherhorn accumulation record. In addition the net accumulation is more sensitive to post-depositional processes and to initial layer assignment than intrinsic core parameters like the $\delta^{18}O$. Spatial correlation analysis showed the two glaciers to be influenced by different precipitation regimes, with the Grenzgletscher reflecting the characteristic precipitation regime south of the Alps and the Fiescherhorn accumulation showing a pattern more closely linked to northern Alpine stations.

A further study involving seasonal $\delta^{18}O$ and deuterium excess from three GNIP stations and the Fiescherhorn ice core was conducted. The aim was to analyze the spatial coherence of the signal in terms of altitudinal changes since all the sites are less than 20 km distant and are assumed to be affected by the same precipitation regimes. The $\delta^{18}O$ was well correlated between all the sites and with temperature and showed an altitude effect slightly higher in summer compared to the other seasons, explainable with partial re-enrichment at the lower altitude sites. For the ice core, the absence of subannual stratigraphic markers introduces an additional uncertainty in the attribution of the winter and summer signal and may in part explain the low correlations obtained. The deuterium excess, characterized by high frequency fluctuations, showed no correlation between the ice core signal and the lower elevation sites and tends to increase nonlinearly with altitude. For this parameter a weak seasonal cycle was observed, with lower values in spring and higher in fall that might be explained in terms of in-cloud and sub-cloud kinetic processes. No homogeneous relationship with the meteorological parameters was found. The common increasing trend of summer deuterium excess over 1993-2011 was explained with the increasing frequency of South-Westerly weather situations, carrying moisture from the high-deuterium excess Mediterranean basin. In winter, the medium altitude site Grimsel Hospiz showed significant anticorrelation between the deuterium excess and the NAO, suggesting for the first time a connection between the second order parameter and the atmospheric circulation over the Alpine region.

Part of this project was dedicated to the setup and characterization of a Wavelength-Scanned Cavity Ring Down Spectrometer (Picarro L2130-i). This laser technique is now widely used in isotope hydrology because of the advantage of measuring both the $\delta^{18}O$ and the δD with high precision and easier operation compared to other methods. The instrument was characterized through the evaluation of memory effect and drift. The analytical uncertainty was quantified as 0.1‰ for the $\delta^{18}O$ and 0.5‰ for the δD. Three internal laboratory standards

were prepared to represent the Alpine isotopic range and were calibrated against International Atomic Energy Agency (IAEA) reference materials. The Grenzgletscher samples were measured allowing for a comparison with previous measurement performed with another technique, Isotopic Ratio Mass Spectrometry. Results showed good agreement within the analytical uncertainty.

Although it was not straightforward to interpret the isotopic signal in the two ice cores at seasonal and interannual timescale, major changes in temperature, precipitation or atmospheric circulation patterns might nevertheless be accessible on longer timescales. Future work will be directed toward detailed interpretation of the 350 years information contained in the Fiescherhorn ice core and the even longer record from Colle Gnifetti.

Contents

1 Introduction

1.1 Climate change and paleoclimate research

Climate change has become a general concern in recent years. The global temperature increase since the preindustrial period is the most outstanding aspect, with an estimated change of 0.74±0.18 °C for the 20th century (1906-2005). During the last 50 years the warming rate is almost double compared to the last 100 years (0.13±0.03 °C/decade versus 0.07±0.02 °C/decade, (IPCC, 2007)). The Fifth IPCC Assessment Report (IPCC, 2013), whose final draft was released during the time this thesis was written, confirms a warming trend of 0.85±0.21 °C for the period 1880-2012, although a reduction in surface warming over the period 1998-2012 was observed compared to the period 1950-2012 and was attributed to reduced forcing combined with internal variability (IPCC, 2013). The anthropogenic forcing in the energy balance, i.e. the enhanced emission of greenhouse gases, was recognized as the main driver of the temperature increase since the mid 19th century (IPCC, 2007). Due to higher temperatures the atmosphere increases its water-holding capacity, affecting the whole hydrological cycle (Trenberth et al., 2003). Although no uniform global precipitation trend was detected, there is a tendency toward an increase of extreme precipitation events (Easterling et al., 2000). Additional effects of climate change on the hydrological cycle are more frequent droughts and floods, with strong impact on the society.

Focusing on Europe, projections predict an increase in annual mean temperature higher than the global mean. The largest warming is expected during winter (summer) in northern (southern) Europe (IPCC, 2007). Besides, precipitation would tend to intensify in northern Europe and decrease in the Mediterranean region, increasing the probability of summer droughts (Figure 1). For the snow season an overall shortening is expected, with snow depth decreasing over most Europe (IPCC, 2007).

With respect to Switzerland the CH2050 regional climate scenario was used to discuss the main impacts over the region until the year 2050 (OcCC, 2007). The major trends are predicted for temperature, with largest warming occurring in summer (2.7-2.8°C depending on the region) and moderate increase in winter (1.8°C). Due to predicted higher summer temperature variability, higher frequency of hot spells is expected in that season, whereas in winter the increase of the mean temperature would lead to a general decrease of cold extremes. The hydrological cycle is also expected to significantly change. The largest change in precipitation amount is predicted in summer, with a general decrease of 17-19% (depending on the region) compared to the other seasons (a few percent), but this estimate has

large uncertainties. Due to the increase of winter temperatures, in that season precipitation is expected to change from solid to liquid especially at mid-low altitudes with consequent increase of flooding events. The glacier extent is projected to be reduced dramatically, with a medium loss of 75% of the extent. This would impact on both, the hydrological cycle (especially on the watercourses mainly fed by glaciers and snow, showing large runoff variations) and the Swiss economy, where 56% of the domestic electricity production relies on hydropower (data from the Swiss Federal Office of Energy SFOE, http://www.bfe.admin.ch/). Winter tourism, which nowadays significantly contributes to the financial resources, is affected as well.
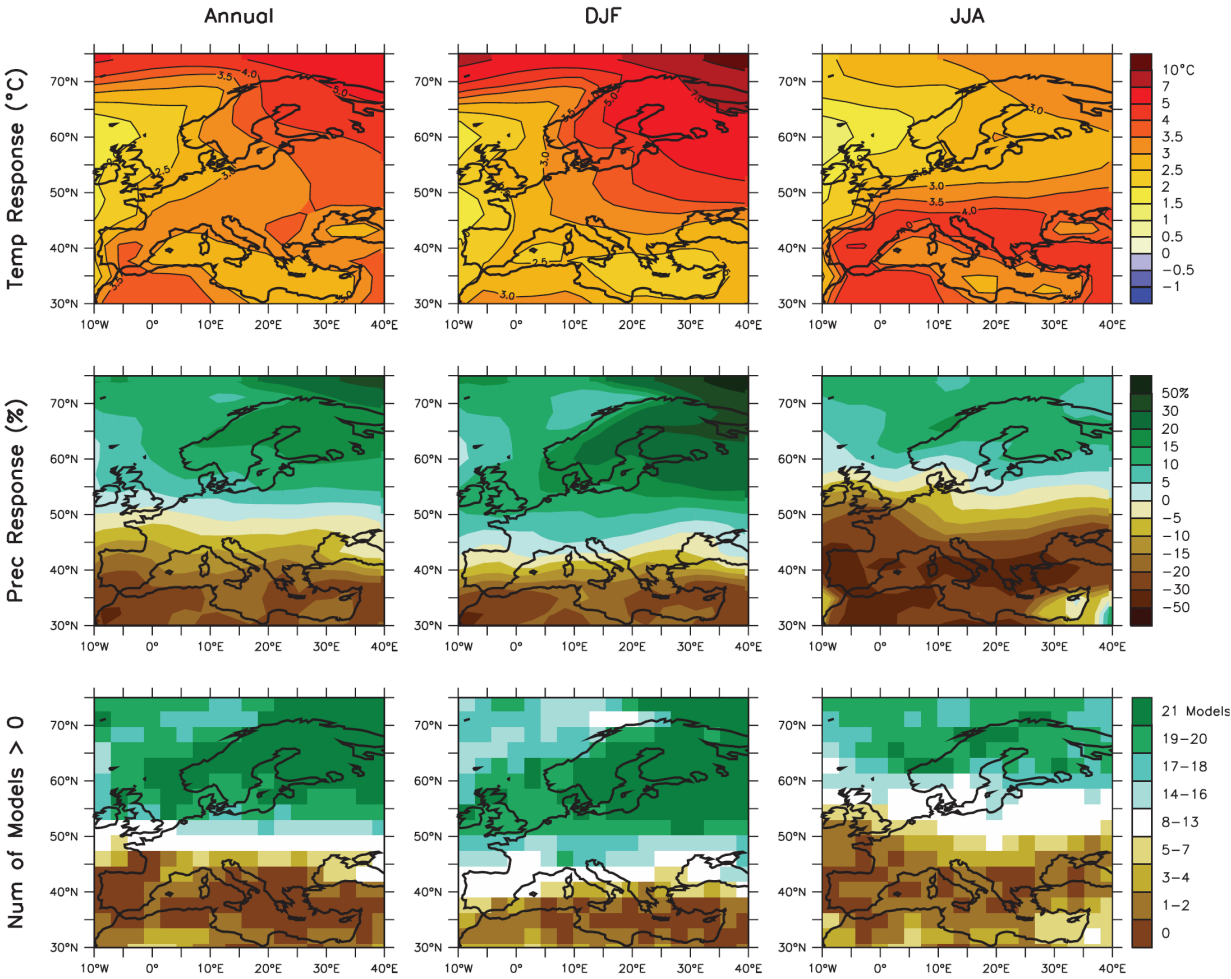

Figure 1 Temperature and precipitation changes over Europe from MMD-A1B simulations. (Upper panels): Annual mean, winter and summer temperature change between 1980 to 1999 and 2080 to 2099 (averaged over 21 models). (Middle panels) same as top, but for fractional change in precipitation. (Bottom panels): number of models out of 21 that project increases in precipitation (IPCC, 2007).

The understanding of the driving factors of climatic change needs identification and quantification of the processes causing climatic variability at different timescales. Extracting and estimating the anthropogenic forcing is challenging since affected parameters are as well influenced by internal climate variability. Moreover external forcing on the globe's energy balance such as solar activity variation, volcanic eruptions and orbital changes need to be taken into account. A vast series of modeling studies has been developed in order to describe these changes by a physical approach (IPCC, 2007).

Most instrumental observations of meteorological parameters started in the mid-19th century, in coincidence with the beginning of the anthropogenic forcing (IPCC, 2007). Additional data is required to better separate human induced changes from natural climate variability. To extend the information further back in time, two approaches are available: (i) the use of modeling studies that may simulate physical processes in the past and (ii) proxy data i.e. parameters extracted from natural archives that can be linked to climate variables. In this thesis the focus is on the second aspect of the so-called paleoclimatic research i.e. the study of the climate of the past using proxy data.

Proxies extracted from natural archives offer information about e.g. past temperature, humidity, precipitation, greenhouse gases concentrations or solar radiation. The most used natural archives are ice cores, tree rings, sea or lake sediments, (e.g. Bradley, 1999). Every natural archive offers advantages and disadvantages with respect to its particular proxies. Polar ice cores for example give the opportunity to reconstruct past climatic changes going hundred thousands of years back in time showing the last glacial-interglacial transitions (e.g. Jouzel et al., 2007; Wolff et al., 2010) for Antarctica ice cores, or investigate the interstadials in detail (e.g. Johnsen et al., 1992; Dansgaard et al., 1993) for Greenland. Recently, in the North Greenland Eemian Ice Drilling (NEEM) project a new ice core from Greenland was retrieved with the purpose of studying the last interglacial period (NEEM community members, 2013).

In paleoclimatic research the study of the past temperature and atmospheric circulation changes is one of the most investigated aspects. For this purpose the so-called isotope paleoclimatology resulted to be a successful method (Jouzel, 2003). This approach is based on the different physicochemical properties, basically saturation vapor pressure and molecular diffusivity, of the water molecules that are formed by the different isotopes of hydrogen and oxygen. Because these properties are to a first approximation, temperature and relative humidity dependent, the concentrations of the different molecules that change differently throughout the water cycle can be used as proxies for temperature and atmospheric circulation

conditions. These concentrations, expressed as the ratio between the heavier to lighter water molecules, are given as the deviation from an international standard, and are commonly indicated as $\delta^{18}O$ and δD (Chapters 2 and 3). It was shown that the $\delta^{18}O$ (or δD) relationship with temperature is generally linear (Dansgaard, 1964 and Chapter 2). Once the relationship, or transfer function, between temperature and $\delta^{18}O$ (δD) is established, it is in principle possible to derive the so-called "paleothermometer", i.e. quantifying the past temperature changes from the variations of the water stable isotope records measured in the archive (Jouzel et al., 1997; Jouzel, 2003). Historically, this approach was first applied to the polar ice cores, where temperature reconstructions extending back to the last glacial period were obtained, with the help of modeling studies. The latter are fundamental to simulate the different conditions that led to precipitation, since the calibration of $\delta^{18}O$ (δD) with temperature is necessarily based on the present state of climate and may considerably change over geologic timescales, due to the different atmospheric conditions (Fricke and O'Neil, 1999; Jouzel et al., 2000; Jouzel, 2003). In the Last Glacial Maximum temperatures inferred from six ice cores in Greenland resulted to be ~20°C lower than present, and temperature oscillations of ~15°C were observed during the Dansgaard-Oeschger events (Johnsen et al., 2001). These are only two examples from the vast literature available from Greenland ice cores. Up to now, the longest ice core stable isotope record was retrieved in the frame of the European Project for Ice Coring in Antarctica (EPICA) core and covers the last 800 ka (Jouzel et al., 2007). The record shows reconstructed glacial-interglacial temperature oscillations of ~15°C over this period, with coldest periods being ~10°C colder than the present and warmer periods having anomalies up to +4.5°C (Figure 2). Models can explain what driving factors affected the isotopic signal in the past. Over these timescales such changes are mainly triggered by variations of the Earth's orbital parameters, but are also affected by internal feedbacks such as ice-albedo, heat transport by ocean, and greenhouse gases (e.g. Petit et al., 1999; Stenni et al., 2001; Jouzel et al. 2007).

Besides the $\delta^{18}O$ (δD) parameter another proxy extracted from the water molecules is commonly used. This second-order parameter is called deuterium excess (d) and is derived from the equation $d=\delta D-8\delta^{18}O$ (Chapter 2). At a first approximation the deuterium excess is a valuable indicator for moisture source conditions, in terms of sea surface temperature (Stenni et al., 2001; Masson-Delmotte et al., 2005) or relative humidity (Jouzel et al., 1982; Pfahl and Wernli, 2008), through its close relationship with the diffusivities of the different water molecules (Chapter 2). Together with the $\delta^{18}O$ the deuterium excess in polar ice cores is used in the so-called co-isotopic approach to integrate the information about past temperature

changes with the moisture source conditions in order to obtain a more comprehensive picture of the atmospheric conditions in the past (e.g. Stenni et al., 2001; Masson-Delmotte et al., 2005).
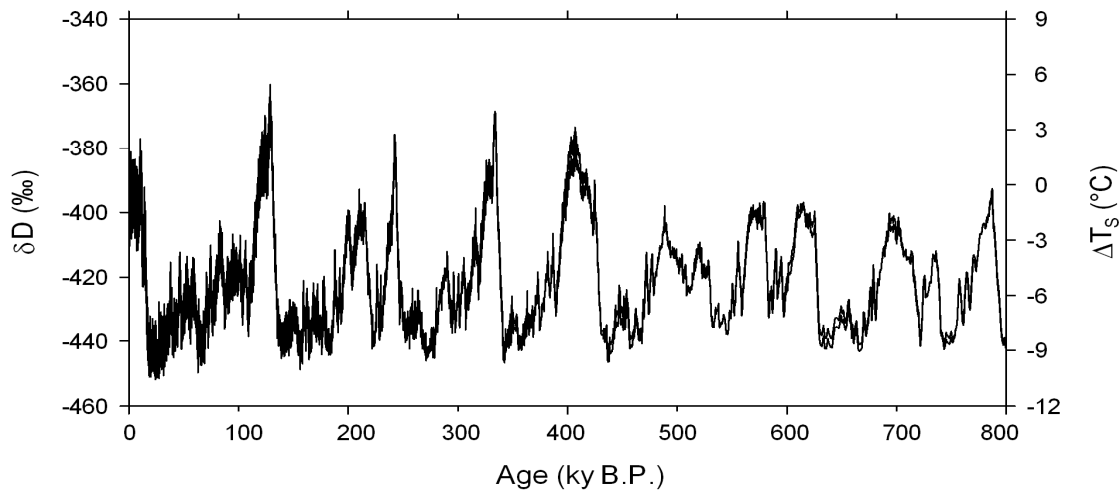
Figure 2 EPICA Dome C δD record (left y axis), together with the reconstructed surface temperature anomaly compared to present-day (right y axis). Data from (Jouzel et al., 2007), EPICA Dome C Ice Core 800KYr Deuterium Data and Temperature Estimates. IGBP PAGES/World Data Center for Paleoclimatology. Data Contribution Series # 2007-091. NOAA/NCDC Paleoclimatology Program, Boulder CO, USA.

1.2 Aim of this study

Despite their remote location, polar regions have most extensively been studied with respect to water stable isotopes as paleoclimatic proxies in the ice cores, for reviews see for example (Jouzel et al., 1997; Jouzel, 2003; Masson-Delmotte et al., 2008).

For mid- and low latitude glaciers, however, there is a limited number of investigations attempting to relate the water stable isotopes in ice cores to the atmospheric parameters. In very few cases a transfer function for the δ^{18}O/temperature relationship was established, like in the case of Tibetan (Yao et al., 1996), European Alpine (Schotterer et al., 1997; Eichler et al., 2001; Bohleber et al., 2013) or Northern American glaciers (Naftz et al., 2002). In other cases, the isotopic records were only discussed without a direct calibration with temperature, deducing it from comparison with the polar ice cores δ^{18}O/temperature relationships (Thompson, 2000) or reporting only the degree of correlation (Davis et al., 1995).

In the European Alpine region, where the atmospheric circulation is dominated by different driving factors, the interpretation of the water stable isotope signal results particularly challenging due also to the complex interactions of air masses with topography. The Alpine

region experiences high intraseasonal and interannual precipitation and moisture sources variability. This might introduce two additional complications in the interpretation of the $\delta^{18}O$/temperature relationship: (i) the seasonal change of moisture sources introduces additional effects altering the isotopic-temperature relationship and (ii) the seasonality, or more in general, precipitation intermittency may bias the annual value of $\delta^{18}O$ toward the season with more precipitation, as was shown for example by Persson et al. (2011) for Greenland. In this latter case the comparison of the isotope record with temperature might thus considerably deviate from the case of uniform precipitation and a more appropriate precipitation-weighted temperature parameter should be used, with implications for paleoclimatic reconstructions (Jouzel et al., 1997).

In order to extend the knowledge and improve the understanding of the water stable isotopes from Alpine glaciers, this PhD project was developed with specific focus on the Swiss Alpine region for two reasons: (i) several ice cores were drilled there and isotopic records from different glaciers are available, enabling the possibility to investigate the spatial variability of the isotopic signal at high altitudes (ii) the Swiss area offers a unique long-term, high quality, and high spatially resolved meteorological dataset that can be used for improving the understanding of the isotopic processes. The investigation focuses mainly on the instrumental period to study the processes affecting the proxy deposition at the site.

This PhD study was embedded in the projects "Varves, Ice cores, and Treerings" (VITA) and "Paleoclimate Variability and Extreme Events" (PALVAREX) funded by the NCCR Climate program (www.nccr-climate.unibe.ch) of the Swiss National Science Foundation (SNF). Part of this project consisted in the characterization of a new laser spectrometer for the analysis of stable isotopes in liquid samples.

The outline of this thesis is the following. In Chapter 2 the theoretical framework of the water stable isotopes is given together with the description of the regional setting. The methods used to measure the water stable isotopes in ice cores are presented in Chapter 3, with particular focus on the setup and characterization of a new laser spectrometer installed in the laboratory in comparison to the Isotopic Ratio Mass Spectrometer analytical technique applied before. The $\delta^{18}O$/temperature and accumulation/precipitation relationship for the Fiescherhorn and Grenzgletscher is discussed in Chapter 4. In Chapter 5 the analysis of the $\delta^{18}O$ and deuterium excess of the Fiescherhorn ice core compared to the nearby GNIP data is presented. Suggestions regarding the use of the Fiescherhorn record together with the long-term Colle Gnifetti data set in future studies are given in the Outlook.

References

Bradley, R. S.: Paleoclimatology: Reconstructing Climates of the Quaternary, Academic Press, 1999.

Dansgaard, W.: Stable isotopes in precipitation, Tellus, 16(4), 436–468, doi:10.1111/j.2153-3490.1964.tb00181.x, 1964.

Dansgaard, W., Johnsen, S. J., Clausen, H. B., Dahl-Jensen, D., Gundestrup, N. S., Hammer, C. U., Hvidberg, C. S., Steffensen, J. P., Sveinbjornsdottir, A. E. and Jouzel, J.: Evidence for general instability of past climate from a 250-kyr ice-core record, Nature, 364, 218–220, doi:10.1038/364218a0, 1993.

Davis, M. E., Thompson, L. G., Mosley-Thompson, E., Lin, P. N., Mikhalenko, V. N. and Dai, J.: Recent ice-core climate records from the Cordillera Blanca, Peru, Ann. Glaciol., 1995.

Easterling, D. R., Meehl, G. A., Parmesan, C., Changnon, S. A., Karl, T. R. and Mearns, L. O.: Climate extremes: observations, modeling, and impacts, Science, 289(5487), 2068–2074, doi:10.1126/science.289.5487.2068, 2000.

Eichler, A., Schwikowski, M. and Gäggeler, H. W.: Meltwater-induced relocation of chemical species in Alpine firn, Tellus B, 53(2), 192–203, doi:10.1034/j.1600-0889.2001.d01-15.x, 2001.

Fricke, H. C. and O'Neil, J. R.: The correlation between $^{18}O/^{16}O$ ratios of meteoric water and surface temperature: its use in investigating terrestrial climate change over geologic time, Earth Planet. Sci. Lett., 170(3), 181–196, doi:10.1016/S0012-821X(99)00105-3, 1999.

IAEA/WMO: Global Network of Isotopes in Precipitation. The GNIP Database. Accessible at: http://www.iaea.org/water, 2013.

IPCC: Climate Change 2007: The Physical Science Basis. Contribution of Working Group I to the Fourth Assessment Report of the Intergovernmental Panel on Climate Change, Cambridge University Press, Cambridge and New York, 2007.

IPCC: Climate Change 2013: The Physical Science Basis. Contribution of Working Group I to the Fifth Assessment Report of the Intergovernmental Panel on Climate Change, Final Draft, Available on: http://www.ipcc.ch/, 2013.

Johnsen, S. J., Clausen, H. B., Dansgaard, W., Fuhrer, K., Gundestrup, N., Hammer, C. U., Iversen, P., Jouzel, J., Stauffer, B. and Steffensen, J. P.: Irregular glacial interstadials recorded in a new Greenland ice core, Nature, 359, 311–313, doi:10.1038/359311a0, 1992.

Johnsen, S. J., Dahl-Jensen, D., Gundestrup, N., Steffensen, J. P., Clausen, H. B., Miller, H., Masson-Delmotte, V., Sveinbjörnsdottir, A. E. and White, J.: Oxygen isotope and palaeotemperature records from six Greenland ice-core stations: Camp Century, Dye-3, GRIP, GISP2, Renland and NorthGRIP, J. Quat. Sci., 16(4), 299–307, doi:10.1002/jqs.622, 2001.

Jouzel, J., Merlivat, L. and Lorius, C.: Deuterium excess in an East Antarctic ice core suggests higher relative humidity at the oceanic surface during the last glacial maximum, Nature, 299(5885), 688–691, doi:10.1038/299688a0, 1982.

Jouzel, J., Alley, R. B., Cuffey, K. M., Dansgaard, W., Grootes, P., Hoffmann, G., Johnsen, S. J., Koster, R. D., Peel, D., Shuman, C. A., Stievenard, M., Stuiver, M. and White, J.: Validity of the temperature reconstruction from water isotopes in ice cores, J. Geophys. Res. Oceans, 102(C12), 26471–26487, doi:10.1029/97JC01283, 1997.

Jouzel, J.: Water stable isotopes: Atmospheric composition and applications in polar ice core studies, in Treatise on geochemistry, vol. 4, pp. 213–243, 2003.

Jouzel, J., Masson-Delmotte, V., Cattani, O., Dreyfus, G., Falourd, S., Hoffmann, G., Minster, B., Nouet, J., Barnola, J. M., Chappellaz, J., Fischer, H., Gallet, J. C., Johnsen, S., Leuenberger, M., Loulergue, L., Luethi, D., Oerter, H., Parrenin, F., Raisbeck, G., Raynaud, D., Schilt, A., Schwander, J., Selmo, E., Souchez, R., Spahni, R., Stauffer, B., Steffensen, J. P., Stenni, B., Stocker, T. F., Tison, J. L., Werner, M. and Wolff, E. W.: Orbital and millennial Antarctic climate variability over the past 800,000 years, Science, 317(5839), 793–796, doi:10.1126/science.1141038, 2007.

Masson-Delmotte, V., Jouzel, J., Landais, A., Stievenard, M., Johnsen, S. J., White, J. W. C., Werner, M., Sveinbjornsdottir, A. and Fuhrer, K.: GRIP deuterium excess reveals rapid and orbital-scale changes in Greenland moisture origin, Science, 309(5731), 118–121, doi:10.1126/science.1108575, 2005.

Masson-Delmotte, V., Hou, S., Ekaykin, A., Jouzel, J., Aristarain, A., Bernardo, R. T., Bromwich, D., Cattani, O., Delmotte, M., Falourd, S., Frezzotti, M., Gallée, H., Genoni, L., Isaksson, E., Landais, A., Helsen, M. M., Hoffmann, G., Lopez, J., Morgan, V., Motoyama, H., Noone, D., Oerter, H., Petit, J. R., Royer, A., Uemura, R., Schmidt, G. A., Schlosser, E., Simões, J. C., Steig, E. J., Stenni, B., Stievenard, M., van den Broeke, M. R., van de Wal, R. S. W., van de Berg, W. J., Vimeux, F. and White, J. W. C.: A review of Antarctic surface snow isotopic composition: observations, atmospheric circulation, and isotopic modeling, J. Clim., 21(13), 3359–3387, doi:10.1175/2007JCLI2139.1, 2008.

Naftz, D. L., Susong, D. D., Schuster, P. F., Cecil, L. D., Dettinger, M. D., Michel, R. L. and Kendall, C.: Ice core evidence of rapid air temperature increases since 1960 in alpine areas of the Wind River Range, Wyoming, United States, J. Geophys. Res.-Atmos., 107(D13), ACL 3–1–ACL 3–16, doi:10.1029/2001JD000621, 2002.

NEEM community members: Eemian interglacial reconstructed from a Greenland folded ice core, Nature, 493(7433), 489–494, doi:10.1038/nature11789, 2013.

OcCC: Climate Change and Switzerland 2050 - Expected Impacts on Environment, Society and Economy, Available from: http://proclimweb.scnat.ch/Products/ch2050/PDF_E/CH2050-E.pdf, 2007.

Persson, A., Langen, P. L., Ditlevsen, P. and Vinther, B. M.: The influence of precipitation weighting on interannual variability of stable water isotopes in Greenland, J. Geophys. Res., 116(D20), D20120, doi:10.1029/2010JD015517, 2011.

Petit, J. R., Jouzel, J., Raynaud, D., Barkov, N. I., Barnola, J.-M., Basile, I., Bender, M., Chappellaz, J., Davis, M., Delaygue, G., Delmotte, M., Kotlyakov, V. M., Legrand, M., Lipenkov, V. Y., Lorius, C., PÉpin, L., Ritz, C., Saltzman, E. and Stievenard, M.: Climate and atmospheric history of the past 420,000 years from the Vostok ice core, Antarctica, Nature, 399(6735), 429–436, doi:10.1038/20859, 1999.

Pfahl, S. and Wernli, H.: Air parcel trajectory analysis of stable isotopes in water vapor in the eastern Mediterranean, J. Geophys. Res. Atmos., 113(D20), doi:10.1029/2008JD009839, 2008.

Schotterer, U., Fröhlich, K., Gäggeler, H. W., Sandjordj, S. and Stichler, W.: Isotope records from Mongolian and Alpine ice cores as climate indicators, Clim. Change, 36(3-4), 519–530, doi:10.1023/A:1005338427567, 1997.

Stenni, B., Masson-Delmotte, V., Johnsen, S., Jouzel, J., Longinelli, A., Monnin, E., Röthlisberger, R. and Selmo, E.: An oceanic cold reversal during the last deglaciation, Science, 293(5537), 2074–2077, doi:10.1126/science.1059702, 2001.

Thompson, L. G.: Ice core evidence for climate change in the Tropics: implications for our future, Quat. Sci. Rev., 19(1–5), 19–35, doi:10.1016/S0277-3791(99)00052-9, 2000.

Trenberth, K. E., Dai, A., Rasmussen, R. M. and Parsons, D. B.: The changing character of precipitation, Bull. Am. Meteorol. Soc., 84(9), 1205–1217, doi:10.1175/BAMS-84-9-1205, 2003.

Wolff, E. W., Barbante, C., Becagli, S., Bigler, M., Boutron, C. F., Castellano, E., de Angelis, M., Federer, U., Fischer, H., Fundel, F., Hansson, M., Hutterli, M., Jonsell, U., Karlin, T., Kaufmann, P., Lambert, F., Littot, G. C., Mulvaney, R., Röthlisberger, R., Ruth, U., Severi, M., Siggaard-Andersen, M. L., Sime, L. C., Steffensen, J. P., Stocker, T. F., Traversi, R., Twarloh, B., Udisti, R., Wagenbach, D. and Wegner, A.: Changes in environment over the last 800,000 years from chemical analysis of the EPICA Dome C ice core, Quat. Sci. Rev., 29(1–2), 285–295, doi:10.1016/j.quascirev.2009.06.013, 2010.

Yao, T., Thompson, L. G., Mosley-Thompson, E., Zhihong, Y., Xingping, Z. and Lin, P.-N.: Climatological significance of $\delta^{18}O$ in north Tibetan ice cores, J. Geophys. Res.-Atmos., 101(D23), 29531–29537, doi:10.1029/96JD02683, 1996.

18

2 Ice core proxies, regional setting and study sites

This Chapter is structured as follows. The ice core proxies investigated in this study, which are the water stable isotope ratios δ^{18}O, δD, the deuterium excess, and the reconstructed accumulation, are presented in section 2.1 and 2.2, respectively. The regional setting is discussed in section 2.3 where the climatological description of the Alpine area is given. In section 2.4 the ice core drilling sites and the records used in this study are shown.

2.1 Water stable isotopes

The hydrological cycle can be investigated using several approaches. One of them, the isotope hydrology, aims to track the hydrological processes by means of the different oxygen and hydrogen isotopes forming the water molecule (e.g. Clark and Fritz, 1997; Hoefs, 2009). In climate science this approach is used to give insights into the processes occurring in the water cycle related to climatic changes and one refers more specifically to the so-called isotope paleoclimatology. The first comprehensive theoretical framework of the water stable isotopes as proxies for temperature was introduced by Dansgaard in 1964, analyzing samples collected all over the world (Dansgaard, 1964). Water stable isotopes are measured in precipitation (IAEA/WMO, 2013), groundwater, and rivers. The data acquisition is global in order to cover the complexity of the cycle. Recently two major achievements in the investigation of the water cycle were obtained with (i) the development of new optical laser system techniques allowing for continuous in-situ measurements of water vapor in the atmosphere, enabling an almost complete tracking of the water cycle (Aemisegger et al., 2012; Steen-Larsen et al., 2013) and (ii) the introduction of a new parameter related only to the relative humidity conditions, the ^{17}O excess (Landais et al., 2012). Besides, modeling studies using both in-cloud microphysics concepts and more complex isotope-equipped GCMs allow investigating the underlying physical processes. This is fundamental to reconstruct the past conditions where the atmospheric circulation was substantially different from the present, like in the case of the Last Glacial Maximum, (e.g. Jouzel et al., 1997; Vimeux et al., 1999; Jouzel, 2003). The next subsections present the theoretical framework of the water stable isotopes, introducing first their physico-chemical properties and then showing their application in climate science studies.

2.1.1 Physical principles and equilibrium fractionation

Hydrogen and oxygen forming the water molecule occur in different stable isotopes in nature (Table 1). For the hydrogen they are ^{1}H, ^{2}H (or D, called deuterium) and for the oxygen they are ^{16}O, ^{17}O, ^{18}O. The lighter isotopes are more frequent in nature: for the oxygen there is approximately one heavy isotope (^{18}O) every 500 light isotopes (^{16}O) whereas the ratio of deuterium to hydrogen is about 1 isotope every 6400.

The focus in isotope paleoclimatology is mainly on three isotopologues, i.e. the combinations of the isotopes forming the water molecule: $H_2{}^{16}O$ (most abundant), $H_2{}^{18}O$ (rare) and HDO (very rare). Due to mass differences these molecules have different physicochemical properties. This effect is particularly strong for isotopes with low atomic number, like hydrogen where the mass ratio D/H is 2 compared to oxygen whose ratio ^{18}O/^{16}O is 1.125. The main two physical properties of relevance here are the vapor pressure, discussed below, and the diffusivity (section 2.1.4).

Element	Z	N	A	Abundance (%)	Symbol
Hydrogen	1	0	1	99.985	H
	1	1	2	0.0155	^{2}H; D
Oxygen	8	8	16	99.759	^{16}O
	8	9	17	0.037	^{17}O
	8	10	18	0.204	^{18}O

Table 1 Stable isotopes of hydrogen and oxygen (adapted from Gat et al. 2001). Z is the atomic (or proton) number, N neutron number and A the relative atomic mass.

For the water isotopologues the lighter molecules require a smaller energy to evaporate. In other words, they have a higher vapor pressure than the heavier ones (Table 2). Thereby, changes in relative concentrations of the isotopologues from one phase to the other occur during a change of phase (e.g. evaporation, condensation). This discrimination is called *isotopic fractionation.*

When the energy (i.e. temperature) of the system increases, the relative vapor pressure increases according to the Clausius-Clapeyron equation and more evaporation occurs. The isotopic fractionation, on the other hand, decreases because the heavier isotopologues tend to evaporate more relative to lower temperature conditions and the discrimination with the lighter molecules diminishes.

Isotopologue	Vapor pressure at 100°C (mbar)
$^{1}H_2^{16}O$	1013 mbar
$D_2^{16}O$	962 mbar

Table 2 Vapor pressure at 100°C for the light and heavy molecule of water. Adapted from Hoefs (2009).

This behavior can be described in analogy to a chemical reaction. With respect to the hydrological cycle the main type of reaction is the physical change of state, e.g. evaporation or condensation. In this case it can be written as:

$aL+bH \leftrightarrow bL + aH$
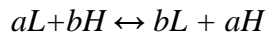
where L is the light and H the heavy isotope of an element and a, b are their concentrations in the two phases. At chemical equilibrium the forward and backward rates of reaction are equal. The equilibrium constant K can then be defined as:

$$K = \frac{[L]^b[H]^a}{[L]^a[H]^b} = \frac{\left(\frac{[H]}{[L]}\right)^a}{\left(\frac{[H]}{[L]}\right)^b}$$

Because of their different vapor pressures the reaction rates of the heavy and light molecules differ. As discussed above, in the case of evaporation the heavier molecules tend to stay more in the lower energy state (liquid phase) whereas the lighter ones evaporate more.

In isotope studies one refers to the *equilibrium fractionation factor* α_{eq} rather than to the equilibrium constant. It can be written as

$\alpha_{eq}=K=R_2/R_1$ (1)

where R_1 and R_2 are the isotope ratios *[H]/[L]* in the phases 1 and 2 (that can be for example liquid and vapor).

In the hydrological cycle the isotopic fractionation during a change of phase has a small effect, since there is only a slight difference of the vapor pressures of the heavy and the light molecules (Table 2). The vapor pressure difference of $H_2^{16}O$ and $H_2^{18}O$ is 1%, while the vapor pressure of $H_2^{16}O$ is about 10% higher than of HDO (Dansgaard et al., 1973).

The isotopic fractionation at equilibrium is temperature dependent, with lower fractionation at higher temperatures. Ideally, at very high temperatures there are no fractionation effects. In general the equilibrium constant (or fractionation factor) can be described by:

$$\ln K = c_1 + \frac{c_2}{T} + \frac{c_3}{T^2}$$

At temperatures much below room temperature lnK is given by $1/T$ whereas at higher temperatures the term $1/T^2$ dominates with less fractionation with respect to the colder conditions (Hoefs, 2009).

The fractionation factor thus approaches 1. Because the differences in the partitioning are of the order of magnitude of thousandths, the *enrichment factor ε* is often used. It is expressed in permil (‰) and defined as follows:

$\varepsilon=(\alpha-1)*1000$

The fractionation factor α of the water-vapor transition at 20°C is 1.0098 and 1.085 for ^{18}O and D, respectively (Jouzel, 2003, and Table 3). That means that the liquid water is slightly enriched in heavier molecules and the ε is 9.8‰ for ^{18}O and 85‰ for D. For lower temperatures the fractionation increases. At 0°C the coefficients is 1.0117 for ^{18}O and 1.1123 for D, corresponding to ε 11.7‰ and 112‰, respectively. The effect is stronger for the solid-vapor equilibrium transition (e.g. ε=15.2‰ and ε=133‰ at 0°C for ^{18}O and D, respectively) because of the larger energy required compared to the liquid-vapor transition.

	Liquid-vapor		Solid-vapor	
T (°C)	α_{18O}	α_D	α_{18O}	α_D
20	1.0098	1.0850		
0	1.0117	1.1123	1.0152	1.1330
-20	1.0141	1.1492	1.0187	1.1744

Table 3 Fractionation factors at different temperatures, adapted from Jouzel (2003), after Merlivat and Nief (1967) and Majoube (1971).

2.1.2 δ notation

As shown previously the variations of the isotopic compositions due to fractionation processes are in the permil (‰) order. These small changes render absolute isotopic ratio measurements difficult to be performed. Thus, isotope ratios R between the heavy and the light component are measured relative to an international standard R_{VSMOV} (Chapter 33). To express the small variations the "delta" notation was introduced (Craig, 1961):

$$\delta^{18}O = \frac{R_{sample} - R_{VSMOW}}{R_{VSMOW}} = \frac{\left(\frac{^{18}O}{^{16}O}\right)_{sample} - \left(\frac{^{18}O}{^{16}O}\right)_{VSMOW}}{\left(\frac{^{18}O}{^{16}O}\right)_{VSMOW}} \cdot 1000$$

This expression describes the changes of the isotopic ratio with respect to the oxygen isotopes, but an analog relation is used for the hydrogen:

$$\delta D = \frac{R_{sample} - R_{VSMOW}}{R_{VSMOW}} = \frac{\left(\frac{D}{H}\right)_{sample} - \left(\frac{D}{H}\right)_{VSMOW}}{\left(\frac{D}{H}\right)_{VSMOW}} \cdot 1000$$

R_{VSMOW} (Vienna Standard Mean Ocean Water) are the respective isotopic ratios of the international standards that are meant to express the mean isotopic composition of the global ocean. Their values are:

$(^{18}O/^{16}O)_{VSMOW} = (2005.20 \pm 0.45)10^{-6}$ (Baertschi, 1976)

$(D/H)_{VSMOW} = (155.95 \pm 0.08)10^{-6}$ (De Wit et al., 1980)

For further details about the international standards, see Chapter 3.

For better visualization the ratios are expressed in ‰ (unitless). Samples enriched in the heavier molecule with respect to VSMOW have positive values, whereas depleted samples show negative values. The typical range for the delta values in the hydrological cycle is $-450‰ < \delta D < 100‰$ and $-50‰ < \delta^{18}O < 50‰$ (Gat et al., 2001).

Analytical uncertainties of these values depend on the instrument used. Typically precisions of $\pm 1.0‰$ (at best 0.3‰) and $\pm 0.1‰$ (at best 0.03‰) can be achieved for δD and $\delta^{18}O$, respectively (Gat et al., 2001).

2.1.3 Rayleigh fractionation

The first model used to describe the isotopic fractionation in the hydrological cycle was the Rayleigh fractionation model. It assumes that part of the material of the initial reservoir is removed, as the change of phase proceeds. This is the case for example of a cloud where the product (condensate) is removed by precipitation and leaves an isotopic imprint in both, remaining vapor and liquid phase depending upon the particular thermodynamical conditions (temperature) at which the change of phase occurred.

The derivation of the Rayleigh distillation equation here described is based on considerations regarding the two reservoirs, but the equation can also be obtained considering a mass balance approach (Gat, 1996; Gat et al., 2001).

A water reservoir contains both, light and heavy molecules, given by their initial concentrations L_0 and H_0, respectively. When the water starts to evaporate, the concentrations of both isotopologues will change according to their equilibrium constants k_L and k_H. The corresponding equations for both, light and heavy isotopologues will be:

$$dL = -k_L L \tag{2}$$

$$dH = -k_H H \tag{3}$$

Dividing Eq. (2) by Eq. (3), the fractionation coefficient is obtained in Eq. (4) according to Eq. (1):

$$dH/H = \alpha(dL/L) \tag{4}$$

Integrating Eq. (4) between H_0, L_0 the initial concentration in the water reservoir and H, L (after some evaporation occurred), it is obtained:

$$\ln(H/H_0) = \alpha \ln(L/L_0) \rightarrow H/H_0 = (L/L_0)^\alpha$$

Dividing everything by L/L_0

$$(H/L)(L_0/H_0) = (L/L_0)^{(\alpha-1)}$$

Defining the quantities $R_0 = H_0/L_0$ (initial isotopic ratio in the reservoir), $R = H/L$ (isotopic ratio of the reservoir at the time t of the evaporation process) and $f = (H+L)/(H_0+L_0) \approx L/L_0$ (fraction of the material remaining with the reservoir as evaporation proceeds), the *Rayleigh distillation equation* is then derived:

$$R = R_0 f^{(\alpha-1)}$$

This equation describes the ideal condition of a system where product and reservoir are in thermodynamical equilibrium. It states that the isotopic ratio R of a species in the reservoir depends on the initial isotopic ratio R_0, the fraction f of the remaining material as the change of phase proceeds and the fractionation factor α.

2.1.4 Equilibrium and kinetic fractionation

When the rate of the forward reaction is counterbalanced by the rate of the backward reaction, equilibrium conditions are met (Dansgaard, 1964). In the hydrological processes in-cloud condensation may be approximated by equilibrium fractionation. However, pure equilibrium conditions seldom occur in nature.

When fast reactions occur there is not sufficient time to establish equilibrium conditions. Since the molecules have mean kinetic energy $1/2mv^2$, the heavier isotopologues tend to react slower than the lighter ones, inducing a *kinetic fractionation (*e.g. Dansgaard, 1964; O'Neil, 1986*)*. The origin of this fractionation is thus kinetic and can be understood considering the Fick's law of diffusion *F=-DdC/dx*, where *F* is the diffusion flux, *D* the diffusivity and *dC/dx* the concentration gradient. *D* is inversely proportional to the square root of the molecular mass (to be precise, for vapor diffusing in the air the mass is the reduced mass considering the water vapor and the air) and therefore lighter molecules tend to diffuse faster than the heavier ones. For the three main isotopologues this means that the $D(H_2^{16}O)>D(HD^{16}O)>D(H_2^{18}O)$, because the corresponding molecular masses are 18, 19 and 20 g/mol. Kinetic fractionation can be enhanced by increasing the concentration gradient *dC/dx* or providing more energy to the molecules i.e. increasing the temperature.

Regarding the hydrological cycle, seawater evaporation occurs in a very thin layer at the interface with the air. The air above the sea is not stagnant and equilibrium conditions are thus not reached, leading to an undersaturation of water vapor. As result a concentration gradient is present and evaporation continues. Merlivat and Jouzel (1979) and Craig and Gordon (1965) described this process with a model, where the sea-air interface consists in a very thin layer (micrometers thick) ideally at 100% saturation, dominated by equilibrium conditions. Between this layer and the well-mixed air column there is a transition zone where diffusion dominates because the air is undersaturated with water. If the relative humidity above the sea decreases larger diffusion takes place increasing the kinetic fractionation, whereas turbulence and strong mixing due to increased wind speed above the surface reduce the kinetic effects.

The total isotopic fractionation should therefore account for both, equilibrium conditions and kinetic effects. The kinetic fractionation is rather small compared to the one at equilibrium. Since the kinetic effects are similar for oxygen and hydrogen and equilibrium fractionation for HDO/H_2O molecules is ~8 times higher than for $H_2^{18}O/H_2^{16}O$, the relative importance of kinetic to equilibrium effects is much higher for $H_2^{16}O/H_2^{18}O$ than $H_2^{16}O/HDO$.

The processes occurring in nature involve both equilibrium and kinetic fractionations: evaporation from the sea is not an equilibrium process as net evaporation occurs, but is also

not entirely kinetic because some condensation of vapor takes place. In that case it is more generally called non-equilibrium fractionation (Mook, 2001).

Kinetic effects occur also in clouds, when at temperatures below 0°C the saturation vapor pressure over ice is lower than over liquid water and the cloud microphysics is governed by the Bergeron-Findeisen process. At temperatures between 0 and -25°C the three phases of water co-exist (mixed-phase clouds) with the vapor being deposited onto ice and the liquid continuously removed from cloud droplets by evaporation. At lower temperatures the process is dominated by the vapor-ice phases. From an isotopic point of view kinetic fractionation occurs when vapor is deposited onto ice and when liquid water evaporates, leaving in both cases the initial phase more enriched in the heavier isotopes. The extent of the kinetic fractionation in this case depends on supersaturation conditions (Jouzel and Merlivat, 1984; Ciais and Jouzel, 1994).

2.1.5 Global Meteoric Water Line (GMWL) and deuterium excess

Craig (1961) plotted the δD values collected in surface and meteoric waters from all over the world against the corresponding $\delta^{18}O$. His result shows that the δD and $\delta^{18}O$ are linearly related. This equation is known as Global Meteoric Water Line (GMWL): $\delta D = 8\delta^{18}O + 10$. More recently, Rozanski et al. (1993) established a relationship using only data collected in precipitation (Figure 3): $\delta D = (8.20 \pm 0.07) \delta^{18}O + (11.27 \pm 0.65)$.

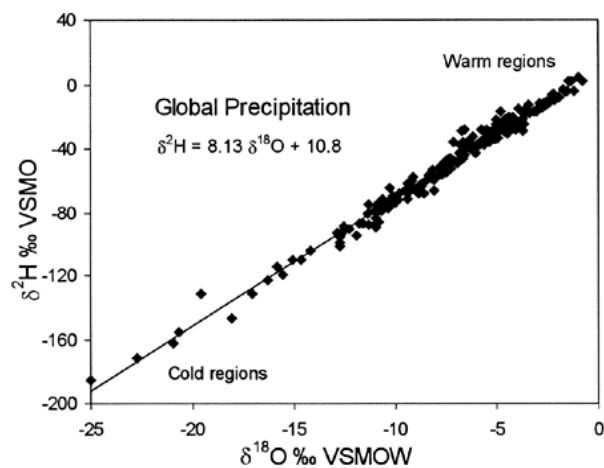**Figure 3** GMWL obtained from the mean annual values of $\delta^{18}O$ and δD in precipitation, from Clark and Fritz (1997), data compiled by Rozanski et al. (1993). Depleted values come from warm regions, more depleted values from cold regions.

This linear relation represents the average of the meteoric waters from all over the world. The slope is ~8 which is in agreement with the ratio of the equilibrium fractionation factors for hydrogen and oxygen at 25°C (Clark and Fritz, 1997). The intercept d, defined by the relation $d=\delta D-8\delta^{18}O$, is called *deuterium excess*. This parameter expresses the deviation from equilibrium conditions and is an indicator for kinetic fractionation. Because of the different isotopologues' diffusivities, the seawater is slightly more enriched with respect to the pure equilibrium conditions when evaporation occurs. The deuterium excess gives the extent of this enrichment.

The GMWL represents global conditions, but locally there might be deviations. It was shown that at sites where strong evaporation occurs the slopes of the so-called Local Meteoric Water Lines (LMWL) are lower than 8 (Gonfiantini, 1986; Rozanski et al., 1993).

Typical values of deuterium excess in meteoric water range from 0‰ to 30‰, the latter ones in regions where strong evaporation occurs. This is the case of the Mediterranean region, especially in the eastern basin (Gat and Carmi, 1970), where kinetic fractionation is particularly enhanced. Moisture recycling, i.e. the mechanism with which moisture is returned to the atmosphere by soil evaporation in summer, results in an increased deuterium excess in the evaporated water (Araguás-Araguás et al., 2000; Fröhlich et al., 2008). Values lower than 10‰ could be indicators of secondary evaporation processes, like sub-cloud re-evaporation. This process tends to decrease the deuterium excess in precipitation and it was shown to partially counteract the effects of moisture recycling in summer (Fröhlich et al., 2008).

Because condensation can be assumed to occur at equilibrium, the deuterium excess would be, unless further kinetic effects occur, a good proxy for the moisture source conditions i.e. relative humidity and temperature at the evaporation site. Several studies related the variability of the deuterium excess in Greenland and Antarctica to sea surface temperature changes, see e.g. Vimeux et al. (1999); Stenni et al. (2001); Masson-Delmotte et al. (2005). Other studies showed that the deuterium excess is rather driven by relative humidity conditions at the moisture source (Jouzel et al., 1982; Pfahl and Wernli, 2008; Pfahl and Sodemann, 2013). Uemura et al. (2008) observed that deuterium excess measured directly in water vapor has significant relationships with both sea surface temperature (positive correlation) and relative humidity (anticorrelation). Lewis et al. (2013) reported that changes in the relative humidity at the source region might affect the deuterium excess-sea surface temperature relationship.

2.1.6 δ^{18}O-temperature relationship

In the air mass the amount of rainout is related to the water vapor-holding capacity, which itself depends on temperature. As temperature decreases higher rainout occurs with progressive distillation, according to the Rayleigh equation. A global relationship between the annual δ^{18}O in precipitation and mean annual temperature was already obtained in 1964 by Dansgaard (Figure 4). He found a linear relationship for both, δ^{18}O and δD:

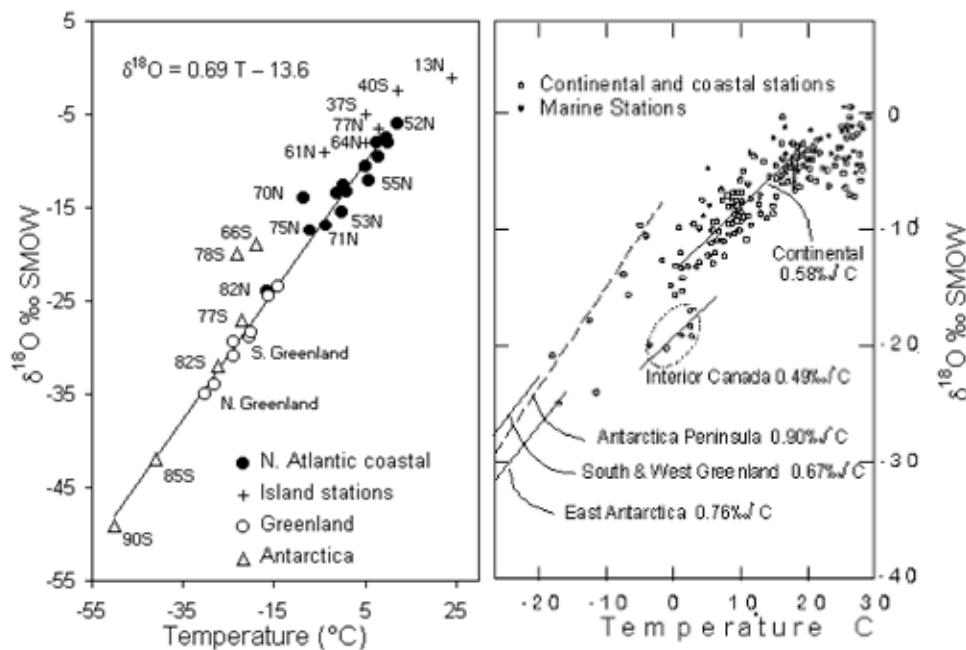$$\delta^{18}O = 0.695T - 13.6‰$$

$$\delta D = 5.6T - 100‰$$

Figure 4 (Left panel) δ^{18}O in precipitation plotted against the mean annual temperature (Clark and Fritz, 1997) after (Dansgaard, 1964). (Right panel) Regional slopes obtained for different stations (Clark and Fritz, 1997) after (Rozanski et al., 1993).

The more enriched isotopic values and temperatures are found at low and mid latitudes, whereas the polar sites occupy the lower part of the line (Figure 4, left panel). Similarly to what was obtained for the GMWL, deviations from the global slope exist due to local effects (Figure 4, right panel). A quite strong deviation was observed at marine stations, where the slope of the relationship is much lower than the GMWL. At these sites the seasonal temperature variations are naturally dampened and the main driving factor is the precipitation (see below). The opposite case tends to occur at continental stations, where the winter to summer temperature excursions are higher than in coastal regions. At the poles the slopes tend to be higher because of the very low temperatures.

The deviations from the global line are a combination of geographical, topographical and seasonal effects, e.g. Yurtsever and Gat (1981); Rozanski et al. (1993); Gat (1996); Clark and Fritz (1997); Fricke and O'Neil (1999); Araguás-Araguás et al. (2000); Gat et al. (2001).

The *latitude effect* is caused by the global water transport from the tropics toward the poles. The decreasing temperature with latitude drives the rainout, resulting in a progressive isotopic depletion of the air masses. In a similar fashion the *continental effect* renders the air masses more and more depleted with increasing distance from the sea (Figure 5).
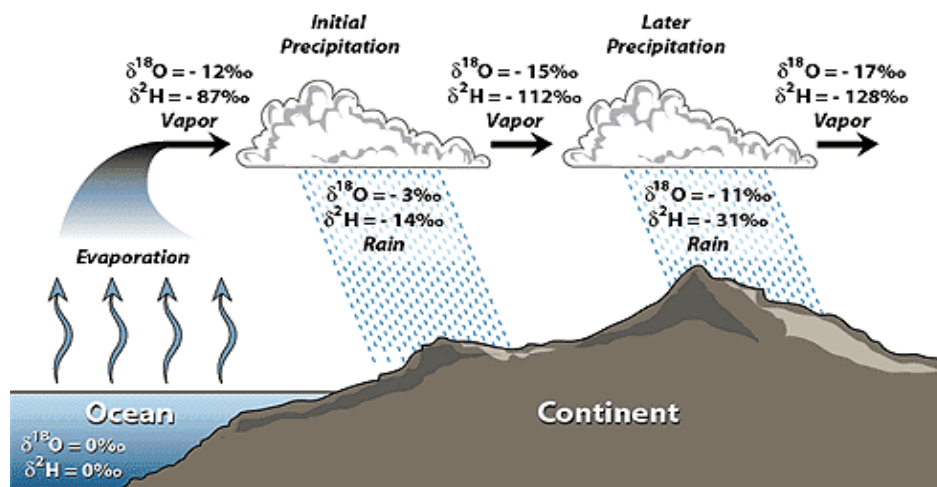

Figure 5 Rainout effect on δD and $\delta^{18}O$ values, based on Coplen et al. (2000) and Hoefs (2009). Source: http://web.sahra.arizona.edu/programs/isotopes/oxygen.html.

The *altitude effect* is observed in presence of mountain chains, when there is a mechanically forced uplift of air masses with consequent adiabatic expansion and cooling. If the uplift is such that the condensation level is reached, orographic precipitation may occur. The remaining water vapor is isotopically depleted as the uplift-driven distillation proceeds. For the European Alps, an altitude effect of $\delta^{18}O/dz \sim -0.2‰/100$ m was observed (Siegenthaler and Oeschger, 1980; Schürch et al., 2003). It was noted that this gradient is homogeneous all over the world with few exceptions especially above 5000 m a.s.l., where the isotopic depletion becomes nonlinear with increasing altitude (Poage and Chamberlain, 2001).

Another process that is more significant at tropical latitudes is the *amount effect*. In these regions $\delta^{18}O$ tends to be anticorrelated with the precipitation amount, i.e. more depleted values are found in correspondence of heavy precipitation (Dansgaard, 1964). This is due to the fact that if the precipitation develops in big towering clouds, like tropical clouds, the droplets will experience in-cloud exchange of water vapor, resulting in a progressive

depletion (Field et al., 2010). Sub-cloud re-evaporation, moreover, may occur, leaving the remaining vapor (hence the successive precipitation) more and more depleted (Risi et al., 2008).

In addition to the spatial variability of $\delta^{18}O$ and δD, temporal variations related to the temperature seasonal cycle affect the isotopic signal. The seasonality of the isotopic signal is particularly pronounced at continental stations, where the summer to winter temperature changes are larger compared to the marine locations (Ronzanski et al., 1993). Over Europe a contribution to the more enriched isotopic values in summer is due to the change of the moisture sources: for example, plant evapotranspiration returns to the atmosphere a considerable amount of water vapor reducing thus the degree of rainout over the continent (Rozanski et al., 1982; Rozanski et al., 1993). Because the focus of this study is on Alpine ice cores, few more considerations have to be taken into account.

2.1.7 Post-depositional processes on glaciers

The discussion has so far focused on $\delta^{18}O$ (δD) in liquid precipitation. When dealing with ice cores, post-depositional effects in the snowpack have to be taken into account (Cooper, 1998; Schotterer et al., 2004). Processes that can alter the isotopic composition in the snowpack are diffusion, meltwater formation, percolation, refreezing, sublimation, and rain precipitation (Stichler and Schotterer, 2000). If the snowpack temperatures are far below 0°C (cold glaciers) fractionation may occur due to the diffusion of the water vapor through the firn pores during snow metamorphosis. Johnsen (1977) showed that diffusion affects the isotopic signal regardless of the accumulation rate and temperature. With a typical diffusion length of 7-8 cm the $\delta^{18}O$ cycles in ice having a wavelength of less than 20 cm are obliterated. The smoothing effect is less strong for δD due to the lower diffusivity difference between the $H_2^{16}O$ and $HD^{16}O$ molecules compared to $H_2^{16}O$ and $H_2^{18}O$, resulting in δD records less affected by this phenomenon (Johnsen et al., 2000). In any case smoothing effect stops when the critical density of 0.55 g/cm^3 is reached (Dansgaard et al., 1973).

In case of polythermal glaciers surface melting can occur. Meltwater can percolate down into the snowpack, where it refreezes. It was shown that due to the very low diffusivity of water in compact ice (10^{-11} cm^2/s, Jouzel and Souchez, 1982) no fractionation occurs during melting. This does not apply if water percolates through porous snow or firn. In that case an initial enrichment in the snowpack and depletion in the meltwater can be observed. As the meltwater progresses it becomes more and more enriched toward the initial snowpack values (Stichler et al., 1981). Refreezing is to be also accompanied by fractionation (Jouzel and Souchez, 1982).

Sublimation would cause enrichment in the snowpack but this effect is usually counterbalanced by condensation of vapor on the surface. Even in extreme dry conditions this effect does not penetrate the snow cover more than 5-10 cm (Moser and Stichler, 1975; Stichler and Schotterer, 2000; Stichler et al., 2001).

Rain might alter the isotopic composition in the snow pack as well (Stichler and Schotterer, 2000), but this is unlikely to occur on the Alpine glaciers considered in this study.

Besides fractionation processes mentioned beforehand, wind erosion at highly exposed sites may considerably bias the isotopic record on annual scale, preserving only part of the total accumulated snow (Schotterer et al., 2004). This was observed at Colle Gnifetti saddle, a wind-exposed, high-altitude glacier saddle, where winter snow is eroded. The $\delta^{18}O$ signal is clearly biased toward summer values compared to the typical Alpine range (Schotterer et al., 1985; Schöner et al., 2002; Sigl, 2009 and section 2.4).

2.2 Precipitation reconstruction

Accumulation reconstruction from ice cores provides an estimation of the past annual precipitation rates and is therefore a useful proxy for the investigation of the hydrological cycle. However, one should consider that the reconstructed surface accumulation rate at the glacier reflects precipitation only to a certain extent, because of local post-depositional effects that may alter/destroy the signal throughout the year. The surface accumulation rate corresponds to the net amount of snow accumulated at the glacier surface within a year. The term "net" indicates that this value is the amount of snow actually preserved and not removed (Cuffey and Paterson, 2010). In order to account for density variations, this parameter is usually expressed in meter water equivalent (m w.e.), which is obtained by multiplying the net surface accumulation in m with the measured density. The density varies from 200-300 kg/m^3 for fresh snow to 400-830 kg/m^3 for firn. The firn-ice transition is defined as the depth where the density becomes 830 kg/m^3 (Cuffey and Paterson, 2010). Annual layers can be identified using parameters with seasonal variability, i.e. identifying the layer thickness from a minimum to the next minimum. This technique, called annual layer counting, is used for dating ice cores (e.g. Schwikowski et al., 1999; Eichler et al., 2000). Every annual layer is buried by new snow and is subjected to iceflow-induced thinning due to the pressure of the above snow column. The layer thickness decreases with depth, not corresponding to the actual net surface accumulation. Several models have been developed in order to correct for this thinning. A simple model assuming constant thinning with depth was presented by Nye (1963) which is usually suitable for the upper two third of the glacier thickness, where interactions with the bedrock are negligible. Focusing on the bottom part of the glacier, Dansgaard and Johnsen (1969) defined a two-layer model where the thinning rate is constant from the surface down to a certain depth and then it decreases linearly to zero at the bottom in order to satisfy the physical boundary condition of ice cap frozen to the bedrock. Thompson et al. (1990) proposed another flow model to account for larger thinning at the near ice divide zone of high-alpine glaciers.

For the final reconstructed surface accumulation it is necessary to account for the mean surface accumulation and the measured layer thickness corrected for thinning. The approach used here was the one adopted by Henderson et al. (2006), where the reconstructed accumulation λ_R is given by the following formula:

$\lambda_R = (\lambda_E/\lambda_M)\lambda_0$

Where λ_E corresponds to the measured annual thickness, λ_M to the annual thickness estimated from an ice flow model and λ_0 to the estimated surface accumulation rate. The latter one is

obtained by averaging the upper layer thicknesses for which thinning can be neglected. One should thus take into account that these reconstructions usually assume stationary conditions in terms of surface accumulation rate, an assumption that may not be valid over long timescales, when significant changes of the precipitation regimes may occur.

2.3 Climate of the Alpine region

The European Alps are in a climatological perspective one of the most challenging regions, due to the complex interaction between the topography and the large-scale processes. The Alps are located in central Europe, in a region extending over 800 km across five countries (France, Switzerland, Italy, Austria and Slovenia, 5°E to 17°E and 44°N to 49°N, Figure 6) with a width ranging from 100 to 250 km. Their orientation roughly follows an arc extending from Southwest to Northeast. The mean altitude is 2500 m, with the Mont Blanc (4810 m a.s.l., at the border between Italy and France) being the highest summit.
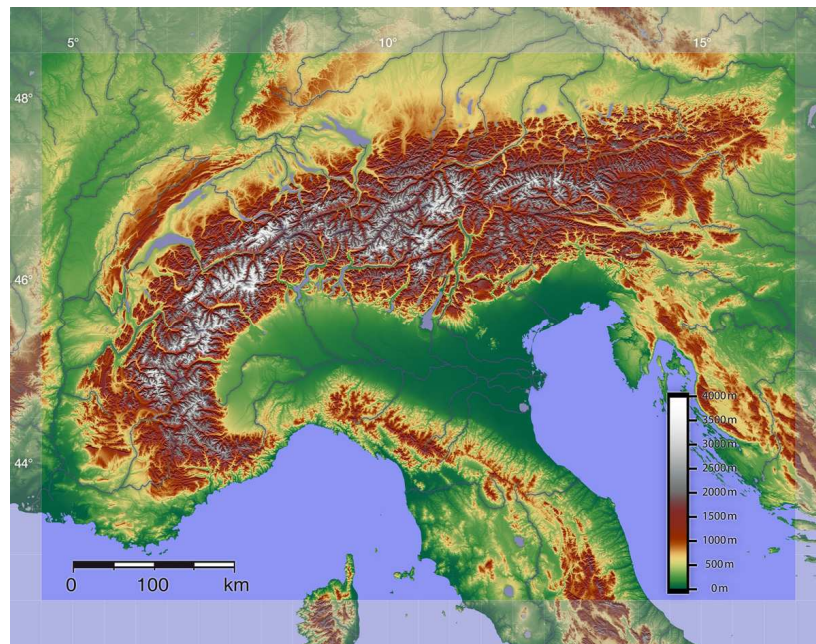

Figure 6 Topographic map of the European Alpine region
(Source: http://en.wikipedia.org/wiki/File:Alpenrelief_01.jpg).

Due to the geographical location in the midlatitudes, the west-east orientation and the altitude the Alps constitute an orographic barrier. Thus, they do not only interact with the incoming air flow with e.g. orographic-induced precipitation, but divide de facto the region in different climatic zones. With respect to Switzerland the region north of the Alps presents continental climate whereas the Southern Alps are more affected by the Mediterranean (Wanner et al., 1997; Beniston, 2006; Barry, 2008).

Therefore the region is heterogeneous in the spatial distribution of precipitation (Figure 7). The northern rim extending over more than 600 km and distinct zones in the southern rim, i.e. Ticino, north-eastern Italy and Slovenia experience higher precipitation with locally more than 2000 mm/year (Frei and Schär, 1998). The northern and the southern wet anomaly in

Switzerland are connected through the St. Gotthard pass. In contrast, drier inner-Alpine areas such as the Valais and Southeastern Switzerland receive typically ~600-700 mm/year (Frei and Schär, 1998). Moreover, precipitation amounts generally increase with altitude.
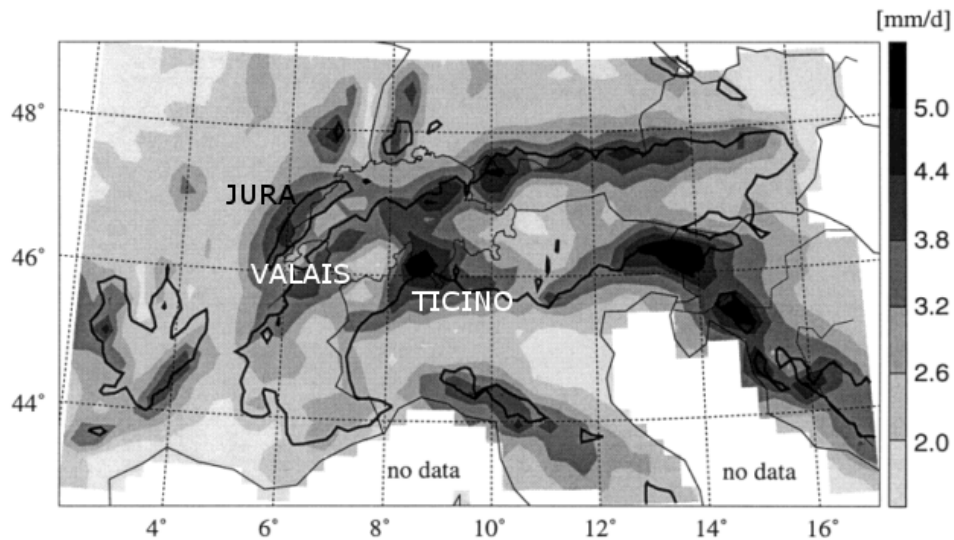

Figure 7 Climatology of the mean annual precipitation in mm/day over the Alps for the period 1971-1990, adapted from Frei and Schär (1998).

2.3.1 Intraseasonal precipitation variability

Focusing now on the Swiss Alpine area a north-south gradient of precipitation exists with the Northern part receiving less precipitation throughout the year relative to the Southern part (~25%, according to Sodemann and Zubler, 2009). Considering two stations indicative for the Northern (Interlaken) and the Southern (Mosogno) Alps (Figure 8), the seasonal distribution of precipitation reveals that the two regions are affected by different regimes, with the Northern Alps generally receiving the maximum of precipitation in summer and the Southern Alps having a bimodal distribution peaking in spring and late summer-fall (Frei and Schär, 1998; Eichler et al., 2004; Barry, 2008; Sodemann and Zubler, 2009). The intraseasonal precipitation variability over the Northern Alps is lower than in the Southern Alps (Figure 8).
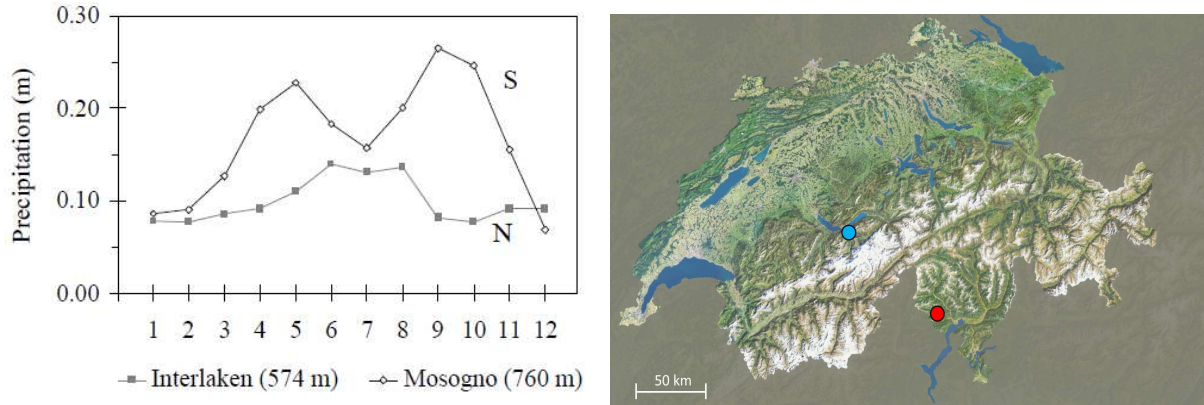
Figure 8 (Left) Climatology of monthly precipitation for the period 1961-1994 for Interlaken, located in the Northern Alps (N) and Mosogno, in the Southern Alps (S) (Eichler et al., 2004). (Right) Locations of the two stations in Switzerland (Interlaken in blue, Mosogno in red).

The moisture sources for precipitation over the Alps are multiple and show quite a high intraseasonal variability. In a climatological study using a Lagrangian diagnostic and reanalysis data Sodemann and Zubler (2009) observed and quantified the different contributions to precipitation over the Alps over the period 1995-2002. The Northern Alps receive in general more moisture from the Northern Atlantic than the Southern Alps, which conversely are more affected by the Mediterranean, confirming the presence of an orographic barrier. In general precipitation over the Northern Alps is dominated by long-range transport from the North Atlantic especially in winter and spring, when precipitation is due to the extratropical cyclones developing over the North Atlantic sector and moving eastward along the storm track. In summer the main moisture source is local land evaporation and precipitation, mainly convective, is due to local instabilities. The Southern Alps show less strong contribution from the North Atlantic in winter and spring, similar local land evaporation contribution in summer and a peak in the Mediterranean moisture source in fall. In general the intermediate seasons show a transition between long range transport and summer local moisture sources (Figure 9).
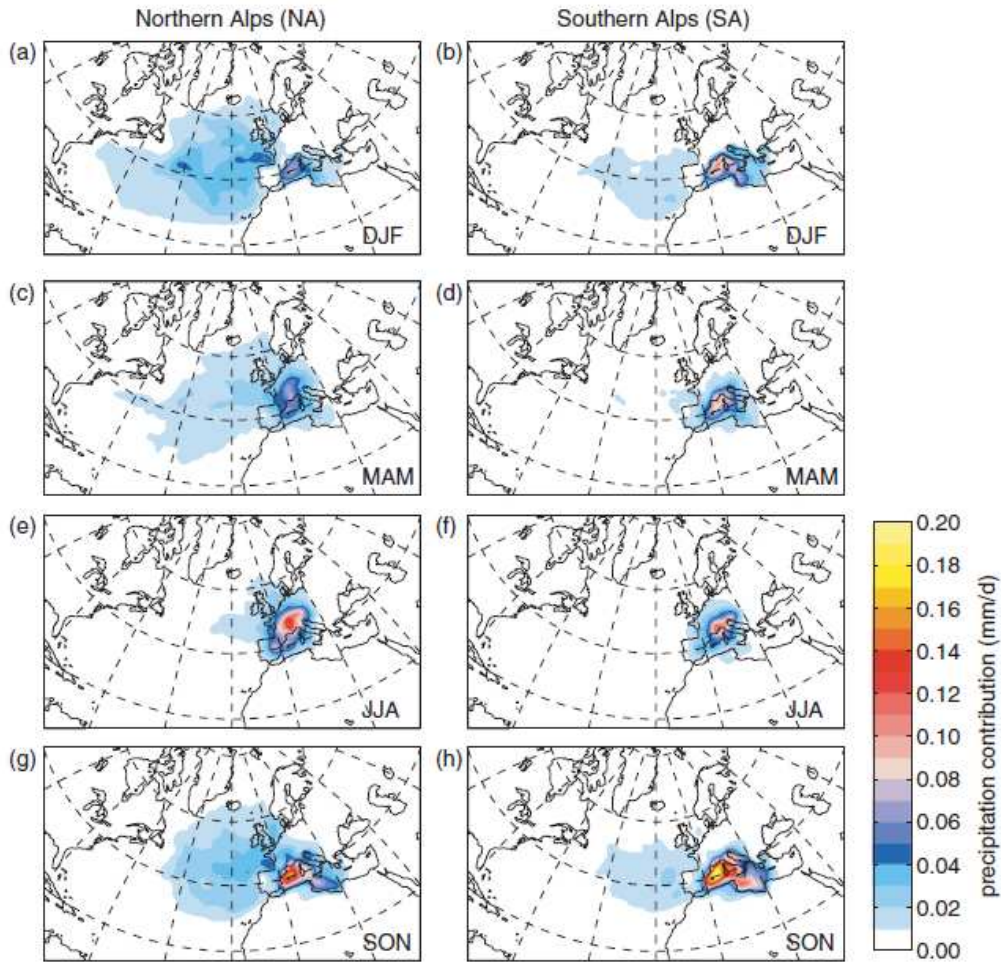
Figure 9 Seasonal mean moisture sources for the Northern Alps and Southern Alps, left and right column, respectively. DJF: winter; MAM: spring; JJA: summer: SON: fall. The shading indicates the contribution of the evaporation to the diagnosed Alpine precipitation in mm/day integrated over 10^4 km^2 (Sodemann and Zubler, 2009).

2.3.2 Interannual variability: the North Atlantic Oscillation

Precipitation over the Alps shows also high variability on longer timescales, from annual to multidecadal (Wanner et al., 1997; Schmidli et al., 2002). On interannual timescales the main teleconnection pattern affecting the European region is the North Atlantic Oscillation (NAO, Hurrell, 1995). The NAO is primarily manifested through an oscillation of winter pressure differences between the Azores high and the Icelandic low (Figure 10). When the normalized sea level pressure between the two centers increases (NAO+), the westerlies strengthen and carry moisture and heat across the North Atlantic inducing precipitation in Scandinavia whereas Southern Europe experiences colder and drier conditions. During the opposite phase the pressure gradient between the Icelandic low and the Azores high is reduced (NAO-), the westerlies weaken and the moisture transport is shifted southward, generating more

precipitation and higher temperature anomalies over Southern Europe and the Mediterranean region. Northern Europe receives less precipitation and the temperatures are below average.
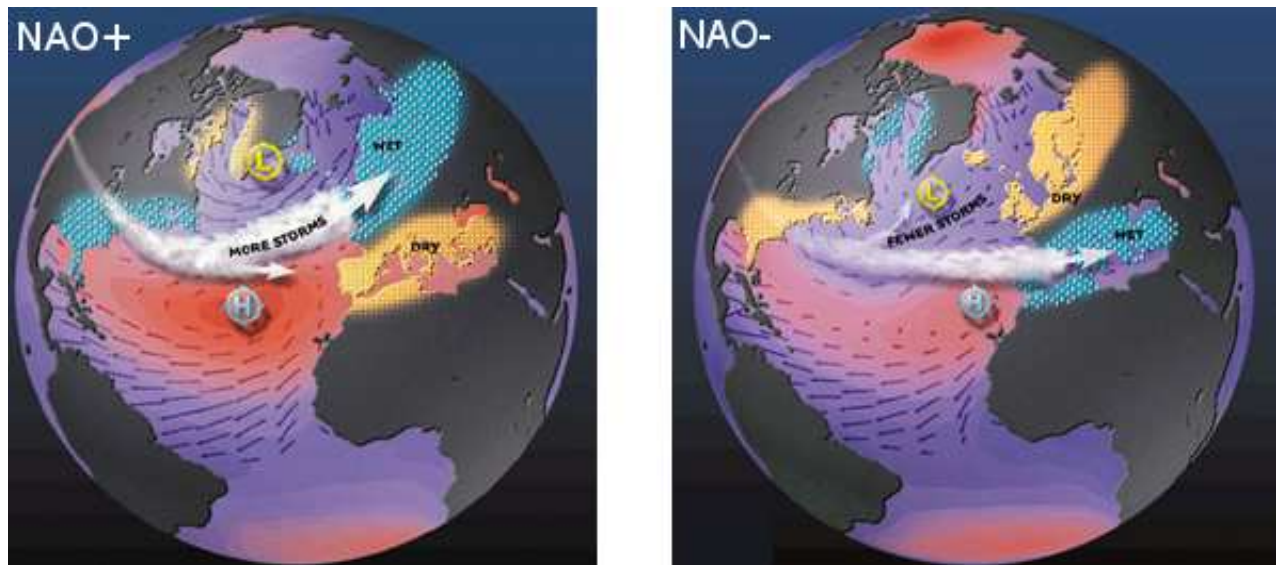

Figure 10 North Atlantic Oscillation main features. (Left) Positive NAO. (Right) Negative NAO. The Azores high and the Icelandic low are indicated by H and L, respectively. The white arrow shows the direction and intensity of the storm track, dry and wet zones are shaded in yellow and light blue, respectively. Sea surface temperature warm and cold anomalies are shown in red and blue, respectively, together with the arrows indicating the surface winds directions and intensities. Adapted from http://www.ldeo.columbia.edu/NAO by Martin Visbeck.

The strength of the NAO is usually expressed with the NAO index. Historically it was conceived as the difference in normalized sea level pressure between two representative locations of the Azores high and the Icelandic low, respectively. For example, the index presented by Hurrell (1995) uses the data from Lisbon, Portugal and Stykkisholmur/Reykjavik, Iceland and reaches back 1864 (Hurrell and National Center for Atmospheric Research Staff (Eds), 2013a). Due to the year-to-year variability of the pressure centers new indexes were created based on Empirical Orthogonal Function analysis (leading EOF of sea level pressure or 500 hPa geopotential heights anomalies over the Atlantic sector, Figure 11), (e.g. Hurrell and National Center for Atmospheric Research Staff (Eds), 2013b).
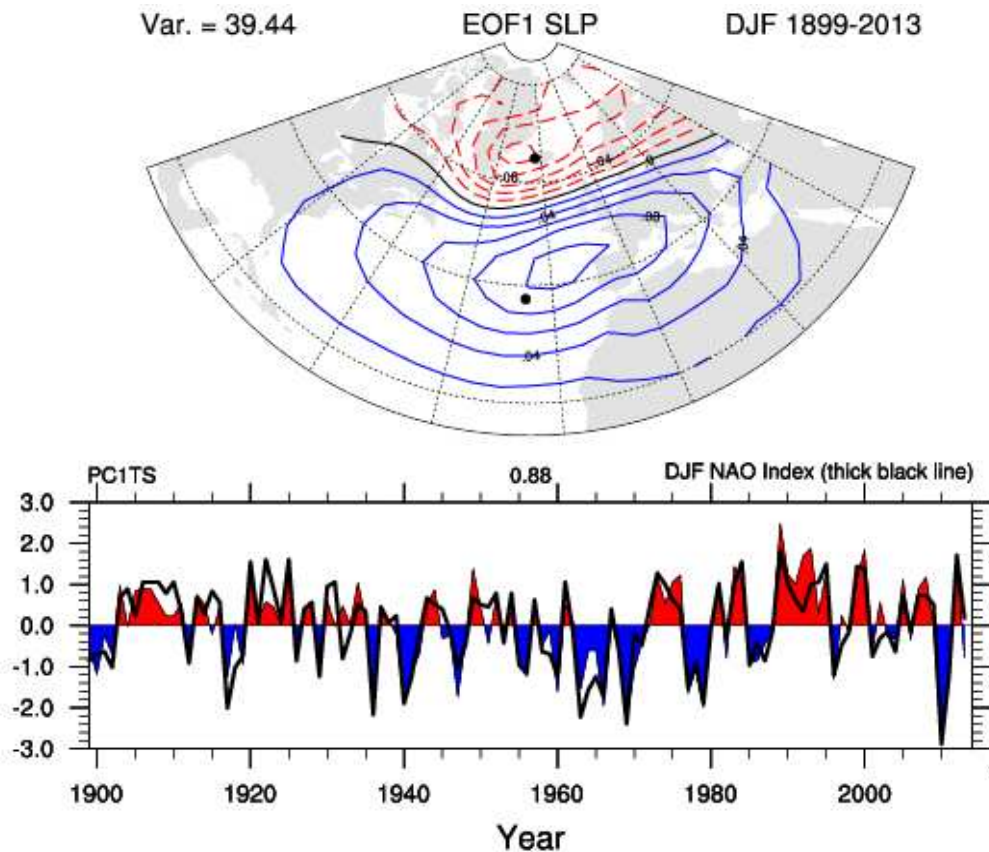
Figure 11 (Above) Leading EOF of the winter (December to February) sea level pressure anomalies over the North Atlantic region (20N-80N, 90W-40E) used to define the principal component (PC)-based NAO index, together with the location of the two sites used to calculate the normalized pressure differences for the station based-index (black dots). (Below) Time series of the station based index (thick line) together with the PC based- index (shaded) (Hurrell and National Center for Atmospheric Research Staff (Eds), 2013b).

Several reconstructions of the NAO index are now available from literature and extend back to the last centuries: e.g. Cook et al. (1998); Glueck and Stockton (2001); Luterbacher et al. (2001); Trouet et al. (2009). For a critical review regarding the different reconstructions, see e.g. Schmutz et al. (2000). The main influence of the North Atlantic Oscillation occurs during winter, whereas during summer the position of the two pressure centers tends to shift northward. Summer NAO was observed to affect Northwestern Europe (Folland et al., 2009). The NAO was thought to be the regional expression of a hemispheric mode of variability, the Arctic Oscillation (or Northern Annular Mode, Thompson and Wallace, 1998; Marshall et al., 2001). There is no clear evidence for a preferred timescale in the NAO variability (Hurrell and Deser, 2009).

Whether and how the NAO influences the Alpine climate is currently highly debated. Studies suggest that the NAO affects the Alpine precipitation through the Ryd-Scherhag divergence

theory, with positive phases inducing a high pressure over the Alps (Wanner et al., 1997; Beniston and Jungo, 2002). According to that, during positive NAO the jet-axis, determined by the relative position of the Azores high and the Icelandic low, is directed from south-west to north-east and the Alps are located southeast of its exit zone, corresponding to the divergence zone. In that case an ageostrophic component would be generated and cross-isobar mass transport would take place with consequent increase of the surface pressure over the region. Warmer temperatures and less precipitation would occur. In the opposite case, the pressure gradient between the Azores high and the Icelandic low would weaken, reducing the westerlies strength with consequent shift of the storm track southward and development of higher precipitation amounts and lower temperatures over the region (Figure 12). This explanation seems to be in agreement with the higher frequencies of anticyclonic weather situations occurring in winter over the Alps during the periods of higher NAO index (Wanner et al., 1997; Stefanicki et al., 1998). For higher Alpine sites (1500-2000 m) Beniston (1997) explained the anticorrelation between snow accumulation and the high pressure induced by the NAO in terms of reduced snowfall combined with early melting in spring due to reduced snowpack. On the other hand, above those altitudes Alpine sites should not be significantly affected, because even high-pressure situations unlikely would initiate melting. Intermittent or no significant relationships between the winter NAO and precipitation over the Alps were found in other studies, where only the Southern Alps resulted to be anticorrelated with the NAO (Schmidli et al., 2002; Casty et al., 2005; Bartolini et al., 2009).
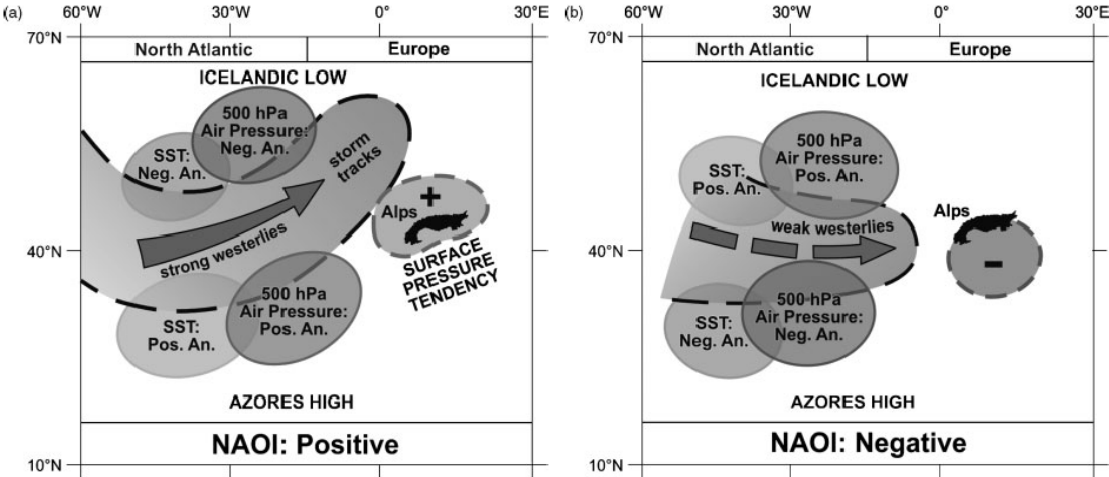

Figure 12 Schematics of the sea surface temperatures (SST) and geopotential height at 500 hPa anomalies, together with the position and strength of the storm track and the pressure tendency over the Alps during a positive (a) and negative (b) NAO. Adapted from Casty et al. (2005).

2.3.3 Climate change in the Alps in the last two centuries

The climate variability over the Alps has been extensively investigated on different timescales. With focus on the last two centuries the ALPCLIM (Böhm et al., 2001) and HISTALP (Auer et al., 2007) projects developed gridded datasets of temperature and precipitation over the Alpine region, providing detailed information. Böhm et al., (2001) noticed a general increase of temperature of 1.1 °C since 1890. Accordingly, Auer et al., (2007) quantified the temperature increase since 1900 to 1.0-1.4 °C depending on the region. This estimated change is almost double of the global temperature change (IPCC, 2007), indicating the high sensitivity of the Alpine region to global warming. A change in the seasonal distribution of precipitation was noticed, with a strong increase in fall precipitation for the period 1975-2000 (23-35% depending on the region) and correspondingly drier winters (-44%).

Although the snow height parameters in the Alps are affected by relatively high interannual to decadal variability (Laternser and Schneebeli, 2003; Scherrer et al., 2013), a decrease of the Alpine snow pack was observed since the mid-1980s especially at stations lower than 1300 m a.s.l. This change was attributed to an increase in local temperature (Scherrer et al., 2004). Analyzing the long-term (1915-2007) mass balance from different glaciers in the Swiss Alps, Huss and Bauder (2009) noted melt rate increase of 10% per decade since 1975. Also the snowfall frequency has changed dramatically. Serquet et al. (2011) observed a significant decrease in snowfall days relative to precipitation days over the periods 1961-2008 and 1979-2008, at stations with temperatures close to the melting point (i.e. lower altitudes). This especially applies to the spring season. The investigation of different snow parameters (mean snow depth, duration of continuous snow cover and number of snowfall days) showed that the 1990s were the least snowy decade since the 1930s (Laternser and Schneebeli, 2003). Beniston (1997) attributed the decrease in the snow amount to the presence of persistent high pressure fields over the Alps in late fall and winter, caused by positive NAO phases.

Over multidecadal timescales a link between the Swiss glaciers mass balances and the Atlantic Multidecadal Oscillation (AMO) was found by Huss et al. (2010). The AMO is an oscillation of the sea surface temperatures over the North Atlantic, with periodicity of 65-70 years (Schlesinger and Ramankutty, 1994) and amplitude ~0.4 °C (Enfield et al., 2001). The strength of the AMO is measured through the AMO index, basically the average sea surface temperature over the North Atlantic detrended for the recent anthropogenic warming (Trenberth and Shea, 2006; van Oldenborgh et al., 2009). When the AMO is in its positive phase sea surface temperatures over the North Atlantic show positive anomalies. Huss et al.

(2010) found an anticorrelation between the AMO and the extent of the Swiss glaciers over the last 250 years, with a lag between the oceanic forcing and the glaciers response of few decades and negative mass balance since 1985.

2.3.4 Water stable isotope research in the Alpine area

The Alpine region has a long tradition of measurements and analysis of water stable isotopes. For Switzerland $\delta^{18}O$ was analyzed in terms of spatial coherence (Rozanski et al., 1992; Schürch et al., 2003), altitudinal changes (Siegenthaler and Oeschger, 1980; Schotterer et al., 1997; Schürch et al., 2003) and isotopic/temperature calibration, from both, GNIP station (Rozanski et al., 1992; IAEA/WMO, 2013) and ice cores data (Schotterer et al., 1997; Eichler et al., 2001).

The investigation of the altitude effect confirmed that a linear $\delta^{18}O$ decrease of -0.2‰/100 m occurs with altitude (Siegenthaler and Oeschger, 1980; Schürch et al., 2003), but also highlighted that over such limited region the lower altitude stations located approximately 50 km northwest (Bern) and southeast (Locarno) from the Alpine arc deviate from these trend, indicating different precipitation regimes and rainout processes (Schürch et al., 2003).

Some evidences of a north-south isotopic gradient were found (Schotterer et al., 2001). The more enriched isotopic values at the southern sites were explained with the generally higher local temperatures and the influence of the Mediterranean Sea (Schürch et al., 2003).

The analysis of the $\delta^{18}O$/temperature relationship revealed higher isotope sensitivity over the Swiss Alpine area, with a higher long-term slope of (0.93±0.07)‰/°C compared to the value (0.63±0.04)‰/°C for the European region (Rozanski et al., 1992).

The deuterium excess was extensively studied in the Austrian Alps. Results show that differences arise depending on the altitude and location with respect to the mountain range, with valley stations having a minimum in summer and the higher elevation sites a maximum between June and October (Rank and Papesch, 2005; Liebminger et al., 2006). The authors explained this difference with the fact that the deuterium excess in precipitation tends to decrease due to sub-cloud evaporation processes, and the extent of this decrease depends on the cloud-earth distance (Kaiser et al., 2001; Fröhlich et al., 2008). A similar seasonality with lower deuterium excess in summer was observed at the low altitude Locarno station in Switzerland (Schotterer et al., 1993). Moreover, they found that the Bergeron-Findeisen process is particularly strong in late summer-fall. Additional kinetic fractionation induces the beforehand-described seasonality (Liebminger et al., 2006). The influence of the atmospheric circulation on the isotopic composition in meteoric water was investigated using European

winter precipitation data (Baldini et al., 2008). Significant positive correlation between the NAO and δ^{18}O in precipitation in central Europe was found. This was explained by enhanced warm westerlies that carry isotopically enriched moisture from the North Atlantic and the Mediterranean, whereas in negative phases cold air coming from Eastern Europe would lead to more depleted values. Accordingly, Field (2010) observed a correlation pattern of observed and modeled δ^{18}O in precipitation with the sea level pressure coherent with the NAO, although shifted eastward. A similar pattern was obtained with the 500 hPa height and interpreted as a possible link with Arctic Oscillation or the Northern Annular mode (Thompson and Wallace, 1998). Recently it was also shown that over central Europe the precipitation intermittency (i.e. the bias introduced from the difference between the seasonal mean temperature and precipitation-weighted temperature) does not alter the main correlation pattern of the winter NAO with winter central European temperature or δ^{18}O (Casado et al., 2013). This confirmed the validity of isotopic signal as proxy for NAO reconstructions. The influence of atmospheric circulation pattern on the isotopic signal was also detected in tree-rings, showing that summer δ^{18}O signal over the Alpine region is positively correlated with a high pressure over central Europe (Saurer et al., 2012).

2.4 Alpine ice cores investigated in this study

The ice cores used in this study come from two glaciers in the Swiss Alps (Figure 13 and 14), the Fiescherhorn glacier (Northern Alps), and the Grenzgletscher (Southern Alps).
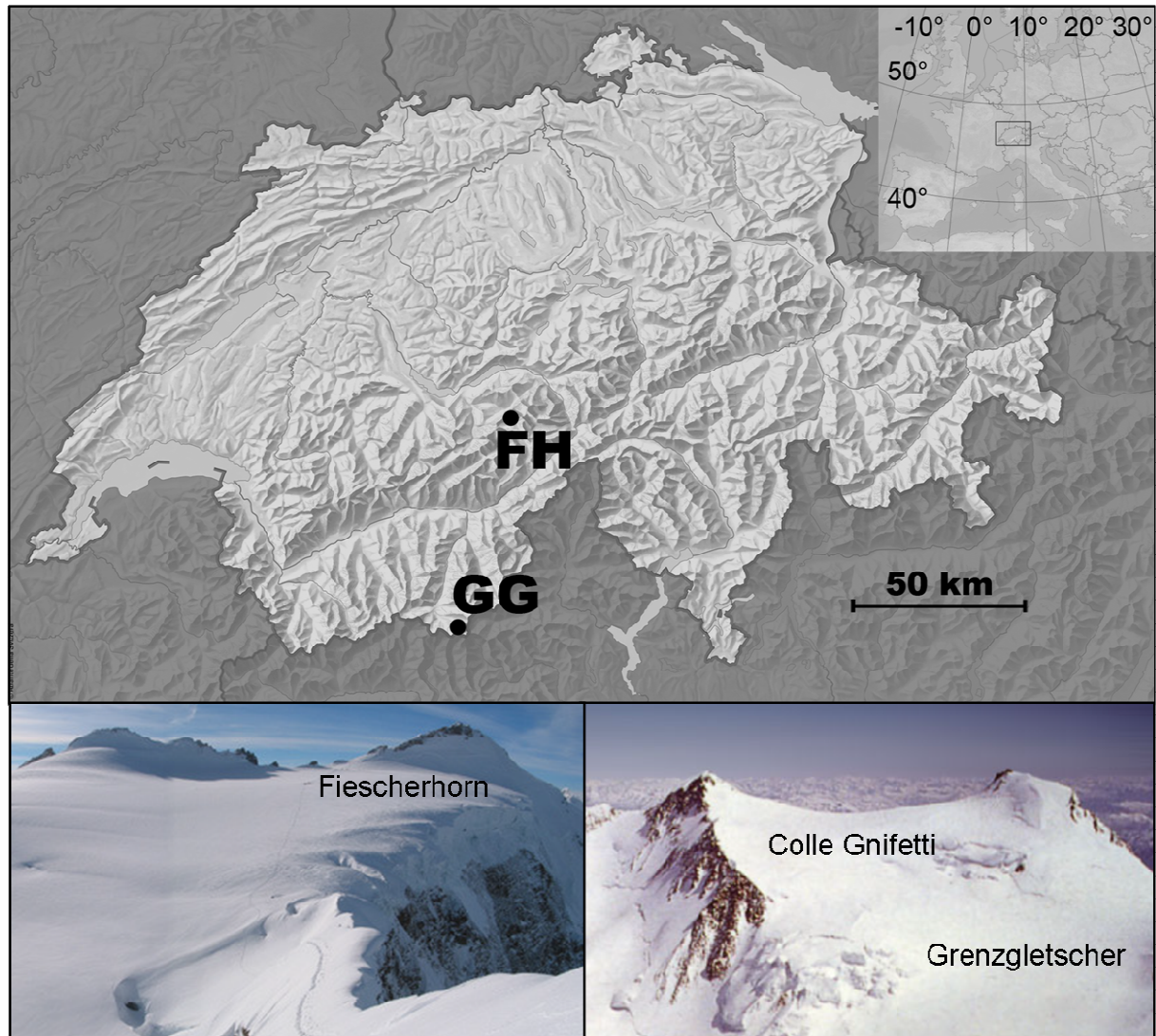

Figure 13 (Upper panel) Location of the two glaciers in Switzerland. The insert gives the location of Switzerland in Europe. (Lower panels) Fiescherhorn glacier (left, photo by Aurel Schwerzmann), Colle Gnifetti and Grenzgletscher drilling sites (right, photo by Kai Hassler).
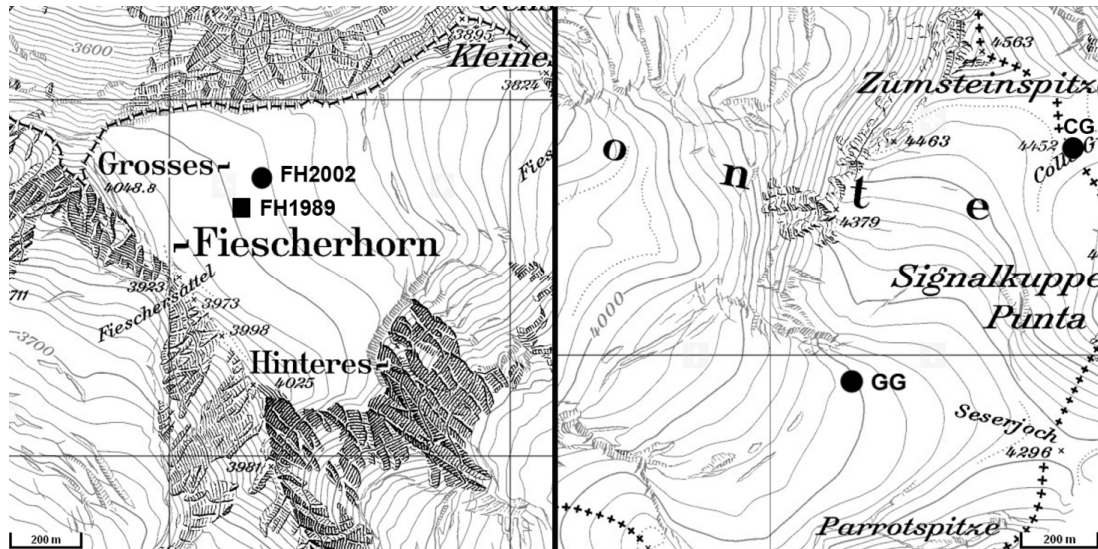
Figure 14 Topographic maps of the glaciers and drilling sites. (Left panel) Fiescherhorn, where FH1989 and FH2002 indicate the two different drilling sites only 100 m distant (Jenk, 2006; Schwikowski et al., 1999). (Right panel) Grenzgletscher (GG) and Colle Gnifetti (CG). Source: Atlas of Switzerland, http://www.atlasderschweiz.ch/).

The Fiescherhorn glacier (FH) is located in the Northern Alps (46º33'3.2" N, 8º04'0.4" E), at an altitude of 3900 m a.s.l. and has an extended relatively flat accumulation area with a steep cliff to the North (Figure 14). Two ice cores were drilled on this glacier (Schwikowski et al., 1999; Jenk et al., 2006; Schotterer et al., 1997, 2004). Here the main investigations were conducted on the core extracted in December 2002, reaching bedrock at a depth of 151 m. In Chapter 4 the results from another ice core, drilled in 1989 and only 100 m distant are used to assess the reproducibility of the records (46°33'6.28" N, 8°04'4.02" E, 3900 m a.s.l., Schotterer et al., 1997; Schwikowski et al., 1999). Borehole temperatures indicate that this is a cold glacier, frozen to the bedrock (Jenk, 2006; Schwerzmann et al., 2006). The firn-ice transition occurs at a depth of ~50 m (Jenk, 2006). The Fiescherhorn FH2002 ice core covers the period ~1680-2002, with a dating uncertainty of ±2 years back to 1899 rising to ±5 years over the period 1818-1899. At the bottom the dating uncertainty is ±30 years (Jenk et al., 2006). Dating was performed with annual layer counting using the stable isotope record and wiggle matching with the FH1989 ice core by identification of stratigraphic markers. Details about the dating of the Fiescherhorn ice core are also described in Jenk (2006). The surface accumulation was estimated to be 1.7 m w.e./year (Jenk, 2006). The stable isotope record covers almost the whole period, except two gaps in the δD record over the periods ~1893-1895 and ~1935-1939 due to bad core quality and missing data. For δ¹⁸O the gaps cover the periods ~1890-1895, ~1897-1899 and ~1916-1939. The stable isotopes were

measured with Isotopic Ratio Mass Spectrometry (IRMS) after CO_2 equilibration for $\delta^{18}O$ or chromium reduction for the δD in the group of Climate and Environmental Physics at the University of Bern. The analytical uncertainty of $\delta^{18}O$ and δD was <0.05‰ and <0.5‰, respectively (Jenk, 2006 and Chapter 3). Melt features were observed, with low to moderate relocation of ions toward lower depths (Jenk, 2006). Nevertheless, the stable isotope record was not significantly affected as shown by Schotterer et al. (1997) and Schwikowski et al. (1999). Past accumulation rate reconstructions were attempted by Jenk (2006) for the whole record, revealing questionable results before 1800 due to dating uncertainty and resolution loss. In Schwerzmann et al. (2006) a novel technique measuring the vertical velocity of firn in the borehole was used and compared to a reconstruction based on a simple Nye model (Nye, 1963), for the period 1940-2002. In this study, after completing analyses of the stable isotopes and concentrations of major ions, the dating was partially revised and the accumulation reconstruction covering the uppermost 60 m w.e. (back to 1950) is presented in Chapter 4.

The ice core from Grenzgletscher (GG) located in the Monte Rosa massif, Southern Alps (45º55'28" N, 7º52'3" E), was drilled in October 1994, reaching the depth of 125 m (Eichler et al., 2000, 2001). The estimated glacier thickness at the drilling site deducted from radar survey is 190 m (Eichler et al., 2000). The drilling site is located at an altitude of 4200 m a.s.l. in the accumulation area southwest and downstream of the Colle Gnifetti saddle (Figure 14). This ice core presents melt features and the borehole temperatures indicate partly temperate ice (Eichler et al., 2001). The firn-ice transition is located at ~20 m w.e. depth (Eichler et al., 2001). The record covers the period ~1937-1994, with a dating uncertainty <1 year over the period 1970-1994 and ±2 years over 1937-1969 (Eichler et al., 2000). The surface accumulation at the Grenzgletscher is high, 2.7 m w.e./year (Eichler et al., 2000). For this reason the $\delta^{18}O$ record was obtained measuring the values every other sample resulting in the upper layers in sample numbers up to 90 samples/year. A small gap is present over the period ~1968-1970, due to bad core quality and a failure in the cooling system of the cold room with consequent melting of the corresponding ice core sections (Eichler et al., 2000). The δD was measured only over a short period, ~1977-1983. The $\delta^{18}O$ was measured with IRMS after CO_2 equilibration and the δD after chromium reduction at the Paul Scherrer Institut. The analytical uncertainties of the measurements are 0.1‰ for $\delta^{18}O$ and 1‰ for δD (Eichler et al., 2000, 2001 and Chapter 3). A second sampling of the Grenzgletscher ice core covering the period 1961-1983 was recently performed in order to extend back in time the record of the deuterium excess, measured with a Wavelength-Scanned Cavity Ring-Down Spectrometer (Chapter 3). The analytical uncertainty on the measurement was 0.1‰ and 0.5‰ for the $\delta^{18}O$

and δD, respectively. Melt features observed in the Grenzgletscher ice core over the period 1985-1989 did not significantly alter the stable isotope signal (Eichler et al., 2001).

The Colle Gnifetti ice core is only one of the several cores drilled at this site (e.g. Wagenbach et al., 1988; Sigl, 2009; Bohleber et al., 2013). Colle Gnifetti is a saddle located just 300 m upstream of the Grenzgletscher drilling site, in the Monte Rosa massif. The drilling site is located at an altitude of 4450 m a.s.l. (45°55'50.41''N, 07°52°33.50''E) where the glacier is cold, as borehole temperatures ranged between -12 and -14°C (Haeberli and Funk, 1991). The firn-ice transition occurs at about 40 m (Sigl, 2009). Colle Gnifetti, one of the highest glacier saddles in the Alps, is orientated in a west-east direction, parallel to the main wind direction (westerlies). In winter, when the wind speeds are high, preferential snow erosion occurs due to the fact that the snow is cold and not sticky. Due to the partial loss of the annual signal, accumulation rates at this site are particularly low (0.33 m w.e., Sigl, 2009), rendering the Colle Gnifetti records exceptionally extended back in time for an Alpine ice core. Using a novel dating technique based on the radiocarbon content of carbonaceous particles, Jenk et al. (2009) showed that Colle Gnifetti core covers the entire Holocene with evidences of Pleistocene ice at the bottom. The accumulation rates exhibit a strong spatial variability over the saddle, due to varying wind exposure conditions (Schöner et al., 2002; Sigl, 2009; Bohleber et al., 2013). The record discussed here is called "CG03" from an ice core drilled in September 2003 and reaching bedrock at a depth of 81.9 m, with an update in 2008 through the drilling of a 10.5 m firn core (Sigl, 2009). The stable isotopes ($\delta^{18}O$ and δD) were measured along the whole ice core with IRMS after pyrolysis reaction (analytical uncertainties 0.1‰ and 0.5‰ for $\delta^{18}O$ and δD, respectively, Sigl, 2009). The Colle Gnifetti ice core did not contain significant melt features (Sigl, 2009).

A qualitative comparison of the $\delta^{18}O$ signal from these three Alpine ice cores is shown in Figure 15, to make the reader immediately familiar with the type of record he/she will be confronted to. Two main features are notable: the quite good seasonality found in Fiescherhorn and Grenzgletscher, with maxima/minima corresponding to summer/winter and the relative strong smoothing of the signal for the Colle Gnifetti record, with notable bias toward summer values.
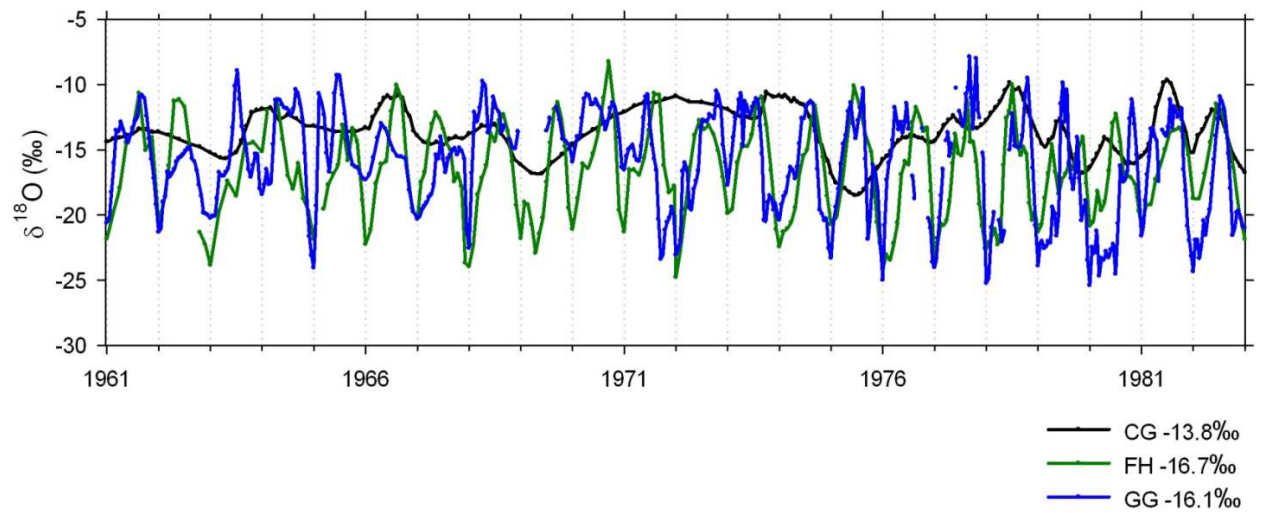
Figure 15 Raw $\delta^{18}O$ data from the three Alpine ice cores Colle Gnifetti (CG, black), Fiescherhorn (FH, green) and Grenzgletscher (GG, blue) over the common period 1961-1983, together with their mean values.

References

Aemisegger, F., Sturm, P., Graf, P., Sodemann, H., Pfahl, S., Knohl, A. and Wernli, H.: Measuring variations of $\delta^{18}O$ and δ^2H in atmospheric water vapour using two commercial laser-based spectrometers: an instrument characterisation study, Atmospheric Meas. Tech., 5(7), 1491–1511, doi:10.5194/amt-5-1491-2012, 2012.

Araguás-Araguás, L., Fröhlich, K. and Rozanski, K.: Deuterium and oxygen-18 isotope composition of precipitation and atmospheric moisture, Hydrol. Process., 14(8), 1341–1355, doi:10.1002/1099-1085(20000615)14:8<1341::AID-HYP983>3.0.CO;2-Z, 2000.

Auer, I., Böhm, R., Jurkovic, A., Lipa, W., Orlik, A., Potzmann, R., Schöner, W., Ungersböck, M., Matulla, C., Briffa, K., Jones, P., Efthymiadis, D., Brunetti, M., Nanni, T., Maugeri, M., Mercalli, L., Mestre, O., Moisselin, J.-M., Begert, M., Müller-Westermeier, G., Kveton, V., Bochnicek, O., Stastny, P., Lapin, M., Szalai, S., Szentimrey, T., Cegnar, T., Dolinar, M., Gajic-Capka, M., Zaninovic, K., Majstorovic, Z. and Nieplova, E.: HISTALP — historical instrumental climatological surface time series of the Greater Alpine Region, Int. J. Clim., 27(1), 17–46, doi:10.1002/joc.1377, 2007.

Baertschi, P.: Absolute ^{18}O content of standard mean ocean water, Earth Planet. Sc. Lett., 31(3), 341–344, doi:10.1016/0012-821X(76)90115-1, 1976.

Baldini, L. M., McDermott, F., Foley, A. M. and Baldini, J. U. L.: Spatial variability in the European winter precipitation $\delta^{18}O$-NAO relationship: Implications for reconstructing NAO-mode climate variability in the Holocene, Geophys. Res. Lett., 35(4), doi:10.1029/2007GL032027, 2008.

Barry, R. G.: Mountain Weather and Climate, 3rd ed., Cambridge University Press., 2008.

Bartolini, E., Claps, P. and D'Odorico, P.: Interannual variability of winter precipitation in the European Alps: relations with the North Atlantic Oscillation., Hydrol. Earth Syst. Sci., 13, 17–25, 2009.

Beniston, M.: Variations of snow depth and duration in the Swiss Alps over the last 50 years: links to changes in large-scale climatic forcings, Clim. Change, 36(3-4), 281–300, doi:10.1023/A:1005310214361, 1997.

Beniston, M. and Jungo, P.: Shifts in the distributions of pressure, temperature and moisture and changes in the typical weather patterns in the Alpine region in response to the behavior of the North Atlantic Oscillation, Theor. Appl. Clim., 71(1-2), 29–42, doi:10.1007/s704-002-8206-7, 2002.

Beniston, M.: Mountain Weather and Climate: A general overview and a focus on climatic change in the Alps, Hydrobiologia, 562(1), 3–16, doi:10.1007/s10750-005-1802-0, 2006.

Bohleber, P., Wagenbach, D. and Schöner, W.: To what extent do water isotope records from low accumulation Alpine ice cores reproduce instrumental temperature series?, Tellus B, 65(0), doi:10.3402/tellusb.v65i0.20148, 2013.

Böhm, R., Auer, I., Brunetti, M., Maugeri, M., Nanni, T. and Schöner, W.: Regional temperature variability in the European Alps: 1760–1998 from homogenized instrumental time series, Int. J. Clim., 21(14), 1779–1801, doi:10.1002/joc.689, 2001.

Casado, M., Ortega, P., Masson-Delmotte, V., Risi, C., Swingedouw, D., Daux, V., Genty, D., Maignan, F., Solomina, O., Vinther, B., Viovy, N. and Yiou, P.: Impact of precipitation intermittency on NAO-temperature signals in proxy records, Clim. Past, 9(2), 871–886, doi:10.5194/cp-9-871-2013, 2013.

Casty, C., Wanner, H., Luterbacher, J., Esper, J. and Böhm, R.: Temperature and precipitation variability in the European Alps since 1500, Int. J. Clim., 25(14), 1855–1880, doi:10.1002/joc.1216, 2005.

Ciais, P. and Jouzel, J.: Deuterium and oxygen 18 in precipitation: Isotopic model, including mixed cloud processes, J. Geophys. Res., 99(D8), 16793–16,803, doi:10.1029/94JD00412, 1994.

Clark, I. D. and Fritz, P.: Environmental Isotopes in Hydrogeology, CRC Press/Lewis Publishers, New York, 1997.

Cook, E. R., D'Arrigo, R. D. and Briffa, K. R.: A reconstruction of the North Atlantic Oscillation using tree-ring chronologies from North America and Europe, The Holocene, 8(1), 9–17, doi:10.1191/095968398677793725, 1998.

Cooper, L.W.: Isotopic fractionation in snow cover, in Isotope tracers in catchment hydrology, Elsevier, Amsterdam, 1998.

Coplen, T. B., Herczeg, A. L. and Barnes, C.: Isotope engineering—Using stable isotopes of the water molecule to solve practical problems, in Environmental Tracers in Subsurface Hydrology, edited by P. G. Cook and A. L. Herczeg, pp. 79–110, Springer US., 2000.

Craig, H.: Isotopic variations in meteoric waters, Science, 133, 1702–1703, doi:10.1126/science.133.3465.1702, 1961.

Craig, H. and Gordon, L.: Deuterium and oxygen 18 variation in the ocean and marine atmosphere, in Stable Isotopes in Oceanographic Studies and Palaeotemperatures, pp. 9–130, E. Tongiorgi, Cons. Naz. delle Ric., Pisa, Italy, 1965.

Cuffey, K. and Paterson, W. S. B.: The Physics of Glaciers, Elsevier, USA, 2010.

Dansgaard, W.: Stable isotopes in precipitation, Tellus, 16(4), 436–468, 1964.

Dansgaard, W. and Johnsen, S. J.: A flow model and a time scale for the ice core from Camp Century, Greenland, J. Glaciol., 8, 215–223, 1969.

Dansgaard, W., Johnsen, S. J., Clausen, H. B. and Gundenstrup, N.: Stable isotope glaciology, CA Reitzel, 1973.

Dansgaard, W., Johnsen, S. J., Clausen, H. B., Dahl-Jensen, D., Gundestrup, N. S., Hammer, C. U., Hvidberg, C. S., Steffensen, J. P., Sveinbjornsdottir, A. E. and Jouzel, J.: Evidence for general instability of past climate from a 250-kyr ice-core record, Nature, 364, 218–220, doi:10.1038/364218a0, 1993.

Eichler, A., Schwikowski, M., Gäggeler, H. W., Furrer, V., Synal, H.-A., Beer, J., Saurer, M. and Funk, M.: Glaciochemical dating of an ice core from upper Grenzgletscher (4200 m a.s.l.), J. Glaciol., 46(154), 507–515, doi:10.3189/172756500781833098, 2000.

Eichler, A., Schwikowski, M. and Gäggeler, H. W.: Meltwater-induced relocation of chemical species in Alpine firn, Tellus B, 53(2), 192–203, doi:10.1034/j.1600-0889.2001.d01-15.x, 2001.

Eichler, A., Schwikowski, M., Furger, M., Schotterer, U., Gäggeler, H. W.: Sources and distribution of trace species in Alpine precipitation inferred from two 60-year ice core paleorecords, Atmos. Chem. Phys. Discuss., 4(1), 71–108, 2004.

Enfield, D. B., Mestas-Nuñez, A. M. and Trimble, P. J.: The Atlantic Multidecadal Oscillation and its relation to rainfall and river flows in the continental U.S., Geophys. Res. Lett., 28(10), 2077–2080, doi:10.1029/2000GL012745, 2001.

Field, R. D.: Observed and modeled controls on precipitation δ^{18}O over Europe: From local temperature to the Northern Annular Mode, J. Geophys. Res. Atmos., 115(D12), D12101, doi:10.1029/2009JD013370, 2010.

Field, R. D., Jones, D. B. A. and Brown, D. P.: Effects of postcondensation exchange on the isotopic composition of water in the atmosphere, J. Geophys. Res.-Atmos., 115(D24), D24305, doi:10.1029/2010JD014334, 2010.

Folland, C. K., Knight, J., Linderholm, H. W., Fereday, D., Ineson, S. and Hurrell, J. W.: The summer North Atlantic Oscillation: past, present, and future, J. Clim., 22(5), 1082–1103, doi:10.1175/2008JCLI2459.1, 2009.

Frei, C. and Schär, C.: A precipitation climatology of the Alps from high-resolution rain-gauge observations, Int. J. Clim., 18(8), 873–900, doi:10.1002/(SICI)1097-0088(19980630)18:8<873::AID-JOC255>3.0.CO;2-9, 1998.

Fricke, H. C. and O'Neil, J. R.: The correlation between ^{18}O/^{16}O ratios of meteoric water and surface temperature: its use in investigating terrestrial climate change over geologic time, Earth Planet. Sci. Lett., 170(3), 181–196, doi:10.1016/S0012-821X(99)00105-3, 1999.

Fröhlich, K., Kralik, M., Papesch, W., Rank, D., Scheifinger, H. and Stichler, W.: Deuterium excess in precipitation of Alpine regions – moisture recycling, Isot. Env. Healt. S., 44(1), 61–70, doi:10.1080/10256010801887208, 2008.

Gat, J. R. and Carmi, I.: Evolution of the isotopic composition of atmospheric waters in the Mediterranean Sea area, Journ. Geophys. Res., 75(15), 3039–3048, 1970.

Gat, J. R.: Oxygen and hydrogen isotopes in the hydrologic cycle, Annu. Rev. Earth Planet. Sci., 24, 225–262, doi:DOI: 10.1146/annurev.earth.24.1.225, 1996.

Gat, J. R., Mook, W. G. and Meijer, H. A. J.: Isotope Methodology, in Environmental isotopes in the hydrological cycle, vol. 2: Atmospheric water, 113 pp., Paris, 2001.

Glueck, M. F. and Stockton, C. W.: Reconstruction of the North Atlantic Oscillation, 1429–1983, Int. J. Clim., 21(12), 1453–1465, doi:10.1002/joc.684, 2001.

Gonfiantini, R.: Environmental isotopes in lake studies, in Handbook of environmental isotope geochemistry, V. 2: The Terrestrial Environment B, ed. Fritz P. and Fortes, J.C., 113–168, Elsevier Press, 1986.

Haeberli, W. and Funk, M.: Borehole temperatures at the Colle Gnifetti core-drilling site (Monte Rosa, Swiss Alps), J Glaciol, 37(125), 37–46, 1991.

Henderson, K., Laube, A., Gäggeler, H. W., Olivier, S., Papina, T. and Schwikowski, M.: Temporal variations of accumulation and temperature during the past two centuries from Belukha ice core, Siberian Altai, J. Geophys. Res., 111(D3), D03104, 2006.

Hoefs, J.: Stable Isotope Geochemistry, Springer, 2009.

Hurrell, J. W.: Decadal Trends in the North Atlantic Oscillation: Regional Temperatures and Precipitation, Science, 269(5224), 676–679, doi:10.1126/science.269.5224.676, 1995.

Hurrell, J. W. and Deser, C.: North Atlantic climate variability: The role of the North Atlantic Oscillation, J. Mar. Syst., 78(1), 28–41, doi:10.1016/j.jmarsys.2008.11.026, 2009.

Hurrell, J. and National Center for Atmospheric Research Staff (Eds): The Climate Data Guide: Hurrell North Atlantic Oscillation (NAO) Index (station-based), Available from: http://climatedataguide.ucar.edu/guidance/hurrell-north-atlantic-oscillation-nao-index-station-based, 2013a.

Hurrell, J. and National Center for Atmospheric Research Staff (Eds): The Climate Data Guide: Hurrell North Atlantic Oscillation (NAO) Index (PC-based), Available from: http://climatedataguide.ucar.edu/guidance/hurrell-north-atlantic-oscillation-nao-index-pc-based, 2013b.

Huss, M. and Bauder, A.: 20th-century climate change inferred from four long-term point observations of seasonal mass balance, Ann. Glaciol., 50(50), 207–214, doi:10.3189/172756409787769645, 2009.

Huss, M., Hock, R., Bauder, A. and Funk, M.: 100-year mass changes in the Swiss Alps linked to the Atlantic Multidecadal Oscillation, Geophys. Res. Lett., 37(10), L10501, doi:10.1029/2010GL042616, 2010.

IAEA/WMO: Global Network of Isotopes in Precipitation. The GNIP Database. Accessible at: http://www.iaea.org/water, 2013.

IPCC: Climate Change 2007: The Physical Science Basis. Contribution of Working Group I to the Fourth Assessment Report of the Intergovernmental Panel on Climate Change, Cambridge University Press, Cambridge and New York, 2007.

Jenk, T. M.: Ice Core Based Reconstruction of Past Climate Conditions and Air Pollution in the Alps Using Radiocarbon, PhD thesis, Departement für Chemie und Biochemie, Univ. of Bern, Bern, Switzerland, 2006.

Jenk, T. M., Szidat, S., Schwikowski, M., Gäggeler, H. W., Brütsch, S., Wacker, L., Synal, H.-A. and Saurer, M.: Radiocarbon analysis in an Alpine ice core: record of anthropogenic and biogenic contributions to carbonaceous aerosols in the past (1650–1940), Atmos. Chem. Phys., 6(12), 5381–5390, 2006.

Jenk, T. M., Szidat, S., Bolius, D., Sigl, M., Gäggeler, H. W., Wacker, L., Ruff, M., Barbante, C., Boutron, C. F. and Schwikowski, M.: A novel radiocarbon dating technique applied to an ice core from the Alps indicating late Pleistocene ages, J. Geophys. Res. Atmos., 114(D14), D14305, doi:10.1029/2009JD011860, 2009.

Johnsen, S. J.: Stable isotope homogenization of polar firn and ice, in Proc. Symp. on Isotopes and Impurities in Snow and Ice, I.U.G.G.XVI, General Assembly, Grenoble Aug. Sept. 1975, vol. 15, pp. 210–219, Washington, 1977.

Johnsen, S. J., Clausen, H. B., Dansgaard, W., Fuhrer, K., Gundestrup, N., Hammer, C. U., Iversen, P., Jouzel, J., Stauffer, B. and Steffensen, J. P.: Irregular glacial interstadials recorded in a new Greenland ice core, Nature, 359, 311–313, doi:10.1038/359311a0, 1992.

Johnsen, S. J., Clausen, H. B., Cuffey, K. M., Hoffmann, G., Schwander, J. and Creyts, T.: Diffusion of stable isotopes in polar firn and ice: The isotope effect in firn diffusion, in Physics of Ice Core Records, pp. 121–140, Hondoh T., Sapporo, 2000.

Jouzel, J., Merlivat, L. and Lorius, C.: Deuterium excess in an East Antarctic ice core suggests higher relative humidity at the oceanic surface during the last glacial maximum, Nature, 299(5885), 688–691, doi:10.1038/299688a0, 1982.

Jouzel, J. and Souchez, R. A.: Melting-refreezing at the glacier sole and the isotopic composition of the ice, J. Glaciol., 28(98), 1982.

Jouzel, J. and Merlivat, L.: Deuterium and oxygen 18 in precipitation: modeling of the isotopic effects during snow formation, J. Geophys. Res., 89(D7), 11749–11,757, doi:10.1029/JD089iD07p11749, 1984.

Jouzel, J., Alley, R. B., Cuffey, K. M., Dansgaard, W., Grootes, P., Hoffmann, G., Johnsen, S. J., Koster, R. D., Peel, D., Shuman, C. A., Stievenard, M., Stuiver, M. and White, J.: Validity of the temperature reconstruction from water isotopes in ice cores, J. Geophys. Res. Oceans, 102(C12), 26471–26487, doi:10.1029/97JC01283, 1997.

Jouzel, J.: Water stable isotopes: Atmospheric composition and applications in polar ice core studies, in Treatise on geochemistry, vol. 4, pp. 213–243, 2003.

Kaiser, A., Scheifinger, H., Kralik, M., Papesch, W., Rank, D. and Stichler, W.: Links between meteorological conditions and spatial/temporal variations in long-term isotope records from the Austrian Precipitation Network, pp. 67–76, 2001.

Landais, A., Steen-Larsen, H. C., Guillevic, M., Masson-Delmotte, V., Vinther, B. and Winkler, R.: Triple isotopic composition of oxygen in surface snow and water vapor at NEEM (Greenland), Geochim. Cosmochim. Acta, 77, 304–316, doi:10.1016/j.gca.2011.11.022, 2012.

Laternser, M. and Schneebeli, M.: Long-term snow climate trends of the Swiss Alps (1931–99), Int. J. Clim., 23(7), 733–750, doi:10.1002/joc.912, 2003.

Lewis, S. C., LeGrande, A. N., Kelley, M. and Schmidt, G. A.: Modeling insights into deuterium excess as an indicator of water vapor source conditions, J. Geophys. Res. Atmospheres, 118(2), 243–262, doi:10.1029/2012JD017804, 2013.

Liebminger, A., Haberhauer, G., Papesch, W. and Heiss, G.: Correlation of the isotopic composition in precipitation with local conditions in alpine regions, J. Geophys. Res. Atmos., 111(D5), D05104, doi:10.1029/2005JD006258, 2006.

Luterbacher, J., Xoplaki, E., Dietrich, D., Jones, P. ., Davies, T. ., Portis, D., Gonzalez-Rouco, J., von Storch, H., Gyalistras, D., Casty, C. and Wanner, H.: Extending North Atlantic

Oscillation reconstructions back to 1500, Atmospheric Sci. Lett., 2(1–4), 114–124, doi:10.1006/asle.2001.0044, 2001.

Majoube, M.: Fractionnement en oxygene-18 et en deuterium entre l'eau et sa vapeur, J. Chim. Phys., 10, 1423–14336, 1971.

Marshall, J., Kushnir, Y., Battisti, D., Chang, P., Czaja, A., Dickson, R., Hurrell, J., McCartney, M., Saravanan, R. and Visbeck, M.: North Atlantic climate variability: phenomena, impacts and mechanisms, Int. J. Clim., 21(15), 1863–1898, doi:10.1002/joc.693, 2001.

Masson-Delmotte, V., Jouzel, J., Landais, A., Stievenard, M., Johnsen, S. J., White, J. W. C., Werner, M., Sveinbjornsdottir, A. and Fuhrer, K.: GRIP deuterium excess reveals rapid and orbital-scale changes in Greenland moisture origin, Science, 309(5731), 118–121, doi:10.1126/science.1108575, 2005.

Merlivat, L. and Nief, G.: Fractionnement isotopique lors des changements d "état solide-vapeur et liquide-vapeur de l'eau à des températures inférieures à 0° C, Tellus, 19(1), 122–127, 1967.

Merlivat, L. and Jouzel, J.: Global climatic interpretation of the deuterium-oxygen 18 relationship for precipitation, J. Geophys. Res. Oceans, 84(C8), 5029–5033, doi:10.1029/JC084iC08p05029, 1979.

Mook, W. G.: Abundance and fractionation of stable isotopes, in Environmental isotopes in the hydrological cycle, vol. 1: Introduction: Theory, Methods, Review, 164 pp., Vienna, 2001.

Moser, H. and Stichler, W.: Deuterium and oxygen-18 contents as an index of the properties of snow covers, Int. Assoc. Hydrol. Sci. Publ., 114, 122–135, 1975.

Nye, J. F.: Correction factor for accumulation measured by the thickness of the annual layers in an ice sheet, J. Glaciol., 4(36), 785–788, 1963.

OcCC: Climate Change and Switzerland 2050 - Expected impacts on environment, society and economy, Available from: http://proclimweb.scnat.ch/Products/ch2050/PDF_E/CH2050-E.pdf, 2007.

O'Neil, J.R.: Theoretical and experimental aspects of isotopic fractionation, Rev. Mineral. Geochem., 16.1, 1–40, 1986.

Van Oldenborgh, G. J., te Raa, L. A., Dijkstra, H. A. and Philip, S. Y.: Frequency- or amplitude-dependent effects of the Atlantic meridional overturning on the tropical Pacific Ocean, Ocean Sci, 5(3), 293–301, doi:10.5194/os-5-293-2009, 2009.

Pfahl, S. and Wernli, H.: Air parcel trajectory analysis of stable isotopes in water vapor in the eastern Mediterranean, J. Geophys. Res.-Atmos., 113(D20), doi:10.1029/2008JD009839, 2008.

Pfahl, S. and Sodemann, H.: What controls deuterium excess in global precipitation?, Clim. Past Discuss., 9(4), 4745–4770, doi:10.5194/cpd-9-4745-2013, 2013.

Poage, M. A. and Chamberlain, C. P.: Empirical relationships between elevation and the stable isotope composition of precipitation and surface waters: considerations for studies of paleoelevation change, Am. J. Sci., 301(1), 1–15, doi:10.2475/ajs.301.1.1, 2001.

Rank, D. and Papesch, W.: Isotopic composition of precipitation in Austria in relation to air circulation patterns and climate, in Isotopic composition of precipitation in the Mediterranean Basin in relation to air circulation patterns and climate: final report of a coordinated research project, 2000-2004, International Atomic Energy Agency, Vienna., 2005.

Risi, C., Bony, S. and Vimeux, F.: Influence of convective processes on the isotopic composition (δ^{18}O and δD) of precipitation and water vapor in the tropics: 2. Physical interpretation of the amount effect, J. Geophys. Res. Atmos., 113(D19), doi:10.1029/2008JD009943, 2008.

Rozanski, K., Sonntag, C. and Münnich, K. O.: Factors controlling stable isotope composition of European precipitation, Tellus, 34(2), 142–150, doi:10.1111/j.2153-3490.1982.tb01801.x, 1982.

Rozanski, K., Araguas-Araguas, L. and Gonfiantini, R.: Relation between long-term trends of oxygen-18 isotope composition of precipitation and climate, Science, 258, 981–985, doi:10.1126/science.258.5084.981, 1992.

Rozanski, K., Araguás-Araguás, L. and Gonfiantini, R.: Isotopic patterns in modern global precipitation, in Geophysical Monograph Series, vol. 78, edited by P. K. Swart, K. C. Lohmann, J. McKenzie, and S. Savin, pp. 1–36, American Geophysical Union, Washington, D. C., 1993.

Saurer, M., Kress, A., Leuenberger, M., Rinne, K. T., Treydte, K. S. and Siegwolf, R. T. W.: Influence of atmospheric circulation patterns on the oxygen isotope ratio of tree rings in the Alpine region, J. Geophys. Res. Atmos., 117(D5), doi:10.1029/2011JD016861, 2012.

Scherrer, S. C., Appenzeller, C. and Laternser, M.: Trends in Swiss Alpine snow days: The role of local- and large-scale climate variability, Geophys. Res. Lett., 31(13), doi:10.1029/2004GL020255, 2004.

Scherrer, S. C., Wüthrich, C., Croci-Maspoli, M., Weingartner, R. and Appenzeller, C.: Snow variability in the Swiss Alps 1864–2009, Int. J. Clim., doi:10.1002/joc.3653, 2013.

Schlesinger, M. E. and Ramankutty, N.: An oscillation in the global climate system of period 65–70 years, Nature, 367(6465), 723–726, doi:10.1038/367723a0, 1994.

Schmidli, J., Schmutz, C., Frei, C., Wanner, H. and Schär, C.: Mesoscale precipitation variability in the region of the European Alps during the 20th century, Int. J. Clim., 22(9), 1049–1074, doi:10.1002/joc.769, 2002.

Schmutz, C., Luterbacher, J., Gyalistras, D., Xoplaki, E. and Wanner, H.: Can we trust proxy-based NAO index reconstructions?, Geophys. Res. Lett., 27(8), 1135–1138, doi:10.1029/1999GL011045, 2000.

Schöner, W., Auer, I., Bohm, R., Keck, L. and Wagenbach, D.: Spatial representativity of air-temperature information from instrumental and ice-core-based isotope records in the European Alps, Ann. Glaciol., 35(1), 157–161, doi:10.3189/172756402781816717, 2002.

Schotterer, U., Oeschger, H., Wagenbach, D. and Münnich, K. O.: Information on paleo-precipitation on a high altitude glacier Monte Rosa, Switzerland, Z. Gletscherkunde Glazialgeol, 21: 379–388, 1985.

Schotterer, U., Fröhlich, K., Stichler, W. and Trimborn, P.: Temporal variations of oxygen-18 and deuterium excess in Alpine regions of Switzerland, in Isotope Techniques in the study of Past and Current Environmental Changes in the Hydrosphere and the Atmosphere, Proceedings of an international Symposium organized by the International Atomic Energy Agency, Vienna, 19 – 23 April 1993, pp. 53–64, IAEA Vienna, 1993.

Schotterer, U., Fröhlich, K., Gäggeler, H. W., Sandjordj, S. and Stichler, W.: Isotope records from Mongolian and Alpine ice cores as climate indicators, Clim. Change, 36(3-4), 519–530, doi:10.1023/A:1005338427567, 1997.

Schotterer, U., Stichler, W., Graf, W., Gourcy, L., Huber, T., and Ginot, P.: Stable isotopes in alpine ice cores: do they record climate variability?, Proc. Intern. Conf. on Isotope Techniques in the Study of Environmental Change, IAEA Vienna, 1998.

Schotterer, U., Stichler, W. and Ginot, P.: The influence of post-depositional effects on ice core studies: examples from the Alps, Andes, and Altai, in Earth Paleoenvironments: Records Preserved in Mid- and Low-Latitude Glaciers, edited by L. D. Cecil, J. R. Green, and L. G. Thompson, pp. 39–59, Springer Netherlands, 2004.

Schürch, M., Kozel, R., Schotterer, U. and Tripet, J.-P.: Observation of isotopes in the water cycle—the Swiss National Network (NISOT), Environ. Geol., 45(1), 1–11, 2003.

Schwerzmann, A., Funk, M., Blatter, H., Lüthi, M., Schwikowski, M. and Palmer, A.: A method to reconstruct past accumulation rates in alpine firn regions: A study on Fiescherhorn, Swiss Alps, J. Geophys. Res., 111(F1), doi:10.1029/2005JF000283, 2006.

Schwikowski, M., Brütsch, S., Gäggeler, H. W. and Schotterer, U.: A high-resolution air chemistry record from an Alpine ice core: Fiescherhorn glacier, Swiss Alps, J. Geophys. Res., 104(D11), 13709–13,719, doi:10.1029/1998JD100112, 1999.

Serquet, G., Marty, C., Dulex, J.-P. and Rebetez, M.: Seasonal trends and temperature dependence of the snowfall/precipitation-day ratio in Switzerland, Geophys. Res. Lett., 38, 07703, doi:DOI: 10.1029/2011GL046976, 2011.

Siegenthaler, U. and Oeschger, H.: Correlation of ^{18}O in precipitation with temperature and altitude, Nature, 285, 314–317, doi:DOI: 10.1038/285314a0, 1980.

Sigl: Ice core based reconstruction of past climate conditions from Colle Gnifetti, Swiss Alps, PhD thesis, Departement für Chemie und Biochemie, Univ. of Bern, Bern, Switzerland, 2009.

Sodemann, H. and Zubler, E.: Seasonal and inter–annual variability of the moisture sources for Alpine precipitation during 1995–2002, Int. J. Clim., 30(7), 947–961, doi:10.1002/joc.1932, 2009.

Steen-Larsen, H. C., Johnsen, S. J., Masson-Delmotte, V., Stenni, B., Risi, C., Sodemann, H., Balslev-Clausen, D., Blunier, T., Dahl-Jensen, D., Ellehøj, M. D., Falourd, S., Grindsted, A., Gkinis, V., Jouzel, J., Popp, T., Sheldon, S., Simonsen, S. B., Sjolte, J., Steffensen, J. P., Sperlich, P., Sveinbjörnsdóttir, A. E., Vinther, B. M. and White, J. W. C.: Continuous

monitoring of summer surface water vapor isotopic composition above the Greenland Ice Sheet, Atmos. Chem. Phys., 13(9), 4815–4828, doi:10.5194/acp-13-4815-2013, 2013.

Stenni, B., Masson-Delmotte, V., Johnsen, S., Jouzel, J., Longinelli, A., Monnin, E., Röthlisberger, R. and Selmo, E.: An oceanic cold reversal during the last deglaciation, Science, 293(5537), 2074–2077, doi:10.1126/science.1059702, 2001.

Stichler, W., Rauert, W. and Martinec, J.: Environmental isotope studies of an alpine snowpack, Nordic Hydrol., 1981.

Stichler, W. and Schotterer, U.: From accumulation to discharge: modification of stable isotopes during glacial and post-glacial processes, Hydrol. Process., 14(8), 1423–1438, doi:10.1002/1099-1085(20000615)14:8<1423::AID-HYP991>3.0.CO;2-X, 2000.

Stichler, W., Schotterer, U., Fröhlich, K., Ginot, P., Kull, C., Gäggeler, H. and Pouyaud, B.: Influence of sublimation on stable isotope records recovered from high-altitude glaciers in the tropical Andes, J. Geophys. Res. Atmos., 106(D19), 22613–22620, doi:10.1029/2001JD900179, 2001.

Thompson, L. G., Mosley-Thompson, E., Davis, M. E., Bolzan, J. F., Dai, J., Klein, L., Gundestrup, N., Yao, T., Wu, X. and Xie, Z.: Glacial stage ice-core records from the subtropical Dunde Ice Cap, China, Ann. Glaciol., 14, 288–297, 1990.

Thompson, D. W. J. and Wallace, J. M.: The Arctic oscillation signature in the wintertime geopotential height and temperature fields, Geophys. Res. Lett., 25(9), 1297–1300, doi:10.1029/98GL00950, 1998.

Trenberth, K. E. and Shea, D. J.: Atlantic hurricanes and natural variability in 2005, Geophys. Res. Lett., 33(12), L12704, doi:10.1029/2006GL026894, 2006.

Trouet, V., Esper, J., Graham, N. E., Baker, A., Scourse, J. D. and Frank, D. C.: Persistent positive North Atlantic Oscillation mode dominated the Medieval Climate Anomaly, Science, 324(5923), 78–80, doi:10.1126/science.1166349, 2009.

Uemura, R., Matsui, Y., Yoshimura, K., Motoyama, H. and Yoshida, N.: Evidence of deuterium excess in water vapor as an indicator of ocean surface conditions, J. Geophys. Res. Atmos., 113(D19), doi:10.1029/2008JD010209, 2008.

Vimeux, F., Masson, V., Jouzel, J., Stievenard, M. and Petit, J. R.: Glacial–interglacial changes in ocean surface conditions in the Southern Hemisphere, Nature, 398(6726), 410–413, doi:10.1038/18860, 1999.

Wagenbach, D., Münnich, K. O., Schotterer, U. and Oeschger, H.: The anthropogenic impact on snow chemistry at Colle Gnifetti, Swiss Alps, Ann. Glaciol., 10, 183–187, 1988.

Wanner, H., Rickli, R., Salvisberg, E., Schmutz, C. and Schüepp, M.: Global climate change and variability and its influence on Alpine climate — concepts and observations, Theor. Appl. Clim., 58(3-4), 221–243, doi:10.1007/BF00865022, 1997.

De Wit, J. C., Van der Straaten, C. M. and Mook, W. G.: Determination of the absolute hydrogen isotopic ratio of V-SMOW and SLAP, Geostand. Newsl., 4(1), 33–36, doi:10.1111/j.1751-908X.1980.tb00270.x, 1980.

Yurtsever, Y. and Gat, J.R.: Atmospheric waters, in Stable isotope hydrology: deuterium and oxygen-18 in the water cycle, Tech. Rep. Ser. 210, pp. 103–142, IAEA, Vienna, 1981.

3 Analysis of $\delta^{18}O$ and δD in liquid samples with a laser spectrometer

3.1 Introduction and motivation

The measurement of water stable isotopes ratios in ice cores is one of the bases of ice core research and is nowadays a routine operation. Many methods are available and offer different solutions depending on the needs of the user (e.g. time optimization, low analytical uncertainty). A comprehensive description of the most used techniques can be found in de Groot (2004).

Conventional Isotopic Ratio Mass Spectrometry (IRMS) is one of the most used methods for the measurement of isotopic ratios of the water molecule (Mook, 2000). The principle of IRMS is to measure the different compounds by separating them according to their different mass/charge ratio. In the IRMS the molecules are positively ionized by electronic bombardment and subsequently accelerated using a high voltage electric field (~MV). The ion beam enters a magnetic field perpendicular to the electric field, where due to the Lorentz force their trajectory is circularly deflected. Because of their different masses the ions follow different paths, with the heavier travelling along a larger curvature trajectory with respect to the lighter ones. The ions are eventually collected in Faraday cups where the signal is converted in electric current and their relative abundances can be obtained compared to a reference standard.

Although it is in principle possible to directly measure the water ions with the IRMS, it is commonly preferred to convert them into other compounds as water tends to be adsorbed on surfaces introducing strong memory effects (Platzner, 1997). Different methods are available and the examples presented here illustrate the techniques previously used for the ice cores analyzed by the Group of Analytical Chemistry in the Laboratory of Radiochemistry and Environmental Chemistry (LCH) at the Paul Scherrer Institut, Switzerland. Some of them, as specified below, were employed in collaboration with the Ecosystems Fluxes Group of the Laboratory of Atmospheric Chemistry (LAC) at the Paul Scherrer Institut and with the Climate and Environmental Physics Group from the Climate Physics Department (KUP) at the University of Bern. For the measurement of the $\delta^{18}O$ one of the most used techniques for IRMS is the CO_2 equilibration (Epstein and Mayeda, 1953), where a vial volume is filled with an aliquot of the sample water and with CO_2 gas.

Through the intermediate formation of H_2CO_3, the equilibration of the products is obtained after few hours according to the following reaction:

$$H_2^{18}O + C^{16}O_2 \rightarrow H_2^{16}O + C^{16}O^{18}O$$
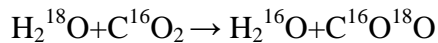
The different CO_2 isotopologues are then measured with the IRMS and through the ratio $C^{16}O^{18}O/C^{16}O_2$ the $\delta^{18}O$ is obtained. $\delta^{18}O$ in the Grenzgletscher ice core was measured by Eichler et al. (2000) with this technique in the LAC at the Paul Scherrer Institut, using a Finnigan MAT Delta S spectrometer. The analytical uncertainty was <0.1‰. The Fiescherhorn ice core $\delta^{18}O$ values were also obtained with this method and were measured in the KUP at the University of Bern with a Finnigan MAT250 system. The analytical uncertainty was <0.05‰ (Jenk, 2006).

The IRMS can also analyze the δD, but a different reaction is needed to reduce water to hydrogen (H_2). For the Grenzgletscher and the Fiescherhorn ice cores the chromium reduction technique was used, in the first case in the LAC at the Paul Scherrer Institut (Eichler, personal communication) and in the second case in the KUP at the University of Bern (Jenk, 2006). This method is based on the following chemical reaction (Gehre et al., 1996):

$$2Cr + 3H_2O \rightarrow Cr_2O_3 + 3H_2$$
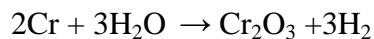
The reaction, i.e. water reduced with chromium, occurs in a reactor kept at temperatures higher than 800°C. The hydrogen thereby produced is then analyzed with the IRMS, a Finnigan MAT Delta S (LAC, Paul Scherrer Institut) and Finnigan MAT250 (KUP, Bern). The analytical uncertainties of δD was <0.5‰ in both cases.

Another technique that in principle can be used for both $\delta^{18}O$ and δD is based on pyrolysis. This method is described here in greater detail because it was applied for a second set of samples from Grenzgletscher ice core covering the period 1961-1983 (see below). The technique is based on conversion of the oxygen in the water to CO in a pyrolysis reaction and subsequent measurement with a mass spectrometer for separation of the different isotopes. The IRMS used is a Finnigan DeltaPlusXP installed in the Ecosystems Fluxes Group (LAC) at the Paul Scherrer Institut (Figure 1).

The sample water is injected into the Temperature Conversion Elemental Analyzer (TC/EA) mainly consisting of a glassy carbon tube kept at 1400°C and filled with carbon grit in order to maximize the yield of the following reaction (Kornexl et al., 1999; Saurer and Siegwolf, 2004):

$$H_2O + C \rightarrow CO + H_2$$
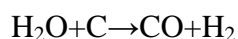
The CO produced is then transported with carrier gas (helium) through a GC column maintained at 70°C where a kinetic separation of CO from interfering gases with the same

mass like N_2 occurs. The three main CO isotopologues are separated in the mass spectrometer. The ions with mass 28 ($^{12}C^{16}O$), 29 ($^{13}C^{16}O$), 30 ($^{12}C^{18}O$) are collected in Faraday cups and compared to a CO reference gas. Other rarer isotopologues can be present due to the different isotopes of carbon and oxygen (e.g. ^{13}C, ^{17}O). In this case a correction accounting for their concentration is automatically performed. Through the determination of the mass ratio 30/28 it is possible to determine the $^{18}O/^{16}O$ ratio hence the $\delta^{18}O$. The calibration to the international standard (VSMOW, see section 3.3.4) is done by measuring internal laboratory standards every 15 samples.
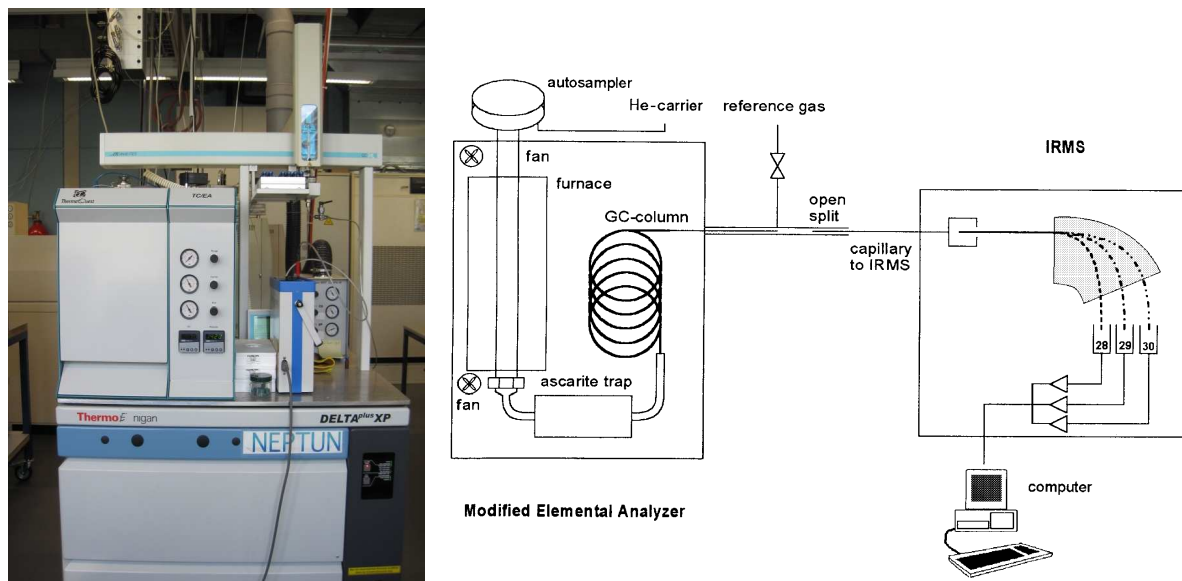

Figure 1 (Left) Finnigan DeltaPlus XP mass-spectrometer used for the measurement of the second set of Grenzgletscher $\delta^{18}O$ samples (Table 1). On top the autosampler, on the left the TC/EA module (see text) and at the bottom the mass spectrometer. (Right) Scheme of the pyrolysis-IRMS system (Kornexl et al., 1999).

The analytical uncertainty of the $\delta^{18}O$ measurement is <0.2‰ is shown in section 3.3.3 and Table 1. With this instrument it is in principle possible to measure δD from the H_2 produced during the pyrolysis, however the uncertainty showed large variations, achieving values <0.5‰ but mostly approaching ~1‰. This latter value was considered too high and therefore the Grenzgletscher samples were not analyzed for δD with this technique. Neither were they measured using the chromium reduction technique, due to technical issues.

The IRMS can provide through various methods excellent measurements of the water stable isotopes ratios. However, it is not always feasible to measure oxygen and hydrogen isotopes simultaneously due to the different settings of the electro-magnetic fields needed. The

Wavelength-Scanned Cavity Ring Down Spectrometry (WS-CRDS) technique overcomes this problem, measuring $\delta^{18}O$ and δD at the same time. The instrument is technically easier to operate compared to the IRMS and is more robust, allowing application on the field. This is fundamental in the investigation of ice cores, whose length can range from hundreds of meters (Alpine ice cores) to kilometers (polar ice cores).

In December 2011 a WS-CRDS spectrometer (Picarro L2130-i) was purchased by the Analytical Chemistry Group at the Paul Scherrer Institut, for the measurement of the water stable isotopes in ice cores.

This chapter focuses on the setup and characterization of the WS-CRDS spectrometer and on the measurements performed on the samples extracted from the Grenzgletscher ice core. The δD record was incomplete and covered only the limited period 1977-1984. We therefore decided to extend it back to 1961, in order to get more information about the deuterium excess. Because of the high surface accumulation rate at this glacier (2.7 m w.e., Eichler et al., 2000) with negligible thinning in the uppermost part of the core and consequent time cost of the analysis, the analyzed period was limited to 1961-1983.

As explained in the following sections, for the second sampling the $\delta^{18}O$ was measured with two different instruments, allowing for interlaboratory comparison. The techniques used and their analytical uncertainties are summarized in Table 1.

Year	Laboratory	Period covered	Method	Instrument	$\delta^{18}O$ Analytical Uncertainty
2000	PSI, LAC	1937-1994	CO_2 equilibration	DELTA S, Finnigan MAT	< 0.1‰
2011	PSI, LAC	1961-1983	Pyrolysis-CO production	DELTAplusXP, Finnigan MAT	< 0.2‰
2012	PSI, LCH	1961-1983	WS-CRDS	Picarro L2130-i	< 0.1‰

Table 1 Chronology of the $\delta^{18}O$ measurements of the Grenzgletscher samples. First sampling and measurements completed by Eichler (2000, 2001). Second sampling done in 2011 and measurements performed in 2011 (with IRMS) and 2012 (with WS-CRDS), see the following sections.

In section 3.2 the principles of the WS-CRDS technique are presented. The characterization of the instrument is described in section 3.3. In section 3.4 the method comparison of WS-CRDS and the IRMS techniques is shown. Conclusions and outlook are presented in section 3.5.

3.2 Wavelength-Scanned Cavity Ring Down Spectrometry (WS-CRDS) technique

The WS-CRDS technique was initially developed by O'Keefe and Deacon (1988) with the aim of improving the sensitivity of the conventional absorption techniques for the measurements of trace compounds, e.g. in air pollution studies. There is nowadays a broad range of applications, from emission to bio-pharmaceutical monitoring (e.g. Paul and Saykally, 1997). In the case of environmental studies, commercial systems developed by the U.S. company Picarro measure water stable isotope ratios as well trace gas concentrations (www.picarro.com). The focus of this chapter is on the L2130-i spectrometer for the measurement of the oxygen and hydrogen ratios in liquid water samples.

3.2.1 Principle of the WS-CRDS technique

The physical basis of the absorption techniques relies on the Lambert-Beer law Eq. (1), stating that the intensity of the light traveling through a medium decreases due to the interaction with the medium and is described by a decreasing exponential function. The rate of absorption for a determined wavelength depends on the sample concentration and on the path length:

$$I = I_0 \exp(-\alpha x) \tag{1}$$

I_0 and I are the light intensities before and after traversing the medium, $\alpha = \sigma N$ is the absorption coefficient, with $\sigma(\lambda)$ the absorption cross section for a determined wavelength and N the density of the sample, x is the path length.

For conventional absorption techniques, given a sample of thickness L, and measuring I and I_0, the corresponding α coefficient and eventually the species concentration is obtained. However, this approach is not sufficiently sensitive when measuring very low concentrations and the signal to noise ratio is too low.

An alternative way is offered by the WS-CRDS technique (Figure 2). The main idea is to increase the path length in such a way to get an accurate determination of the time constant τ of the intensity decay, hence, of the sample concentration.

This technique is based on infrared (IR) lasers because the main vibration modes of the water molecules are in this frequency range. An IR laser tuned on the water molecule absorption wavelengths enters a cavity containing two high reflectivity mirrors (reflectivity R=99.999%). Three-mirrors cavities like in the case of the Picarro WS-CRDS spectrometer better support the traveling wave. When a threshold is reached, the laser is shut off and the light bounces between the mirrors. Their high reflectivity extends the path length by a factor of 10^5,

allowing for an accurate determination of the decaying light intensity. The intensity obviously decreases due to the not perfect reflectivity of the mirrors, i.e. at each reflection the light is partly transmitted. The intensity decrease follows the Lambert Beer law. A photodetector located behind one of the mirrors measures this exponential decay with high accuracy because the sampling time is much lower than the decay constant (Busch and Busch, 1999).
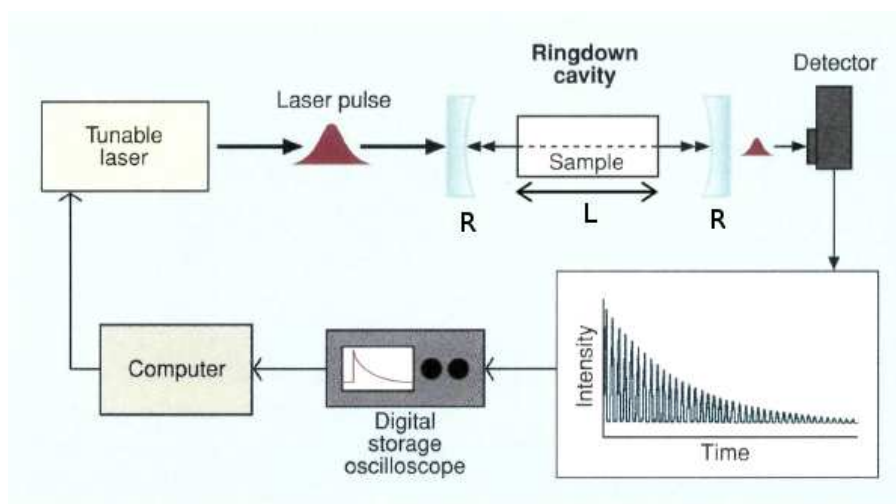

Figure 2 Scheme of a CRDS with a cavity length L and two mirrors of reflectivity R. Adapted from Paul and Saykally (1997). For the Picarro L2130-i a continuous wave (CW) laser is used.

The time constant τ of the decay, called also "ring down" from the analogy with the sound of a bell ringing down, can thus be determined giving the "empty cavity" factor, i.e. the decay only due to the cavity characteristics (size and mirrors reflectivity). When a sample is present in the cavity the intensity decrease is faster due to the additional absorption by the sample (Figure 3).

Measuring the total absorption (though the time constant) and knowing the "empty cavity" factor it is therefore possible to retrieve the decay only due to the sample absorption, hence, its concentration. This technique is particularly suitable in the case of low concentrations where the high time constant of the decay allows an accurate estimation of the absorption coefficient.
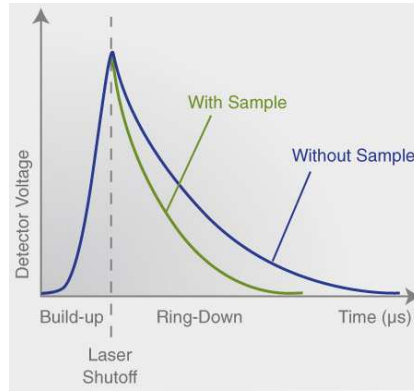
Figure 3 Scheme of the ring down time of the cavity without (blue) and with (green) the absorbing species (sample). Source: www.picarro.com.

3.2.2 Mathematical description

For the mathematical description of the technique please refer to (Busch and Busch, 1999) and Figure 2. Tuneable IR diode laser light enters a two-mirror cavity of reflectivity R and length L, respectively (a completely analogue derivation may be obtained considering three-mirror cavities). If the cavity does not contain any absorbing species, the laser intensity decreases with time following the Lambert-Beer law, with a loss given by the following factors:

$$I(t) = I_0 \exp\left[-\left(\frac{\text{Loss}}{\text{Reflection}}\right)\left(\frac{\text{Number of reflections}}{\text{Round trip}}\right)(\text{Number of round trips})\right]$$

The first factor is simply *1-R*, considering that the transmittivity *T* is given through the Kirchoff's law, with *T=1-R*. The second factor corresponds to the number of the mirrors, in this case 2. The last factor is the path covered at the time *t* by the laser photons travelling at the speed of light ($c=3\cdot10^8$ m/s), i.e. *tc/2L*, where a roundtrip corresponds to the total length of the cavity, in this case 2L. The intensity at the time t is then given by Eq. (2):

$$I(t) = I_0 \exp\left[-(1-R)\left(\frac{tc}{L}\right)\right] \tag{2}$$

The time constant τ_E of the decay due to the empty cavity losses is the time after that the initial intensity I_0 has decayed by a factor e, i.e. *I(t)/I$_0$=e^{-1}*:

$$\tau_E = \frac{t_R}{2(1-R)} \tag{3}$$

where $t_R = 2L/c$ is the transit time for a round trip.

If the cavity contains an absorbing species, the loss is given by the loss per round trip (*2αL*, with α the absorption coefficient usually expressed in cm^{-1}) times the number of round trips (*tc/2L*). The total loss can now be expressed as:

$$\text{Total loss} = (1-R)\frac{tc}{L} + \alpha L\frac{tc}{L} = \left[(1-R) + \alpha L\right]\frac{tc}{L} \tag{4}$$

Eq. (2) thus becomes:

$$I(t) = I_0 \exp\left\{\left[-(1-R) + \alpha L\right]\frac{tc}{L}\right\} \tag{5}$$

Analogue to the empty cavity case it is possible to define a time constant for the total decay τ_T:

$$\tau_T = \frac{t_R}{2\left[(1-R) + \alpha L\right]} \tag{6}$$

Obviously $\tau_T < \tau_E$, because the intensity decay is enhanced by the presence of the absorbing species.

The absorption coefficient α can finally be retrieved combining Eq. (3) and (6):

$$\alpha = \frac{1}{c}\left(\frac{1}{\tau_T} - \frac{1}{\tau_E}\right) \tag{7}$$

Physically this means that knowing τ_E, only depending on the cavity characteristics, and measuring τ_T it is possible to retrieve the absorption coefficient hence the sample concentration.

3.2.3 Description of the L2130-i Picarro laser spectrometer

A photo and a scheme of the Picarro L2130-i spectrometer are shown in Figure 4. The instrument consists of an autosampler (Leap Technologies PAL, model HTC-xt), a vaporizer usually kept at 110°C, a 25 cm long cavity (33 cm^3) inserted in a metallic box containing the hardware as well, two wash stations for the pre- and post-cleaning of the syringe (containing ultrapure water, 18.2 MΩcm at 25°C and methylpyrrolidinone solution, hereafter MPD), and two pumps (external units for the A0211 module). High purity N_2 (>99.999%) is used as carrier gas and is supplied to the instrument at 200 sccm and at a pressure of 2.5 psi (172 hPa). The pre- and post-cleaning procedure can be adapted upon the user's need. The analyzer software controls the measurement and displays it on a screen connected to the instrument.

The measurement procedure we adopted is described as follows. The water samples obtained from molten ice are stored in 2 mL clear glass vials (Infochroma, model G074B-12/032-Si/Te-H). No previous filtering is applied since ice core samples are particularly pure and there is no need of pre-treatment for this type of analysis. The vials are collocated in two autosampler trays with a capacity of 54 samples each. After a pre-cleaning with the sample

(70% of the syringe volume), the syringe extracts 2 µL that are injected into the vaporizer (A0211 module), and vaporized at a temperature of 110°C. The water vapor is flushed into the cavity that is constantly kept at subatmospheric pressure of 67 hPa. This reduces the broadening of the spectral lines. The temperature cavity is stabilized at 80°C. Picarro guarantees both, high pressure and thermal stability (0.003% of an atmosphere and 0.006% of room temperature, respectively, www.picarro.com). The small volume of the cavity allows fast gas exchange rates. The laser used is a 50 mW CW diode laser.
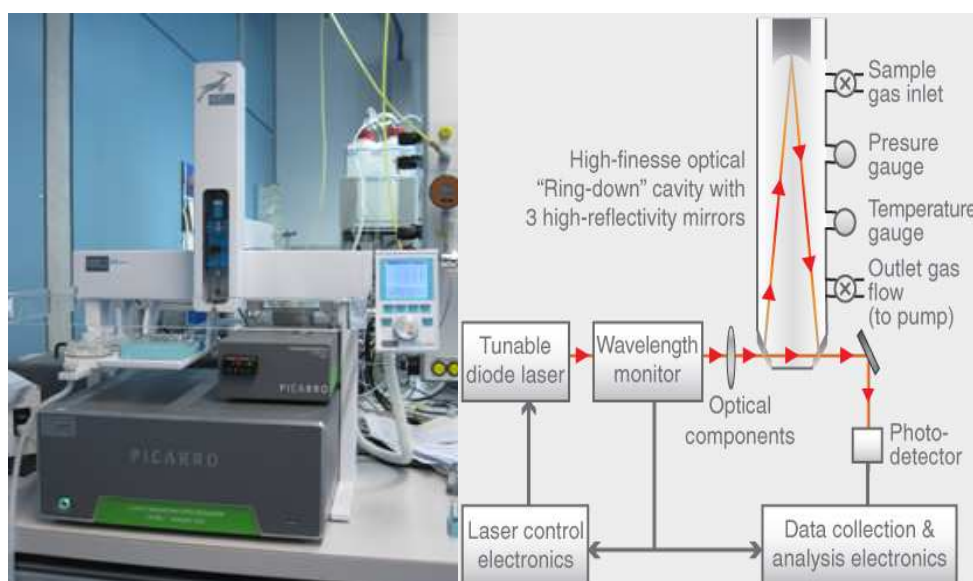

Figure 4 (Left) Photo of the Picarro L2130-i spectrometer in the Analytical Chemistry Laboratory OFLG/203 at Paul Scherrer Institut. (Right) Scheme of the Picarro WS-CRDS (Source: www.picarro.com). The system consists of a tunable diode laser, wavelength monitor, cavity with high reflectivity mirrors with high stability temperature and pressure controls, photodetector and electronics for the data collection and analysis. The water sample is previously vaporized and injected through the gas inlet and after the measurements removed with the pump system.

After the build-up phase lasting tenth of microseconds, the laser is abruptly shut off. The circulating light decreases because of both, "empty cavity" and sample absorption factors. The decay constant (order of magnitude ~10 µs) for a selected wavelength is retrieved and the laser is then tuned to a different wavelength, scanning a range of wavenumbers between 7199.80 cm^{-1} and 7200.40 cm^{-1} (corresponding to 1.3888 µm and 1.3889 µm respectively, see Figure 5). A patented wavelength monitor can sample the spectrum at a very high resolution ($\Delta\lambda/\lambda \approx 10^{-7}$), corresponding to 2MHz for the frequencies considered here (www.picarro.com). The absorption due to the "empty cavity" factor is retrieved using baseline at the wavelengths

without specific absorption. The three peaks in Figure 5 correspond to the concentrations of the three main water isotopologues. The analyzer can indeed measure the absolute concentrations of the different molecules, nevertheless it returns the quantities in the conventional $\delta^{18}O$, δD scale.
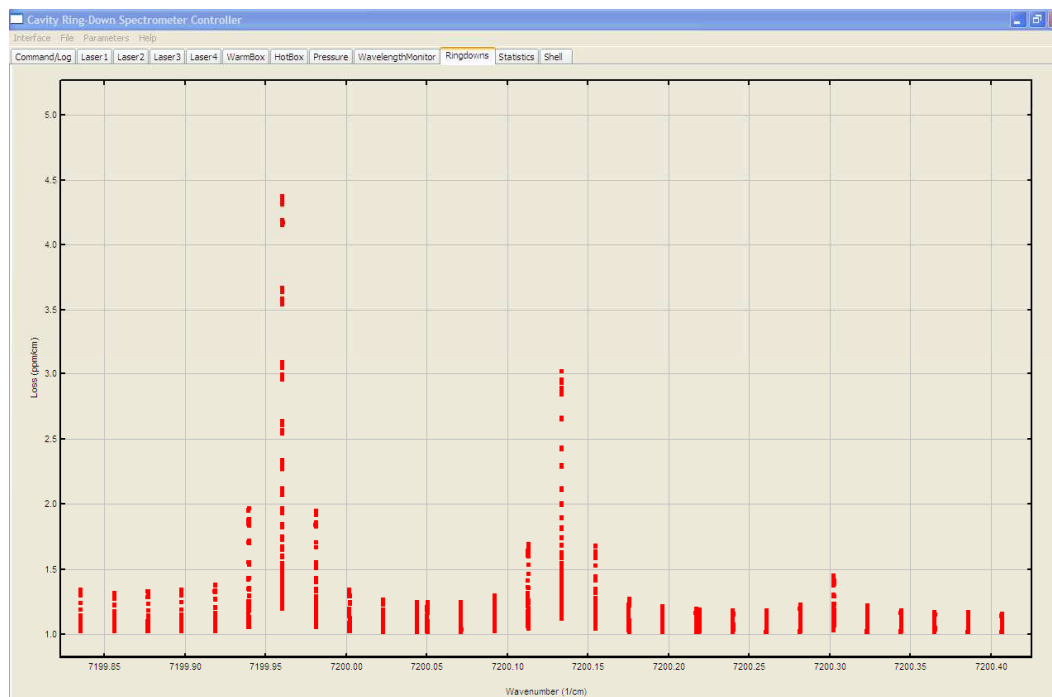

Figure 5 Snapshot of a single scan of the isotopologues absorptions of a water sample as a function of the wavenumber from the Picarro Controller. The loss due to the absorption is expressed in ppm/cm, the wavelengths are given in wavenumbers (cm^{-1}). Each red line shows the absorption for a certain scanned wavelength. The three peaks correspond to the three isotopologues $H_2^{16}O$, $H_2^{18}O$, HDO. When no sample is present in the cavity, the loss is between 1.01 and 1.03 ppm/cm.

Every sample measurement consists of several scans as illustrated above and the corresponding peak for typical water content in the cavity is usually 20000 ppm compared to the 150 ppm of the empty cavity, as shown in the upper panel of Figure 6. Due to the high stability of the instrument, every peak consists of a plateau. Part of this plateau (the red line in the graph) is then selected based on stability criteria and all the measurements in this part are averaged to get the final value. One cycle of measurement including pre-cleaning, injection, analysis and post-cleaning usually lasts ~10 minutes. Due to memory effects, described in section 3.3.1, Picarro suggests repeating the procedure six times. As a result one hour is needed for the complete measurement of one sample. Two pumps are connected to the vaporizer and to the cavity, respectively. They flush the sample away after the measurement

cycle and keep the system at subatmospheric pressure. Right after the injection, the syringe is cleaned once with ultrapure water and once with MPD solution. This substance showed to considerably prolong the syringe's life by reducing the friction of the plunger.
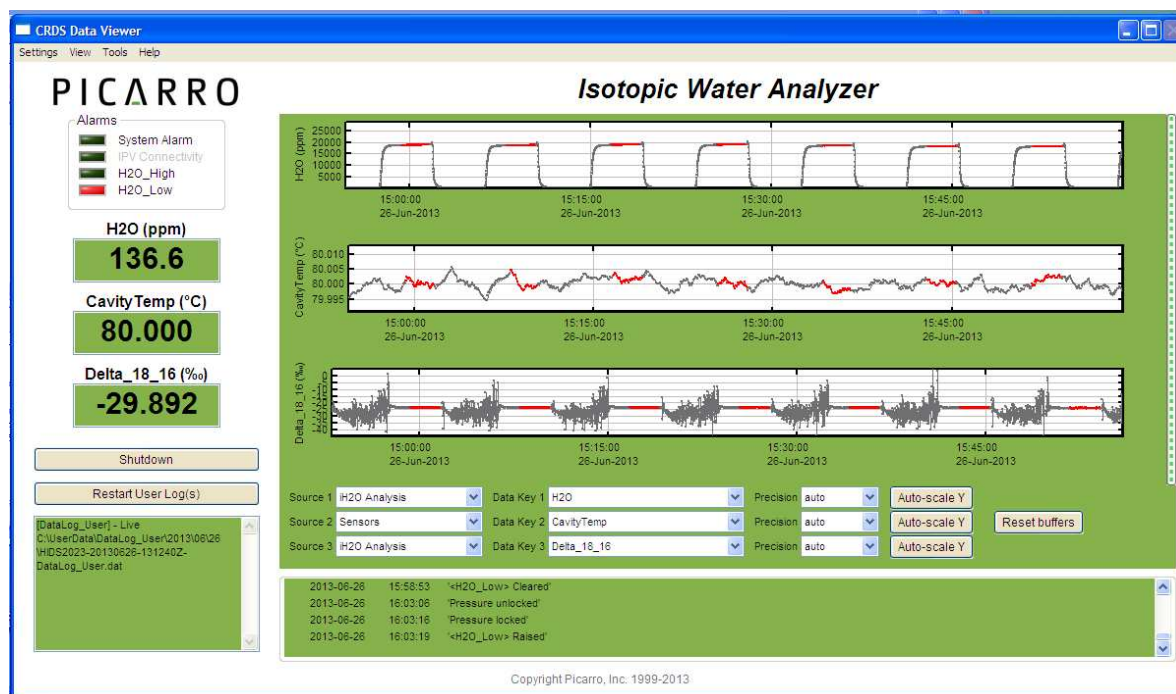

Figure 6 Screenshot of the "DatViewer" interface. The water content, cavity temperature and $\delta^{18}O$ measured with time are shown in the upper, middle and lower panel, respectively. The red highlighted parts correspond to the measurements used by the analyzer for the sample evaluation. Note the high stability of the cavity temperature and of the $\delta^{18}O$ during the sample measurement compared to the empty cavity due to the high water content (~20000 ppm compared to ~135 ppm).

Different types of syringes have been tested. First, a 5 μL Hamilton syringe (number 203189) was tried, adjusting the injection volume to 2 μL. However, the water content injected was unstable, exceeding the recommended value of 20000±3000 ppm. 5 μL SGE syringes (model SG001982) were then used, but the plungers got broken by the autosampler. Other two types of Hamilton syringes were thus tried: a 10 μL (model 80366) and a 10 μL gastight syringe (model 203206). The latter was eventually chosen because good stability in the water content was observed. The amount of water injected was finally set to 2.10 μL.

3.3 Characterization of the instrument and calibration of the laboratory standards

The instrument characterization consisted in the determination of memory effect, drift and analytical uncertainty. For this purpose two internal laboratory standards provided by the Ecosystem Fluxes Group of the Laboratory of Atmospheric Chemistry (LAC) as well as ultrapure water were used (Table 2).

Name	$\delta^{18}O$ (‰)	δD (‰)
Haus3	-10.03‰	-71.7‰
Miki2	-20.2‰	≈-95‰
Ultrapure water	≈-10‰	≈-74‰

Table 2 Isotopic composition of the waters used for the characterization of the WS-CRDS spectrometer. Note that Haus3 and ultrapure water are basically the same water, coming from the Paul Scherrer Institut and that the δD value of the Miki2 standard is only roughly estimated.

For the Miki2 standard only an approximate value of δD is given. Moreover, the approximate values of ultrapure water $\delta^{18}O$ and δD, measured with the laser spectrometer, are due to the fact that no calibration was made at this stage (see section 3.3.4). However, for the determination of the memory effect and drift this does not matter because the evaluations are exclusively made on the measured values. The choice of using more than one water standard at this stage of the instrument characterization was done in order to establish whether drift and memory effect change with the isotopic value.

Subsequently three new internal laboratory standards were prepared and calibrated.

3.3.1 Memory effect

A memory effect is observed when the measurement is affected by the previous one, due to unavoidable traces of the previous sample in the syringe and cavity. In order to reduce this effect, it is suggested to repeat the measurement at least six times and utilize only the last injections for the evaluation of the sample (www.picarro.com).

To determine the memory effect and establish the number of injections to be retained two water standards Haus3 and Miki2 were used. The difference in their $\delta^{18}O$ values reflects the typical summer to winter Alpine ice cores fluctuations (values typically ranging between -10‰ and -25‰, Schwikowski et al., 1999; Jenk, 2006 and Chapter 4). It is notable that the δD difference of the standards is much smaller compared to the Alpine range ($\Delta\delta D\sim25‰$ compared to $\sim100‰$ for the Fiescherhorn record, Jenk, 2006). It results to deviate significantly from the GMWL (Craig, 1961; Rozanski et al., 1993), from which an estimated value of $\delta D\sim-150‰$ should be obtained. This is probably due to strong deuterium enrichment in this water when the standard was prepared.

For the investigation of the memory effect two cases were considered: excursion from less negative to more negative isotopic values and vice versa. In order to do that 15 Haus3 and 15 Miki2 1 mL samples were measured alternatively (six injections for each of them). This way it was additionally possible to estimate the drift (see section 3.3.2).

In Figure 7 the $\delta^{18}O$ value (blue line) and the water content (black) are plotted against time. It is possible to notice the memory effect on the first injections of each sample. The water content resulted to be stable within the requirements.
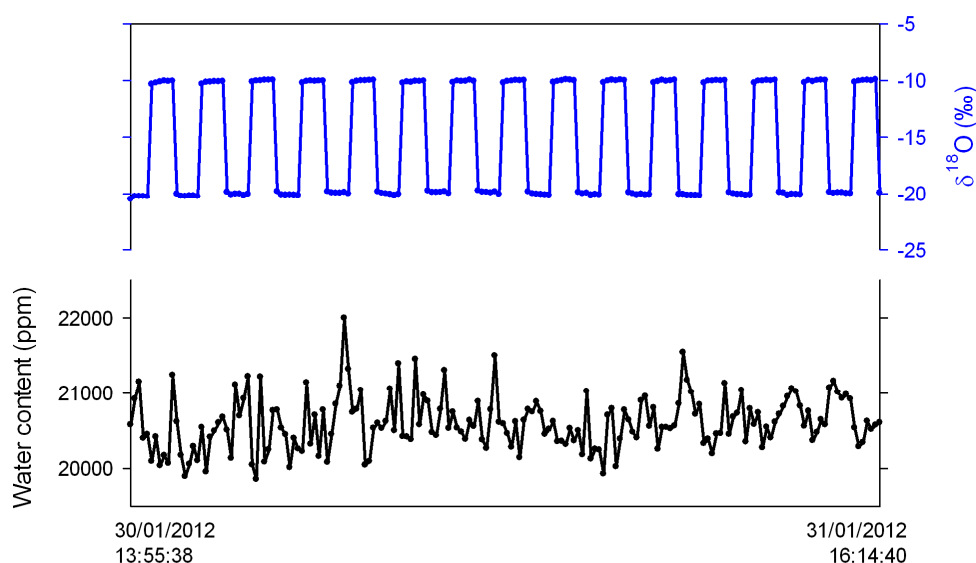

Figure 7 (Blue) $\delta^{18}O$ of the measured standards Haus3 (less negative) and Miki2 (more negative). (Black) Water content detected at each injection.

For the evaluation of the memory effect a simple approach was used. The "true value" was defined as the average of the isotopic value of the last three injections ($\delta^{18}O_{4th\text{-}6th}$, i.e. from the fourth to the sixth injection). The resulting memory coefficient M was then defined as follows:

$$M = \delta^{18}O_i / \delta^{18}O_{4th\text{-}6th} \tag{8}$$

where "i" denotes the i-th injection, from 1 to 6. Without carryover from the previous injections, M would be equal to 1. In reality it tends to 1 with time. After changing from Miki2 to Haus3, the first values of Haus3 tend to be more depleted, giving a coefficient slightly lower than 1. In the opposite case, the coefficient is slightly higher than 1. In order to report both cases the same way, the quantity 1-(M-1) was used for the isotopic changes Miki2-Haus3. The M coefficients obtained for each isotopic change were then averaged and are shown in Figure 8, for both $\delta^{18}O$ and δD.
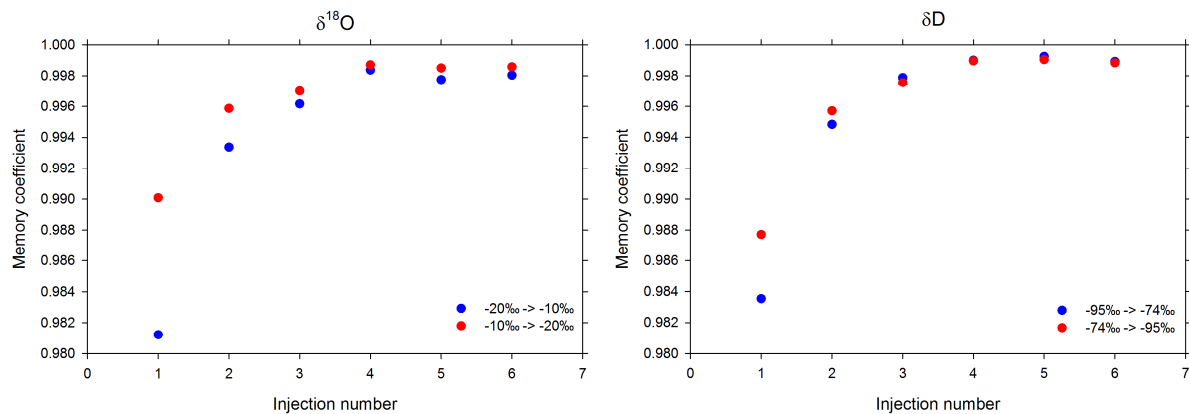

Figure 8 Memory coefficients as defined in Eq. (8) for $\delta^{18}O$ (left) and δD (right). Blue dots indicate the isotopic changes from Miki2 (more depleted) to Haus3 (less depleted), red dots from Haus3 (less depleted) to Miki2 (more depleted).

The first injections are in fact affected by a memory effect of less than 2% in both $\delta^{18}O$ and δD. The memory effect significantly decreases to 2‰ over the last three injections. It was therefore decided to inject each sample six times and use the average of the last three injections as result.

3.3.2 Instrument drift

With the same test it was also possible to estimate the drift of the isotopic values. Picarro guarantees a 24 hours drift below 0.2/0.8‰ for the $\delta^{18}O$ and δD, respectively. In order to characterize the drift for this instrument the $\delta^{18}O$ and δD values as described in section 3.3.1 were taken, averaging the last three injections. Instead of performing the drift test repeating measurement of the same sample several times, it was decided to use the previous test because the alternating isotopic values better reflect a real measurement. Results are shown in Figure 9.

The drift was slightly dependent on the isotopic value, with stronger trends associated to more isotopically depleted samples (Miki2). With respect to the $\delta^{18}O$, it was found a trend of 0.15‰/day for Haus3 and 0.2‰/day for Miki2. For the δD the trend was 0.7‰/day for Haus3 and ~1‰/day for Miki2. In general, a relative change of 1% with respect to the isotopic value was observed over 24 hours. It is also interesting to notice how the $\delta^{18}O$ measurements approach the true value without calibration, whereas this is not the case for the δD.
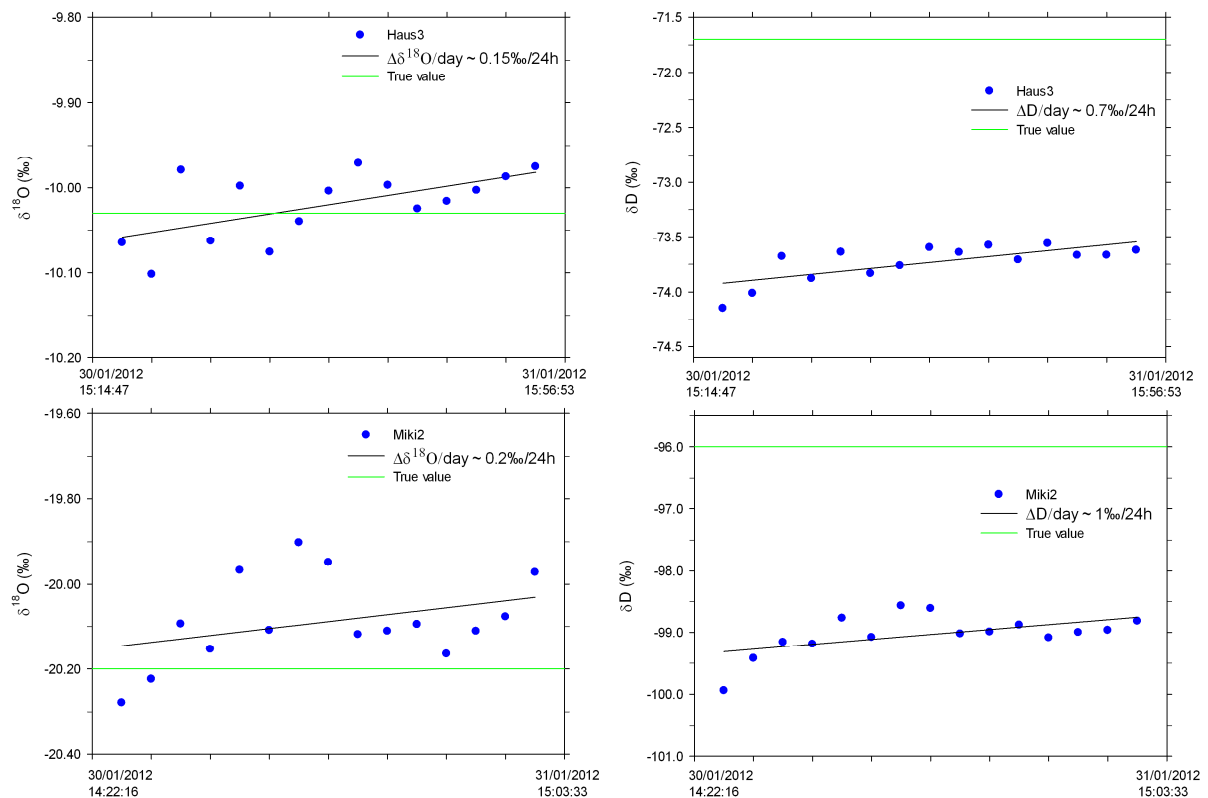

Figure 9 Drift effect for Haus3 (top) and Miki2 (bottom). The $\delta^{18}O$ and δD drift is shown on the left and right, respectively.

3.3.3 Determination of the analytical uncertainty

Before estimating the total analytical uncertainty an evaluation of the instrument precision is presented. Due to memory effect the precision was defined as the standard deviation of the last three injections. Picarro guarantees a precision of 0.025 and 0.100‰ for $\delta^{18}O$ and δD, respectively. In Figure 10 the standard deviation of Haus3 and Miki2 is plotted as a function of the measurement number, i.e. time. The time between one measurement and the following is approximately two hours because of the alternating measurements of Haus3 and Miki2. The graph thus shows the variation of the standard deviation estimate over more than one day. For the $\delta^{18}O$ higher variability is observed in Miki2 whereas for the δD no significant differences are present between the two standards. The errors do not show particular trends over time.
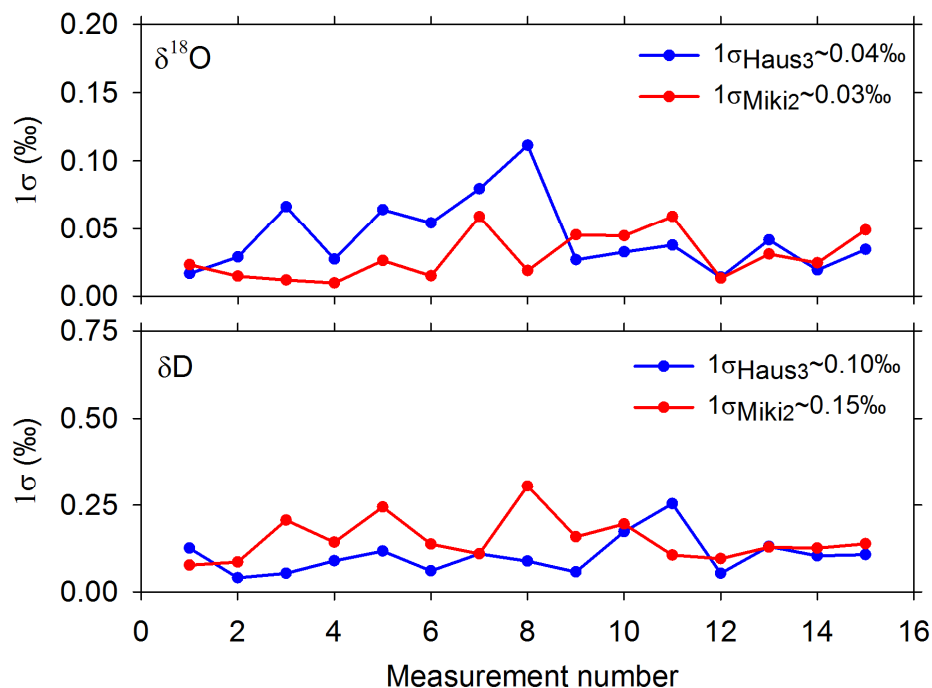

Figure 10 Instrument precision evaluated as the standard deviation of the 4th-6th injection as a function of time, for Haus3 (blue) and Miki2 (red). $\delta^{18}O$ and δD values are shown in the upper and lower panel, respectively.

The estimate of the total analytical uncertainty should take into account the additional sources of error introduced by the memory and drift correction (sections 3.3.1 and 3.3.2), as well as the propagation of the uncertainty associated to the standards used for the calibration. This latter quantity is shown in section 3.3.4, dedicated to the calibration of the internal laboratory standards. The analytical uncertainty accounting for the correction factors was estimated to be 0.1‰ for $\delta^{18}O$ and 0.5‰ for δD.

Compared to the IRMS techniques (pyrolysis and CO_2 equilibration for $\delta^{18}O$ and chromium reduction for δD), the L2130-i spectrometer shows in general comparable to lower uncertainties in both parameters (Table 3).

Laboratory	Method	Instrument	$\delta^{18}O$ Analytical Uncertainty	δD Analytical Uncertainty
PSI, LAC	CO_2 equilibration	Finnigan MAT Delta S	< 0.1‰	
PSI, LAC	Chromium reduction	Finnigan MAT Delta S		< 0.5‰
KUP, Bern	CO_2 equilibration	Finnigan MAT250	< 0.05‰	
KUP, Bern	Chromium reduction	Finnigan MAT250		< 0.5‰
PSI, LAC	Pyrolysis-CO production	DELTAplusXP, Finnigan MAT	< 0.2‰	< 1‰
PSI, LCH	WS-CRDS	Picarro L2130-i	< 0.1‰	< 0.5‰

Table 3 Analytical uncertainties of $\delta^{18}O$ and δD for the different laboratories and techniques.

3.3.4 Laboratory standards calibration

As explained in section 3.2.3, the spectrometer can measure the absolute concentrations of the three main isotopologues. Nevertheless it returns $\delta^{18}O$ and δD values because this is the convention internationally used. Offsets introduced by the instruments could be present. In order to quantify and correct for these offsets it is necessary to measure standards whose isotopic composition is known and transfer this correction factor to the measured samples.

A water standard is a reference material of known isotopic composition ($\delta^{18}O$ and δD in this case) specifically prepared and distributed to the laboratories in order to align the measured values to a common, intercomparable scale. There are different types of reference materials, according to the level of purity reached. The primary reference material or "international standard" is the material against which the sample is expressed (Gröning, 2004). These standards are provided by the International Atomic Energy Agency (IAEA), http://nucleus.iaea.org/rpst/ReferenceProducts/ReferenceMaterials/Stable_Isotopes/2H18O-water-samples/index.htm. Currently they are VSMOW2 (Vienna Standard Mean Ocean Water 2), with $\delta^{18}O=0.00$‰, $\delta D=0.0$‰, and SLAP2, with $\delta^{18}O=-55.50$‰, $\delta D=-427.5$‰ (International Atomic Energy Agency (IAEA), 2009). Those standards substitute the previous VSMOW and SLAP materials that are almost exhausted. Because of the limited amount of these waters, IAEA releases only 20 mL per laboratory every three years. Thus is not possible to use directly these primary reference materials for the measurements. It becomes necessary to prepare internal laboratory standards whose water is easily accessible and available in large amounts and calibrate it against the primary reference materials.

The range of isotopic values from Alpine ice cores is generally between -10‰/-75‰ and -25‰/-175% for $\delta^{18}O/\delta D$ (Schwikowski et al., 1999; Jenk, 2006). It was therefore decided to prepare three different internal laboratory standards, covering approximately this range. That means obtaining a more depleted (~-25‰/-180‰), an intermediate (-17‰/-125‰) and a less depleted (-10‰/-70‰) water standard. In order to do that, snow collected in Alpine regions in Switzerland (Scuol, Rueras) and samples from Antarctica were used. The (uncalibrated) isotopic value of the three waters was adjusted by adding the depleted Antarctica water (uncalibrated $\delta^{18}O$~-32‰, δD~-260‰) and ultrapure water from the Analytical Chemistry Group laboratory at the Paul Scherrer Institut (uncalibrated $\delta^{18}O$~-10‰, δD~-74‰). Eventually approximately four liters of water for each standard were obtained and were distributed in two bottles of 2.5 L each. The material of the bottles, amber glass, is such to isolate as much as possible the material and reduce the fractionation. These three standards

were labeled "Scuol", "Rueras" and "Labwater" depending on the origin of their major component.

For the calibration of the internal laboratory standards it was decided to use other four IAEA standards that better cover the isotopic range than VSMOW2 and SLAP2. These standards were used for the fourth IAEA interlaboratory comparison exercise (WICO 2011, Ahmad et al., 2012). Their isotopic values are given in Table 4.

Name	$\delta^{18}O$ (‰)	δD (‰)
OH-13	-0.96±0.04	-2.29±0.94
OH-14	-5.59±0.05	-37.69±0.82
OH-15	-9.37±0.04	-78.01±0.77
OH-16	-15.41±0.04	-113.81±0.94

Table 4 Isotopic composition of the four WICO2011 standards used for the calibration of the internal laboratory standards. The values were determined at the IAEA Isotope Hydrology Laboratory. The errors indicate the standard uncertainty for a single measurement given at 1σ level (Ahmad et al., 2012).

For each of these standards, provided by the Ecosystem Fluxes Group at the Paul Scherrer Institut, 1.5 mL was taken. In order to minimize the isotopic jumps between the samples, they were measured in the following order: OH-13, OH-14, OH-15, OH-16, Scuol, Rueras, Labwater. As mentioned before, each of the internal laboratory standards is stored in two bottles, thus, one sample from each of the bottles was taken, labeling it with the suffix "1" or "2", respectively. Each sample was measured only once (six injections) to minimize possible drift effects. In total, every run lasted approximately ten hours. After each measurement the caps were replaced with new ones to further reduce additional exchange through the hole produced by the needle. The complete run was repeated six times. After few weeks the entire procedure was repeated using new samples, i.e. taking another 1.5 mL of the WICO and internal laboratory standards. In this second case the runs were repeated eight times.

In total 14 measurements of the WICO standards together with the internal laboratory standards were obtained. For the calibration a least squares linear regression of the certified WICO values versus the measured ones was performed for each of the 14 runs. The "true value" of each internal laboratory standard could be then established from the regression equation, see also Figure 11.

As a quality check of the runs the uncertainties obtained for both the $\delta^{18}O$ and δD were inspected. It was decided to exclude a run whenever a measurement gave simultaneously errors bigger than 0.1‰ for the $\delta^{18}O$ and 0.5‰ for the δD. With this threshold two runs were excluded.
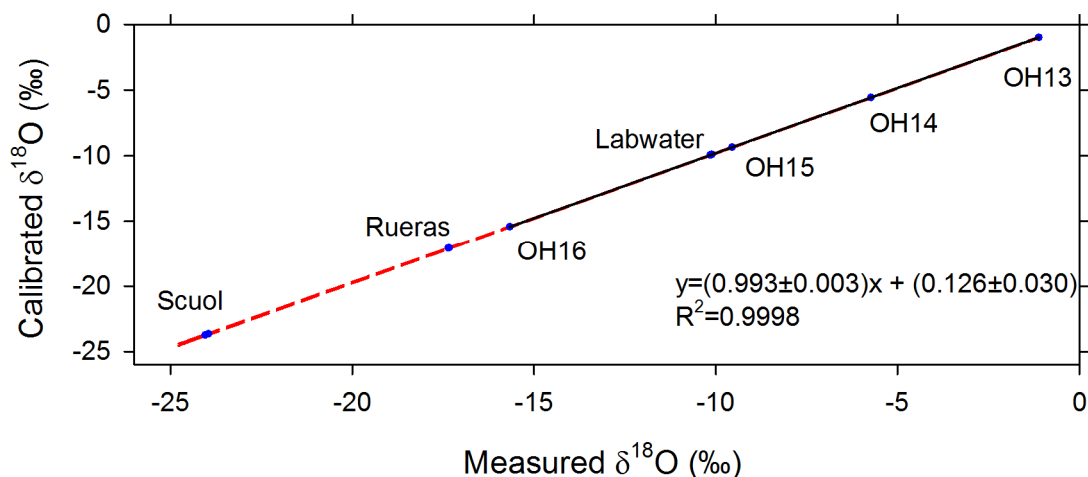

Figure 11 Calibration line (black) obtained from the four WICO standards for the first calibration run. The dashed red lines show prediction bound at 1σ level. The values for Rueras and Scuol are extrapolated from the fit. The standard error of the estimate resulted to be 0.03, not visible at this scale.

The weighted average of the remaining data was used to assess the final calibrated values. For the weights the quantity $1/s^2$ was used, where s^2 was the prediction bound (1σ level) obtained for the sample. This way it was attributed less weight to those measurements that resulted less predictable. The values obtained are shown in Table 5.

The $\delta^{18}O/\delta D$ relationship derived from these values is $\delta D=(8.00\pm0.16)\delta^{18}O+(10.17\pm2.79)$, with a $R^2=0.998$. This result is in agreement with the GMWL obtained by Rozanski et al. (1992) for the long-term annual means: $\delta D=(8.20\pm0.07)\delta^{18}O+(11.27\pm0.65)$.

Name	$\delta^{18}O$ (‰)	δD (‰)
Scuol1	-23.77±0.03	-181.0±0.3
Scuol2	-23.77±0.03	-181.6±0.3
Rueras1	-17.08±0.02	-124.2±0.2
Rueras2	-17.10±0.02	-124.0±0.2
Labwater1	-9.96±0.02	-70.8±0.2
Labwater2	-9.93±0.02	-70.4±0.2

Table 5 Final isotopic values of the internal laboratory standards obtained from the calibration procedure and subsequent weighted averaging. The uncertainties given here were

calculated as the error on the weighted mean, $1/S$, where $S=\Sigma(1/s_i)$ and $i=1,\ldots12$ (the number of the calibration runs utilized). The two values of each standard are compatible within the uncertainties.

3.3.5 Measurement protocol and instrument performance

Here a brief description of the samples preparation and of the evaluation procedure is presented. The samples are obtained by cutting ice. The water obtained from melting the ice samples is transferred into 2 mL vials via pipette and the vials are sealed with caps. No filtering is needed for the stable isotopes measurements. The storage at very low temperatures (-20°C) is suggested to prevent additional fractionation.

For the evaluation of the samples a Microsoft Excel® worksheet is used. Prior to the measurement, the first standard (Scuol) is measured twice (12 injections) in order to reduce memory effects from the previous measurement. Each of the three standards is measured once (6 injections) in the order Scuol-Rueras-Labwater every 10 samples to monitor the drift. The throughput is 20 samples/day, which is lower compared to 60 samples/day achievable with the IRMS. One run can range from 20 samples up to 70 samples depending on the users' needs. Longer measurements are discouraged because of strong drifts and possible instabilities that might arise. The data are saved as .csv files and imported into a Microsoft Excel® file where a series of automatic evaluations is done. The water content of each injection should be always plotted as well as the Data Acquisition System (DAS) temperature in order to see whether there are instabilities. The DAS temperature usually ranges between 40 and 45°C. It was noticed that it tends to oscillate following the diurnal cycle of temperature, with excursions in the order of 1-2°C. In winter it follows the heating system cycle of the laboratory with a peak at around 17:00 and a minimum at 5:00. Outliers in the measurement might be revealed by jumps in the DAS temperature or strong trends. The standard deviation of the last three injections is automatically evaluated in the worksheet where it is immediately possible to verify whether there are measurements exceeding the thresholds established for $\delta^{18}O$ and δD. Plots of the trends of the uncalibrated standards (Labwater, Rueras and Scuol) are generated in order to see whether there are outliers in the measurements. If this is not the case, the calibration is done using the first measurement of the three standards and evaluating the equation of the regression line. The goodness of the fit is assessed through the R^2. All the following samples are then calibrated against this regression line. This procedure differs from what is suggested by Picarro in the PostProcess tool, where a set of 10 samples is evaluated against the previous standards. It was thought that the several

calibrations performed for each set of 10 samples might have introduced discontinuities and therefore it was chosen to use only the first set of standards for the calibration and if necessary to correct for drift secondly. The evaluation of the drift is done by both checking the plotted standards values against time and, if a trend is present, estimating the difference between the lowest and the highest value. If the difference is larger than the analytical uncertainty, as most of the times (indicating also that the major source of uncertainty is given by the drift), a correction is performed.

The reference value for the drift correction is Rueras because it represents intermediate isotopic values. A linear regression is done based on the Rueras standards and the estimated drift is therefore subtracted from all the samples. Usually trends involve all the standards (perhaps with different amplitudes), however it is always suggested to check case by case. In some measurements a drift was detected in the $\delta^{18}O$ values but not in the δD. After the trend correction, a final check of the uncalibrated, calibrated and drift corrected data is done evaluating the average and standard deviation of the final values obtained from the three standards. This way it is possible to monitor the quality of the calibration and correction for each isotopic standard.

Another possibility for the evaluation of the data was proposed by Gröning (2011). In a Microsoft Excel® spreadsheet it is possible to upload the measurements and perform an automatic evaluation procedure similar to what was presented previously. This spreadsheet accounts for different measurement techniques and includes calibration and drift correction. For the memory effect, a special correction including all the injections is used attributing less weight to the first measurements so that it is not necessary to exclude the first injections. This tool might be used in parallel for checking quality of the two evaluation procedures.

The stability of the instrument performance was characterized evaluating the analytical reproducibility over the period April 2012 - January 2013. The three internal laboratory standards Scuol, Rueras and Labwater were selected in order to characterize possible variations of the reproducibility dependent on the isotopic value. Each of the $\delta^{18}O$ and δD values listed in Tables 6 and 7 was extracted from the second measurement block of the three standards, i.e. after the first 10 samples according to the measurement protocol. This block of standards is not used to obtain the calibration curve but instead treated like a block of samples. Therefore the final values contain all the uncertainties due to calibration, correction for memory and drift. The analytical reproducibility can then be defined as the standard deviation of the values obtained from independent measurement series shown in Tables 6 and

7 (twelve different days). The data indicate the high degree of stability of the measurements (Figure 12).

For the three isotopic values the retrieved reproducibility is <0.11‰ and <0.4‰ for δ^{18}O and δD, respectively. This is in good agreement with the analytical uncertainty estimate of 0.1‰ and 0.5‰ given in section 3.3.3. The obtained mean for the individual standards is not different from the reference value (Table 5) within the given analytical uncertainty, which is further indicating that those estimates are reasonable.

	δ^{18}O (‰)					
Date	Scuol1	$\sigma_{\text{4th-6th inj.}}$	Rueras1	$\sigma_{\text{4th-6th inj.}}$	Labwater1	$\sigma_{\text{4th-6th inj.}}$
1) 04/04/2012	-23.69	0.02	-17.05	0.03	-9.89	0.01
2) 13/04/2012	-23.61	0.02	-17.07	0.02	-9.74	0.04
3) 23/04/2012	-23.51	0.04	-17.02	0.01	-9.92	0.01
4) 30/04/2012	-23.49	0.01	-17.04	0.02	-9.94	0.02
5) 07/05/2012	-23.70	0.02	-17.07	0.04	-9.90	0.03
6) 16/05/2012	-23.54	0.03	-17.05	0.02	-9.95	0.05
7) 21/05/2012	-23.71	0.02	-17.07	0.03	-9.92	0.02
8) 30/05/2012	-23.88	0.02	-17.05	0.02	-10.06	0.03
9) 26/06/2012	-23.78	0.02	-17.08	<0.005	-9.91	0.04
10) 13/08/2012	-23.70	<0.005	-17.05	0.01	-9.94	0.01
11) 14/12/2012	-23.61	0.02	-17.15	0.03	-9.99	0.03
12) 25/01/2013	-23.72	0.02	-17.09	<0.005	-9.91	0.02
Mean (‰)	-23.66		-17.07		-9.92	
σ (‰)	0.11		0.03		0.07	

Table 6 δ^{18}O from Scuol1, Rueras1 and Labwater1 samples measured during the period April 2012 - January 2013, together with the the analytical precision given as the standard deviation of the last three injections. The calibrated δ^{18}O was corrected for drift and memory. Mean and reproducibility are shown in the last two rows.

	δD (‰)					
Date	Scuol1	$\sigma_{\text{4th-6th inj.}}$	Rueras1	$\sigma_{\text{4th-6th inj.}}$	Labwater1	$\sigma_{\text{4th-6th inj.}}$
1) 04/04/2012	-181.0	0.2	-124.1	0.2	-70.7	0.1
2) 13/04/2012	-180.2	0.2	-124.0	0.1	-70.7	<0.05
3) 23/04/2012	-180.3	0.2	-123.8	<0.05	-71.0	0.1
4) 30/04/2012	-180.1	0.2	-123.9	0.1	-71.0	0.2
5) 07/05/2012	-181.3	0.2	-124.3	0.1	-71.3	0.2
6) 16/05/2012	-180.5	0.2	-124.1	<0.05	-71.3	0.3
7) 21/05/2012	-181.3	0.2	-124.3	0.2	-71.1	0.2
8) 30/05/2012	-180.9	0.2	-123.4	<0.05	-70.6	0.2
9) 26/06/2012	-181.1	0.2	-124.1	0.2	-71.1	0.2
10) 13/08/2012	-180.9	0.2	-124.1	0.1	-71.3	0.1
11) 14/12/2012	-180.8	0.2	-124.3	0.1	-71.1	0.2
12) 25/01/2013	-181.3	0.2	-124.2	0.1	-71.1	0.2
Mean (‰)	-180.8		-124.1		-71.0	
σ (‰)	0.4		0.3		0.2	

Table 7 δD from Scuol1, Rueras1 and Labwater1 samples measured during the period April 2012 - January 2013, together with the the analytical precision given as the standard deviation of the last three injections. The calibrated δD was corrected for drift and memory. Mean and reproducibility are shown in the last two rows.
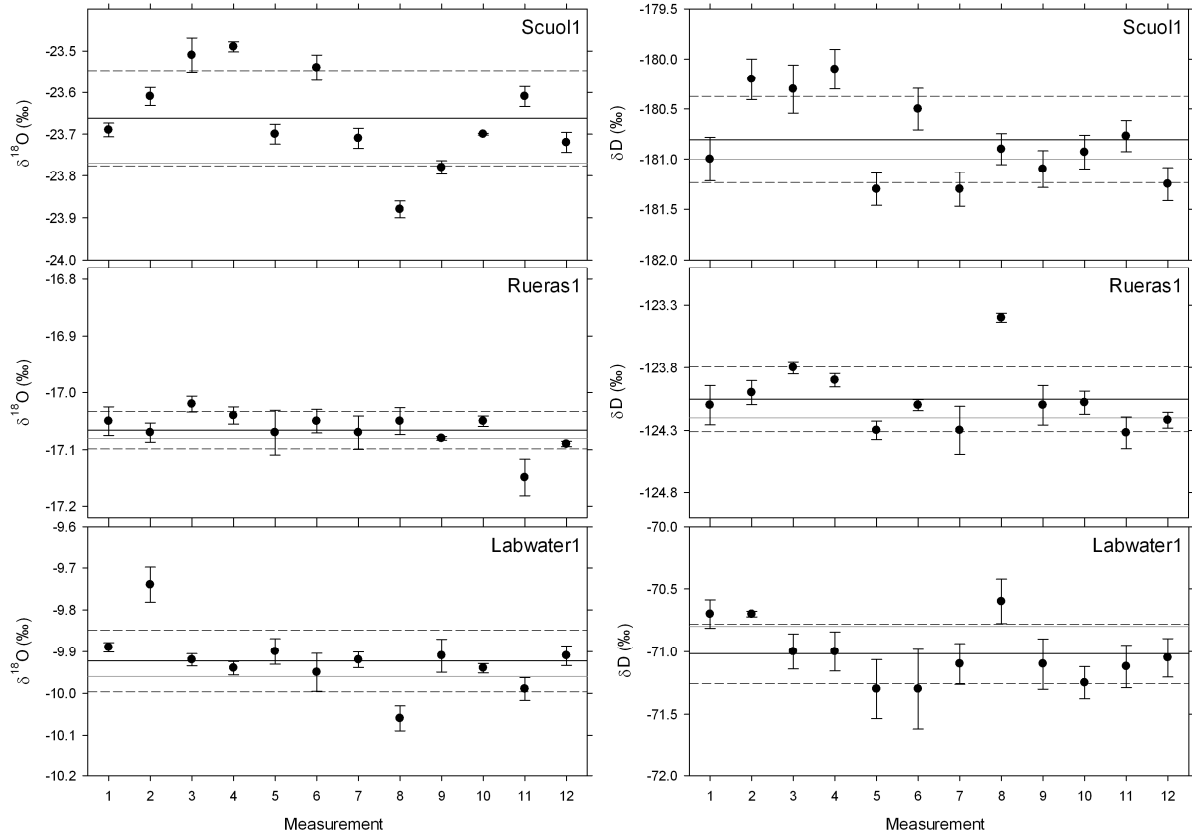
Figure 12 $\delta^{18}O$ (left) and δD (right) from Scuol1, Rueras1 and Labwater1 samples measured during the period April 2012 - January 2013, together with their analytical precision given as the standard deviation of the last three injections (Tables 6 and 7). The mean of the twelve values is indicated with a solid black line, the reproducibility ($\pm 1\sigma$) with dashed lines and the reference values of Table 5 are shown with a gray line.

3.4 Measurement of $\delta^{18}O$ and δD in Grenzgletscher ice core samples

After the calibration procedure was completed it was possible to start measuring $\delta^{18}O$ and δD in samples of the Grenzgletscher ice core. The cutting was done following the dating given in (Eichler et al., 2000). Knowing the time scale, it was possible to select the samples thickness for each core in such a way to get on average 20 samples per year, distributed in an equidistant way. A gap covering approximately the years 1968-1970 is due to the loss of three ice core sections (number B157-B159), that were melted because of a failure in the cold room cooling system. With respect to the previous sampling, it was possible to cut also the section B156, consisting of several chips, covering approximately the second half of the year 1969. The number of samples prepared for this period, covering 100 ice core sections of length 50-55 cm, was finally 523. The samples were melted, 1 mL was transferred into 2 mL vials which were sealed with caps with rubber/PTFE septa (Infochroma, model G003-AC-Ru/Te). The vials were then stored at a temperature of -20° C until analysis.

3.4.1 Comparison of $\delta^{18}O$ measurements with WS-CRDS and IRMS

As explained beforehand, $\delta^{18}O$ from the second set of Grenzgletscher samples was measured in spring 2011 with an IRMS (pyrolysis technique) in the Ecosystems Fluxes Group, LAC at the Paul Scherrer Institut. The measurements of both $\delta^{18}O$ and δD of the same samples were performed with the WS-CRDS, installed in December 2011. This way it was possible to obtain a comparison of the measurements of the $\delta^{18}O$ with two different instruments.

The comparison between the measurements made with the IRMS and with WS-CRDS is shown in Figure 13. They are plotted against the section number. This way it was possible to compare the results with the previous measurements performed by Eichler et al. (2000), where a different sampling resolution was adopted (see below). The general agreement between the IRMS and the WS-CRDS measurements is very good, with a standard deviation of the residuals (root mean square error, RMSE) of 0.3‰ and discrepancies of 0.2‰ on average (mean of the absolute values), within the analytical uncertainties of the two instruments. More generally, the values oscillate between -0.5‰ and +0.5‰ (Figure 13 middle and lower panel). The Pearson correlation coefficient resulted to be 0.996 (p<0.001). There are however several values between the section 120 and section 140 that show systematically higher discrepancies (up to +2‰). This would mean that somehow those samples resulted enriched when measured with the WS-CRDS spectrometer. Probably those samples encountered some isotopic

exchange during the storage period (one year). This might be due to no proper closing of the caps or exchange with the air because of the hole in the cap produced by the needle.

Another comparison was done with the results obtained from the previous sampling by Eichler et al. (2000). In that case the $\delta^{18}O$ was measured with a CO_2 equilibration technique. The analytical uncertainty was estimated to be <0.1‰ (Table 1 and Eichler et al., 2000). Figures 14 and 15 show the comparison of this technique with the WS-CRDS and IRMS (pyrolysis), respectively. For the discrepancies plot the mean $\delta^{18}O$ for each section was evaluated averaging all the points belonging to the section.

In both cases the values are significantly correlated, with a Pearson correlation coefficient of 0.84 (p<0.001) for the comparison with WS-CRDS and 0.85 (p<0.001) with pyrolysis-IRMS measurements ($\delta^{18}O$ averaged over the section). The discrepancies show a mean value of -0.52‰ and -0.40‰ for the first (Figure 14) and second (Figure 15) comparison, respectively, indicating an offset between the two measurements, with isotopically lighter values in Eichler et al. (2000). The RMSE evaluated regressing linearly the WS-CRDS on the IRMS (CO_2 equilibration) and the two IRMS techniques (pyrolysis against CO_2 equilibration) was in both cases 1.9‰, indicating lower agreement between the datasets when considering the averages over the sections.
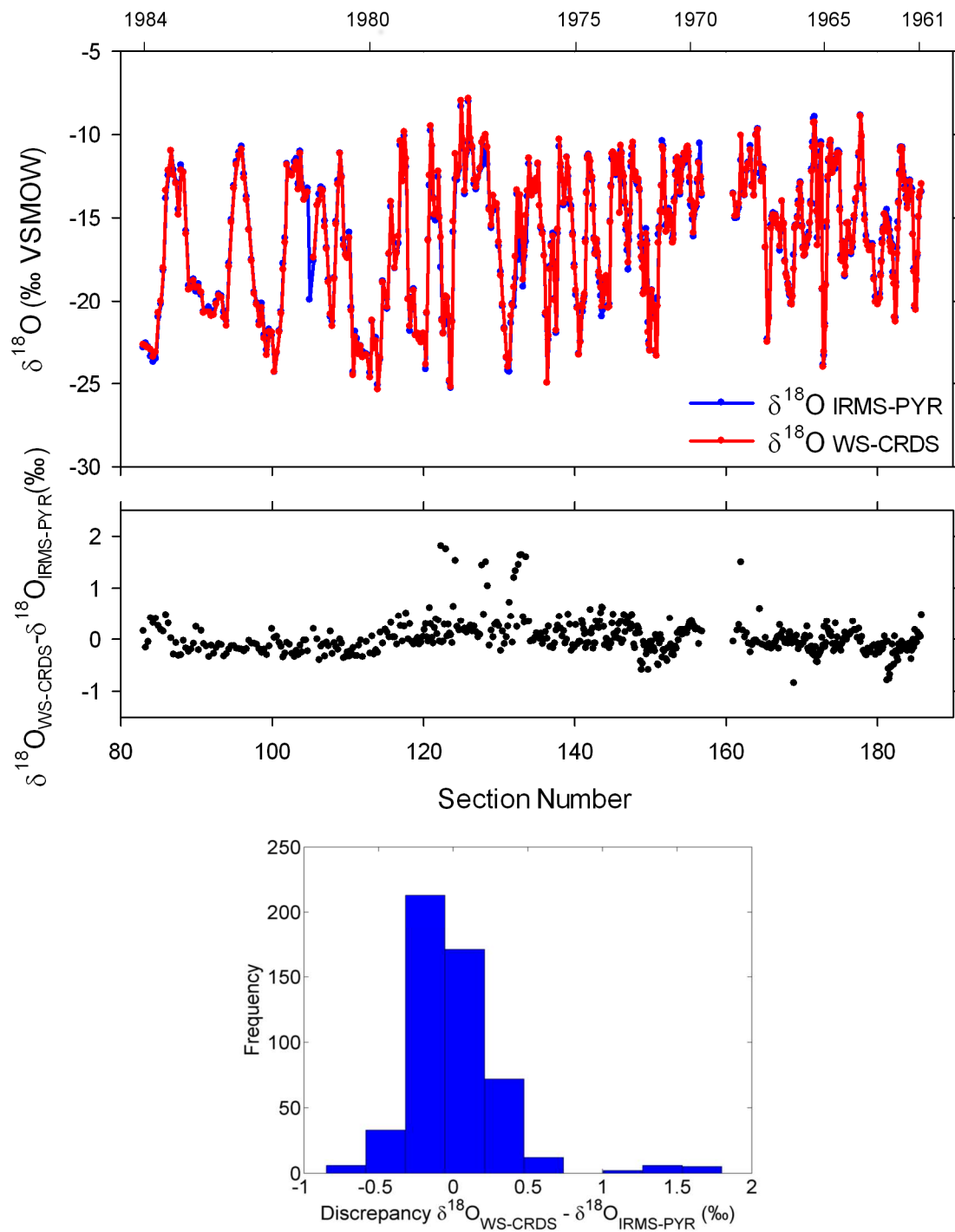
Figure 13 Grenzgletscher $\delta^{18}O$ measured with the IRMS (pyrolysys technique, IRMS-PYR, blue) and WS-CRDS (red). (Upper panel) Raw data. (Middle panel) Discrepancy plot of $\delta^{18}O_{WS-CRDS} - \delta^{18}O_{IRMS-PYR}$. Note that the time axis on top is not linear due to the different number of samples per year. For the complete dating of the Grenzgletscher ice core, see (Eichler et al., 2000) and Chapter 4. (Lower panel) Frequency histogram of the discrepancies.
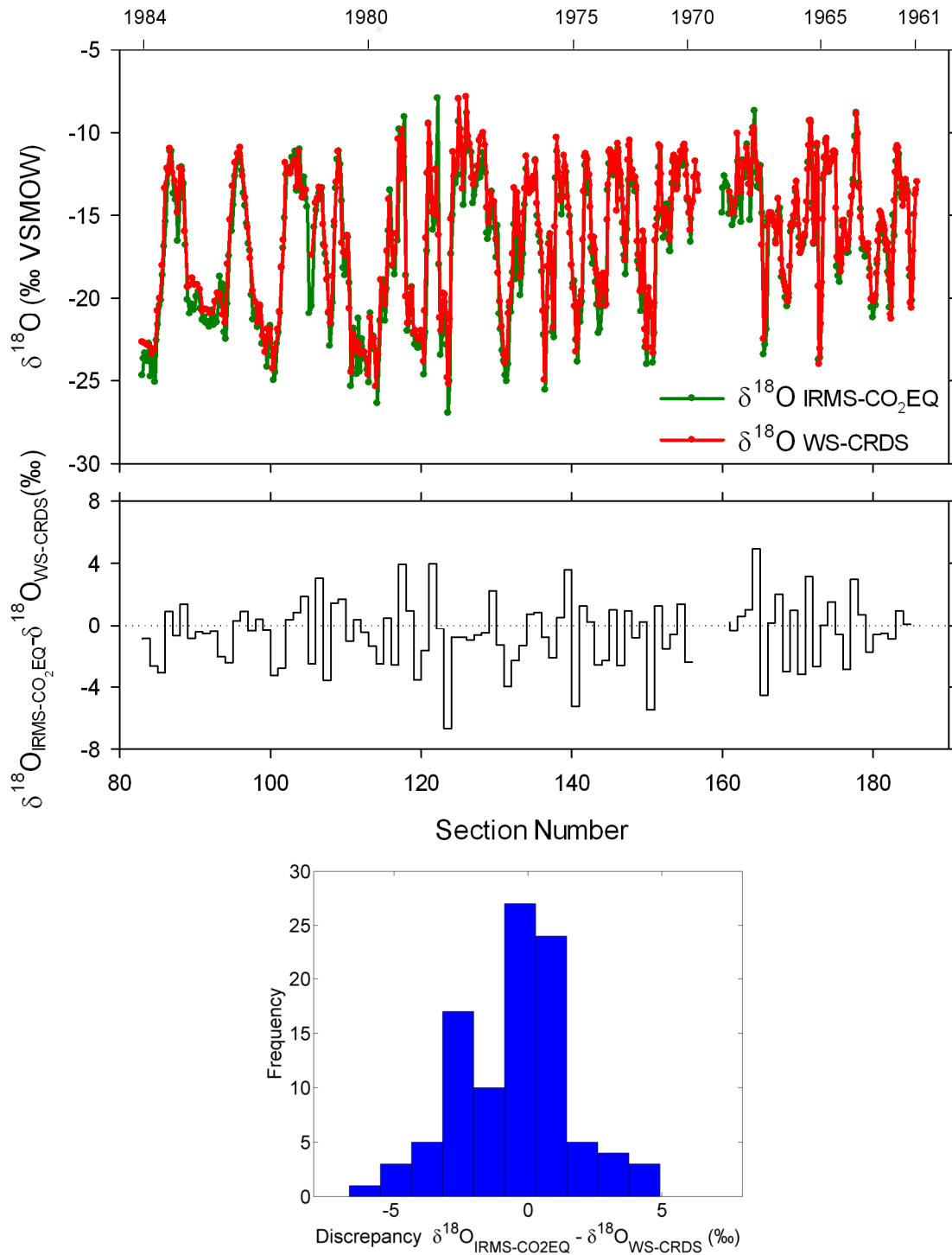
Figure 14 Grenzgletscher $\delta^{18}O$ measured with IRMS (CO_2 equilibration technique, Eichler et al., 2000, green) and WS-CRDS (red). (Upper panel) Raw data. (Middle panel) Discrepancy plot of $\delta^{18}O_{IRMS-CO2EQ}$ - $\delta^{18}O_{WS-CRDS}$ where the $\delta^{18}O$ is the average over the section. The dotted line indicates zero. Note that the time axis on top is not linear due to the different number of samples per year. (Lower panel) Frequency histogram of the discrepancies.
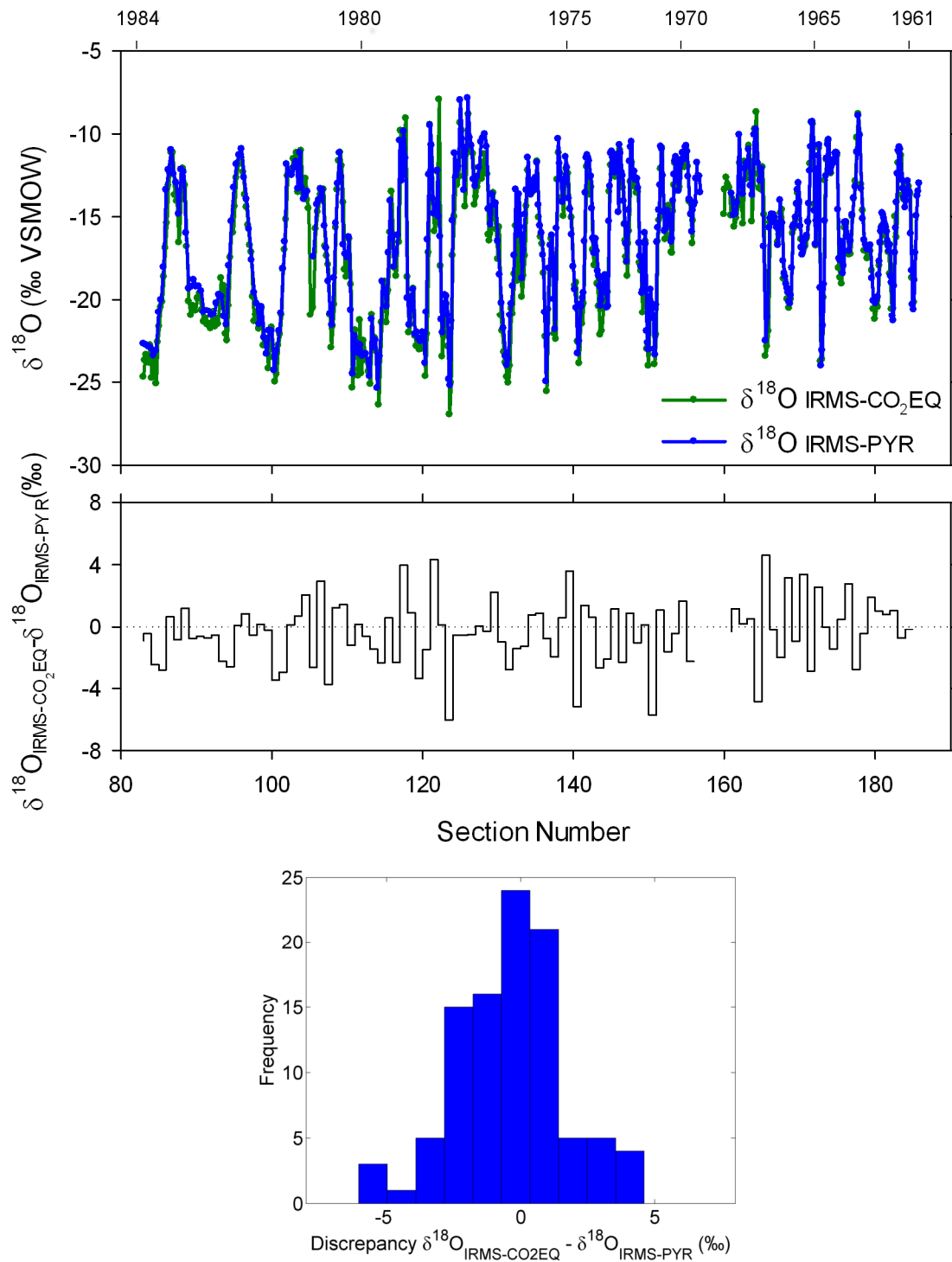
Figure 15 Grenzgletscher $\delta^{18}O$ measured with IRMS (CO_2 equilibration technique, Eichler et al., 2000, green) and IRMS (pyrolysis technique, blue). (Upper panel) Raw data. (Middle panel) Discrepancy plot of $\delta^{18}O_{IRMS-CO2EQ} - \delta^{18}O_{IRMS-PYR}$ where the $\delta^{18}O$ is the average over the section. The dotted line indicates zero. Note that the time axis on top is not linear due to the different number of samples per year. (Lower panel) Frequency histogram of the discrepancies.

3.4.2 Deuterium excess

Figure 16 shows the complete record of $\delta^{18}O$ and deuterium excess measured with the WS-CRDS. The analytical uncertainty of the deuterium excess data is evaluated propagating the uncertainty of both $\delta^{18}O$ and δD. It results to be $(0.1^2+0.5^2)^{1/2} \approx 0.5‰$. Contrarily to the $\delta^{18}O$, the deuterium excess does not show any particular seasonal cycle and the record is affected by high frequency fluctuations.
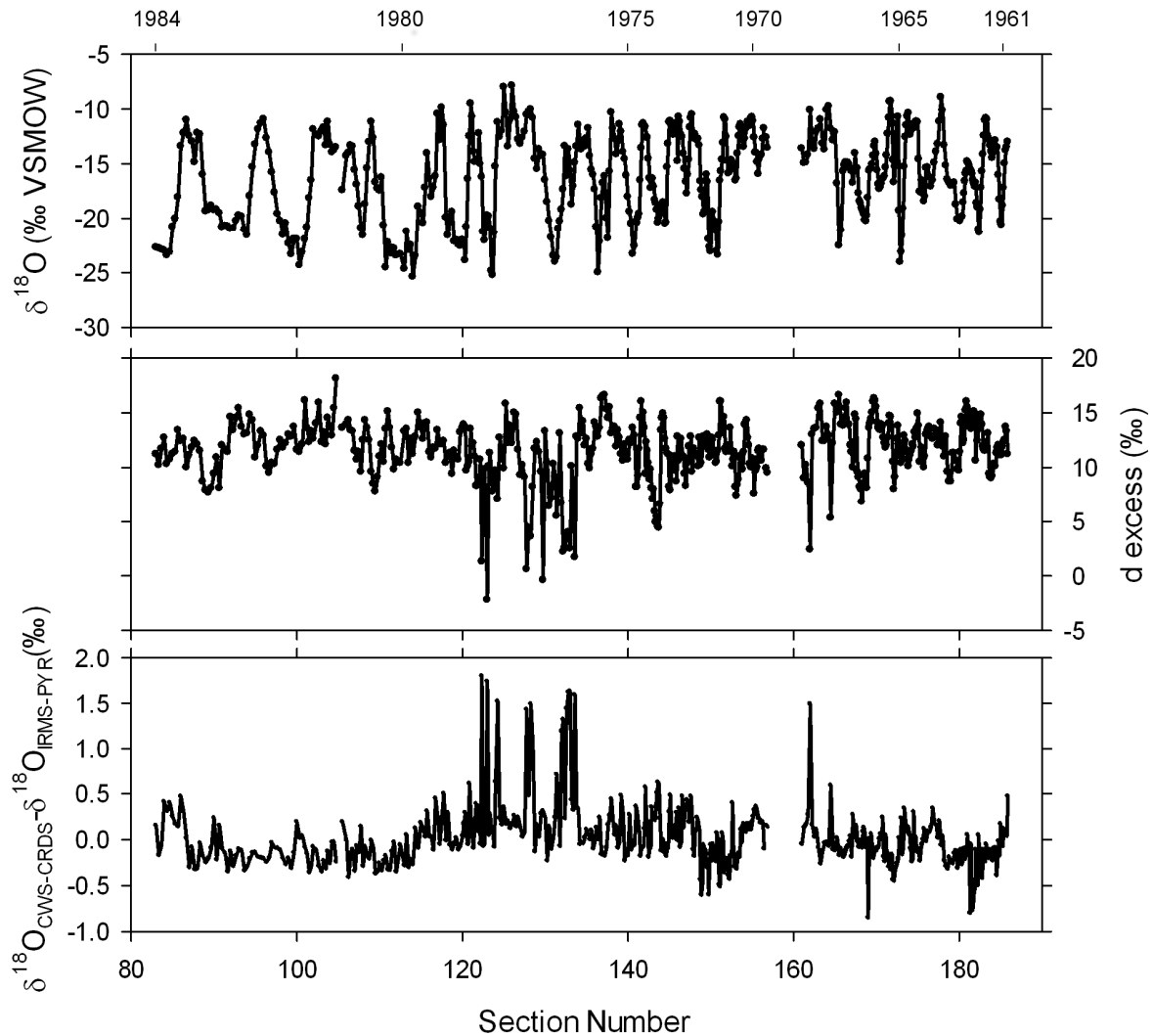

Figure 16 (Upper panel) $\delta^{18}O$ (Middle panel) deuterium excess raw data measured with WS-CRDS. (Lower panel) Discrepancy plot as in Figure 13.

Notably, samples with extremely low deuterium excess also showed the highest discrepancies of the $\delta^{18}O$ measurements with the IRMS. This result seems to confirm that between the first measurement in 2011 and the second one in 2012 for those samples an additional fractionation occurred, most likely due to evaporation from the vial and subsequent enrichment in the $\delta^{18}O$ and decrease in the deuterium excess.

Finally a qualitative comparison with the deuterium excess obtained with CO_2 equilibration ($\delta^{18}O$) and chromium reduction (δD) is shown in Figure 17. The analytical uncertainty of δD was 0.5‰, resulting in an uncertainty for the deuterium excess of ≈0.5‰.

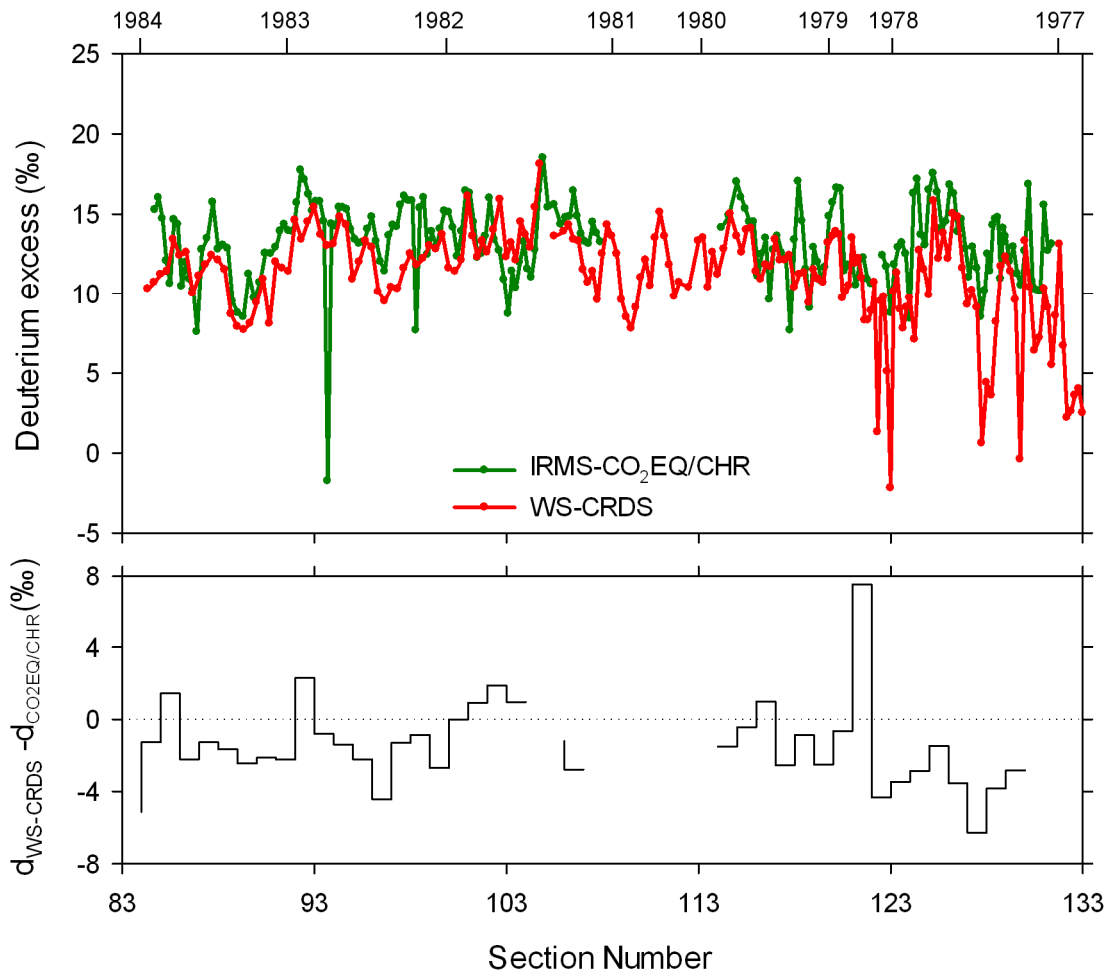**Figure 17** Grenzgletscher deuterium excess retrieved from IRMS with CO_2 equilibration ($\delta^{18}O$) and chromium reduction technique (δD) in green and from WS-CRDS ($\delta^{18}O$ and δD). (Upper panel) Deuterium excess (d) raw data. (Lower panel) Discrepancy plot of $d_{WS-CRDS}$-$d_{IRMS-CO2EQ/CHR}$. Note that the time axis on top is not linear due to the different number of samples per year.

Excluding the part where evaporation occurred in the vials (~1977-1979) the raw data show, except few sparse outliers, that there is a good agreement in the trend, whereas the comparison of the mean values for each core reveals higher discrepancies. This is due to the influence of single point-to-point discrepancies in the averaging process.

3.5 Conclusions and outlook

The WS-CRDS laser spectrometer installed in the Analytical Chemistry Group at the Paul Scherrer Institut was characterized in terms of memory, drift and analytical uncertainty. The calibration of the internal laboratory standards was done considering the typical isotopic range in the Alpine ice cores. The measurement of the ice core samples coming from the Grenzgletscher was performed and was useful in assessing the discrepancies with two measurements previously done, with a pyrolysis-IRMS (same sampling) and with a CO_2 equilibration-IRMS technique (first sampling, Eichler et al., 2000). Results showed a good agreement within the analytical uncertainties of the measurements, although some samples likely experiences evaporation with consequent enrichment in the $\delta^{18}O$. A confirmation of that was obtained from the deuterium excess values, showing accordingly lower values. Compared to the short record of deuterium excess obtained by Eichler et al. (2000), the values measured with WS-CRDS show a good agreement in the trend, whereas the point-to point discrepancies introduce significant differences when comparing the mean core values. The developed method resulted to provide high quality data.

References

Ahmad, M., Aggarwal, P., Duren, M. van, Poltenstein, L., Araguas, L., Kurttas, T. and Wassenaar, L. I.: Final Report on Fourth interlaboratory comparison exercise for δD and δ^{18}O analysis of water samples (WICO2011), 2012.

Busch, K. W. and Busch, M. A.: Introduction to Cavity-Ringdown Spectroscopy, in Cavity-Ringdown Spectroscopy, vol. 720, pp. 7–19, American Chemical Society, 1999.

Craig, H.: Isotopic variations in meteoric waters, Science, 133, 1702–1703, doi:10.1126/science.133.3465.1702, 1961.

Eichler, A., Schwikowski, M., Gäggeler, H. W., Furrer, V., Synal, H.-A., Beer, J., Saurer, M. and Funk, M.: Glaciochemical dating of an ice core from upper Grenzgletscher (4200 m a.s.l.), Journal Glaciol., 46(154), 507–515, doi:10.3189/172756500781833098, 2000.

Eichler, A., Schwikowski, M. and Gäggeler, H. W.: Meltwater-induced relocation of chemical species in Alpine firn, Tellus B, 53(2), 192–203, doi:10.1034/j.1600-0889.2001.d01-15.x, 2001.

Epstein, S. and Mayeda, T.: Variation of O18 content of waters from natural sources, Geochim. Cosmochim. Acta, 4(5), 213–224, doi:10.1016/0016-7037(53)90051-9, 1953.

Gehre, M., Hoefling, R., Kowski, P. and Strauch, G.: Sample preparation device for quantitative hydrogen isotope analysis using chromium metal, Anal. Chem., 68(24), 4414–4417, doi:10.1021/ac9606766, 1996.

Gröning, M.: Improved water δ^2H and δ^{18}O calibration and calculation of measurement uncertainty using a simple software tool, Rapid Commun. Mass Sp., 25(19), 2711–2720, doi:10.1002/rcm.5074, 2011.

De Groot, P. A.: Handbook of Stable Isotope Analytical Techniques, Elsevier, 2004.

International Atomic Energy Agency (IAEA): Reference Sheet for International Measurement Standards. Available from: http://nucleus.iaea.org/rpst/Documents/VSMOW2_SLAP2.pdf (Accessed 10 August 2013), 2009.

Jenk, T. M.: Ice Core Based Reconstruction of Past Climate Conditions and Air Pollution in the Alps Using Radiocarbon, PhD thesis, Departement für Chemie und Biochemie, Univ. of Bern, Bern, Switzerland, 2006.

Kornexl, B. E., Gehre, M., Höfling, R. and Werner, R. A.: On-line δ^{18}O measurement of organic and inorganic substances, Rapid Commun. Mass Sp., 13(16), 1685–1693, doi:10.1002/(SICI)1097-0231(19990830)13:16<1685::AID-RCM699>3.0.CO;2-9, 1999.

Mook, W. G., Environmental Isotopes in the Hydrological Cycle: Principles and Applications, vol. I, Introduction: Theory, Methods, Review, Int. At. Energy Agency, U. N., Paris, 2000.

O'Keefe, A. and Deacon, D. A. G.: Cavity ring-down optical spectrometer for absorption measurements using pulsed laser sources, Rev.Scient. Instr., 59(12), 2544–2551, doi:doi:10.1063/1.1139895, 1988.

Paul, J. B. and Saykally, R. J.: Cavity Ringdown Laser Absorption Spectroscopy, Anal. Chem., 69(9), 287A–292A, doi:10.1021/ac971622e, 1997.

Platzner, I.T., Modern Isotope Ratio Mass Spectrometry, Wiley, Chichester, 514 pp., 1997.

Rozanski, K., Araguas-Araguas, L. and Gonfiantini, R.: Relation between long-term trends of oxygen-18 isotope composition of precipitation and climate, Science, 258, 981–985, doi:10.1126/science.258.5084.981, 1992.

Rozanski, K., Araguás-Araguás, L. and Gonfiantini, R.: Isotopic patterns in modern global precipitation, in Geophysical Monograph Series, vol. 78, edited by P. K. Swart, K. C. Lohmann, J. McKenzie, and S. Savin, pp. 1–36, American Geophysical Union, Washington, D. C., 1993.

Saurer, M. and Siegwolf, R.: Pyrolysis techniques for oxygen isotope analysis of cellulose, in Handbook of stable isotope analytical techniques, vol. 1, Elsevier, 2004.

Schwikowski, M., Brütsch, S., Gäggeler, H. W. and Schotterer, U.: A high-resolution air chemistry record from an Alpine ice core: Fiescherhorn glacier, Swiss Alps, J. Geophys. Res., 104(D11), 13709–13,719, doi:10.1029/1998JD100112, 1999.

4 Temperature and precipitation signal in two Alpine ice cores over the period 1961-2001

I. Mariani[1,2], A. Eichler[1,2], T.M. Jenk[1,2,3], S. Brönnimann[2,4], R. Auchmann[2,4], M.C. Leuenberger[2,5], and M. Schwikowski[1,2,6]

(1){Paul Scherrer Institut, Villigen, Switzerland}

(2){Oeschger Centre for Climate Change Research, University of Bern, Bern, Switzerland}

(3){Centre for Ice and Climate, Niels Bohr Institute, Copenhagen University, Copenhagen, Denmark}

(4){Institute of Geography, University of Bern, Bern, Switzerland}

(5){Physics Institute, University of Bern, Bern, Switzerland}

(6){Department of Chemistry and Biochemistry, University of Bern, Bern, Switzerland}

Correspondence to: M. Schwikowski (margit.schwikowski@psi.ch)

Abstract

Water stable isotope ratios and net snow accumulation in ice cores are commonly interpreted as temperature or precipitation proxies. However, only in a few cases a direct calibration with instrumental data has been attempted. In this study we took advantage of the dense network of observations in the European Alpine region to rigorously test the relationship of the annual and seasonal resolved proxy data from two highly-resolved ice cores with local temperature and precipitation. We focused on the time period 1961-2001 with the highest amount and quality of meteorological data and the minimal uncertainty in ice core dating (± 1 year). The two ice cores were retrieved from the Fiescherhorn glacier (Northern Alps, 3900 m a.s.l.), and Grenzgletscher (Southern Alps, 4200 m a.s.l.). A parallel core from the Fiescherhorn glacier allowed assessing the reproducibility of the ice core proxy data. Due to the orographic barrier, the two flanks of the Alpine chain are affected by distinct patterns of precipitation. The different location of the two glaciers therefore offers a unique opportunity to test if such a specific setting is reflected in the proxy data. On a seasonal scale a high fraction of $\delta^{18}O$ variability was explained by the seasonal cycle of temperature (~60% for the ice cores, ~70% for the nearby stations of the Global Network of Isotopes in Precipitation (GNIP)). When the

seasonality is removed, the correlations decrease for all sites indicating that factors other than temperature such as changing moisture sources and/or precipitation regimes affect the isotopic signal on this timescale. Post-depositional phenomena may additionally modify the ice core data. On an annual scale, the δ^{18}O/temperature relationship was significant at the Fiescherhorn, whereas for Grenzgletscher this was the case only when weighting the temperature with precipitation. In both cases the fraction of interannual temperature variability explained was ~20%, comparable to the values obtained from the GNIP stations data. Consistently with previous studies, we found an altitude effect for the δ^{18}O of -0.17‰/100 m for an extended elevation range combining data of the two ice core sites and four GNIP stations. Significant correlations between net accumulation and precipitation were observed for Grenzgletscher during the entire period of investigation, whereas for Fiescherhorn this was the case only for the less recent period (1961-1977). Local phenomena, probably related to wind, seem to partly disturb the Fiescherhorn accumulation record. Spatial correlation analysis shows the two glaciers to be influenced by different precipitation regimes, with the Grenzgletscher reflecting the characteristic precipitation regime south of the Alps and the Fiescherhorn accumulation showing a pattern more closely linked to northern Alpine stations.

4.1 Introduction

The stable isotopes ratios in meteoric water ($^{18}O/^{16}O$ and, similarly $^2H/^1H$, not discussed in this paper) are widely used as temperature proxies (Craig, 1961; Dansgaard, 1964). Commonly these ratios are reported in the delta notation ($\delta^{18}O$ and δ^2H or δD) with δ denoting the deviation from an international reference standard (e.g. VSMOW, Vienna Standard Mean Ocean Water) in per mil (‰).

To a first approximation, $\delta^{18}O$ in meteoric water can be considered as a proxy for the condensation temperature in the cloud with its variation within the water cycle described by the Rayleigh distillation model. The heavy isotopologues preferentially condense with respect to the lighter ones and progressive distillation occurs as the air mass loses moisture through precipitation (Dansgaard, 1964). The primary microphysical processes affecting this proxy within the water cycle (equilibrium and non-equilibrium fractionations) are known and can be quantified (Dansgaard, 1964; Jouzel and Merlivat, 1984; Ciais and Jouzel, 1994; Gat, 1996; Araguás-Araguás et al., 2000). However, several factors may change the isotopic signal before, during and after the precipitation event. For instance, sub-cloud processes such as exchange and re-evaporation may lead to additional fractionation, leaving an imprint in both, raindrops and remaining vapor (Friedman et al., 1962; Risi et al., 2008; Field et al., 2010).These secondary processes however do not affect solid precipitation in the form of snow (Friedman et al., 1962; Field et al., 2010).

Besides the microphysical processes, changes of the moisture sources may additionally affect the isotopic signal (Rozanski et al., 1993). Precipitation intermittency (Casado et al., 2013) or seasonality (Perrson et al., 2011) may bias the $\delta^{18}O$ toward the season with more precipitation. In this case the $\delta^{18}O$ should be associated with the precipitation-weighted temperature than the mean temperature (Jouzel et al., 1997a; Kohn and Welker, 2005; Sturm et al., 2010). The interpretation of the $\delta^{18}O$ signal in natural archives may be further complicated in the case of ice cores, where post-depositional processes can lead to signal alteration (e.g. Stichler and Schotterer, 2000; Schotterer et al., 2004). These processes may involve melting and refreezing (Jouzel and Souchez, 1982), diffusion (Johnsen, 1977; Johnsen et al., 2000), snow removal by winds (Wagenbach et al., 1988; Schoener et al., 2002) and sublimation (Stichler et al., 2001).

In order to understand such a complex signal the $\delta^{18}O$ in precipitation can be investigated following different approaches: using (i) observational data from global precipitation collection networks such as the GNIP data set (IAEA/WMO, 2013), enabling $\delta^{18}O$/temperature ($\delta^{18}O$/T) calibrations for different regions in the world (Yurtsever and Gat,

1981; Rozanski et al., 1992, 1993), (ii) natural archives such as ice cores, tree rings and lake sediments (e.g. Bradley, 1999) which allow access to records exceeding the period of direct instrumental measurements, (iii) models to investigate the underlying physical processes such as simple Rayleigh distillation models (e.g. Jouzel et al., 1997b) or more complex atmospheric general circulation models (GCMs) allowing to track the water throughout the hydrological cycle, accounting also for other processes such as changing moisture sources, evaporation, and interaction with subcloud water (e.g. Ciais and Jouzel, 1994; Jouzel et al., 2000; Jouzel, 2003; Noone and Sturm, 2010). Meanwhile, several isotope-equipped GCMs are available and their output has recently been investigated through the Stable Water Isotope Intercomparison Group (SWING2) experiment (Sturm et al., 2010; Conroy et al., 2013).

In the European Alpine region and specifically in the Swiss area investigated in this study, the interpretation of the isotopic signal results particularly challenging due to a distinct topography, with the Alps acting as a divide between the Mediterranean and the European continental climate (Barry, 2008). The Northern Alps are dominated by the influence of North Atlantic air masses in winter and land evaporation in summer whereas the Southern Alps are characterized by higher intraseasonal precipitation variability and substantial contribution from the Mediterranean, especially in spring and autumn (Frei and Schär, 1998; Eichler et al., 2004; Sodemann and Zubler, 2009).

Common features in precipitation may be observed in winter under the influence of midlatitude cyclones arriving from the North Atlantic by means of intensified westerlies. Systems advected from the North or the South are also frequent (see e.g., Eichler et al., 2004; Barry, 2008). In this case, precipitation affects especially one flank, often accompanied by Foehn situations on the other side. In winter the prevailing directions of the cyclones are from the Northern and Western quadrants. As a consequence orographic precipitation over the Northern Alps and consequently Foehn over the Southern Alps is a common phenomenon. Similarly, atmospheric disturbances arriving from the southern quadrants especially in spring and autumn generate Foehn situations over the Northern Alps (Barry, 2008). It is nonetheless known that Foehn events are not always associated with precipitation over the other flank, as shown in Seibert (1989). Convective systems contribute to the whole region's precipitation as well, especially in summer (Frei and Schär, 1998; Eichler et al., 2004; Barry, 2008; Sodemann and Zubler, 2009). The resulting climatology is such that in general there is more precipitation over the Southern Alps, peaking in spring and autumn and less precipitation over the Northern Alps, with a large maximum in summer (Frei and Schär, 1998; Eichler et al., 2004; Sodemann and Zubler, 2009).

Both, GCMs and also higher resolved regional models are not able to spatially resolve the Alpine subregions affected by their characteristic precipitation regimes. However, an extended monitoring network exists over this area, and several studies have been conducted for the time where instrumental records are available (Siegenthaler and Oeschger, 1980; Rozanski et al., 1992; Schürch et al., 2003). The relation between altitude and change of the isotopic value as well as the δ^{18}O/T relation has been quantified, using the δ^{18}O data of the GNIP station network. A lapse rate of ~-0.2‰/100 m was obtained (Siegenthaler and Oeschger, 1980; Schürch et al., 2003) and generally higher long-term slopes compared to the rest of Europe were found (Rozanski et al., 1992). Because of the changes in moisture sources, the intraseasonal variability of precipitation is relatively high, especially on the Southern side where a mixture of sources originating from the North Atlantic Ocean, the Mediterranean region, the North Sea and Baltic Sea as well as from European land surface re-evaporation contribute to the total annual precipitation of a specific site (Sodemann and Zubler, 2009) and may thus significantly affect the δ^{18}O signal. Such an influence of changes in large-scale circulation patterns was observed in Alpine tree-rings (Saurer et al., 2012).

There is large potential offered by Alpine ice cores in terms of reconstructing past changes in the climate and the hydrological cycle, but a better understanding of the signal deposited on the glacier is needed. Some studies which combine instrumental and Alpine ice core data are available (e.g. Rozanski et al., 1997; Schotterer et al., 1997; Eichler et al., 2001; Sigl, 2009; Bohleber et al., 2013). Ice cores extracted from the Alps proofed to be valuable tools for the reconstruction of atmospheric pollutants and studies of their transport (e.g. Wagenbach et al., 1988; Schwikowski et al., 1999, 2004). However, as mentioned before, the interpretation of the isotopic signal is not straightforward. δ^{18}O records a signal only when snowfall occurs (Jouzel et al., 1997a; Sturm et al., 2010) and seasonality of precipitation and post-depositional effects can be very local phenomena, causing each high-altitude site to behave uniquely. Investigating the precipitation climatology near the glacier can thus provide fundamental information about the proxy deposition. Using the data from the Grenzgletscher ice core (also investigated in this study) Brönnimann et al. (2013) addressed the problem of irregular sampling of weather events by natural archives. A simple forward model was developed to replicate the ice core on a sample-by-sample basis from daily meteorological data, which well reproduced accumulation and δ^{18}O variations on a sub-seasonal scale over the most recent 15 years of the ice core record. The uncertainties induced by irregular sampling in the relation between ice-core proxies and mean climate were investigated with a new reconstruction method, a Monte Carlo re-sampling approach of long meteorological records. Low

correlations between annual mean temperature and precipitation-weighted temperature were obtained, as a given combination of $\delta^{18}O$ and accumulation can be achieved in many different ways.

Beside $\delta^{18}O$-derived temperatures, also reconstructions of past accumulation rates from mountain glaciers are available (Henderson et al., 2006; Schwerzmann et al., 2006; Herren et al., 2013). The reconstructed net accumulation can be regarded as precipitation proxy, considering few caveats. (i) In order to account for thinning effects, such reconstructions require an accurate description of the glacier ice flow by means of physical models. (ii) The glacier only records the net balance between what was deposited and what was removed during the year, e.g. by partial melting, wind erosion or sublimation. (iii) Precipitation at high-altitudes can be a very local phenomenon. In a region such as the Alps, characterized by high temporal and spatial variability of the climatic parameters, the interpretation of the net snow accumulation rate as a proxy for regional precipitation might thus be limited even in the case of negligible post-depositional effects.

In this study we focus on annually and sub-annually resolved records of $\delta^{18}O$ and net accumulation from two highly resolved ice cores from the Northern and the Southern Alps, in order to investigate whether and how the temperature and precipitation signals are captured at these sites with the final goal to improve the understanding of the ice core proxies $\delta^{18}O$ and net accumulation. We take advantage of the unique opportunity offered by the dense observation station network over this region. For this detailed study, we focus on the most recent decades (1961-2001), where amount and quality of the available instrumental data is highest and the dating uncertainty in the ice cores is minimal. In section 4.2 the datasets are described. The analysis of the $\delta^{18}O$/temperature and the accumulation/precipitation relationship is discussed in section 4.3 and conclusions and implications are presented in section 4.4.

4.2 Data

4.2.1 Ice core sites

In this study we investigate two Alpine ice cores, one from the Northern Alps (Fiescherhorn, FH) and the other from the Southern Alps (Grenzgletscher, GG), see Figure 1. From the Fiescherhorn glacier several ice cores have been collected (Schotterer et al., 1997; Schwikowski et al., 1999; Schotterer et al., 2002; Jenk, 2006). Here we mainly focus on the records from the core extracted in December 2002, reaching bedrock at a depth of 151 m (46º33'3.2" N, 8º04'0.4" E, 3900 m a.s.l., Jenk, 2006). Additionally the results from the core

recovered in 1989 are used to assess the reproducibility of the records (46°33'6.28" N, 8°04'4.02" E, 3900 m a.s.l., Schotterer et al., 1997; Schwikowski et al., 1999). The two drilling sites are 100 meters apart on an extended relatively flat accumulation area with a steep cliff to the North. The ice core from Grenzgletscher in the Southern Alps (Monte Rosa massif, 45°55'28" N, 7°52'3" E, 4200 m a.s.l.) was extracted in October 1994, reaching a depth of 125 m, Eichler et al., 2000, 2001). The drilling site is located in the accumulation area downstream of the Colle Gnifetti saddle, were many other ice core studies were conducted (e.g. Schotterer et al., 1985; Wagenbach et al., 1988; Schwikowski et al., 2004).
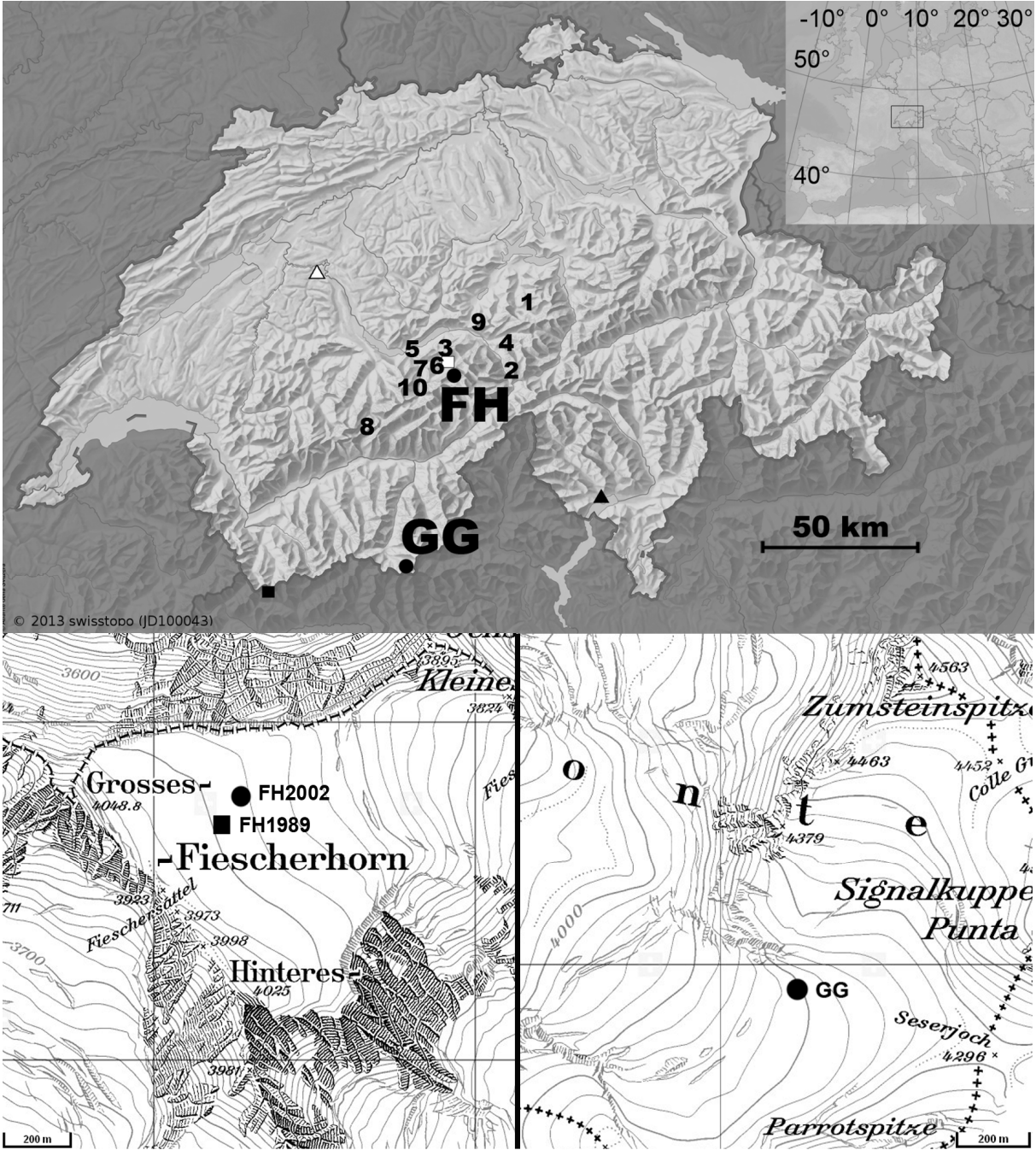
Figure 1. (Upper panel) Topographic map of Switzerland showing the position of the two glaciers, Fiescherhorn (FH), and Grenzgletscher (GG) (source: Atlas of Switzerland, http://www.atlasderschweiz.ch/), together with the location of Switzerland in Europe (insert). The numbers indicate the weather stations near the Fiescherhorn, according to Table 2. Engelberg (1), Grimsel Hospiz (2), Grindelwald (3), Guttannen (4), Interlaken (5), Kleine Scheidegg (6), Lauterbrunnen (7), Leukerbad (8), Meiringen (9), Mürren (10). Squares indicate the location of the Jungfraujoch (white) and Grand Saint Bernard (black) weather stations and the triangle the position of the low-altitude stations Bern (white) and Locarno (black). (Lower panels) Topographic map of the ice core drilling sites (source: Swisstopo, http://map.geo.admin.ch/). The left panel shows the location of the FH1989 and FH2002, the right panel shows the position of the Grenzgletscher drilling site (GG).

4.2.1.1 Dating of the ice cores

The dating of the ice cores was established with a multi-parametric approach involving:

- Annual layer counting of the seasonally varying signals, like $\delta^{18}O$ (see Figure 2) and concentration of NH_4^+, whose maxima correspond to summer and minima to winter (Schwikowski et al., 1999)

- Horizons indicated by spikes in the records of chemical species which correspond to well documented events: e.g., the Ca^{2+} maximum in 2000, 1977, 1990 as a tracer for a prominent Saharan dust fall (Schwikowski et al., 1995; Jenk, 2006, triangles in Figure 2), ^{137}Cs for the Chernobyl accident in 1986 (Schwikowski et al., 1999; Eichler et al., 2000, circles in Figure 2), ^{3}H with a peak in 1963 from thermonuclear bomb tests (Schwikowski et al., 1999; Eichler et al., 2000; Jenk, 2006, squares in Figure 2)

- Nuclear dating using ^{210}Pb (Eichler et al., 2000)

Due to the presence of stratigraphic markers and well preserved $\delta^{18}O$ seasonality (see Figure 3 and section 4.3.1.1) the resulting dating uncertainty for the period considered in this study is ±1 year for both ice cores. This value was empirically estimated as number of ambiguous annual layers that were attributed between the reference horizons. The Fiescherhorn core covers the time period from ~1680-2002 AD, and the Grenzgletscher core the period from ~1937-1994 AD. The latter has a gap in the data for the time period 1968-1970, due to bad core quality and a failure in the cooling system of the cold room with consequent melting of the corresponding ice core sections (Eichler et al., 2000). The FH1989 covers the period 1946-1989 AD, for further details see (Schotterer et al., 1997; Schwikowski et al., 1999).
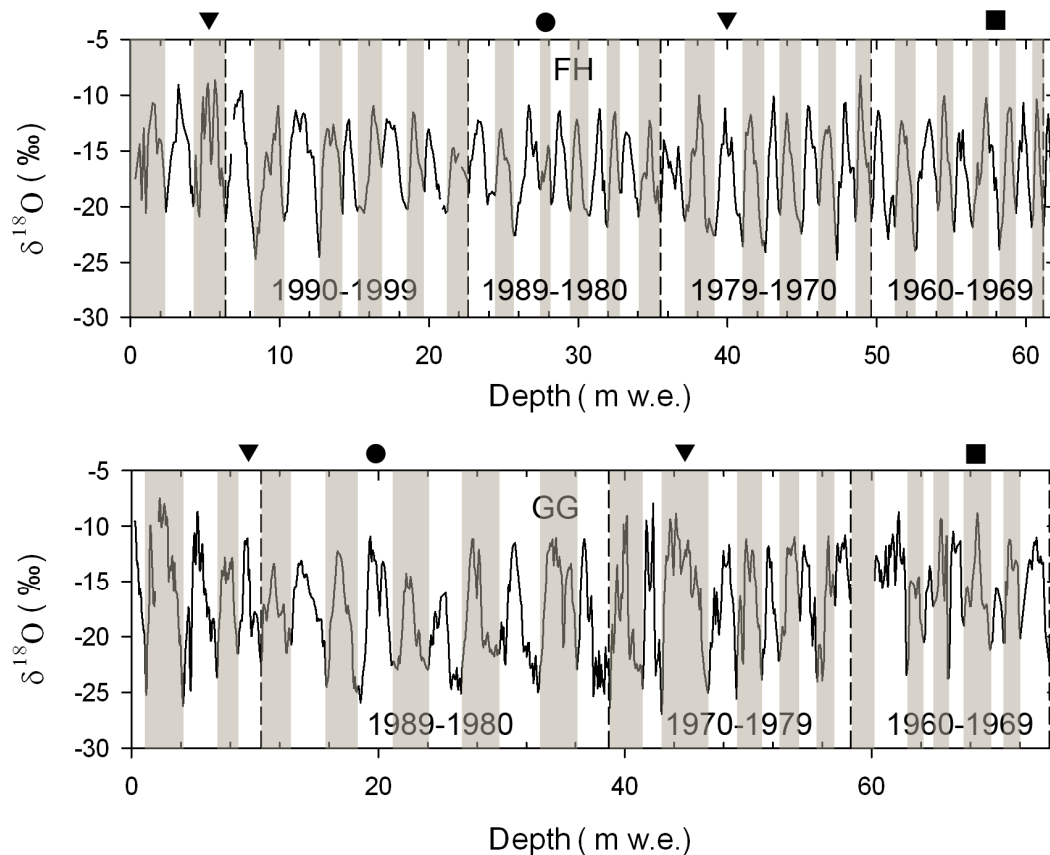
Figure 2. $\delta^{18}O$ raw data from Fiescherhorn core drilled in 2002 (FH, top, first 60 m w.e. corresponding to the period 1961-2001), and Grenzgletscher (GG, bottom, first 70 m w.e., corresponding to the period 1961-1993, with a gap in the period 1968-1970). White and gray alternating bars show the different annual layers. The reference horizons used for the dating are indicated as follows. Triangles: Saharan dust events (2000, 1990, 1977). Circles: Chernobyl accident in 1986. Squares: tritium peak in 1963. The stratigraphy of FH1989 was extensively described in (Schotterer et al., 1997; Schwikowski et al., 1999).

4.2.1.2 Ice core $\delta^{18}O$ data

The $\delta^{18}O$ in both ice cores was measured by Isotope Ratio Mass Spectrometry (IRMS) after CO_2 equilibration in the Climate and Environmental Physics group at the University of Bern, Switzerland for the Fiescherhorn (Jenk, 2006) and at the Paul Scherrer Institut, Switzerland for the Grenzgletscher (Eichler et al., 2000). The analytical uncertainties were <0.05‰ for the Fiescherhorn and <0.1‰ for the Grenzgletscher. More detailed description of the analytical procedures is given in Schwikowski et al. (1999) and Jenk (2006) for the Fiescherhorn cores and in Eichler et al. (2000, 2001) for the Grenzgletscher core. In the upper part discussed here (see also section 4.2.1.3), the Fiescherhorn record contains ~15-25 data points per year and Grenzgletscher ~20-90 points per year. Assuming diffusion lengths of 7-8 cm typical for firn

conditions, smoothing of the isotope signal due to diffusion (Johnsen, 1977) is negligible for the investigated cores due to the high accumulation rates. Annual $\delta^{18}O$ was obtained according to the dating procedure (see section 4.2.1.1), averaging all the values belonging to the same year. To derive subannual values, the year (defined from minimum to minimum) was split into twelve evenly spaced sections after linear interpolation of the raw data and the four seasonal winter to autumn $\delta^{18}O$ averages were calculated according to the convention (DJF, MAM, JJA, SON). This procedure assumes that the signal is uniformly deposited throughout the year, which might not be the case if seasonality or intraseasonal precipitation variability is present. In the Fiescherhorn ice core some melt features were observed, with low to moderate relocation of ions towards lower depths (Jenk, 2006). The Grenzgletscher concentration records were disturbed in the period 1985-1989 for certain major ions, due to the inflow of meltwater (Eichler et al., 2001). In contrast, the $\delta^{18}O$ was not significantly affected by melting as shown in (Schotterer et al., 1997; Schwikowski et al., 1999) for Fiescherhorn and in (Eichler et al., 2001) for Grenzgletscher.

4.2.1.3 Ice core accumulation reconstruction

The annual layer thickness λ_E was obtained from the depth differences between the age markers of subsequent years. In order to correct for the changing density in the firn, results in meters total depth were normalized to meters water equivalent (m w.e.) by multiplying the depth of the sample with the respective density which was derived from measurements of the ice core segments (length typically between 30 and 70 cm).

In order to reconstruct the net accumulation it is necessary to account for the ice thinning with depth (Cuffey and Paterson, 2010). We followed the approach given by Henderson et al. (2006) using Eq. (1):

$$\lambda_R = (\lambda_E/\lambda_M)\lambda_0 \qquad (1)$$

where λ_R is the reconstructed net accumulation, λ_E the annual thickness, λ_M the annual thickness estimated from an ice flow model, and λ_0 the estimated surface accumulation rate. Here the correction factor λ_M was determined with the ice flow model proposed by Nye (1963), which assumes a constant thinning with depth. This assumption is generally only valid for the upper two thirds of the glacier thickness of vast ice sheets (Hammer et al., 1978), but could still be applied in the case of Fiescherhorn and Grenzgletscher ice cores, because we deal with the uppermost ~60 and ~70 m w.e. of a total of 124 and 170 (estimated) m w.e., respectively.

This model was previously used in two studies involving Fiescherhorn and Grenzgletscher. For Fiescherhorn it was compared to a more sophisticated accumulation reconstruction derived from the measurement of the vertical velocity of the ice (Schwerzmann et al., 2006). Here, we do not apply the latter reconstruction, because the dating of the Fiescherhorn ice core was revised and is based now on an extended data set after analyses of the stable isotopes and concentrations of major ions were completed. For Grenzgletscher the Nye model was applied as an additional and independent dating technique (Eichler et al., 2000).

In order to obtain λ_M we first used the reverse Nye function to fit the data (Dansgaard and Johnsen, 1969), using Eq. (2):

$$t = t_0 - \frac{H}{\lambda_0} \ln(\frac{H-z}{H}) \qquad (2)$$

where t is the year, t_0 the drilling date (2002.92 for Fiescherhorn, 1994.67 for Grenzgletscher), H the glacier thickness (124 m w.e. for Fiescherhorn, 170 m w.e. for Grenzgletscher), z the height above the bed in m w.e., and λ_0 the surface accumulation rate in m w.e./year, estimated by averaging the upper layer thicknesses for which thinning can be neglected (1.7 m w.e./year for Fiescherhorn, by averaging the layers from 1990 to 2002 (Jenk, 2006), 2.7 m w.e./year for Grenzgletscher (Eichler et al., 2000)). The fit is characterized by a reduced $\chi^2=0.93$ over the upper ~70 m w.e. in Fiescherhorn, corresponding to the period 1950-2002, and a reduced $\chi^2=0.67$ for Grenzgletscher over the period 1938-1994. We also obtained a reconstructed accumulation for FH1989, with $\lambda_0=1.4$ m w.e./year, after Schwikowski et al. (1999), and $t_0=1989$, giving a reduced $\chi^2=0.39$ for the whole period 1946-1989. The difference between the two Fiescherhorn cores' λ_0 arises only due to the different period used for the estimation of the surface accumulation rate. We retrieved the modeled depth corresponding to the calendar year and formed, in analogy with λ_E, the modeled layer thickness λ_M.

4.2.2 Weather data

For the analysis of the temporal and spatial variability of the ice core proxies we used data collected at weather stations near the glaciers as well as gridded data. The correlation analyses were done by calculating the Pearson coefficient and the relation between $\delta^{18}O$ and temperature was evaluated by regression analysis. The presence of possible outliers was investigated by evaluating the jackknife residuals. The temperature and precipitation data are from the weather stations operated by the Federal Office of Climatology and Meteorology in Switzerland (Meteoswiss). When available, homogenized data were used. For Fiescherhorn this is the homogenized temperature from the high-alpine weather station at the Jungfraujoch, only 6 km west of the site (46°33' N, 7°59'E, 3580 m a.s.l). Since precipitation is not

measured at Jungfraujoch, data from nearby stations were considered instead (section 4.3.2.1). For Grenzgletscher we utilized homogenized temperature and precipitation data from the high-alpine station of the Grand Saint Bernard (45°52'N, 7°10'E, 2472 m a.s.l.), located 50 km west of the site, as explained in sections 4.3.1 and 4.3.2, and from Locarno (46°10'N, 8°47'E, 367 m a.s.l.) in Ticino (Southern Switzerland). The location of the weather stations is shown in Figure 1. For the spatial correlation analysis gridded data of temperature and precipitation were used. We selected the surface temperature and 700 hPa temperature from the Twentieth Century Reanalysis Dataset (Compo et al., 2011), ERA40 (Uppala et al., 2005), and NCEP-NCAR R1 (Kalnay et al., 1996), respectively. Out of these the Twentieth Century Reanalysis has the highest spatial resolution (2° x 2°). We excluded other higher resolution reanalysis products like ERA-INTERIM, MERRA or CFSR because their datasets only start in 1979. We focused on the region from 40°N to 60°N and from 15°W to 25°E. For precipitation, because of its sporadic nature in space and time, we used higher resolution data provided by Meteoswiss (nominally 2.2 km, actually 15-20 km, corresponding to the mean inter-station distance). This monthly, gridded dataset covers the area of Switzerland, starts in 1961, and is based on precipitation data collected within the rain-gauge network of Meteoswiss (Frei and Schär, 1998). Due to the scarcity of weather stations at high-altitude, the uncertainty of precipitation data over the Alps is estimated to be 25-30% (Meteoswiss, 2013). The resulting period of overlap among the different datasets (Twentieth Century Reanalysis, Meteoswiss gridded data) and the ice core data is 1961-1993 for Grenzgletscher (with a gap between 1968 and 1970, as explained in section 4.2.1.1) and 1961-2001 for Fiescherhorn.

We additionally used the δ^{18}O measured in meteoric water at four GNIP stations, Bern (541 m a.s.l.), Meiringen (632 m a.s.l), Guttannen (1055 m a.s.l.), and Grimsel Hospiz (1950 m a.s.l.). For their location we refer to Figure 1. The collection of monthly meteoric water at these stations started in January 1970 for Bern, August 1970 for the others and δ^{18}O measurements were performed by the Climate and Environmental Physics Department of the Physics Institute of the University Bern, Switzerland (IAEA/WMO, 2013). Since July 1992, the data collection at the GNIP stations in Switzerland has been carried on by the Swiss Geological Survey at the Federal Office of the Environment (FOEN), through the NISOT network (Swiss National Network for Isotopes in the Water Cycle, Schürch et al., 2003).

For the comparison between the two ice cores, the resulting common period is 1961-1993 (with a gap in 1968-1970) and for the analysis with the GNIP data is 1971-1993 (1980 excluded, as explained later).

4.3 Results and discussion

4.3.1 δ^{18}O and temperature

4.3.1.1 Seasonal scale

Ice core raw δ^{18}O data from the Fiescherhorn and the Grenzgletscher sites span the characteristic summer-to-winter values between -10‰ and -25‰ (Figure 3) expected for the respective altitudes (Siegenthaler and Oeschger, 1980; Sigl, 2009). Very good agreement is found between the two Fiescherhorn series (r=0.79, p<0.001), indicating that the mean conditions are homogeneously recorded at the glacier. We compared the seasonal δ^{18}O averages of the Fiescherhorn and Grenzgletscher ice core with the temperature data from the weather station Jungfraujoch and Grand Saint Bernard, respectively (see also section 4.2.2). Ice core δ^{18}O records and temperature data agree well for most of the years, clearly showing seasonality in the isotopic records. The seasonal cycle is remarkably well captured in the ice cores (r=0.70, p<0.001 for Fiescherhorn, period 1961-2001, r=0.69, p<0.001 for Grenzgletscher, period 1961-1993). Similar correlation was found for Grenzgletscher when using the precipitation-weighted seasonal temperature at the Grand Saint Bernard (r=0.71, p<0.001, see also section 4.3.1.2).

In the case of Fiescherhorn, precipitation-weighting was not possible because no precipitation data is available for the Jungfraujoch high-altitude station which might be most representative for the Fiescherhorn. Also no clear relation between Fiescherhorn accumulation and precipitation at nearby weather stations was observed; see sections 4.3.1.2 and 4.3.2.1. The results for Grenzgletscher are in good agreement with a previous study by Eichler et al. (2001), using a similar approach based on monthly data from Grenzgletscher and Grand Saint Bernard for the period 1980-1994 (r= 0.7).

In order to investigate the suitability of the ice core δ^{18}O signal as a temperature proxy we compared the established δ^{18}O/T relationship with results from the nearest GNIP stations. To mimic the seasonal distribution of precipitation affecting the δ^{18}O at high-alpine sites, the seasonal precipitation-weighted mean from the monthly δ^{18}O GNIP data was used, following the suggestion by Siegenthaler and Oeschger (1980). No adjustment to the temperature data accounting for the altitude difference between station and ice core sites was applied (moist adiabatic lapse rate of ~-0.6°C/100 m), since only the slope of the δ^{18}O/T regression line is of interest in this context. In order to check whether the obtained relationships are mainly due to the seasonal cycle, seasonal anomalies (e.g. deviation from the mean of the seasonal variation) of both δ^{18}O and temperature were analyzed in addition (Liu et al., 2010).

$\delta^{18}O$ (‰ VSMOW) $\delta^{18}O$ (‰ VSMOW)

T_{GSB}

GG
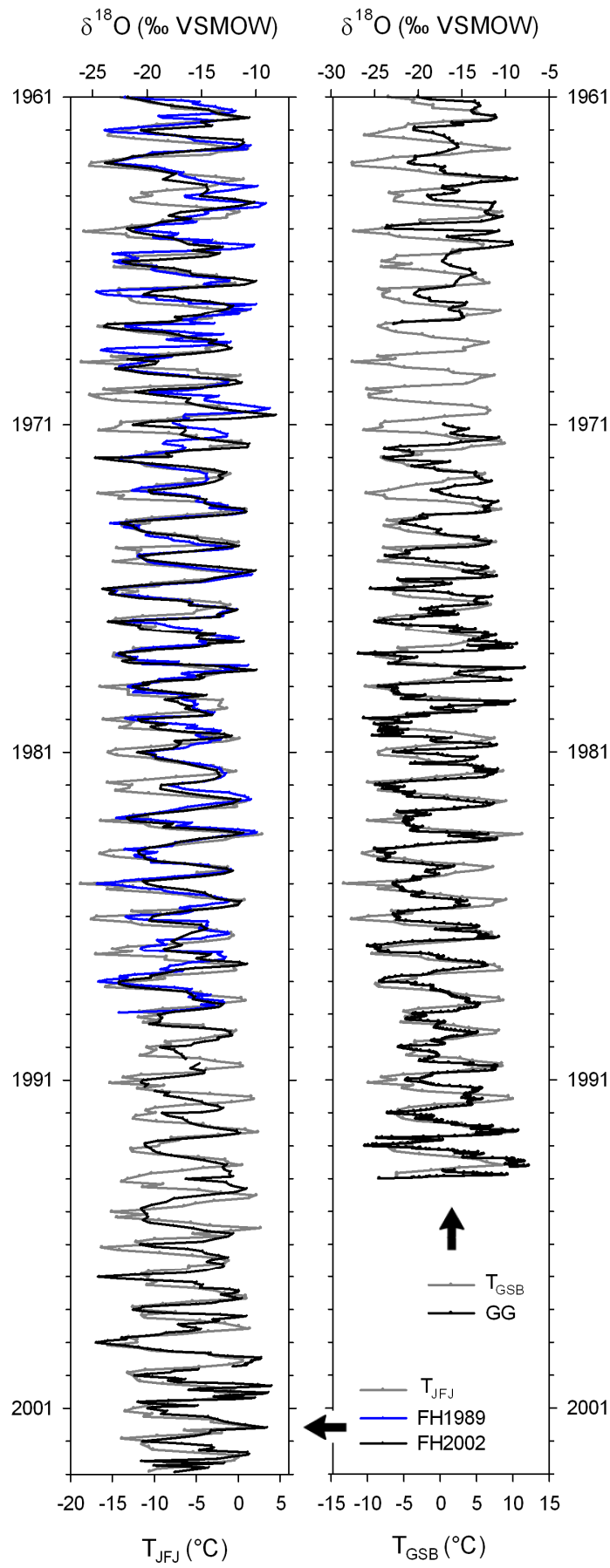
T_{JFJ}

FH1989

FH2002

T_{JFJ} (°C) T_{GSB} (°C)

Figure 3. (Left panel) $\delta^{18}O$ raw data from the Fiescherhorn ice cores (FH2002, black, FH1989, blue), together with the monthly temperature at the Jungfraujoch station (gray). (Right panel) $\delta^{18}O$ raw data from the Grenzgletscher ice core (black), together with the monthly temperature at the Grand Saint Bernard (gray).

The overlapping period with available station and ice core data is 1971-1993. Two years (1971 and 1980) were excluded because of missing values in winter 1971 in the Grenzgletscher record and in summer 1980 in the Guttannen station record. The results are summarized in Table 1.

| | Mean | Seasonal scale | | Seasonal scale (anomalies) | | Annual scale | |
| | | Slope | | Slope | | Slope | |
	(‰)	(‰/°C)	R^2	(‰/°C)	R^2	(‰/°C)	R^2
Bern	-9.89	0.32 ± 0.02	0.69	0.45 ± 0.14	0.11	0.57 ± 0.32	0.14
Meiringen	-11.35	0.42 ± 0.03	0.73	0.67 ± 0.16	0.17	0.88 ± 0.41	0.19
Guttannen	-12.54	0.46 ± 0.03	0.71	0.49 ± 0.15	0.12	0.72 ± 0.35	0.18
Grimsel Hospiz	-14.23	0.43 ± 0.03	0.70	0.57 ± 0.11	0.23	0.68 ± 0.20	0.36
FH2002	-16.53	0.47 ± 0.05	0.55	-0.22 ± 0.16	0.02	0.44 ± 0.22	0.17
GG (with T_{UNW})	-17.34	0.53 ± 0.05	0.56	0.28 ± 0.21	0.02	0.27 ± 0.53	0.01
GG (with T_{PW})	-17.34	0.55 ± 0.05	0.58	0.47 ± 0.20	0.07	0.77 ± 0.32	0.22

Table 1 Mean values of $\delta^{18}O$ from the GNIP stations as well as from the ice cores over the common period 1971-1993, together with the slope of the long-term $\delta^{18}O$/temperature calibration and the R^2 for the seasonal and the annual scale. For the seasonal scale, values were calculated for the common period 1972-1993 (1971 and 1980 excluded because of gaps in the data). For the annual scale, the year 1980 was excluded. The temperatures used to calibrate the GNIP $\delta^{18}O$ were measured at the respective stations, whereas for the ice cores the Jungfraujoch temperature was used for the Fiescherhorn and the Grand Saint Bernard for the Grenzgletscher. The suffix "UNW" stands for the unweighted average and "PW" for precipitation-weighted average.

For the four GNIP stations we obtained slopes ranging between (0.32±0.02)‰/°C (Bern) and (0.46±0.03)‰/°C (Guttannen), comparable to the values found by Siegenthaler and Oeschger (1980) using monthly data over the period 1971-1978 (0.35, 0.53, 0.55, and 0.44‰/°C for Bern, Meiringen, Guttannen, and Grimsel Hospiz, respectively). For the Fiescherhorn/Jungfraujoch δ^{18}O/T relation the slope is (0.47±0.05)‰/°C (R^2=0.55).

Similar values were found for the δ^{18}O/T relation between Grenzgletscher δ^{18}O and Grand Saint Bernard temperature ((0.55±0.05)‰/°C and (0.53±0.05)‰/°C with R^2 = 0.58 and 0.56 for the precipitation-weighted and unweighted temperature, respectively; see also section 4.3.1.2). This does not change significantly when the entire period (1961-2001 for FH2002 and 1961-1993, 1968-1970 excluded for Grenzgletscher) is considered: (0.46±0.04)‰/°C for Fiescherhorn, (0.48±0.05)‰/°C and (0.50±0.05)‰/°C for the Grenzgletscher unweighted and precipitation-weighted temperature, respectively. In general the fraction of δ^{18}O variance explained by temperature changes is ~60% compared to ~70% in the GNIP data. However, when removing the seasonal cycle this value decreases for all sites and ranges between 0-10% for the ice core data and 10-25% for the GNIP station data, indicating that the major part of the correlation is determined by the seasonal cycle. The slopes however, do not change significantly between the seasonal and deseasonalized case and are smaller compared to what would be expected from Rayleigh distillation processes suggesting that other factors such as precipitation intermittency and changes in the moisture source play a role. For the lower elevation stations receiving liquid precipitation, below-cloud processes may further affect the isotopic composition of water whereas for the ice core data, effects due to post-depositional processes need to be assumed as indicated by the very low coefficients.

4.3.1.2 Annual scale

For paleoclimatic reconstructions the δ^{18}O/T relation on an annual scale becomes fundamental because with depth, the proxy resolution decreases to a few points per year due to glacier flow induced layer thinning and seasonal resolution cannot be obtained anymore. The annual averages of δ^{18}O are shown in Figure 4 to highlight the altitude effect. For the common time period, the mean δ^{18}O ice core values decrease with increasing altitude from -16.53‰ at Fiescherhorn (3900 m a.s.l.) to -17.34‰ at Grenzgletscher (4200 m a.s.l.). This result is consistent with the altitude effect resulting in a lapse rate of dδ^{18}O/dz =-0.2‰/100 m reported by Siegenthaler and Oeschger (1980) and Schürch et al. (2003). A similar value of dδ^{18}O/dz = (-0.17±0.02)‰/100 m (R^2=0.94) was found in this study for an extended elevation range combining data of the two ice core sites and the four GNIP stations.

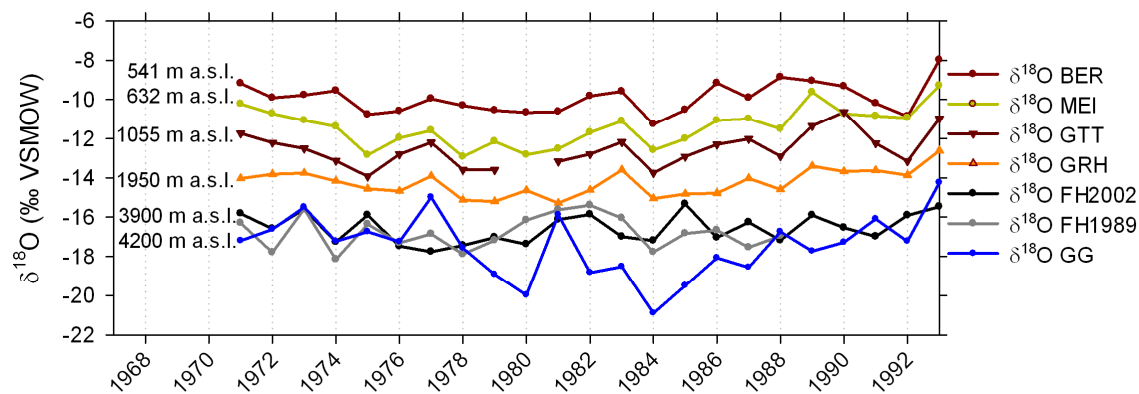**Figure 4**. Annual precipitation-weighted δ^{18}O from the GNIP stations together with the ice core data. The sites are indicated as follows. Bern (BER), Meiringen (MEI), Guttannen (GTT), Grimsel Hospiz (GRH), Fiescherhorn (FH), Grenzgletscher (GG). The gaps in the GNIP data are due to missing data points for the corresponding years. The altitude of each site is indicated on the left.

For the correlation of the two Fiescherhorn δ^{18}O series the resulting high correlation coefficient (Figure 5, r=0.52, p<0.01, period 1961-1988) demonstrates that on an annual scale the two ice cores do representatively capture the conditions at the glacier. In the following we focus on the FH2002 core which also covers the more recent time period.

The recent warming (Appenzeller et al., 2008) is particularly pronounced in the Jungfraujoch temperature with a stepwise increase after the year ~1984. At the Fiescherhorn a more gradual δ^{18}O increase is observed after 1984, more similar to the trends at the Grenzgletscher, the four GNIP stations and the Grand Saint Bernard temperature (Figures 4, 5 and 6).

The annual Fiescherhorn δ^{18}O correlates significantly with the Jungfraujoch annual temperature (r=0.44, p<0.01, period 1961-2001). The resulting slope is (0.50±0.16)‰/°C which is consistent with the result based on the seasonal values. The slope is substantially different from what was found by Schotterer et al. (1997) for the annual values of FH1989 over the period 1969-1989 (1.1‰/°C, R^2=0.74).
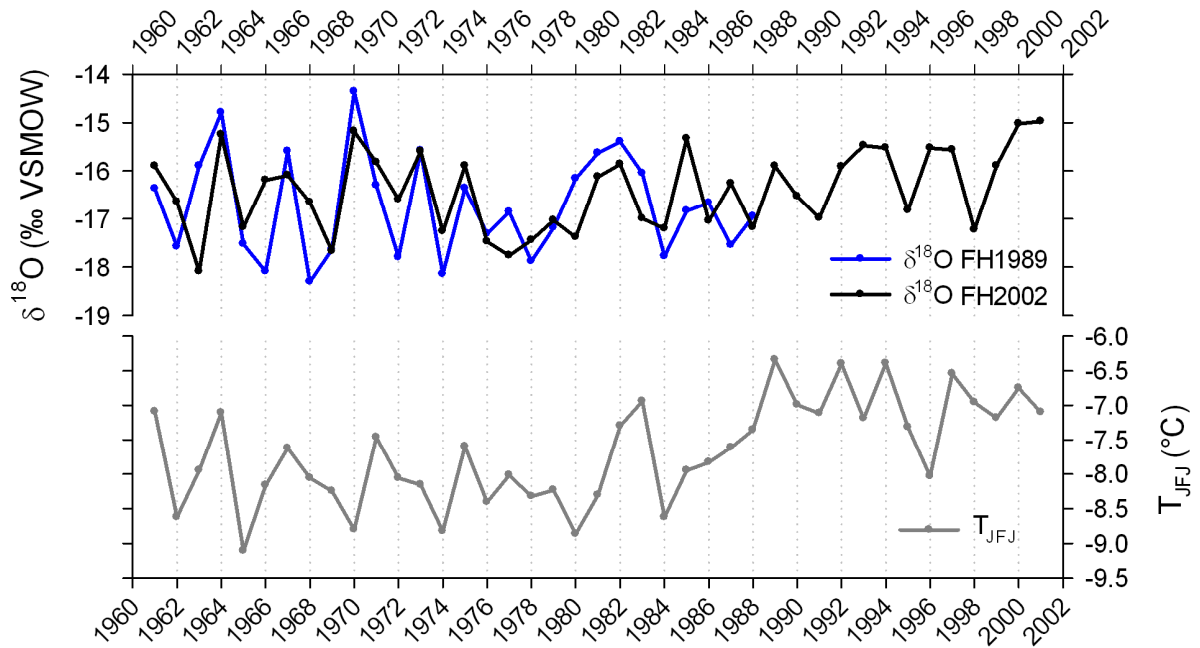
Figure 5. Annual $\delta^{18}O$ from FH2002 ice core (black), FH1989 (blue), together with the annual mean temperature at the Jungfraujoch weather station (gray).
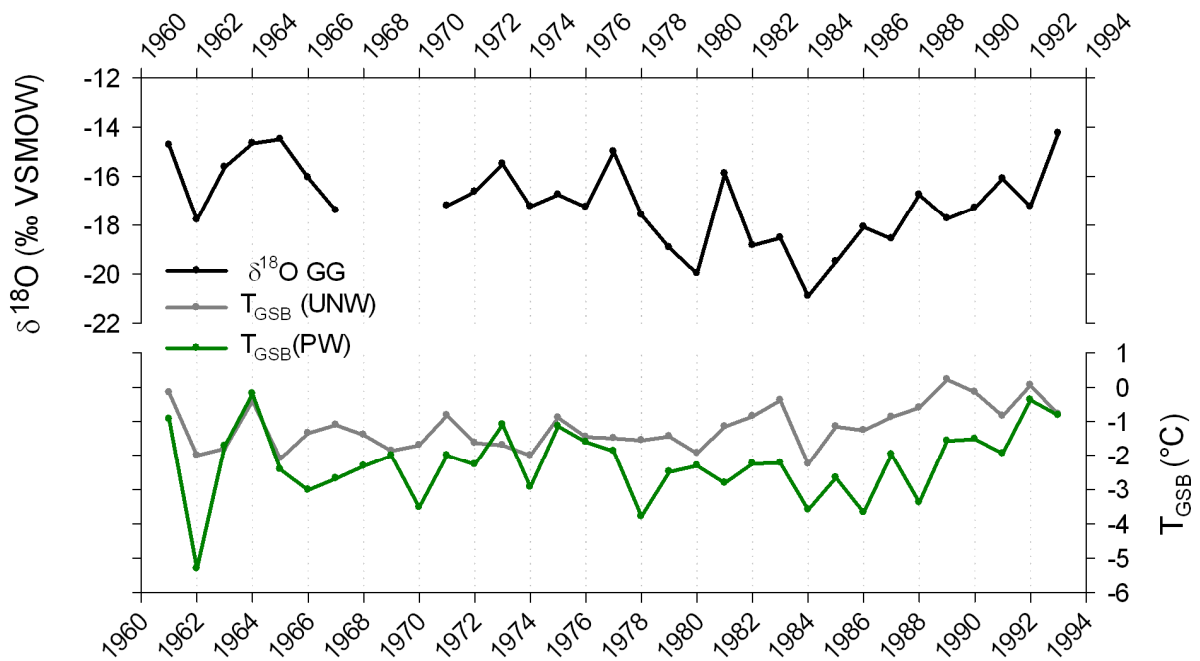

Figure 6. Annual $\delta^{18}O$ from the Grenzgletscher (black), together with the annual mean temperature at the Grand Saint Bernard station. In gray the unweighted (UNW) temperature, in green the precipitation-weighted (PW) temperature, obtained as described in section 4.3.1.2.

In order to get a reasonable correlation, Schotterer et al. (1997) had to exclude four years with strong anomalous data (1971, 1972, 1981, 1988). In the case of FH2002, even when excluding two suspected outliers determined with the jackknife residuals (1963 and 1970), despite a higher Pearson coefficient (r=0.54, p<0.001), the slope does not change significantly ((0.58±0.15)‰/°C). In the case of Grenzgletscher the annual temperature and the $\delta^{18}O$ do not show any significant correlation within the dating uncertainty (-1, 0, +1 year), neither with the Grand Saint Bernard or the Locarno station data nor with the gridded data (not shown). Because in first approximation the $\delta^{18}O$ is a proxy for the in-cloud temperature only when precipitation occurs, one neglects a potential effect due to the seasonal distribution of precipitation, when comparing the $\delta^{18}O$ on the glacier with the mean annual temperature. We assume that at the Grenzgletscher the non-uniform snow deposition throughout the year is more pronounced than at Fiescherhorn (see section 4.3.2.1), as it is generally the case in the Southern Alps compared to the Northern Alps (Frei and Schär, 1998; Eichler et al., 2004; Sodemann and Zubler, 2009). To account for the higher variability of precipitation at the Grenzgletscher we calculated the precipitation-weighted temperature according to Eq. (3):

$$T_{ann} = \frac{\sum_{i=1}^{12} P_i T_i}{P_{ann}} \qquad (3)$$

where T_{ann} is the annual precipitation weighted temperature, P_i the monthly amount of precipitation used to weight the monthly temperature T_i, P_{ann} the annual amount of precipitation. Since it is not possible to get subannual information from the reconstructed accumulation (only annual layer thickness is retrieved), we mimicked the monthly precipitation at the Grenzgletscher using the data from the high-altitude station Grand Saint Bernard, instead. This is reasonable based on the good agreement between the precipitation at that station and accumulation at the site (see section 4.3.2). The unweighted and precipitation-weighted annual temperatures are shown in Figure 6. The precipitation-weighted annual temperatures are lower than the unweighted temperatures (mean of -2.2°C compared to -1.1°C), because of the observed higher precipitation in winter compared to summer at the Grand Saint Bernard (607, 611, 419, 568 mm in winter, spring, summer, and autumn, respectively, over 1961-1993, data provided by Meteoswiss). As expected the correlation significantly increases (r=0.45, p<0.05) with respect to the unweighted temperature (r=0.16, p=0.20). We obtained a similar result when using the unweighted and precipitation-weighted data from the lower altitude station of Locarno, with the correlation coefficients increasing from r=0.12 (p=0.27) to r=0.21 (p=0.14). Due to the better agreement with the Grand Saint

Bernard station, the corresponding slope δ^{18}O/T for Grenzgletscher was determined using high-Alpine temperature data from this site and is (0.68±0.26)‰/°C (precipitation-weighted temperature) compared to (0.39±0.47)‰/°C (unweighted temperature) for the time period 1961-1993. The obtained δ^{18}O/T relationship based on the annual ice core data was compared with results from the near GNIP stations (Table 1) to infer differences between seasonal and annual information. We considered again the common period 1971-1993 (Figure 7). Suspected outliers were evaluated with the jackknife residuals, but the exclusion of these points did not significantly change the slopes. In all cases except for the GG unweighted data, i.e. for both the ice core and station data, the general capability to reproduce the temperature is significant (at least $p<0.10$ for all sites). The percentage of δ^{18}O variance explained by temperature changes is about 20% on an annual scale which is comparable to the value obtained for the deseasonalized data and is explained by the reduced data set and the stronger bias of the non-uniformity of precipitation on the annual compared to the seasonal scale as well as by changes in the moisture sources throughout the year and post-depositional processes. As described above, no correlation exists with the annual mean temperature for the Grenzgletscher indicating that precipitation intermittency and variability plays a fundamental role there (Persson et al., 2011).
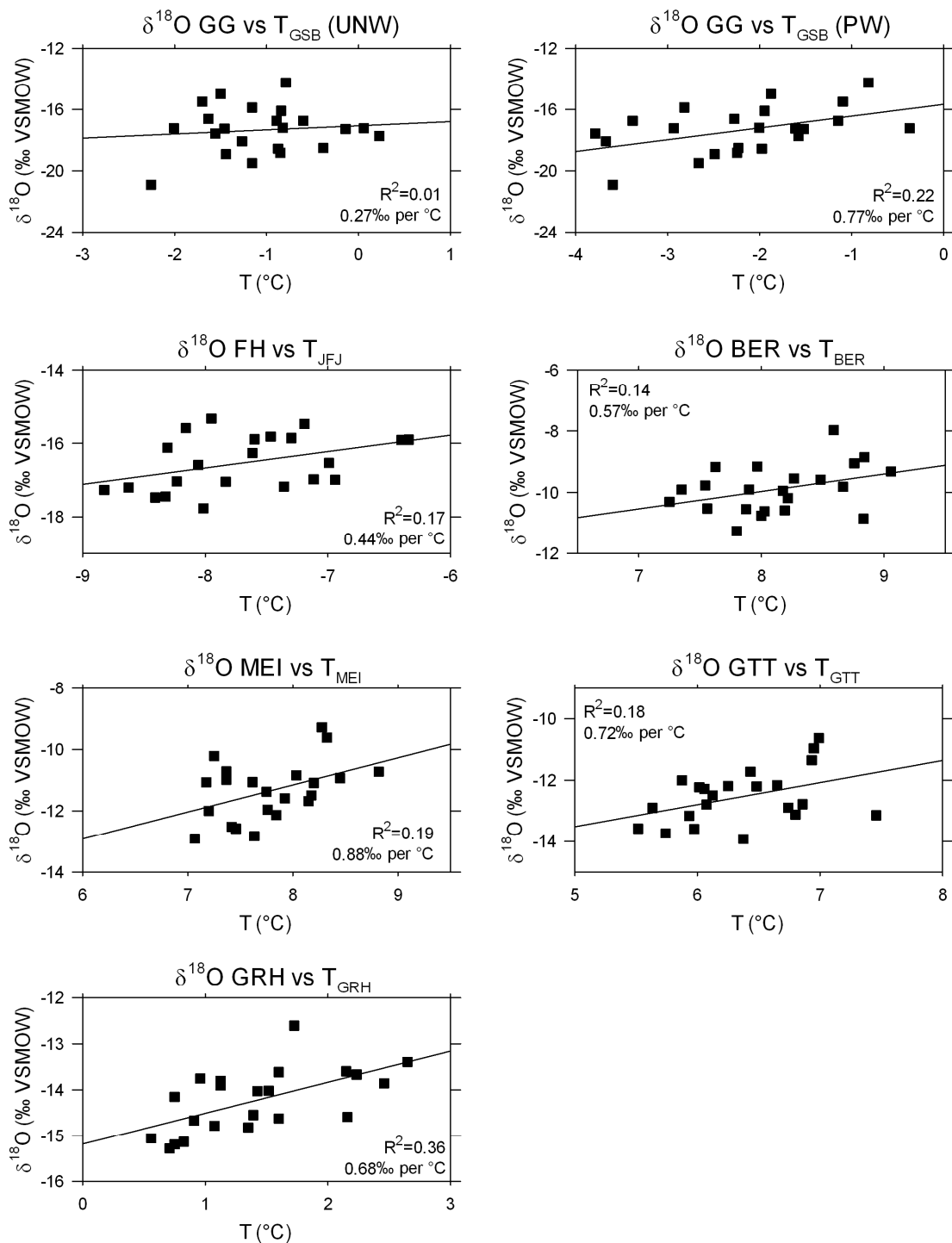
Figure 7. Scatterplots of annual temperature and $\delta^{18}O$ data over the common period 1971-1993. The sites are denoted as follows: Grenzgletscher (GG), Grand Saint Bernard (GSB), Fiescherhorn (FH), Jungfraujoch (JFJ), Bern (BER), Meiringen (MEI), Guttannen (GTT), Grimsel Hospiz (GRH). "UNW" stands for the unweighted temperature and "PW" for precipitation-weighted temperature.

4.3.1.3 Spatial correlations

We finally investigated the capability of the ice core δ^{18}O to capture the regional temperature, performing a spatial correlation analysis with gridded instrumental data. The analysis was done with the KNMI Climate Explorer tool available on http://climexp.knmi.nl (Trouet and Van Oldenborgh, 2013). Figure 8a shows the spatial correlation between Fiescherhorn annual δ^{18}O and the Twentieth Century Reanalysis temperature at 700 hPa, which was considered to be most representative for the high elevation of the studied glacier sites. We observed significant correlation with temperature in Central and Southern Europe at 700 hPa and at the surface level (not shown). Similar patterns were seen with the ERA40 and NCEP-NCAR R1 reanalyses (not shown), indicating no significant differences between the reanalyses datasets. We compared this result with the spatial correlation pattern of the Jungfraujoch temperature with the gridded data. Figure 8b shows the pattern centered over Switzerland with coefficients higher than 0.7 for most of Europe. If comparing the two patterns it is clear that the δ^{18}O captures less variability and is representative for a smaller region only, which is not unexpected based on the fact that the temperature explains only 20% of the isotopic variance. For Grenzgletscher we found significant correlations at both 700hPa and surface level (not shown) with the Twentieth Century Reanalysis precipitation-weighted temperature (each grid point was weighted with the monthly Grand Saint Bernard precipitation). This is in agreement with the previous results where the ice core data compared to the Grand Saint Bernard and Locarno station data showed a correlation with the precipitation-weighted temperatures. A similar pattern slightly shifted westwards and elongated towards a west-east direction was observed (Figure 8c, for the 700hPa temperature), compared to the imprint of the regional temperature on the Southern Alpine station (Figure 8d). The latter is very similar to the pattern obtained in Figure 8b for the northern Alpine station.

The results obtained for the station data indicate that temperature variations on an annual scale are rather homogenous over entire Europe. This suggests that ice core based temperature reconstructions (precipitation-weighted in the case of Grenzgletscher) are in principal valid on a regional scale and could be interpreted even as a Central European temperature. The result further underlines that the two glaciers, distant only 60 km, behave significantly different in the way the isotopic signal is recorded. At Fiescherhorn the annual δ^{18}O in precipitation reasonably represents the mean annual temperature, implying a nearly homogeneous preservation of precipitation throughout the year. At Grenzgletscher because of the high variability in precipitation throughout the seasons, the average temperature during

precipitation deduced from the ice core $\delta^{18}O$ differs significantly from the annual mean temperature.

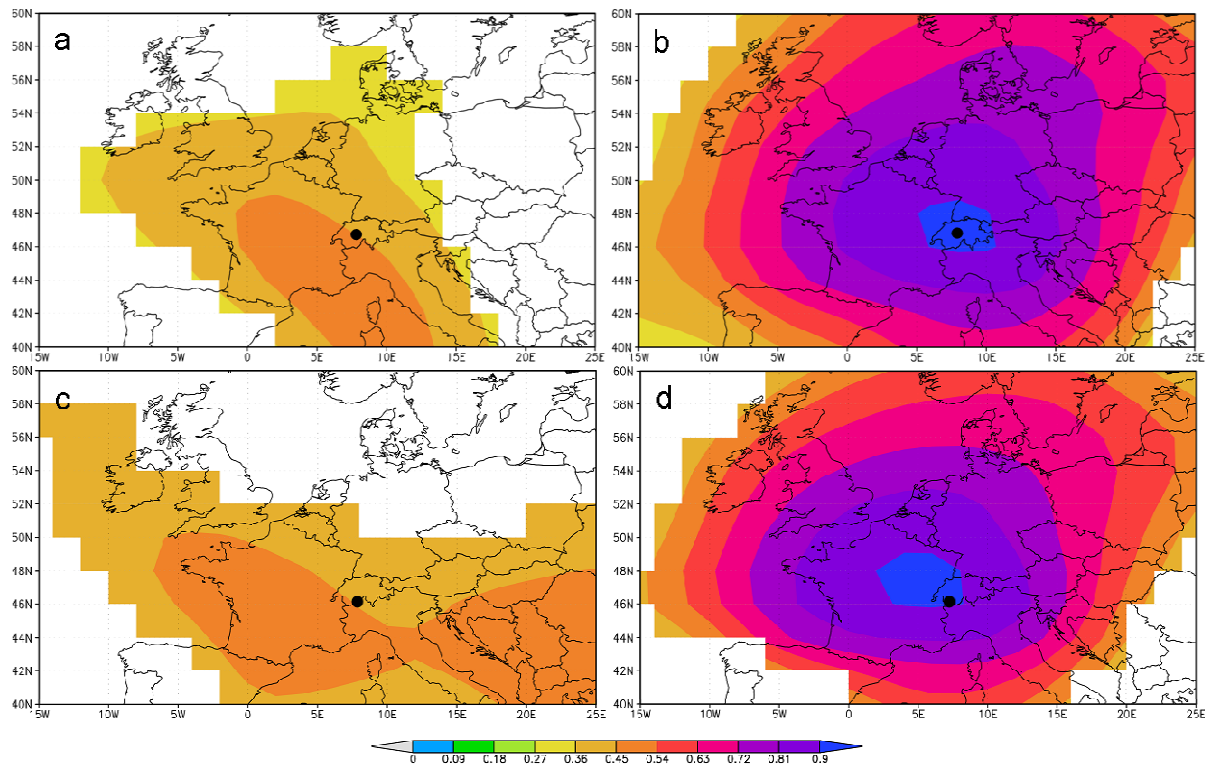**Figure 8**. Spatial correlation maps of annual $\delta^{18}O$ and temperature records with the Twentieth Century Renalysis 700 hPa temperature, for Northern Alpine (upper panels, period 1961-2001) and Southern Alpine sites (lower panels, period 1961-1993, 1968-1970 excluded). Correlation with a) Fiescherhorn $\delta^{18}O$, b) Jungfraujoch temperature c) Grenzgletscher $\delta^{18}O$ (using the Twentieth Century Reanalysis 700 hPa precipitation-weighted temperature, Grand Saint Bernard precipitation utilized to weight the temperature), d) Grand Saint Bernard temperature. Black dots indicate the location of the sites. Areas with correlation coefficients statistically significant at the 5% level are shaded.

4.3.2 Net accumulation and precipitation

4.3.2.1 Comparison with the station data

The time series of the reconstructed annual net accumulation at Fiescherhorn and Grenzgletscher together with the annual precipitation from nearby weather stations are shown in Figure 9a-b and 9c-d, respectively. For the northern and southern sites we selected a low-altitude (Interlaken, 577 m a.s.l. and Locarno, 367 m a.s.l., respectively) and a high-altitude station (Grimsel Hospiz, and Grand Saint Bernard, respectively). For their geographic locations we refer to Figure 1.

117

The two Fiescherhorn reconstructions are well correlated with each other (r=0.66, p<0.001), indicating similar preservation of the precipitation at the two sites, 100 m apart. With focus on the common period 1961-1993, Grenzgletscher has a higher mean accumulation and interannual variability (2.7 m w.e., 1σ=0.8 m w.e. ~30%) compared to the Fiescherhorn record (1.7 m w.e., 1σ=0.4 m w.e. ~23%), see Figure 9. This is in agreement with higher precipitation for stations in the Southern Alps. The two stations in the Northern Alps reveal a mean precipitation and interannual variability of 1183 mm and 12% (Interlaken), 1881 mm and 18% (Grimsel Hospiz), and the southern stations 1858 mm and 19% (Locarno), 2214 mm and 14% (Grand Saint Bernard). As shown in Figure 9, precipitation increases with altitude at the southern sites including the Grenzgletscher. For the northern stations the increase is even more pronounced. However, Fiescherhorn accumulation is lower than precipitation at the Grimsel Hospiz. This could be explained by local phenomena, probably related to wind erosion at the exposed Fiescherhorn saddle. Post-depositional processes could also be responsible for the higher interannual variability at the glacier sites compared to the stations.

Comparing the precipitation records of the northern stations with the Fiescherhorn record (Figure 9, Table 2), we found a significant correlation with most stations only in the earlier part (1961-1977) when allowing the ice core series to be shifted by -1 year, which is within the given dating uncertainty. The Fiescherhorn accumulation maximum around 1977 is not recorded in the northern station data, but pronounced at southern sites including the Grenzgletscher. This might indicate that the common precipitation features between the Northern and the Southern sites are better captured at the Fiescherhorn than at the respective low altitude stations. No correspondence with precipitation in the most recent period (1978-2001) was found, probably indicating a general change in the pattern of received precipitation or the local influence of post-depositional processes such as wind erosion, but this is not understood at this point. The earlier part dominates the overall correlation over the whole period 1961-2001, as shown in Table 2.

For the Grenzgletscher we found a significant correlation between the reconstructed ice core accumulation, the Grand Saint Bernard (r=0.58, p<0.001) and the Locarno precipitation (r=0.59, p<0.001), indicating that the sites located in the Southern Alps are likely affected by the same precipitation regime (Figure 9c-d).

In order to test how the precipitation and temperature proxies potentially affect each other we correlated the ice cores δ^{18}O with the respective reconstructed accumulations. However, we did not find significant correlations between the Grenzgletscher and Fiescherhorn δ^{18}O and the respective reconstructed accumulation.
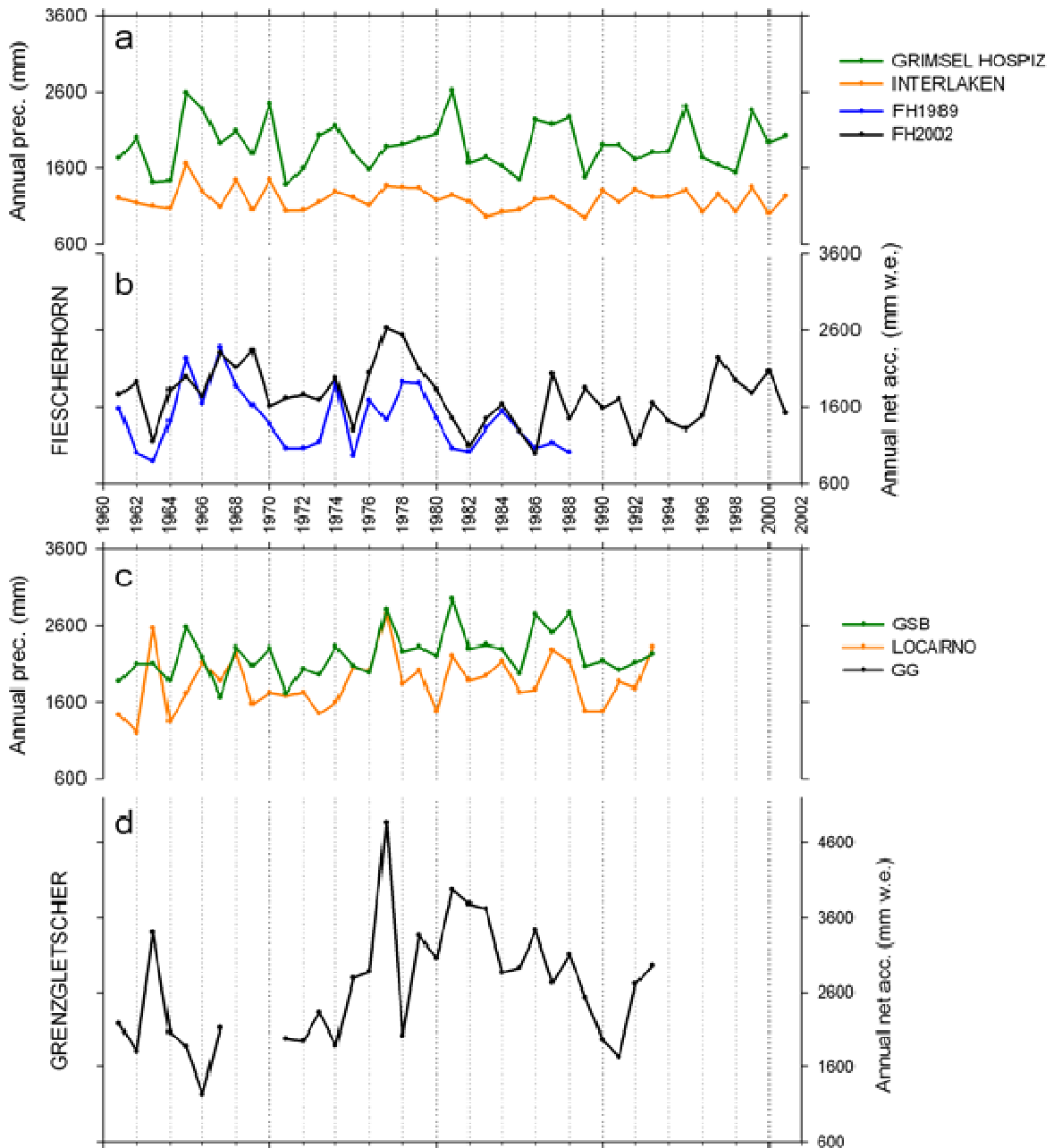
Figure 9. a) Annual sum of precipitation from the high and low-altitude stations Grimsel Hospiz (1950 m a.s.l., green) and Interlaken (577 m a.s.l., orange). b) Reconstructed annual accumulation at the Fiescherhorn glacier for FH2002 (black) and FH1989 (blue). c) Annual sum of precipitation from the high and low-altitude stations Grand Saint Bernard (2472 m a.s.l., green) and Locarno (367 m a.s.l., orange). d) Reconstructed annual accumulation at the Grenzgletscher (black). Note that the panels are shown on the same scale, to allow a direct comparison of the records.

Station	Latitude	Longitude	Altitude (m a.s.l.)	Mean Annual Precipitation (1961-2001) (mm)	r (1961-2001)	r (1961-1977)
1. Engelberg *	46°49' N	8°25' E	1035	1533 (11%)	0.25	**0.54**
2. Grimsel Hospiz *	46°34' N	8°20' E	1950	1908 (17%)	0.26	**0.53**
3. Grindelwald	46°38' N	8°02' E	1158	1398 (14%)	0.20	**0.49**
4. Guttannen	46°39' N	8°17' E	1055	1732 (13%)	**0.32**	**0.66**
5. Interlaken	46°40' N	7°52' E	577	1192 (13%)	**0.41**	**0.51**
6. Kleine Scheidegg	46°35' N	7°58' E	2061	1586 (14%)	0.13	**0.42**
7. Lauterbrunnen	46°36' N	7°54' E	818	1181 (13%)	**0.28**	**0.56**
8. Leukerbad	46°23' N	7°38' E	1390	1224 (19%)	**0.40**	**0.55**
9. Meiringen	46°44' N	8°10' E	632	1353 (13%)	**0.37**	**0.60**
10. Mürren	46°33' N	7°53' E	1638	1462 (14%)	**0.33**	**0.43**

Table 2 Mean annual precipitation over the period 1961-2001 for the stations near the Fiescherhorn glacier, together with their interannual variability, expressed as 1σ / mean value in percent (in parenthesis). Asterisks indicate homogenized data. Pearson correlation coefficient of the precipitation with the annual net accumulation (offset = -1 year) at Fiescherhorn glacier. Values of correlation coefficients statistically significant at the 5% level are bold.

4.3.2.2 Spatial correlations

In order to see whether the two glaciers record the different precipitation patterns expected due to the orographic barrier, a spatial correlation analysis was performed using the higher resolution Meteoswiss gridded data. Figure 10a shows significant correlations of Fiescherhorn accumulation with precipitation in regions extending from the Southwest to the Northeast ($0.3<r<0.5$). However, this was found only when introducing an offset of -1 year as discussed in section 4.3.2.1.
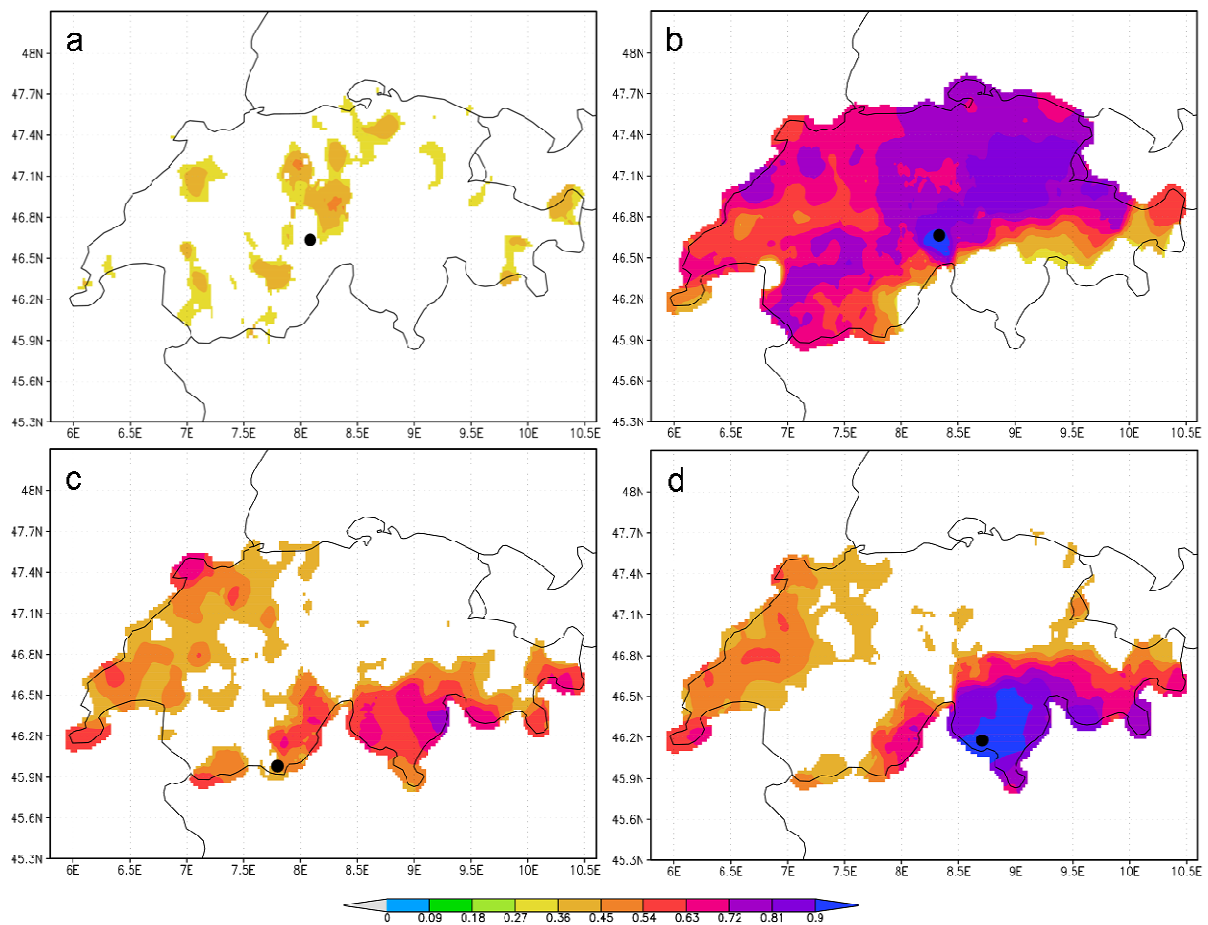

Figure 10. Spatial correlation map of annual records with the Meteoswiss gridded precipitation for Northern Alpine (upper panels, period 1961-2001) and Southern Alpine sites (lower panels, period 1961-1993, 1968-1970 excluded). Correlation with a) Fiescherhorn annual net accumulation (where an offset of -1 year was introduced), b) Grimsel Hospiz annual precipitation c) Grenzgletscher annual net accumulation, d) Locarno annual precipitation. Black dots indicate the location of the sites. Areas with correlation coefficients statistically significant at the 5% level are shaded.

The observed pattern gets more pronounced when considering the period 1961-1977 (not shown) for which the highest correlation was found (see section 4.3.1.2). We investigated whether the latter precipitation regime is reflected in the spatial correlations with the nearby northern station (Grimsel Hospiz). We found that the annual station precipitation is strongly correlated with almost the entire Swiss area except Ticino (Figure 10b). A similar correlation pattern was found for Interlaken (not shown).

For Grenzgletscher, despite the considerable intraseasonal to interannual variability of precipitation (Figure 9d) a good correlation with the instrumental data was observed (Figure 10c). The most significant results ($0.4<r<0.8$) found over Ticino, Southern Alps, and Northwestern Switzerland are consistent with the expected spatial pattern over the region. No uniform correlations were obtained nearby the Grenzgletscher region. This may be explained by the sparseness of the weather stations especially at such high altitudes, resulting in less accurate precipitation interpolation in the gridded data. In an analogue approach the correlation of the Southern Alpine station precipitation data from Locarno with the gridded data gave very similar results, confirming the Grenzgletscher to be representative for southern Alpine precipitation (Figure 10d). These results confirm that the two selected ice core sites represent different precipitation regimes.

4.4 Conclusions and implications

The study conducted with two Alpine ice cores has important implications on the way how temperature and precipitation from high-alpine sites should be reconstructed in order to prevent from over-, or even faulty interpretation of the records.

1. The seasonal cycle is strongly affecting the correlation of the isotopic signal with temperature, with the fraction of variance explained being ~60% and decreasing to 0-10% when removing the seasonality. Accordingly, the GNIP stations showed a decrease in the fraction of variance explained from ~70% to 10-20% indicating that over the Alpine area the seasonal temperature is only partially recorded in the $\delta^{18}O$ and additional factors such as changes in the moisture sources and below-cloud processes have a significant impact on the isotopic signal. Ice core data may further be affected by post-depositional effects.

2. On an annual scale the high variability of precipitation, especially at high-altitude sites, might considerably bias the isotopic signal toward the season with more precipitation. For a glacier site with homogeneously preserved accumulation throughout the year the mean temperature signal is partly preserved on annual scale. In case of strong intraseasonal precipitation variability the annual mean of $\delta^{18}O$ is only representative for temperature during precipitation and not for annual mean temperature. For such a glacier site, a paleotemperature reconstruction is not feasible.

3. Even for glacier sites in close proximity (only 60 km) within the same mountain range, distinct local precipitation patterns can result in variations how the temperature proxy signal is preserved. Thus, a careful individual calibration of the local $\delta^{18}O/T$ relation is essential for every ice core site.

4. The precipitation reconstruction from accumulation is critical, since it is more sensitive to post-depositional processes such as wind erosion and to initial layer assignment than the intrinsic core parameters like the $\delta^{18}O$. Further, precipitation at a high-alpine glacier may reflect very local conditions not captured in weather data obtained at lower elevation stations. Nevertheless, the distinct precipitation regimes for the Northern and Southern sites were observed in the respective accumulation records. At the Grenzgletscher the typical Southern Alpine precipitation pattern was obtained in agreement with the Southern Alpine stations.

5. Even for high-resolution ice core records with a pronounced seasonal signal, the dating uncertainty is rarely below ± 1 year and cannot be neglected. The dating uncertainty cannot be overcome but its influence can be minimized by averaging or smoothing of the annual data still allowing for valuable ice core based temperature or precipitation reconstructions of the past climate.

Acknowledgements

References

Appenzeller, C., Begert, M., Zenklusen, E. and Scherrer, S. C.: Monitoring climate at Jungfraujoch in the high Swiss Alpine region, Sci. Total Environ., 391(2–3), 262–268, doi:10.1016/j.scitotenv.2007.10.005, 2008.

Araguás-Araguás, L., Fröhlich, K., and Rozanski, K.: Deuterium and oxygen-18 isotope composition of precipitation and atmospheric moisture, Hydrolog. Process., 14, 1341–1355, doi:10.1002/1099-1085(20000615)14:8<1341::AID-HYP983>3.0.CO;2-Z, 2000.

Barry, R. G.: Mountain Weather and Climate, 3rd ed., Cambridge University Press, 386-397, 2008.

Bohleber, P., Wagenbach, D. and Schöner, W.: To what extent do water isotope records from low accumulation Alpine ice cores reproduce instrumental temperature series?, Tellus B, 65(0), doi:10.3402/tellusb.v65i0.20148, 2013.

Bradley, R.S.: Paleoclimatology: Reconstructing Climates of the Quaternary, in: International Geophysics Series, 64, edited by Dmowska, R., and Holton J.R., Academic Press, San Diego, Calif., 1999.

Brönnimann, S., Mariani, I., Schwikowski, M., Auchmann, R., and Eichler, A.: Simulating the temperature and precipitation signal in an Alpine ice core, Clim. Past, 9, 2013-2022, doi:10.5194/cp-9-2013-2013, 2013.

Casado, M., Ortega, P., Masson-Delmotte, V., Risi, C., Swingedouw, D., Daux, V., Genty, D., Maignan, F., Solomina, O., Vinther, B., Viovy, N. and Yiou, P.: Impact of precipitation intermittency on NAO-temperature signals in proxy records, Clim. Past, 9(2), 871–886, doi:10.5194/cp-9-871-2013, 2013.

Ciais, P. and Jouzel, J.: Deuterium and oxygen 18 in precipitation: isotopic model, including mixed cloud processes, J. Geophys. Res., 99, 16793–16803, doi:10.1029/94JD00412, 1994.

Compo, G. P., Whitaker, J. S., Sardeshmukh, P. D., Matsui, N., Allan, R. J., Yin, X., Gleason, B. E., Vose, R. S., Rutledge, G., Bessemoulin, P., Brönnimann, S., Brunet, M., Crouthamel, R. I., Grant, A. N., Groisman, P. Y., Jones, P. D., Kruk, M., Kruger, A. C., Marshall, G. J., Maugeri, M., Mok, H. Y., Nordli, Ø., Ross, T. F., Trigo, R. M., Wang, X. L., Woodruff, S. D., and Worley, S. J.: The Twentieth Century Reanalysis Project, Q. J. Roy. Meteorol. Soc., 137, 1–28, doi:10.1002/qj.776, 2011.

Conroy, J.L., Cobb, K.M., and Noone, D.: Comparison of precipitation isotope variability across the tropical Pacific in observations and SWING2 model simulations, J. Geophys. Res. Atmos., doi: 10.1002/jgrd.50412, 2013.

Craig, H.: Isotopic variations in meteoric waters, Science, 133, 1702–1703, doi:10.1126/science.133.3465.1702, 1961.

Cuffey, K., and Paterson, W.S.B.: Ice core studies, in: The physics of the glaciers, 4th ed., Elsevier, Butterworth-Heinemann, USA, 611-674, 2010.

Dansgaard, W.: Stable isotopes in precipitation, Tellus, 16(4), 436–468, doi:10.1111/j.2153-3490.1964.tb00181.x, 1964.

Dansgaard, W., and Johnsen, S.J.: A flow model and a time scale for the ice core from Camp Century, Greenland, J. Glaciol., 846(53), 215-223, 1969.

Eichler, A., Schwikowski M., Gäggeler H.W., Furrer V., Synal H.-A., Beer J., Saurer M., and Funk M.: Glaciochemical dating of an ice core from upper Grenzgletscher (4200 m a.s.l.), J. Glaciol., 46(154), 507-515, doi:10.3189/172756500781833098, 2000.

Eichler, A., Schwikoski M., and Gäggeler H. W.: Meltwater-induced relocation of chemical species in Alpine firn, Tellus B, 53(2), 192-203, doi:10.1034/j.1600-0889.2001.d01-15.x, 2001.

Eichler, A., Schwikowski M., Furger M., Schotterer U., and Gäggeler H.W.: Sources and distribution of trace species in Alpine precipitation inferred from two 60-year ice core paleorecords, Atmos. Chem. Phys. Dicuss., 4, 71-108, 2004.

Field, R. D., Jones, D. B. A. and Brown, D. P.: Effects of postcondensation exchange on the isotopic composition of water in the atmosphere, J. Geophys. Res.-Atmos., 115(D24), doi:10.1029/2010JD014334, 2010.

Frei, C., and Schär, C.: A precipitation climatology of the Alps from high-resolution rain-gauge observations, Int. J. Climatol., 18, 873-900, doi:10.1002/(SICI)1097-0088(19980630)18:8<873::AID-JOC255>3.0.CO;2-9, 1998.

Friedman, I., Machta, L. and Soller, R.: Water-vapor exchange between a water droplet and its environment, J. Geophys. Res., 67(7), 2761–2766, doi:10.1029/JZ067i007p02761, 1962.

Fröhlich, K., Kralik M., Papesch W., Rank D., Scheifinger H., and Stichler W.: Deuterium excess in precipitation of Alpine regions – moisture recycling, Isot. Environ. Heal. S. 44, 61-70, doi:10.1080/10256010801887208, 2008.

Gat, J.R.: Oxygen and hydrogen isotopes in the hydrologic cycle, Annu. Rev. Earth Ol. Sc., 24, 225-262, doi:10.1146/annurev.earth.24.1.225, 1996.

Hammer, C. U., Clausen, H. B., Dansgaard, W., Gundestrup, N., Johnsen, S. J. and Reeh, N.: Dating of Greenland ice cores by flow models, isotopes, volcanic debris, and continental dust, J. Glaciol., 20, 3–26, 1978.

Henderson, K., Laube, A., Gäggeler, H. W., Olivier, S., Papina, T., and Schwikowski, M.: Temporal variations of accumulation and temperature during the past two centuries from Belukha ice core, Siberian Altai, J. Geophys. Res., 111, D03104, 2006.

Herren, P.-A., Eichler, A., Machguth, H., Papina, T., Tobler, L., Zapf, A. and Schwikowski, M.: The onset of Neoglaciation 6000 years ago in western Mongolia revealed by an ice core from the Tsambagarav mountain range, Quat. Sci. Rev., 69, 59–68, doi:10.1016/j.quascirev.2013.02.025, 2013.

IAEA/WMO, Global Network of Isotopes in Precipitation. The GNIP Database. Accessible at: http://www.iaea.org/water (2013).

Jenk, T.M.: Ice core based reconstruction of past climate conditions and air pollution in the Alps using radiocarbon, Ph.D. thesis, Department of Chemistry and Biochemistry, University of Bern, Bern, Switzerland, 165 pp., 2006.

Johnsen, S. J.: Stable isotope homogenization of polar firn and ice, Proc. Symp. on Isotopes and Impurities in Snow and Ice, I.U.G.G.XVI, General Assembly, Grenoble Aug. Sept. 1975, 15, 210–219, Washington 1977, 1977.

Johnsen, S. J., Clausen, H. B., Cuffey, K. M., Hoffmann, G., Schwander, J., and Creyts, T.: Diffusion of stable isotopes in polar firn and ice: the isotope effect in firn diffusion, in: Physics of Ice Core Records, edited by: Hondoh, T., Hokkaido University Press, Sapporo, 2000.

Jouzel, J. and Souchez, R. A.: Melting-refreezing at the glacier sole and the isotopic composition of the ice, J. Glaciol., 28(98), 1982.

Jouzel, J., and Merlivat, L.: Deuterium and oxygen 18 in precipitation: modeling of the isotopic effects during snow formation, J. Geophys. Res., 89, 11749–11757, doi:10.1029/JD089iD07p11749, 1984.

Jouzel, J., Alley, R. B., Cuffey, K. M., Dansgaard, W., Grootes, P., Hoffmann, G., Johnsen, S. J., Koster, R. D., Peel, D., Shuman, C. A., Stievenard, M., Stuiver, M. and White, J.: Validity of the temperature reconstruction from water isotopes in ice cores, J. Geophys. Res. Oceans, 102(C12), 26471–26487, doi:10.1029/97JC01283, 1997a.

Jouzel, J., Fröhlich, K. and Schotterer, U.: Deuterium and oxygen-18 in present-day precipitation: data and modelling, Hydrol. Sci. J., 42(5), 747–763, doi:10.1080/02626669709492070, 1997b.

Jouzel, J., Hoffmann, G., Koster, R. D. and Masson, V.: Water isotopes in precipitation: data/model comparison for present-day and past climates, Quat. Sci. Rev., 19(1–5), 363–379, doi:10.1016/S0277-3791(99)00069-4, 2000.

Jouzel, J.: Water stable isotopes: Atmospheric composition and applications in polar ice core studies, in Treatise on geochemistry, vol. 4, pp. 213–243, 2003.

Kalnay, E., Kanamitsu, M., Kistler, R., Collins, W., Deaven, D., Gandin, L., Iredell, M., Saha, S., White, G.,Woollen, J., Zhu, Y., Leetmaa, A., Reynolds, R., Chelliah, M., Ebisuzaki,W., Higgins, W., Janowiak, J., Mo, K. C., Ropelewski, C.,Wang, J., Jenne, R., and Joseph, D.: The NCEP/NCAR 40-Year Reanalysis Project, B. Am. Meteorol. Soc., 77, 437–471, 1996.

Kohn, M. J. and Welker, J. M.: On the temperature correlation of $\delta^{18}O$ in modern precipitation, Earth Planet. Sci. Lett., 231(1–2), 87–96, doi:10.1016/j.epsl.2004.12.004, 2005.

Liu, J., Fu, G., Song, X., Charles, S. P., Zhang, Y., Han, D. and Wang, S.: Stable isotopic compositions in Australian precipitation, J. Geophys. Res.-Atmos, 115(D23), D23307, doi:10.1029/2010JD014403, 2010.

Meteoswiss, Documentation of MeteoSwiss Grid-Data Products - Monthly and Yearly Precipitation: RhiresM and RhiresY. Accessible at http://www.meteosuisse.admin.ch/web/de/services/datenportal/gitterdaten/precip/RhiresM.Par.0006.DownloadFile.tmp/proddocrhiresm.pdf, 2013.

Noone, D. and Sturm, C.: Comprehensive Dynamical Models of Global and Regional Water Isotope Distributions, in Isoscapes, edited by West, J. B., Bowen, G. J., Dawson, T. E., and Tu, K. P., pp. 195–219, Springer, Netherlands, 2010.

Nye, J. F.: Correction factor for accumulation measured by the thickness of the annual layers in an ice sheet, J. Glaciol., 4, 785–788, 1963.

Persson, A., Langen, P. L., Ditlevsen, P., and Vinther, B. M.: The influence of precipitation weighting on interannual variability of stable water isotopes in Greenland, J. Geophys. Res., 116, D20120, doi:10.1029/2010JD015517, 2011.

Risi, C., Bony, S. and Vimeux, F.: Influence of convective processes on the isotopic composition (δ^{18}O and δD) of precipitation and water vapor in the tropics: 2. Physical interpretation of the amount effect, J. Geophys. Res.-Atmos., 113(D19), doi:10.1029/2008JD009943, 2008.

Rozanski, K., Araguas-Araguas, L. and Gonfiantini, R.: Relation between long-term trends of oxygen-18 isotope composition of precipitation and climate, Science, 258, 981–985, 1992.

Rozanski, K., Araguas-Araguas, L., and Gonfiantini, R.: Isotopic patterns in modern global precipitation, Geophys. Monogr., 78, 1–36, 1993.

Rozanski, K., Johnsen, S. J., Schotterer, U. and Thompson, L. G.: Reconstruction of past climates from stable isotope records of palaeo-precipitation preserved in continental archives, Hydrolog. Sci. J., 42(5), 725–745, doi:10.1080/02626669709492069, 1997.

Saurer, M., Kress, A., Leuenberger, M., Rinne, K. T., Treydte, K. S. and Siegwolf, R. T. W.: Influence of atmospheric circulation patterns on the oxygen isotope ratio of tree rings in the Alpine region, J. Geophys. Res-Atmos., 117, doi:10.1029/2011JD016861, 2012.

Schoener, W., Auer, I., Bohm, R., Keck, L. and Wagenbach, D.: Spatial representativity of air-temperature information from instrumental and ice-core-based isotope records in the European Alps, Ann. Glaciol., 35(1), 157–161, doi:10.3189/172756402781816717, 2002.

Schotterer, U., Oeschger, H., Wagenbach, D. and Münnich, K. O.: Information on paleo-precipitation on a high altitude glacier Monte Rosa, Switzerland.. Z. Gletscherkunde Glazialgeol, 21: 379–388, 1985.

Schotterer, U., Fröhlich, K., Gäggeler, H. W., Sandjordj, S. and Stichler, W.: Isotope records from Mongolian and Alpine ice cores as climate indicators, Climatic Change, 36(3-4), 519–530, doi:10.1023/A:1005338427567, 1997.

Schotterer, U., Stichler, W., Graf, W., Bürki, H.U., Gourcey, L., Ginot, P., Huber, T.: Stable isotopes in alpine ice cores: do they record climate variability? In: Proc. Of an International Symposium on the Study of Environmental Change using Isotope Techniques, IAEA Vienna, 23-27 April 2001, IAEA, Vienna, 2002.

Schotterer, U., Stichler, W., and Ginot, P.: The influence of post-depositional effects on ice core studies: examples from the Alps, Andes, and Altaı, in: Earth Paleoenvironments: Records preserved in Mid- and Low-Latitude Glaciers, edited by: De Wayne Ceciel, L., Green, J.R., and Thompson, L. G., Developments in Paleoenvironmental Research Series, Kluwer Academic Publishers, 39–60, 2004.

Schürch, M., Kozel, R., Schotterer, U. and Tripet, J.-P.: Observation of isotopes in the water cycle—the Swiss National Network (NISOT), Environ. Geol., 45(1), 1–11, doi:10.1007/s00254-003-0843-9, 2003.

Schwerzmann, A., Funk M., Blatter H., Lüthi M., Schwikowski M., and Palmer A.: A method to reconstruct past accumulation rates in alpine firn regions: A study on Fiescherhorn, Swiss Alps, J. Geophys. Res., 111, F01014, doi:10.1029/2005JF000283, 2006.

Schwikowski, M., Seibert, P., Baltensperger, U. and Gaggeler, H. W.: A study of an outstanding Saharan dust event at the high-alpine site Jungfraujoch, Switzerland, Atmos. Environ., 29(15), 1829–1842, doi:10.1016/1352-2310(95)00060-C, 1995.

Schwikowski, M., Brütsch, S., Gäggeler, H. W., and Schotterer, U.: A high-resolution air chemistry record from an Alpine ice core: Fiescherhorn glacier, Swiss Alps, J. Geophys. Res., 104(D11), 13709–13719, doi:10.1029/1998JD100112, 1999.

Schwikowski, M., Barbante, C., Doering, T., Gaeggeler, H. W., Boutron, C., Schotterer, U., Tobler, L., Van de Velde, K., Ferrari, C., Cozzi, G., Rosman, K. and Cescon, P.: Post-17th-century changes of European lead emissions recorded in high-altitude alpine snow and ice, Environ. Sci. Technol., 38(4), 957–964, doi:10.1021/es034715o, 2004.

Seibert, D. P.: South foehn studies since the ALPEX experiment, Meteorol. Atmos. Phys., 43(1-4), 91–103, doi:10.1007/BF01028112, 1990.

Siegenthaler, U., and Oeschger, H.: Correlation of ^{18}O in precipitation with temperature and altitude, Nature, 285, 314–317, doi:10.1038/285314a0, 1980.

Sigl, M.: Ice core based reconstruction of past climate conditions from Colle Gnifetti, Swiss Alps, Ph.D. thesis, Department of Chemistry and Biochemistry, University of Bern, Bern, Switzerland, 200 pp., 2009.

Sodemann, H., and Zubler E.: Seasonal and inter-annual variability of the moisture sources for Alpine precipitation during 1995-2002, Int. J. Climatol., 30, 947-961, 2009.

Stichler, W. and Schotterer, U.: From accumulation to discharge: modification of stable isotopes during glacial and post-glacial processes, Hydrol. Process., 14(8), 1423–1438, 2000.

Stichler, W., Schotterer, U., Fröhlich, K., Ginot, P., Kull, C., Gäggeler, H. and Pouyaud, B.: Influence of sublimation on stable isotope records recovered from high-altitude glaciers in the tropical Andes, J. Geophys. Res.-Atmos., 106(D19), 22613–22620, doi:10.1029/2001JD900179, 2001.

Sturm, C., Zhang, Q., and Noone, D.: An introduction to stable water isotopes in climate models: benefits of forward proxy modelling for paleoclimatology, Clim. Past, 6, 115–129, doi:10.5194/cp-6-115-2010, 2010.

Trouet, V. and Van Oldenborgh, G. J.: KNMI Climate Explorer: A Web-Based Research Tool for High-Resolution Paleoclimatology, Tree-Ring Res., 69(1), 3–13, doi:10.3959/1536-1098-69.1.3, 2013.

Uppala, S. M., Kallberg, P. W., Simmons, A. J., Andrae, U., Bechtold, V. D., Fiorino, M., Gibson, J. K., Haseler, J., Hernandez, A., Kelly, G. A., Li, X., Onogi, K., Saarinen, S., Sokka, N., Allan, R. P., Andersson, E., Arpe, K., Balmaseda, M. A., Beljaars, A. C. M., Van De Berg, L., Bidlot, J., Bormann, N., Caires, S., Chevallier, F., Dethof, A., Dragosavac, M., Fisher, M., Fuentes, M., Hagemann, S., Holm, E., Hoskins, B. J., Isaksen, L., Janssen, P. A. E. M., Jenne, R., McNally, A. P., Mahfouf, J. F., Morcrette, J. J., Rayner, N. A., Saunders, R.

W., Simon, P., Sterl, A., Trenberth, K. E., Untch, A., Vasiljevic, D., Viterbo, P., and Woollen, J.: The ERA-40 re-analysis, Q. J. Roy. Meteor. Soc., 131, 2961–3012, 2005.

Wagenbach, D., Münnich, K. O., Schotterer, U. and Oeschger, H.: The anthropogenic impact on snow chemistry at Colle Gnifetti, Swiss Alps, Ann. Glaciol., 10, 183–187, 1988.

Yurtsever, Y., and Gat, J.R., Atmospheric waters, in: Stable Isotope Hydrology: Deuterium and Oxygen-18 in the Water Cycle, edited by: Gat, J. R., and Gonfiantini, R., Tech. Rep. Ser. 210, 103-142, Int. At. Energy Agency, Vienna, 1981.

5 Investigation of seasonal δ^{18}O and deuterium excess in the Swiss Alps

5.1 Fiescherhorn ice core versus the nearby Northern Alpine stations

Abstract

The interpretation of water stable isotopes in the European Alpine region is challenging due to both, topographic-induced effects and high variability of the moisture sources. Here we present a study involving seasonal δ^{18}O and deuterium excess from three Global Network of Isotopes in Precipitation (GNIP) stations and a high-altitude ice core from the Fiescherhorn glacier (3900 m a.s.l.), all the sites being <20 km distant and assumed to be affected by the same precipitation regimes. Within such limited region it was possible to analyze the spatial coherence of the signal in terms of altitudinal changes. The δ^{18}O was well correlated between all the sites and with temperature and showed an altitude effect slightly higher in summer compared to the other seasons, explainable with partial re-enrichment at the lower altitude sites. Accordingly, significant relationship was observed with summer relative humidity. For the ice core low correlations were obtained, due to precipitation seasonality and post-depositional effects such as smoothing and wind erosion in winter. Additionally, the absence of subannual stratigraphic markers introduces an uncertainty in the attribution of the ice core winter and summer signal. The deuterium excess, characterized by high frequency fluctuations, showed no correlation between the ice core signal and the lower elevation sites and tends to increase nonlinearly with altitude. For this parameter we observed a weak seasonal cycle, with lower values in spring and higher in fall that might be explained in terms of in-cloud and sub-cloud kinetic processes. No homogeneous relationship with the meteorological parameters was found. The common increasing trend of summer deuterium excess over 1993-2011 was explained with the increasing frequency of South-Westerly weather situations, carrying moisture from the high-deuterium excess Mediterranean basin. In winter, the medium altitude site Grimsel Hospiz showed significant anticorrelation between the deuterium excess and the NAO, suggesting for the first time a connection between the second order parameter and the atmospheric circulation over the Alpine region.

5.1.1 Introduction

Water stable isotopes are commonly used to investigate the hydrological cycle and temperature changes. The first evidences of the $\delta^{18}O$ as temperature proxy were given by Craig (1961) and Dansgaard (1964). The processes affecting the $\delta^{18}O$ can vary depending on different factors such as latitude, altitude, continentality, amount of precipitation (Dansgaard, 1964; Rozanski et al., 1993; Clark and Fritz, 1997). At mid-high latitudes however, the main driving factor is the rainout distillation controlled by temperature, e.g. (Dansgaard, 1964; Rozanski et al., 1992, 1993). The second order parameter deuterium excess (d) retrieved from the equation $d=\delta D-8\delta^{18}O$ depends on kinetic effects and can provide additional information about the moisture source conditions (Merlivat and Jouzel, 1979). Supported by the results obtained by GCM simulations, studies involving both Greenland and Antarctica polar ice cores interpreted the deuterium excess as proxy for sea surface temperature conditions of the source area, e.g. (Vimeux et al., 1999; Stenni et al., 2001; Masson-Delmotte et al., 2005). Other studies however suggest that the relative humidity at the source region is the main driver of the deuterium excess (Jouzel et al., 1982; Pfahl and Wernli, 2008; Pfahl and Sodemann, 2013).

In Central Europe and more specifically in the Alpine region the interpretation of both $\delta^{18}O$ and deuterium excess is complicated by topographically-induced effects (Siegenthaler and Oeschger, 1980; Schürch et al., 2003; Liebminger et al., 2006) and high intraseasonal variability of the moisture sources (Frei and Schär, 1998; Sodemann and Zubler, 2009).

Several studies have been conducted over the region in order to better understand the spatial variability of the isotopic signal in the Alps. The mountain chain extending approximately for 2000 km over Europe acts as a climatological divide between North Atlantic, continental and Mediterranean influence (Wanner et al., 1997; Barry, 2008). For the Swiss Alps two main regions can be distinguished: Northern and Southern Alps. The first one is more dominated by North Atlantic air masses and continental climate, the latter is more directly affected by the Mediterranean (Wanner et al., 1997; Sodemann and Zubler, 2009). The precipitation regimes result are quite different, with the Northern Alps getting more precipitation in summer and the Southern Alps receiving most of it in spring and fall, with generally higher amounts throughout the year. The variability of precipitation is also higher at the Southern sites (Frei and Schär, 1998; Eichler et al., 2004). In the Swiss Alps analyses conducted using the GNIP data (IAEA/WMO, 2013) as well as ice cores (Schotterer et al., 1997; Eichler et al., 2001) showed generally higher $\delta^{18}O$/temperature sensitivity with respect to other continental stations (Rozanski et al., 1992). Differences in the isotopic compositions were observed between

Northern and Southern Alps (Schotterer et al., 2001), the latter sites being more enriched due to generally higher average temperatures and the proximity to the Mediterranean sea (Schürch et al., 2003). The altitude effect (i.e. the progressive depletion of the air mass in the heavier isotopes with height due to orographic-forced uplift and distillation) was quantified as -0.2‰/100 m over the Alps using annual data (Schotterer et al., 1997 and Chapter 4) or seasonal data considering medium-low altitude sites (Siegenthaler and Oeschger, 1980; Schürch et al., 2003; Kern et al., 2013). However, it was also shown that over such limited region the lower altitude stations located approximately 50 km northwest (Bern) and southeast (Locarno) from the Alpine arc deviate from these trends, indicating other precipitation regimes with different rainout processes.

The deuterium excess was extensively analyzed only in the Austrian Alps. Different seasonality was observed at valley and higher altitude stations, the former showing a minimum in summer and the latter a maximum between June and October (Rank and Papesch, 2005; Liebminger et al., 2006). This difference was explained in terms of (i) subcloud re-evaporation processes that tend to decrease the deuterium excess in precipitation and whose effect clearly increases with cloud base-earth distance i.e. at lower elevation sites (Kaiser et al., 2001; Fröhlich et al., 2008), and (ii) enhanced Bergeron-Findeisen process in late summer-fall leading to increased kinetic fractionation and higher deuterium excess at the higher altitude sites (Liebminger et al., 2006). Accordingly, at the low elevation station Locarno, Switzerland, a minimum in the deuterium excess in summer was observed (Schotterer et al., 1993).

In this study we present and compare the seasonal $\delta^{18}O$ and deuterium excess records in precipitation from three GNIP stations in the Northern Swiss Alps and from an ice core record extracted from the near Fiescherhorn glacier in 2002 (Figure 1). The aim is to systematically investigate the spatial coherence of the isotopic signal on seasonal scale in a region affected by the same precipitation regimes, but at locations at different altitudes. For the seasonal scale the particular focus is on the winter and summer signal. Data from the three GNIP stations Meiringen, Guttannen, and Grimsel Hospiz, only 15 km distant from the glacier were considered, reaching a spatial resolution not achievable by any GCM or regional model (Figure 1). The stations were selected since they belong to the same climatic region, the Northern Alps as the Fiescherhorn glacier. The time period is limited by the short period covered by the GNIP stations (data collection started in 1971 for the $\delta^{18}O$ and in 1992 for the deuterium excess). The sites and datasets are described in section 5.1.2. The $\delta^{18}O$ and the deuterium excess are analyzed in section 5.1.3 and 5.1.4, respectively.

A discussion of seasonality and altitude effect of the isotopic signal is given in the subsections 5.1.3.1 and 5.1.4.1 for $\delta^{18}O$ and deuterium excess, respectively. The investigation of the winter and summer signal is presented in subsection 5.1.3.2 ($\delta^{18}O$) and 5.1.4.2 (deuterium excess). Summary and concluding remarks are given in section 5.1.5.

5.1.2 Sites and datasets description

The three GNIP stations (Meiringen, MEI in Figure 1, Guttannen, GTT and Grimsel Hospiz, GRH) and the Fiescherhorn glacier (FH) are located in the Northern Swiss Alps, at a relative distance <20 km (Table1 and Figure 1). One peculiarity of the GNIP stations is that they are located in different points along the Haslital valley, orientated approximately from north-west to south-east, extending from the Lake of Brienz (Brienzersee in Figure 1) toward the Alps. Meiringen is situated at a lower altitude (632 m a.s.l.) and is 10 km distant from the Lake of Brienz located at north-west. Guttannen is in a central position with respect to the valley length at about 10 km distance from Meiringen and at an altitude of 1055 m a.s.l.. Grimsel Hospiz, 10 km away from Guttannen, is located at medium altitude (1950 m a.s.l.), close to the lake and the pass of Grimsel at 2164 m a.s.l..

The drilling site at Fiescherhorn glacier is situated in the flat accumulation area at 3900 m a.s.l., with a steep cliff to the north (Jenk et al., 2006; Chapters 2 and 4 of this thesis).

All the sites belong climatologically to the Northern Alpine region. The main contribution to precipitation in winter is from extratropical cyclones developed along the storm track in the North Atlantic sector. In summer the main moisture sources are local land evaporation and precipitation assumes more convective features (Frei and Schär, 1998; Eichler et al., 2004; Barry, 2008; Sodemann and Zubler, 2009). The peak of precipitation is usually in summer.

For the GNIP stations the data used are $\delta^{18}O$ and deuterium excess in monthly precipitation together with temperature, precipitation and relative humidity (IAEA/WMO, 2013). Since 1992 the Federal Office for Water and Geology (FOWG), now Federal Office of the Environment (FOEN), has been the responsible for the analysis and data submission for the GNIP stations in Switzerland (Schürch et al., 2003).

The Fiescherhorn ice core was drilled in December 2002 (Jenk et al., 2006). Another ice core was previously drilled on this glacier, e.g. Schwikowski et al., (1999); Schotterer et al., (1997, 2004). In the 2002 campaign the bedrock was reached at a depth of 151 m and borehole temperatures indicate that the ice is frozen to the bedrock (Jenk, 2006). Melting features were observed and there is indication of low to moderate relocation of ions toward lower depths. However, the isotopic signal does not appear to be disturbed (Jenk, 2006).
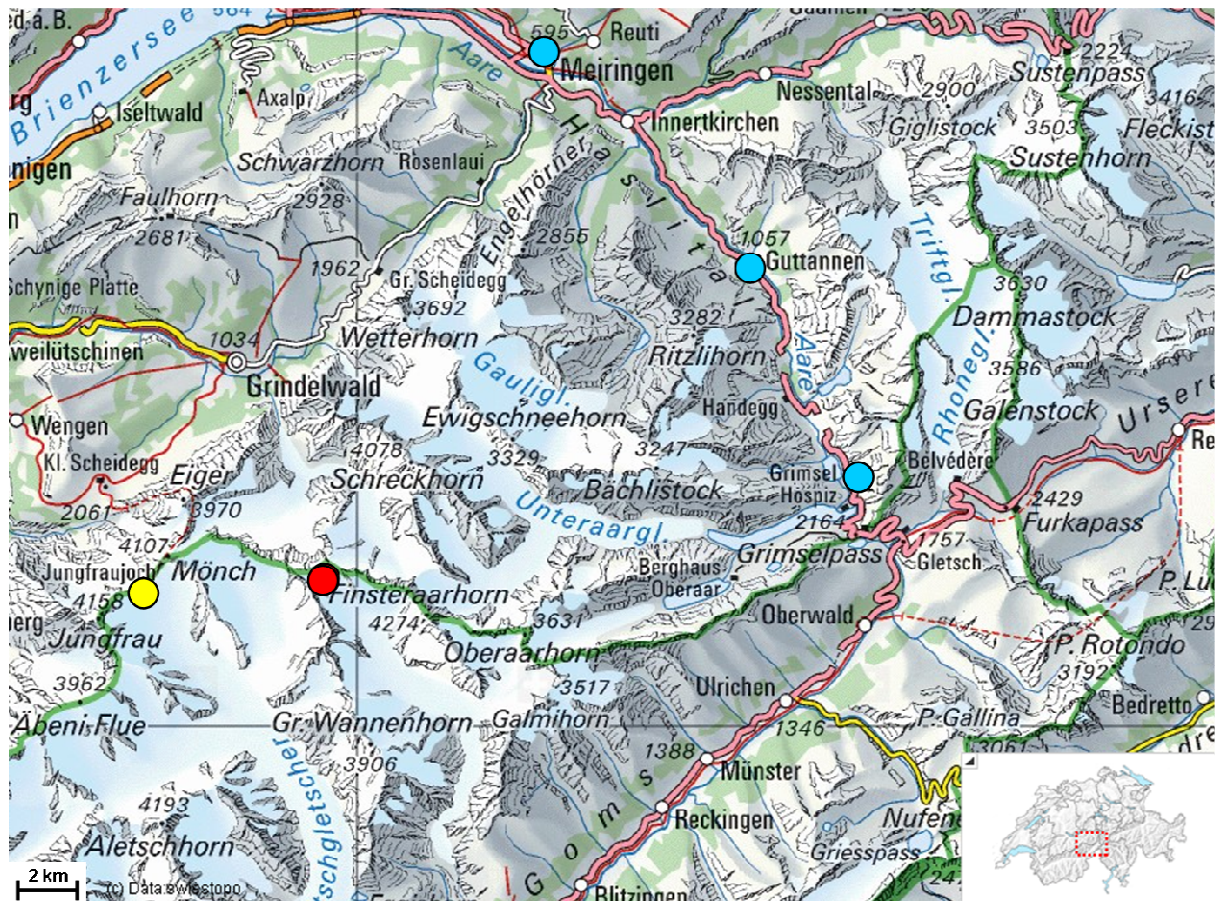
Figure 1 Location of the three GNIP stations Meiringen (632 m a.s.l.), Guttannen (1055 m a.s.l.), Grimsel Hospiz (1950 m a.s.l.), (light blue dots), Fiescherhorn glacier (red) and the Jungfraujoch weather station (yellow). The insert gives the location of this region in Switzerland. Source: Swisstopo, http://map.geo.admin.ch/).

The ice core covers approximately the last three hundred years with a dating uncertainty constrained by the reference horizons of ±1 year for the period ~1960-2002 (Chapter 4). The estimated surface accumulation rate is ~1.7 m water equivalent/year (Jenk, 2006). The data resolution for the period 1971-2001 considered here is ~8-25 points/year. The δ^{18}O and δD were measured with Isotopic Ratio Mass Spectrometry at the Climate and Environmental Physics department (KUP) at the University of Bern and the analytical uncertainty is <0.05‰ and <0.5‰, respectively (Jenk, 2006). The resulting uncertainty of the deuterium excess given by the propagation of the errors is ≈0.5‰.

The time period analyzed in this study is constrained by the overlap of the different datasets and the dating uncertainty of the ice core that has to be sufficiently low for the correlation analysis at interannual timescale. For the δ^{18}O we investigated the common period 1971-2001. For the deuterium excess no long common period is available. We therefore took the shorter period 1993-2001 for the comparison of the deuterium excess between the sites and a longer

period for the correlation analysis of the summer and winter signals (1971-2001 for Fiescherhorn and 1993-2011 for the GNIP stations) with the meteorological data and the relative $\delta^{18}O$. Datasets were tested for extreme outliers with 3σ and 3-interquartile range criteria. Trends significance was evaluated with a Mann-Kendall test. The time resolution considered in this study is seasonal. For the ice core isotopic record it is difficult to achieve higher time resolution (Stichler and Schotterer, 2000). This is due to the fact that, although a seasonal variability can be seen in the ice core record, the attribution of monthly values might be questionable due to the absence of subannual stratigraphic markers. Moreover only in the ideal case of uniform precipitation throughout the year the isotopic signal matches the actual cycle of temperature. This is almost never the case because seasonal cycles of precipitation (Persson et al., 2011) or post-depositional processes such winter wind erosion or diffusion (smoothing) both affect and may partially alter the signal (Stichler et al., 2001). Therefore the peaks and dips observed in an apparent well preserved seasonal record might actually be shifted or altered with respect to the temperature signal. The seasonal values of the ice core $\delta^{18}O$ and deuterium excess were obtained assuming constant seasonal distribution of snow, linearly interpolating the raw data and then evaluating the seasonal averages. For the GNIP data the precipitation-weighted seasonal mean of $\delta^{18}O$ and deuterium excess was taken. In the few cases where gaps were present the seasonal mean was approximated using two months instead of three.

Site	Coordinates	Altitude (m a.s.l.)
Meiringen	46°43'33.93"N, 8°11'8.60"E	632
Guttannen	46°39'23.18"N, 8°17'29.87"E	1055
Grimsel Hospiz	46°34'16.25"N, 8°19'53.90"E	1950
Fiescherhorn ice core	46°33'3.2"N, 8°04'0.4"E	3900

Table 1 Location and altitude of the four sites used in this study.

5.1.3 δ^{18}O

Figure 2 shows the monthly δ^{18}O data from the three stations Meiringen, Guttannen and Grimsel Hospiz together with the δ^{18}O record extracted from the Fiescherhorn ice core over the period 1971-2001.
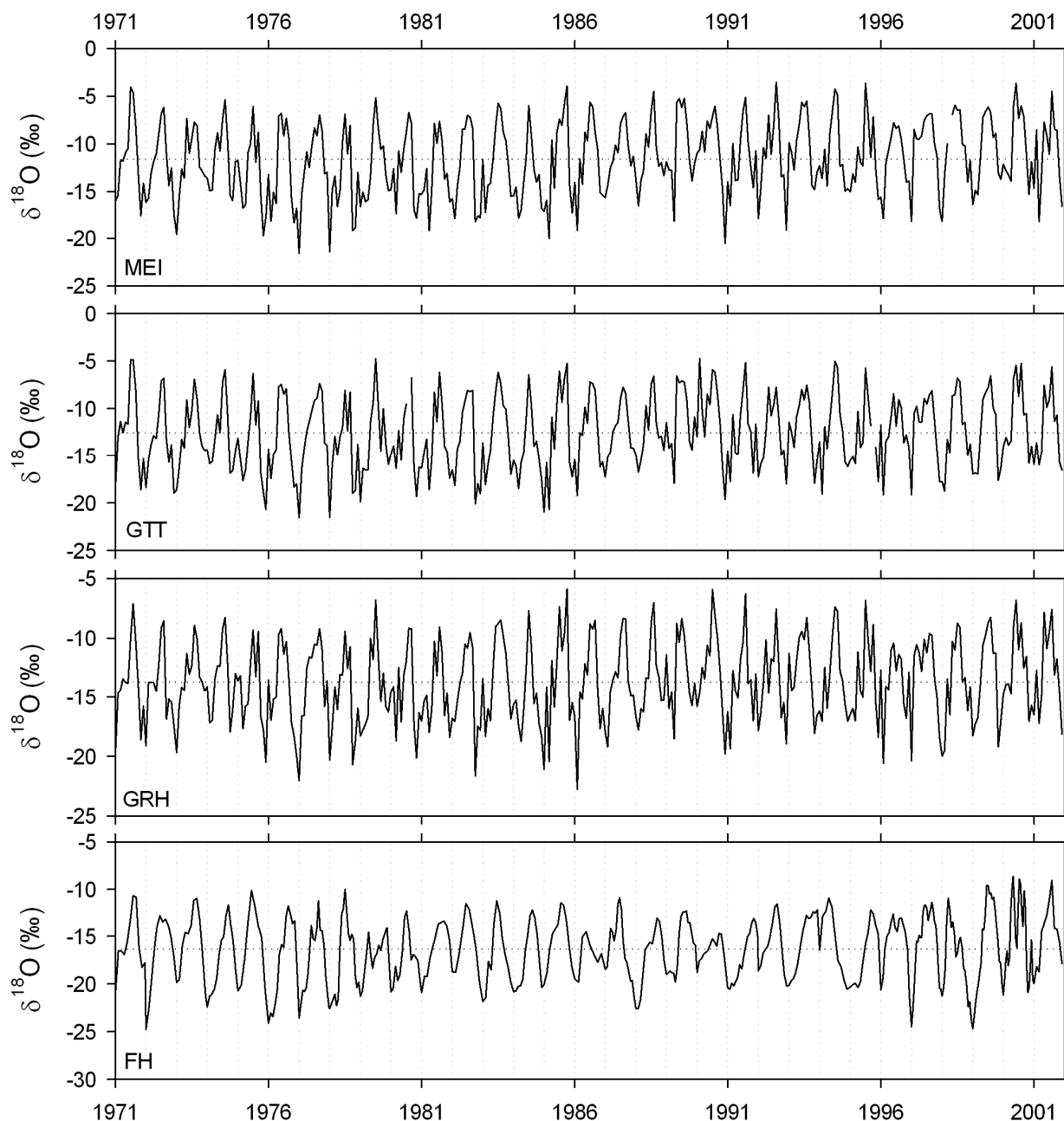

Figure 2 Monthly data of δ^{18}O from Meiringen, Guttannen, Grimsel Hospiz and Fiescherhorn ice core δ^{18}O (sampling resolution, 8-25 points/year) over the period 1971-2001. Dotted lines indicate the mean value: -11.61‰ (MEI), -12.57‰ (GTT), -13.69‰ (GRH), -16.36‰ (FH), see also Table 2, column (a).

All the records well reproduce the seasonal cycle of temperature in agreement with previous studies (Siegenthaler and Oeschger, 1980; Schürch et al., 2003 and Chapter 4). The GNIP δ^{18}O data show similar structures (see e.g. the years 1975, 1982-1983, 1985, 1991). The apparent smoothing in the Fiescherhorn δ^{18}O is due to both, diffusion in the firn (Johnsen, 1977; Johnsen et al., 2000) and reduced number of samples per year (e.g. in 1982, 1986, 1994 with less than 10 samples per year). Nevertheless structures coherent with the GNIP data are obvious e.g. in the years 1989-1990 and are generally present in the more recent part. The isotopic variability over the whole record, here expressed as 1σ, is 3-4‰ (Table 2).

	(a)	(b)	(c)	(d)	(e)
Site	All data (‰)	Winter (‰)	Spring (‰)	Summer (‰)	Fall (‰)
MEI	-11.61 (3.86)	-14.74 (1.75)	-11.98 (1.94)	-7.65 (1.22)	-12.17 (1.70)
GTT	-12.57 (3.82)	-15.60 (2.18)	-13.08 (1.41)	-8.74 (1.08)	-13.13 (1.42)
GRH	-13.69 (3.41)	-16.26 (1.75)	-14.16 (1.40)	-10.43 (1.01)	-14.73 (1.28)
FH	-16.36 (3.39)	-19.70 (1.93)	-16.98 (2.27)	-13.78 (1.72)	-16.59 (1.89)

Table 2 Mean value of the δ^{18}O at the GNIP stations and the Fiescherhorn ice core over the period 1971-2001. Numbers in parenthesis indicate 1σ. (a) Mean evaluated on the monthly and sampling resolution data for the GNIP stations and Fiescherhorn, respectively. (b), (c), (d), (e) Mean of the seasonal values, i.e. December to February for winter, March to May for spring, June to August for summer and September to November for fall. For the GNIP data the precipitation-weighted mean was used.

To qualitatively assess the degree of correlation of the seasonal δ^{18}O over the region we calculated the Spearman correlation coefficient ρ between all the series (Table 3). All the sites are as expected significantly correlated, with ρ exceeding 0.9 between the three GNIP sites and 0.6 between the stations and the Fiescherhorn.

ρ	MEI	GTT	GRH	FH
MEI		0.95	0.94	0.69
GTT			0.93	0.67
GRH				0.62

Table 3 Spearman correlation coefficients of the seasonal $\delta^{18}O$ at the sites, over the period 1971-2001, statistically significant at the 0.1 % level.

5.1.3.1 Seasonality and altitudinal change

The seasonality of the $\delta^{18}O$ signal and its variability are shown in Table 2 columns (b), (c), (d), (e) and Figure 3. At all sites the $\delta^{18}O$ clearly follows the seasonal temperature cycle. For the GNIP stations there is a particular strong enrichment in summer.
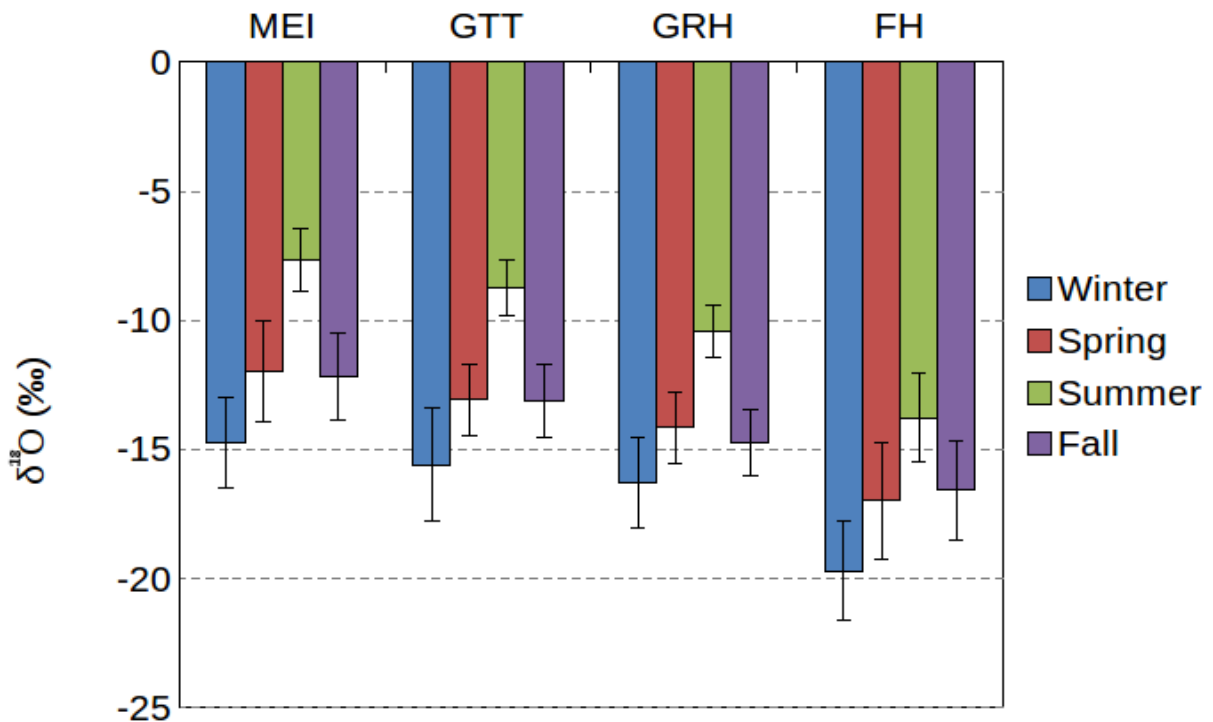
Figure 3 Seasonal means of the isotopic values over the period 1971-2001 at the four sites. The error bars indicate 1σ (Table 2).

In all the seasons it is possible to identify the altitude effect as can be seen from the mean values, see Table 2 column (a). In previous studies over the Swiss Alps a lapse rate of -0.2‰/100 m was reported (Siegenthaler and Oeschger, 1980; Schotterer et al., 1997, 2001; Schürch et al., 2003; Chapter 4 of this thesis). Here we quantify the change of altitude effect throughout the seasons including the Fiescherhorn ice core (Figure 4). In all the cases a linear relationship was found. In winter, spring and fall the variation of the $\delta^{18}O$ signal with height

is the same within the error (-0.15‰/100 m), whereas in summer it is slightly higher (-0.18‰/100 m). This is in contrast with a recent study using a new precipitation isoscape, a spatial map of isotopic variation involving several stations over Switzerland and its border zone for the years 1995-1996 (Kern et al., 2013). The authors observed a steeper gradient in winter with the higher altitude sites (>1000 m a.s.l.) hardly affected by altitudinal difference. They explained this outcome with the seasonal variation of the planetary boundary layer (PBL). In winter the PBL is located below the higher elevation sites that are thus affected by more well-mixed conditions with higher isotopic homogeneity compared to the lower stations. In our study we used only the stations close to the Fiescherhorn glacier and explain our result in terms of partial re-enrichment at the lower altitudes due to subcloud re-evaporation, especially strong in summer (Ambach et al., 1968; Liebminger et al., 2006; Fröhlich et al., 2008; Risi et al., 2008). This is consistent with the fact that Alpine precipitation in summer is mainly due to convective systems (Frei and Schär, 1998; Eichler et al., 2004; Sodemann and Zubler, 2009).
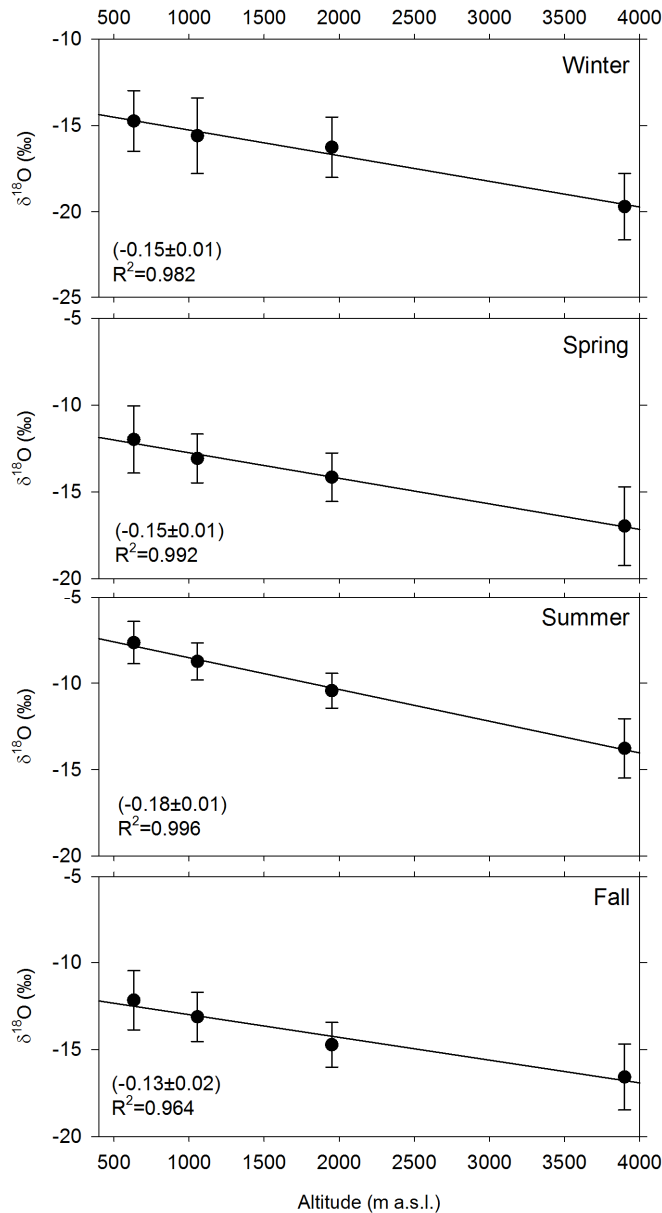
Figure 4 Seasonal $\delta^{18}O$ mean from the sites against their altitude. Mean values calculated over the period 1971-2001, the error bars indicate 1σ. The regression line obtained by least squares regression is given together with the corresponding slope and R^2.

5.1.3.2 Analysis of seasonal $\delta^{18}O$

In order to investigate to what extent the $\delta^{18}O$ signal is coherent over the studied region we analyzed its seasonality together with the respective temperature, precipitation-weighted temperature, relative humidity and seasonal sum of precipitation at the sites. For the Fiescherhorn the temperature and relative humidity data measured at the nearby high-alpine Jungfraujoch station (6 km west, 3500 m a.s.l.) by the Federal Office of Meteorology and Climatology (Meteoswiss) were used. Precipitation is not quantified at this site due to strong wind drift (Schotterer et al., 2001). We therefore tested the assumption of approximating the

ice core seasonal distribution of precipitation with the medium altitude Grimsel Hospiz precipitation data. However, caution should be used in the association of this parameter to the Fiescherhorn ice core accumulation. Although previous studies showed some agreement between the two sites (Schotterer et al., 2001), in this study no clear relationship between the local annual precipitation and the reconstructed accumulation at the glacier was observed (Chapter 4). This might be due to very local processes (e.g. local, sporadic precipitation events and partial snow removal in winter by winds) occurring at the glacier probably altering the relationship between the annual accumulation signal and the precipitation at the near sites. For the Guttannen station the temperature and relative humidity data are available only for the period 1971-2008 and 1971-1996, respectively.

The seasonality of these parameters is shown in Figure 5 and Table 4. We considered both the unweighted and the precipitation-weighted temperature, the first one to later investigate the δ^{18}O/temperature slope, the latter to see to what extent the relationship changes/improves including precipitation weighting that ideally better mimics the temperature signal deposition occurring only during precipitation (e.g. Jouzel et al., 1997a; Kohn and Welker, 2005; Persson et al., 2011; Brönnimann et al., 2013). At all the sites the precipitation-weighted temperature follows the seasonal cycle of temperature and no strong distinctions can be made from the unweighted case. As observed in Figure 2 the δ^{18}O well reflects the temperature cycle. Precipitation shows different seasonality for Meiringen and Guttannen with a peak in summer, whereas for the medium-altitude station Grimsel Hospiz it occurs in winter. This is due to the location of this station, close to a mountain pass probably receiving precipitation from both the flanks of the mountain. Not surprisingly, the relative humidity shows opposite cycles between low and high elevations. At low altitude minima (maxima) occur in summer (winter) due to the higher (lower) temperatures and higher (lower) humidity capacity. At higher elevations the relative humidity is lower in winter whereas in summer it increases due to the higher vertical extent of the planetary boundary layer. Temperature and relative humidity tend to decrease with altitude, precipitation to increase. In the case of Grimsel Hospiz and Fiescherhorn, the precipitation is mainly solid throughout the year, due to temperatures usually below 0°C (Table 4).

Site	Season	T (unw) (°C)	1σ (°C)	T (pw) (°C)	1σ (°C)	P (mm)	1σ (mm)	RH (%)	1σ (%)
MEI	Winter	-0.6	1.4	-0.5	1.5	272	100	84	3
	Spring	8.0	1.0	8.2	1.5	315	86	75	3
	Summer	16.1	1.0	16.0	0.9	456	69	81	4
	Fall	8.3	0.8	8.2	1.4	291	85	84	2
GTT	Winter	-0.6	1.6	-0.6	1.8	367	117	78	5
	Spring	6.2	1.9	6.0	2.0	453	127	75	3
	Summer	14.4	1.5	14.2	1.5	482	87	77	3
	Fall	7.2	1.2	7.0	1.6	403	122	79	3
GRH	Winter	-4.8	1.2	-5.1	1.4	558	205	68	6
	Spring	-0.5	1.1	-1.2	1.5	481	132	75	5
	Summer	8.4	1.0	8.1	1.0	400	69	76	6
	Fall	2.8	1.2	2.1	1.6	437	145	72	6
FH	Winter	-12.8	1.4	-13.3	1.6	558	205	69	8
	Spring	-9.9	1.1	-10.6	1.5	481	132	78	6
	Summer	-1.4	0.9	-1.7	0.8	400	69	78	5
	Fall	-6.1	1.2	-6.9	1.6	437	145	70	5

Table 4 Seasonal values of unweighted mean temperature ("unw"), precipitation-weighted temperature ("pw"), precipitation, relative humidity for Meiringen (MEI), Guttannen (GTT), Grimsel Hospiz (GRH) and Fiescherhorn (FH) over the period 1971-2001. The standard deviation is indicated by 1σ. For Guttannen, the relative humidity was calculated over the period 1971-1996. For Fiescherhorn the Jungfraujoch temperature and relative humidity and Grimsel Hospiz precipitation were used.
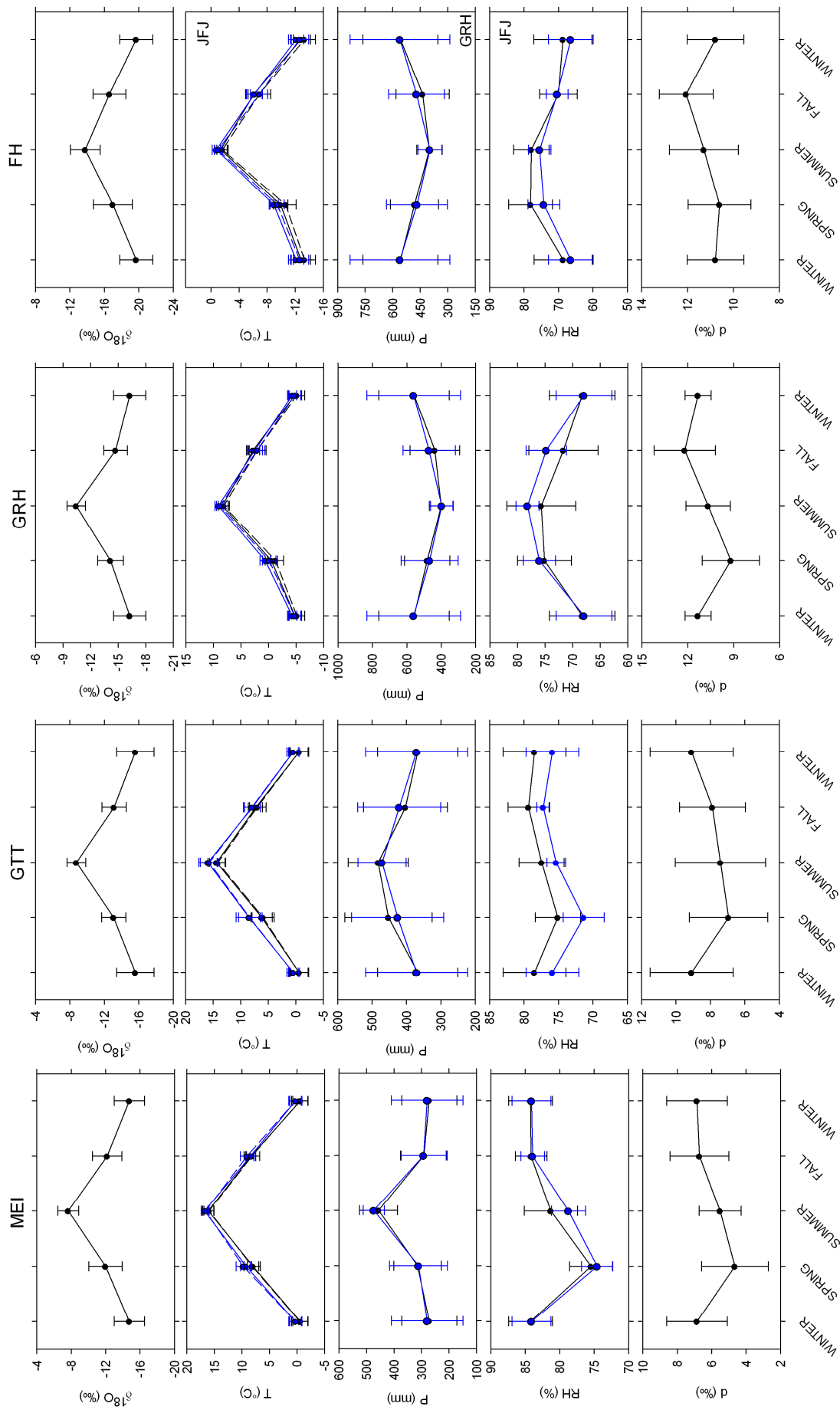
Figure 5 Seasonality of $\delta^{18}O$, unweighted and precipitation-weighted temperature (solid and dashed lines respectively), precipitation, relative humidity and deuterium excess for Meiringen (MEI), Guttannen (GTT), Grimsel Hospiz (GRH) and Fiescherhorn (FH). Winter to winter values are shown for better visualization of the seasonal cycle. In black the climatology related to the period 1971-2001, in blue for the common period of deuterium excess data (1993-2001). Error bars indicate 1σ evaluated over the respective periods, see Table 2, 4 and 7. For Guttannen the relative humidity was calculated over the period 1971-1996 (black) and 1993-1996 (blue). For Fiescherhorn the Jungfraujoch temperature and relative humidity and Grimsel Hospiz precipitation were used. For the precipitation-weighted temperature the Jungfraujoch temperature was weighted with the Grimsel Hospiz precipitation.

Because of the easier detection of minima and maxima, for the correlation analysis we focused on the winter and summer seasons. We considered the December to February and June to August precipitation-weighted mean $\delta^{18}O$ and correlated it with the corresponding seasonal temperature, precipitation and relative humidity. For the Fiescherhorn, because of the uncertainty introduced by both the precipitation sampling and the attribution of the season, we compared the $\delta^{18}O$ with different averages of the Jungfraujoch temperature in order to see in what period the ice core "winter/summer" $\delta^{18}O$ presumably records most of the temperature. This might be only a portion of the season, or might be shifted with respect to the actual winter and summer. In order to verify that, we took for winter the period from October to April and considered all the possible averages of contiguous months i.e. two, three, four months means. For the summer $\delta^{18}O$ we analogously investigated the period April-October. We repeated the same procedure also for the precipitation-weighted temperature using the Grimsel Hospiz precipitation. For winter $\delta^{18}O$ the highest correlation was found with the January-February (JF) unweighted mean temperature and October-November (ON) precipitation-weighted temperature, respectively. For summer $\delta^{18}O$ the highest correlations were obtained in both cases with August-September mean temperature (AS). We reported in Table 5 only the Spearman coefficients for which we found the highest correlations. The corresponding precipitation and relative humidity values were hence selected based on the $\delta^{18}O$/temperature relation (i.e. JF, ON, AS values).

	Winter				Summer			
	(a)	(b)	(c)	(d)	(e)	(f)	(g)	(h)
	T (unw)	T (pw)	P	RH	T (unw)	T (pw)	P	RH
MEI	**0.48**	**0.58**	-0.09	-0.15	**0.67**	**0.65**	-0.04	**-0.63**
GTT	**0.33**	**0.39**	-0.16	-0.13	**0.53**	**0.58**	**-0.36**	*0.38*
GRH	**0.50**	**0.54**	-0.13	*0.33*	**0.64**	**0.69**	*0.32*	-0.19
FH(*)	0.18		-0.07	*0.32*	*0.26*		0.01	0.003
FH(**)		0.18	-0.18	-0.26			0.22	0.01	0.003

Table 5 Spearman correlation coefficients between the winter precipitation-weighted $\delta^{18}O$ and the corresponding (a) unweighted, (b) precipitation-weighted temperature, (c) precipitation, (d) relative humidity over the period 1971-2001. (f), (g), (h), (i) As before, for summer values. (d) and (i) for Guttannen were evaluated over the period 1971-1996. For the Fiescherhorn marks (*) indicates the results based on the correlation with the unweighted temperature for JF mean in winter and AS in summer, (**) with the precipitation-weighted temperature ON mean in winter and AS in summer. Values statistically significant at a 10% and 5% level are shown in italic and bold, respectively.

For the GNIP stations $\delta^{18}O$ correlates significantly with temperature in both the seasons, with higher coefficients in summer slightly increasing with the precipitation-weighted temperature (Table 5). Guttannen shows generally lower correlations. In winter no significant relation was found between $\delta^{18}O$ and precipitation for neither of the sites. The correlations with winter relative humidity are negative at higher altitude. This would mean that drier surface air conditions might lead to sublimation and $\delta^{18}O$ enrichment in the snow at these sites although this effect is known to be small (Stichler and Schotterer, 2000). In summer $\delta^{18}O$ is anticorrelated with precipitation in Guttannen and Grimsel Hospiz indicating a possible amount effect (Dansgaard, 1964; Risi et al., 2008). In this case the negative correlation with summer relative humidity is only observed at lower elevations. We explain that in terms of possible re-evaporation processes that tend to leave the precipitation more enriched at lower elevations stations, but do not affect significantly the isotopic composition at higher stations, similarly to what was found by Liebminger et al. (2006).

The time series of winter $\delta^{18}O$, temperature, precipitation and relative humidity are shown in Figure 6. At all the sites the relationship between $\delta^{18}O$ and temperature can be observed inspecting common peaks and dips of $\delta^{18}O$ e.g. in 1975, 1990, 1997 (maxima), 1973, 1977, 1991 (minima). Interestingly the temperature minimum in winter 1981 is not accompanied by

correspondingly low $\delta^{18}O$. Higher precipitation occurred at all the GNIP stations but opposite relative humidity conditions were observed between the low and medium altitude station. It is possible that different factors may have led to a decoupling between the isotopic signal and temperature in that winter.

The summer values show significant increasing trends reflecting the temperature change (Figure 7 and Appenzeller et al., (2008)). In Meiringen and Grimsel Hospiz the $\delta^{18}O$ has been changing with a rate of (0.06 ± 0.02)‰/year and (0.05 ± 0.02)‰/year respectively, following an increase in temperature of 0.06-0.07°C/year. In Guttannen a similar trend was observed in temperature and $\delta^{18}O$, but the $\delta^{18}O$ trend was not significant. The relative humidity in both Meiringen and Guttannen shows a significant decreasing trend of (-0.27 ± 0.06)‰/year and (-0.25 ± 0.07)‰/year respectively, indicating a possible transition toward drier summers in the valley. The hot summer 1983 (Ropelewski, 1984) was recorded at all sites. The peak in the $\delta^{18}O$ might have resulted from high temperatures in combination with low precipitation and relative humidity. Interestingly, the $\delta^{18}O$ peak in 1989 seems not to be clearly associated to any of the other parameters.
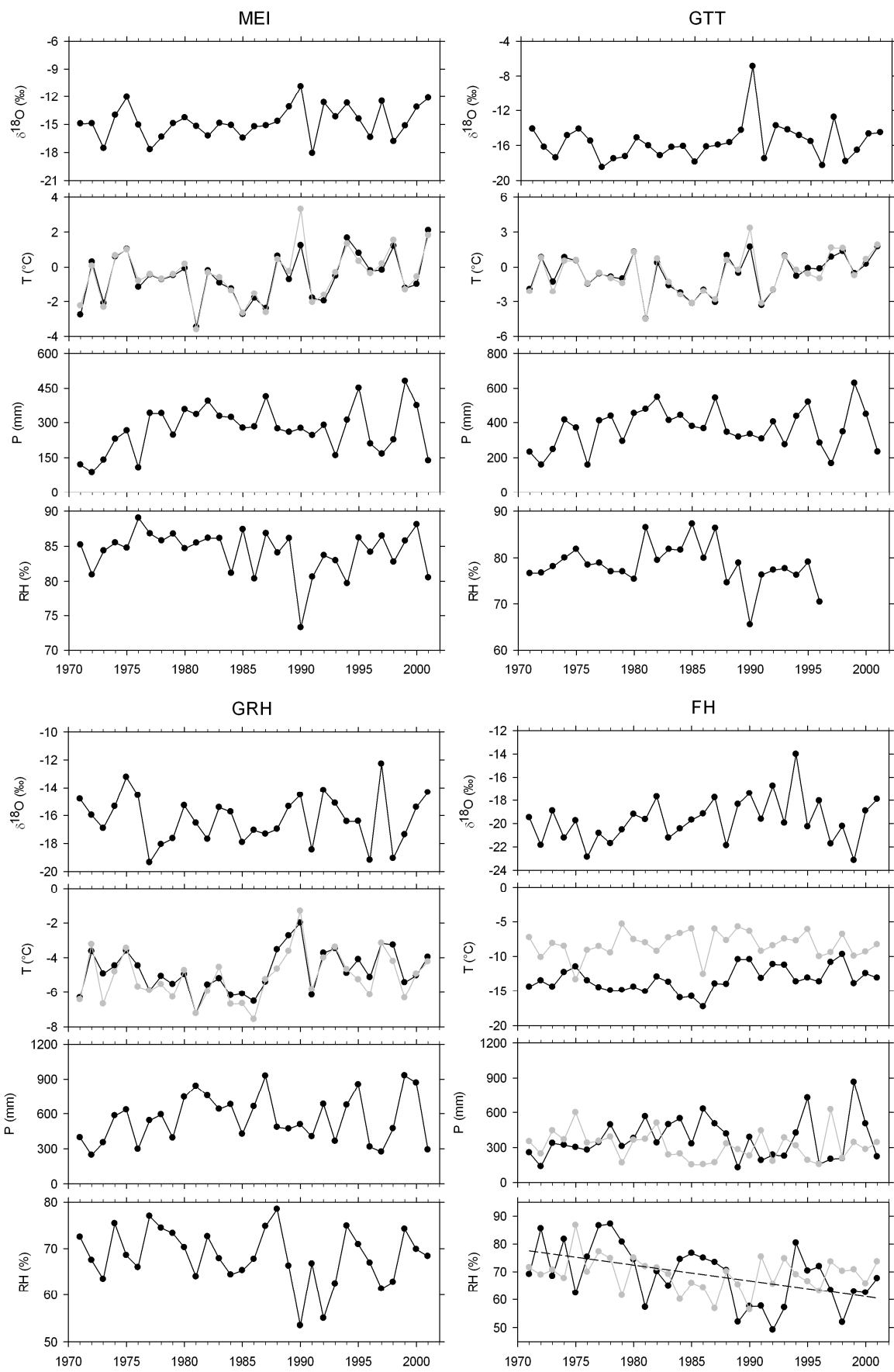
**Figure 6** Time series of winter $\delta^{18}O$ in Meiringen (MEI), Guttannen (GTT), Grimsel Hospiz (GRH) and Fiescherhorn (FH) together with the respective temperature, precipitation, relative humidity. In gray the precipitation-weighted temperature. For the Fiescherhorn the temperature and relative humidity from the Jungfraujoch station was used according to the results shown in Table 5. In black the JF mean temperature, in gray ON precipitation-weighted temperature using the Grimsel Hospiz precipitation data as weights. For the relative humidity JF mean in black and ON mean in gray). Significant trends ($p<0.05$) are shown with a dashed line.
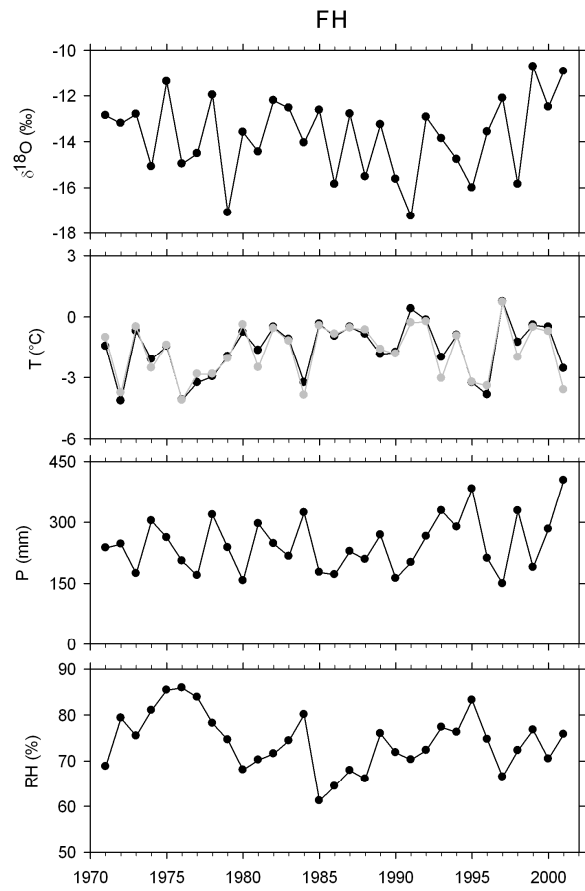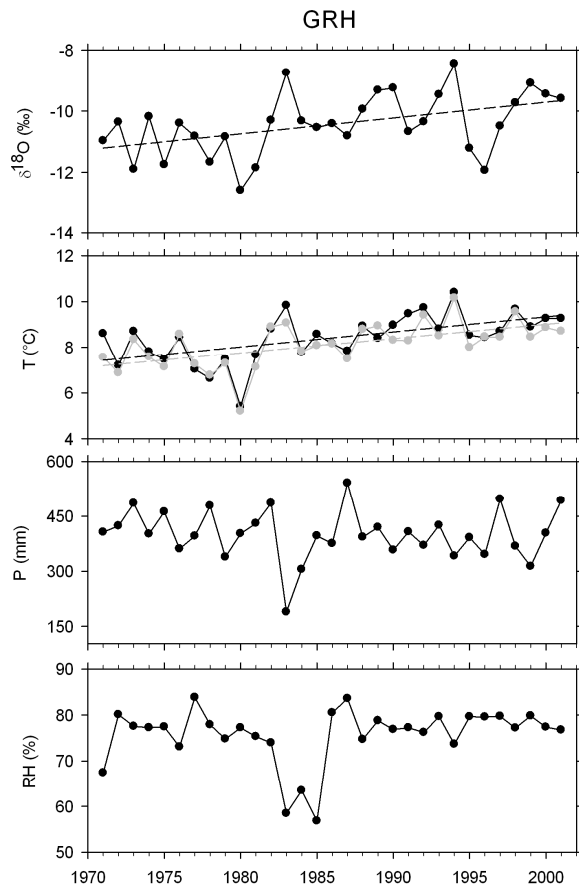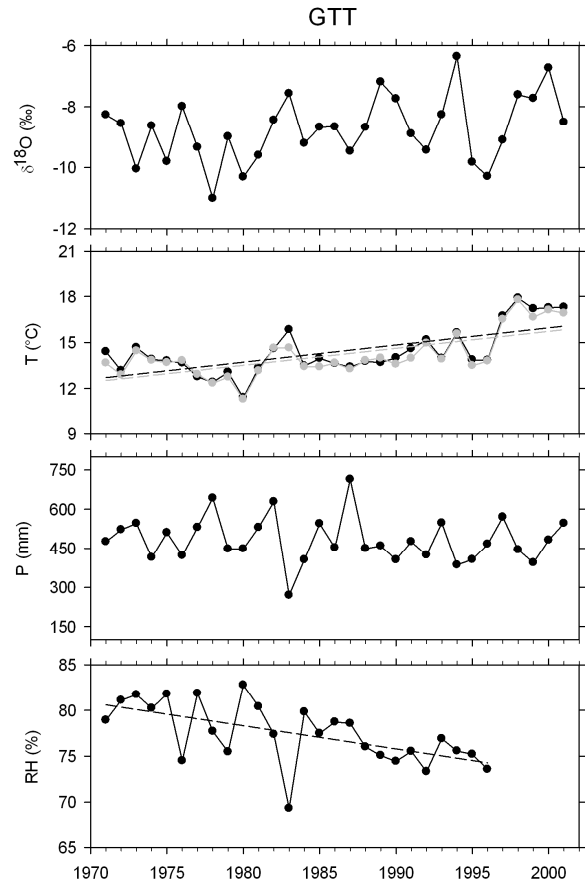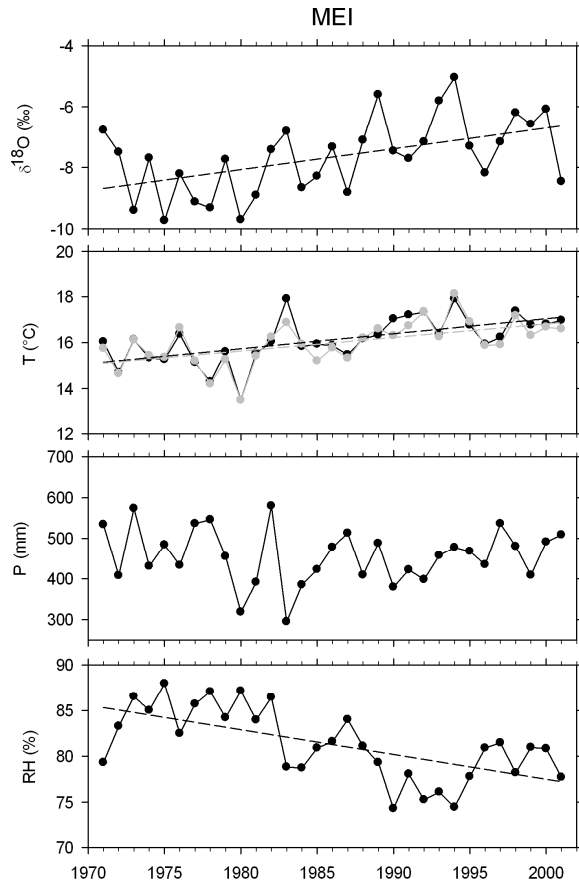
Figure 7 As Figure 6, but for summer. In gray the precipitation-weighted temperature. For the Fiescherhorn the temperature and relative humidity from the Jungfraujoch station was used according to the results shown in Table 5 (in black the AS mean temperature, in gray AS precipitation-weighted temperature using the Grimsel Hospiz precipitation data as weights. For precipitation and relative humidity AS values from Grimsel Hospiz and Jungfraujoch stations were used. Significant trends ($p < 0.05$) are shown with a dashed line.

The $\delta^{18}O$/temperature relation was evaluated with a least square linear regression of the data (previously inspected with jackknife residuals) and is shown in Table 6. In agreement with what was observed by (Schotterer et al., 1997) there is a general tendency for the lower stations toward higher slopes in summer. For Fiescherhorn the variability of $\delta^{18}O$ explained by temperature is quite low, as already shown in the correlation analysis (Table 5). This result is in agreement with what obtained in Chapter 4, where after removing the seasonal cycle the correlations significantly decreased.

	Winter		Summer	
	Slope	R^2	Slope	R^2
MEI	(0.56±0.21)	0.20	(0.82±0.17)	0.44
GTT	(0.25±0.17)	0.07	(0.39±0.11)	0.32
GRH	(0.65±0.23)	0.22	(0.67±0.13)	0.48
FH (*)	(0.16±0.20)	0.02	(0.17±0.24)	0.02
FH (**)	(0.17±0.19)	0.02	(0.17±0.25)	0.02

Table 6 $\delta^{18}O$/temperature relation indicated by the slopes and R^2 obtained for winter and summer, respectively. For Fiescherhorn (*) marks indicates the relation with the unweighted temperature (JF mean for winter and AS for summer) (**) with the precipitation-weighted temperature (ON mean for winter and AS for summer).

5.1.4 Deuterium excess

For the analysis of the deuterium excess record the common period 1993-2001 was considered. Figure 8 (a) shows the raw deuterium excess from the Fiescherhorn ice core over the period 1971-2001 together with the GNIP monthly data (panels (b)). At all the sites the deuterium excess is characterized by high frequency fluctuations (at monthly scale in the GNIP stations). Similar trends were observed at Grimsel Hospiz and Fiescherhorn (panel (c)), with the higher altitude sites showing lower variability compared to the lower elevation stations Meiringen and Guttannen. Interestingly, a decreasing trend throughout the whole 1999 and 2000 was observed. The apparent smoothing in the Fiescherhorn signal over the years 1993-1996 and 2001 is due a smaller number of data per year (<15 compared to 20-25 of the other years).

The mean values over the period are shown in Table 7 column (a), together with the standard deviation. A general increase of the deuterium excess with altitude is observed, with Fiescherhorn and Grimsel Hospiz showing similar values and the Fiescherhorn having a smaller variability than at the other sites.

Site	(a) All data (‰)	(b) Winter (‰)	(c) Spring (‰)	(d) Summer (‰)	(e) Fall (‰)
MEI	5.90 (3.36)	6.85 (1.21)	4.65 (1.57)	5.51 (2.02)	6.70 (1.85)
GTT	7.77 (3.97)	9.09 (2.41)	6.94 (2.28)	7.41 (2.63)	7.88 (1.92)
GRH	10.76 (3.22)	11.33 (0.85)	9.19 (1.87)	10.66 (1.46)	12.20 (2.00)
FH	11.15 (1.99)	10.78 (1.24)	10.60 (1.37)	11.28 (1.50)	12.06 (1.18)

Table 7 Mean values of the deuterium excess at the GNIP stations and the Fiescherhorn ice core over the period 1993-2001. Numbers in parenthesis indicate 1σ. (a) Average calculated from the monthly and raw data for the GNIP stations and Fiescherhorn, respectively. (b),(c),(d),(e) Mean of the seasonal values, i.e. December to February for winter, March to May for spring, June to August for summer and September to November for fall. For the GNIP data the precipitation-weighted mean was used.
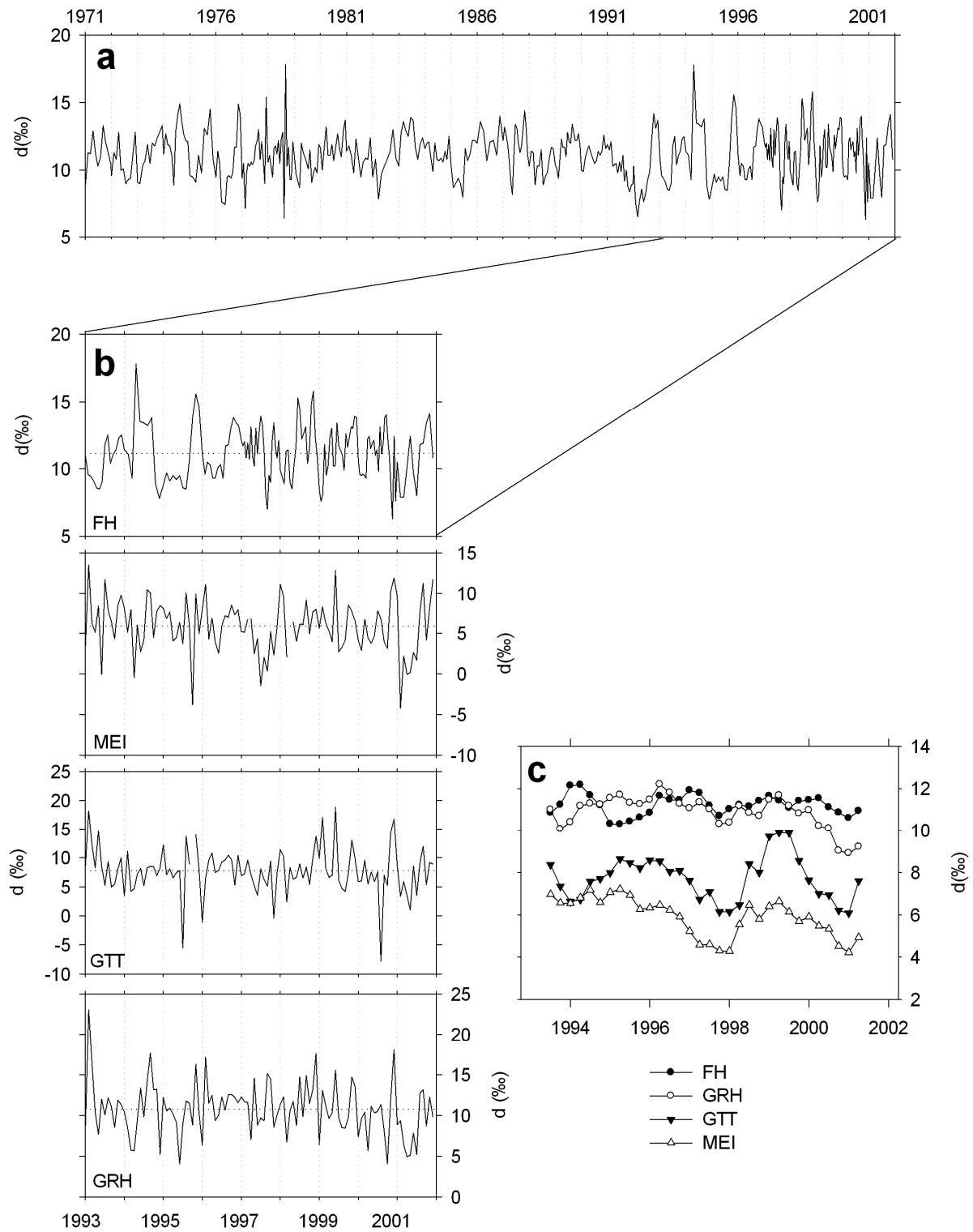
Figure 8 (a) Deuterium excess data from the Fiescherhorn ice core over the period 1971-2001 (sampling resolution). (b) Data over the period 1993-2001 for Fiescherhorn (FH), Meiringen (MEI), Guttannen (GTT), Grimsel Hospiz (GTT), monthly resolution for the GNIP stations. Dotted lines indicate the mean value over the period: 5.90‰ (MEI), 7.77‰ (GTT), 10.76‰ (GRH), 11.11‰ (FH over 1971-2001), 11.15‰ (FH over 1993-2001) see also Table 2.

153

(c) Time series of the seasonal averages of deuterium excess smoothed with a 5 points running mean filter.

The Local Meteoric Water Lines (LMWL) of the monthly data (sampling resolution for Fiescherhorn) for the period 1993-2001 show different behavior for the lower and the higher elevations sites (Figure 9). Meiringen and Guttannen have both lower slope and deuterium excess than Grimsel Hospiz and Fiescherhorn, indicating the presence of kinetic effects such as sub-cloud re-evaporation for the former sites, as it will be explained in section 5.1.4.2.
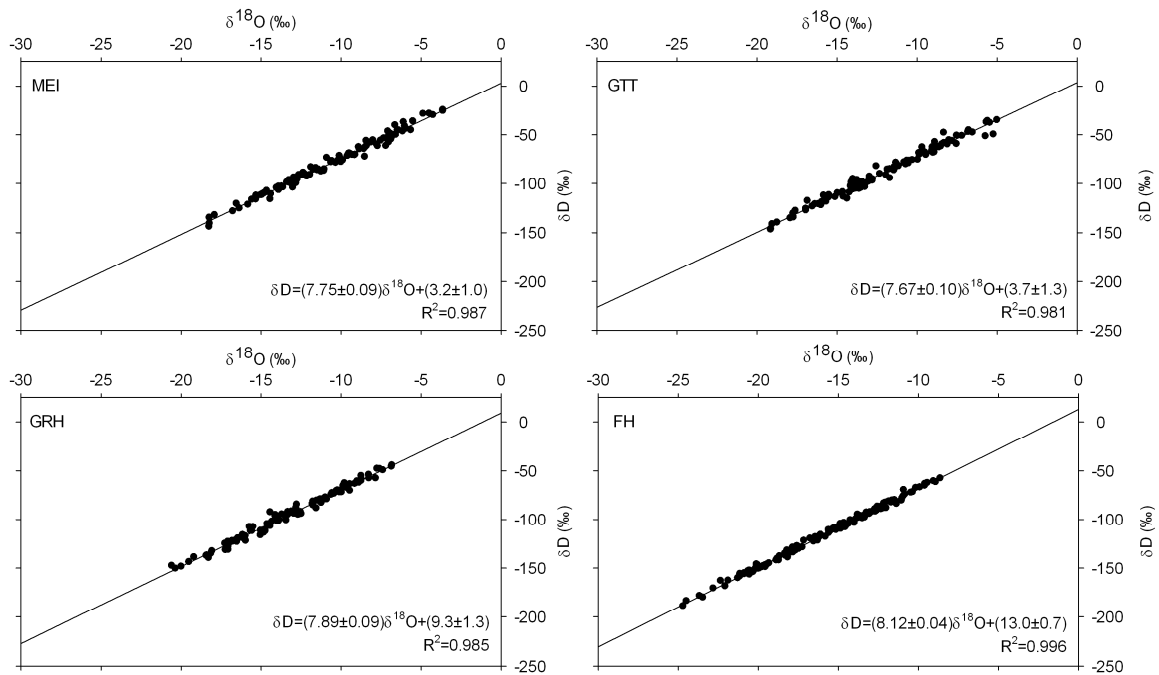
Figure 9 LMWL for Meiringen (MEI), Guttannen (GTT), Grimsel Hospiz (GRH) and Fiescherhorn (FH) for the period 1993-2001. The slope and intercept (deuterium excess) of the regression line is shown together with the coefficient of determination R^2.

On seasonal scale the deuterium excess is correlated between the GNIP stations. The Fiescherhorn shows significant correlations only with the high altitude Grimsel Hospiz station, implying possible common processes at the two high Alpine sites. Therefore Grimsel Hospiz presents common features with both the low and high altitude sites.

ρ	MEI	GTT	GRH	FH
MEI		**0.52**	**0.56**	0.10
GTT			**0.42**	-0.11
GRH				**0.35**

Table 8 Spearman correlation coefficients of the seasonal deuterium excess at the different sites, over the period 1993-2001. In bold coefficients statistically significant at a 5% level.

5.1.4.1 Seasonality and altitudinal change

The raw data of the deuterium excess show less pronounced seasonality than $\delta^{18}O$ as indicated by the seasonal averages and 1σ values in Figure 10 and Table 7 (b)-(e).
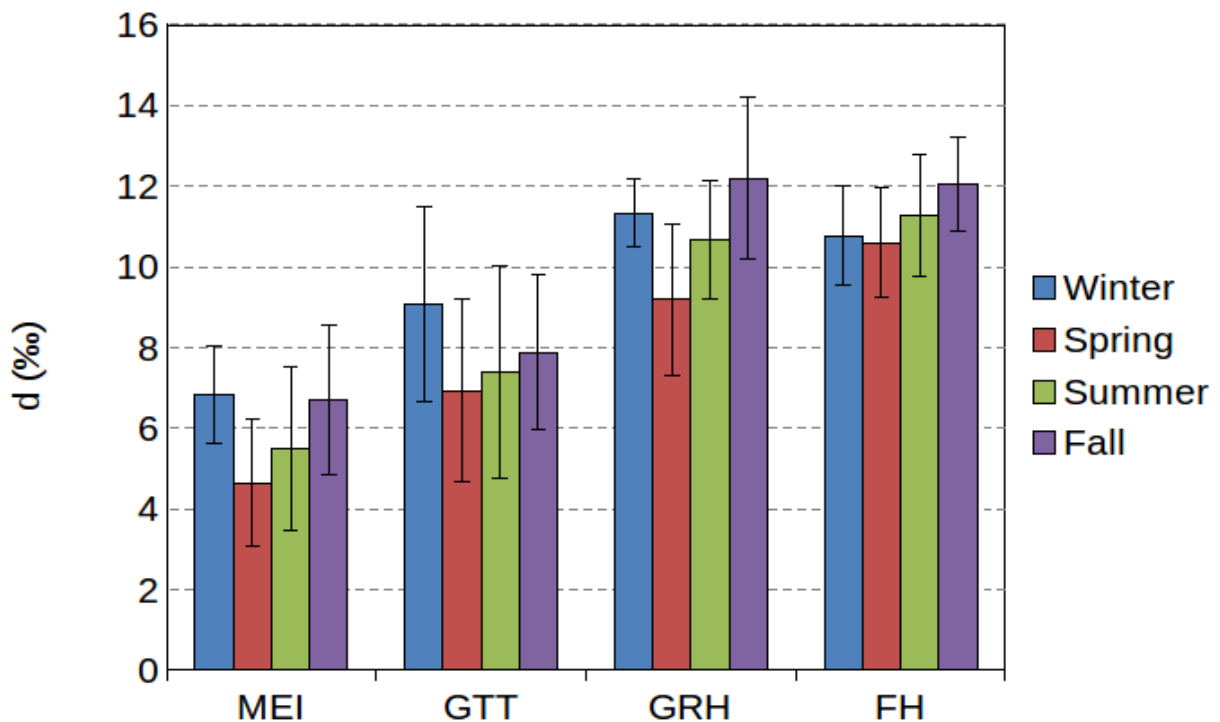
Figure 10 Seasonal means of the deuterium excess in precipitation over the period 1993-2001 at the four sites. The bars indicate 1σ.

All the sites show a general tendency toward higher values in fall-winter and lower deuterium excess in spring, but they are also affected by large variability in contrast to $\delta^{18}O$ for which a clear seasonality over the same period was found (analogously to Figure 3, not shown). Generally, the deuterium excess in this region shows a maximum (minimum) in winter (summer) due to lower (higher) relative humidity conditions related to the sea surface temperature in the oceanic source regions (Jouzel et al., 1997b; Schotterer et al., 1997). Due to topographic effects and precipitation seasonality local variations of the deuterium excess

seasonality might occur. Similarly to what we observed here, some of the Alpine Austrian stations show a peak in fall and lower values in spring (Rank and Papesch, 2005; Liebminger et al., 2006). According to that, we suggest that the parameter is similarly driven by local factors in the Swiss Alps, i.e. Bergeron-Findeisen processes and sub-cloud re-evaporation creating a sort of altitude effect (Liebminger et al., 2006). Changes in the moisture sources with stronger contribution from the Mediterranean in fall might as well affect the deuterium excess over the region. We investigated the altitudinal change of the deuterium excess throughout the seasons and observed an apparent nonlinear increase with altitude, with Grimsel Hospiz and Fiescherhorn deuterium excess resulting undistinguishable (Figure 11). A similar decoupling between lower and higher elevation sites was found in Antarctica by Masson-Delmotte et al. (2008), with more homogenous deuterium excess at lower altitudes and a linear increase with height above 2000 m a.s.l. This feature was attributed to different moisture sources. In the case of this limited region in the Alps the altitudinal change of deuterium excess with more homogeneous conditions at higher elevations is probably related to in-cloud and sub-cloud processes. At the lower elevation sites the deuterium excess tends to decrease because of sub-cloud re-evaporation whereas at higher altitudes it is more directly affected by in-cloud kinetic processes.
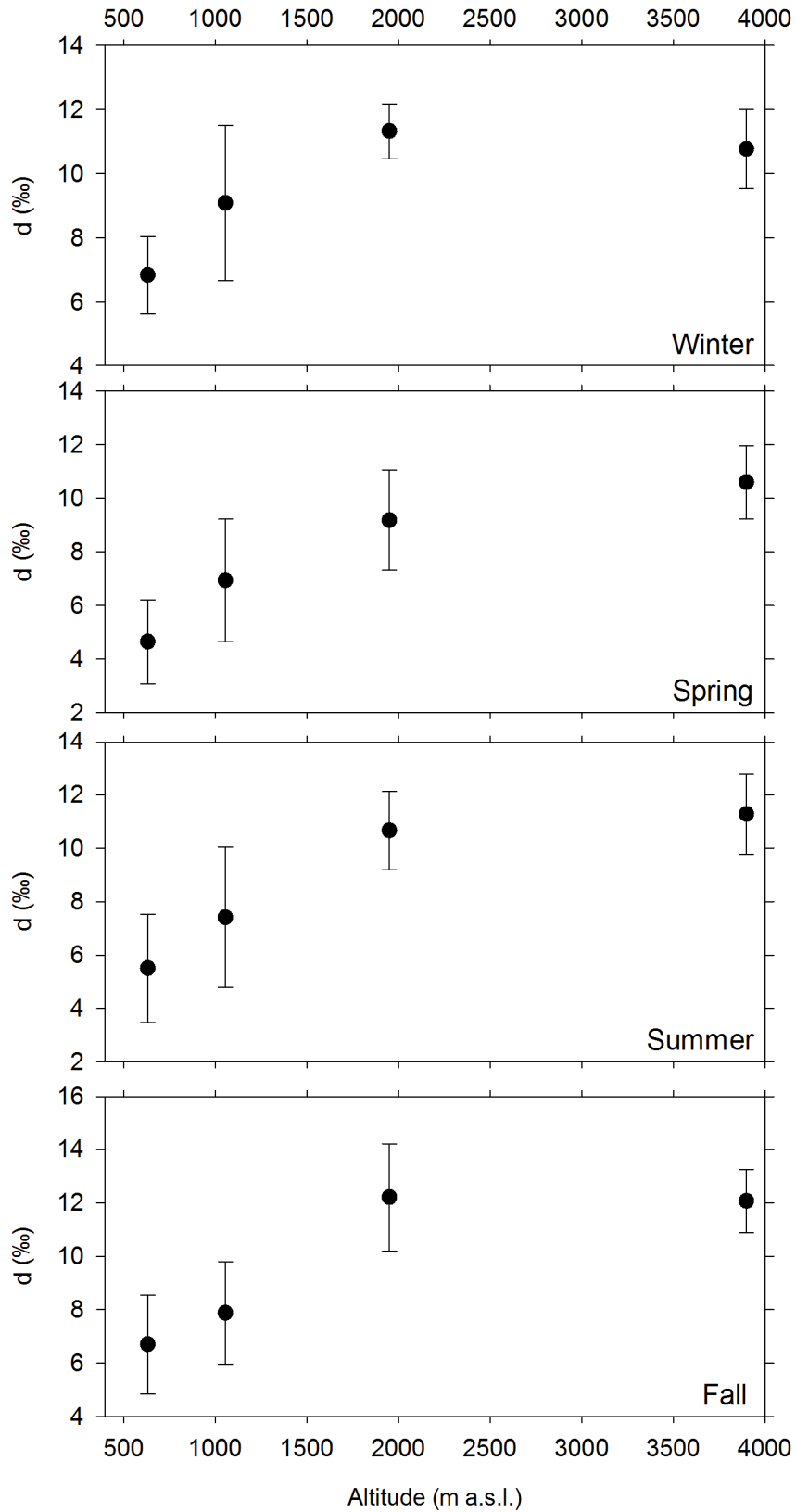
Figure 11 Seasonal deuterium excess d against altitude. Mean values calculated over the period 1993-2001, the error bars indicate 1σ.

5.1.4.2 Analysis of seasonal deuterium excess

For the comparison with the weather parameters we evaluated the climatology over the years 1993-2001, clearly not differing significantly from the longer period 1971-2001 (Figure 5). The corresponding data are shown in Table 9.

Site	Season	T (unw) (°C)	1σ (°C)	T (pw) (°C)	1σ (°C)	P (mm)	1σ (mm)	RH (%)	1σ (%)
MEI	Winter	0.3	1.2	0.3	1.0	279	130	84	3
	Spring	9.3	1.0	9.8	1.3	311	105	75	2
	Summer	16.8	0.6	16.6	0.7	474	38	79	2
	Fall	8.4	0.9	9.1	1.2	293	82	84	2
GTT	Winter	0.4	0.9	0.5	1.1	371	148	76	4
	Spring	8.5	2.4	8.4	2	426	134	71	3
	Summer	16.0	1.7	15.7	1.6	471	70	75	1
	Fall	7.9	1.4	8.0	1.5	421	121	77	1
GRH	Winter	-4.3	0.8	-4.7	1.1	560	272	68	5
	Spring	0.6	1.0	-0.1	1.2	468	166	76	3
	Summer	9.1	0.6	8.8	0.7	397	65	78	2
	Fall	2.5	1.4	2.1	1.4	470	153	75	4
FH	Winter	-12.1	1.1	-12.6	1.3	560	272	66	6
	Spring	-9.0	0.6	-9.4	1.0	468	166	74	5
	Summer	-0.8	0.6	-1.0	0.6	397	65	75	3
	Fall	-6.2	1.2	-6.9	1.2	470	153	70	3

Table 9 Climatology of the seasonal values of temperature ("unw"), precipitation-weighted temperature ("pw"), precipitation, relative humidity for Meiringen, Guttannen, Grimsel Hospiz and Fiescherhorn over the period 1993-2001. The standard deviation is indicated by the 1σ. For Guttannen, the climatology of relative humidity was evaluated over the period 1993-1996. For Fiescherhorn the Jungfraujoch temperature and relative humidity and Grimsel Hospiz precipitation were used.

There is apparently no link between the deuterium excess seasonality with minimum in spring and the other parameters, except for Meiringen and Guttannen where the cycle follows the relative humidity. For the correlation analysis with the weather parameters and the $\delta^{18}O$ a

longer time period is needed. We used the period 1971-2001 for the Fiescherhorn and 1993-2011 for the GNIP data. In contrast to $\delta^{18}O$, there is no clear relationship with the meteorological parameters, indicating that the deuterium excess behavior is rather complex over the region (Table 10). Generally summer temperatures are positively correlated with the deuterium excess at Grimsel Hospiz. The corresponding relative humidity shows a significant anticorrelation only in Meiringen. From the results obtained with the summer $\delta^{18}O$ we would expect a positive correlation with the deuterium excess, as re-evaporation would enrich the precipitation in the heavier isotopes and accordingly decrease the deuterium excess. It is therefore possible that other processes dominate the deuterium excess at this site.

A negative correlation was found between Grimsel Hospiz deuterium excess and temperature in winter. Such anticorrelation between the two parameters was also observed in Antarctica by Masson-Delmotte et al. (2008) and was explained in terms of (i) possible changes in the in equilibrium fractionation coefficients at low temperatures, (ii) kinetic fractionation related to supersaturation conditions and (iii) changes in moisture origin. However, the anticorrelation between winter deuterium excess and temperature in Grimsel Hospiz and in Meiringen with $\delta^{18}O$ are not reflected in the respective isotopic and temperature parameters (columns (e) and (a, b), respectively in Table 10), indicating that complex phenomena affect this isotopic parameter at these sites. This result is not understood at this point. No significant results were obtained with the precipitation.

	Winter					Summer				
	(a)	(b)	(c)	(d)	(e)	(f)	(g)	(h)	(i)	(j)
	T (unw)	T (pw)	P	RH	$\delta^{18}O$	T (unw)	T (pw)	P	RH	$\delta^{18}O$
MEI	0.02	0.06	0.14	-0.15	*-0.45*	0.04	0.07	0.27	**-0.58**	-0.17
GTT	-0.02	-0.17	0.16	/	-0.30	*0.35*	0.34	-0.11	/	0.23
GRH	**-0.50**	**-0.53**	-0.30	-0.14	-0.10	**0.40**	**0.54**	-0.15	-0.18	0.28
FH(*)	-0.24		0.19	-0.09	0.01	0.24		-0.06	-0.06	0.10
FH(**)		-0.17	0.12	0.11			0.23	-0.06	-0.06	

Table 10 Spearman correlation coefficients between the winter precipitation-weighted deuterium excess and the corresponding (a) unweighted, (b) precipitation-weighted temperature, (c) precipitation, (d) relative humidity, (e) $\delta^{18}O$ over the period 1993-2011 (GNIP stations) and 1971-2001 (Fiescherhorn ice core). (f), (g), (h), (i), (j) As before, for the summer values. (a), (b), (f), (g) for Guttannen were calculated over the period 1993-2008, (d) and (i) were not evaluated because no relative humidity data are available after 1996. For the

Fiescherhorn (*) indicates the results based on the correlation with the unweighted temperature (JF mean in winter and AS in summer), (**) with the precipitation-weighted temperature (ON mean in winter and AS in summer), see section 5.1.3.2. Values statistically significant at a 10% and 5% level are shown in italic and bold, respectively.

Figure 12 confirms that the winter deuterium excess at the sites is quite heterogeneous, with no common features at the stations.

In order to understand if the signal is affected by more complex atmospheric driver we investigated the connection with the main teleconnection pattern driving winter conditions over Europe, the North Atlantic Oscillation (NAO, Hurrell, 1995). Previous studies analyzed the relationship between the NAO and δ^{18}O in Europe (Field, 2010), including the GNIP stations here used (Baldini et al., 2008) and observing a general positive correlation between the two parameters.

Here we extended the investigation to the deuterium excess parameter. We took the DJF Principal Component (PC)-based NAO index available on the NCAR Climate Data Webpage (Hurrell and National Center for Atmospheric Research Staff (Eds), 2013) for the GNIP stations over the period 1993-2011 and over the period 1971-2001 for the Fiescherhorn.

The correlation analysis between the winter deuterium excess and the NAO shows an overall negative coefficient, although only in Grimsel Hospiz this is significant (ρ=-0.53, p<0.05). The Spearman correlation coefficients for Meiringen, Guttannen and Fiescherhorn are -0.04, 0.14 and -0.18 (over 1971-2001), respectively. For the ice core no significant correlation between the δ^{18}O and the NAO index was found (ρ=0.04).

The spatial correlation pattern of Grimsel Hospiz deuterium excess with the ERA-INTERIM (Dee et al., 2011) sea level pressure confirms that there is a NAO-like structure, although shifted eastward (Figure 13). The mechanism leading to a higher deuterium excess in more negative NAO phases might be related to the higher frequency of cold and drier easterlies over central Europe, whereas during positive phases precipitation over the Alps originates from milder, low Atlantic deuterium excess air masses. The fact that such feature is not coherently observed in the other nearby GNIP sites is not understood at this point.
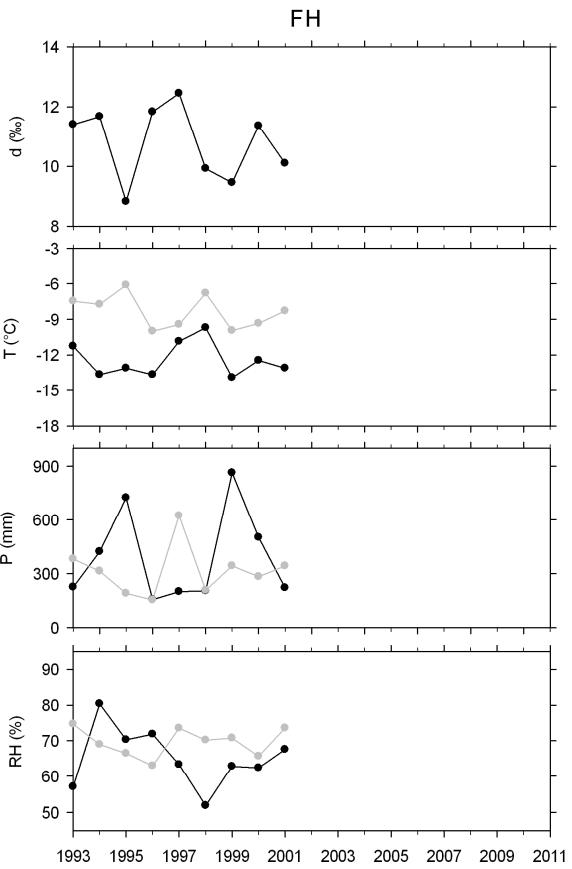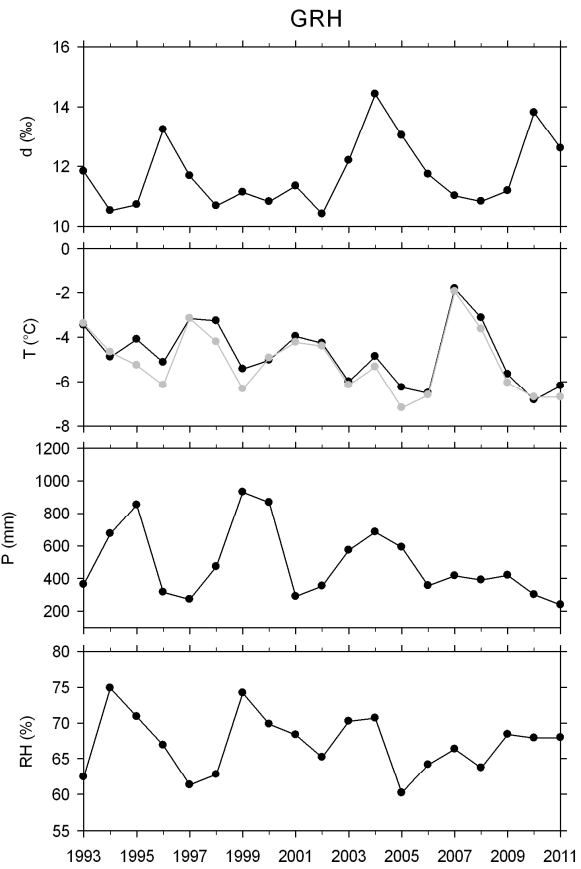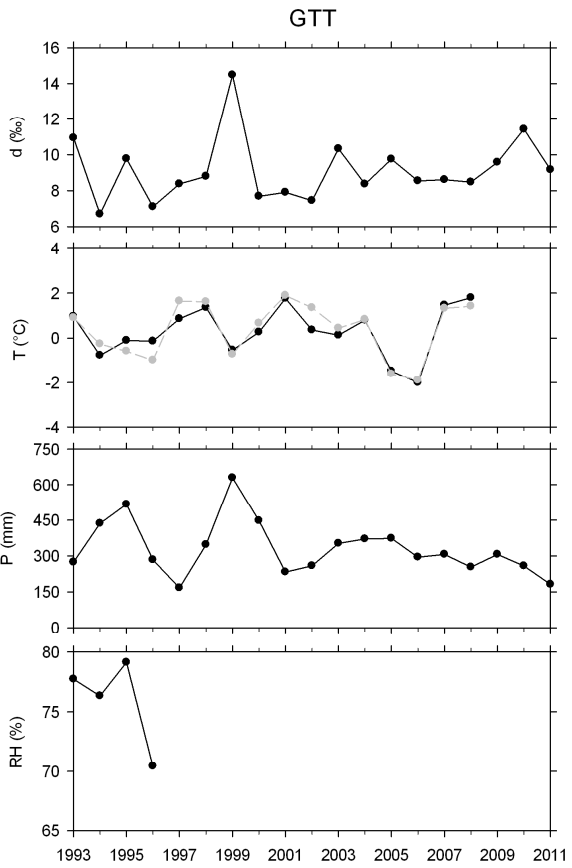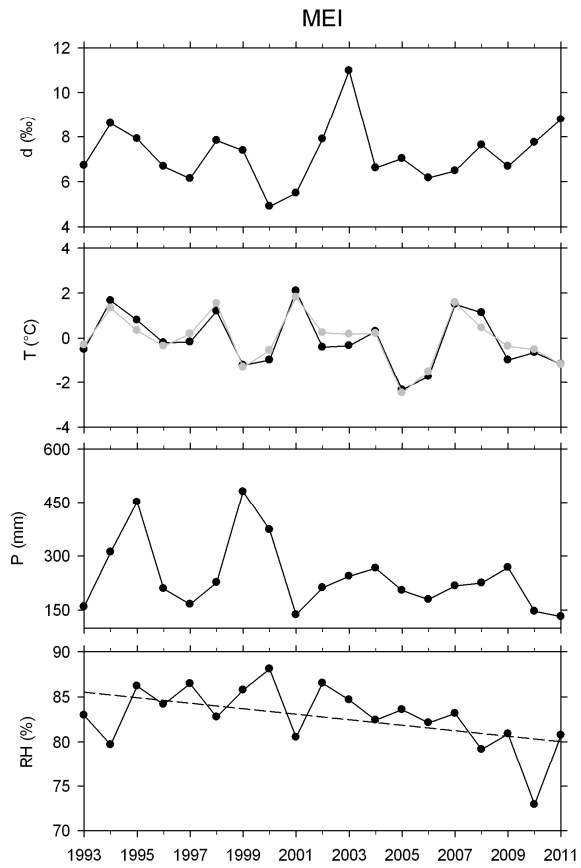
Figure 12 Time series of winter deuterium excess in Meiringen, Guttannen, Grimsel Hospiz and Fiescherhorn together with the respective temperature, precipitation, relative humidity signal. In gray the precipitation-weighted temperature. For the Fiescherhorn the temperature and relative humidity from the Jungfraujoch station was used according to the results shown in Table 5 (in black the JF mean temperature, in gray ON precipitation-weighted temperature using the Grimsel Hospiz precipitation data as weights. For the relative humidity JF mean in black and ON mean in gray). Significant trends (p<0.05) are shown with a dashed line.
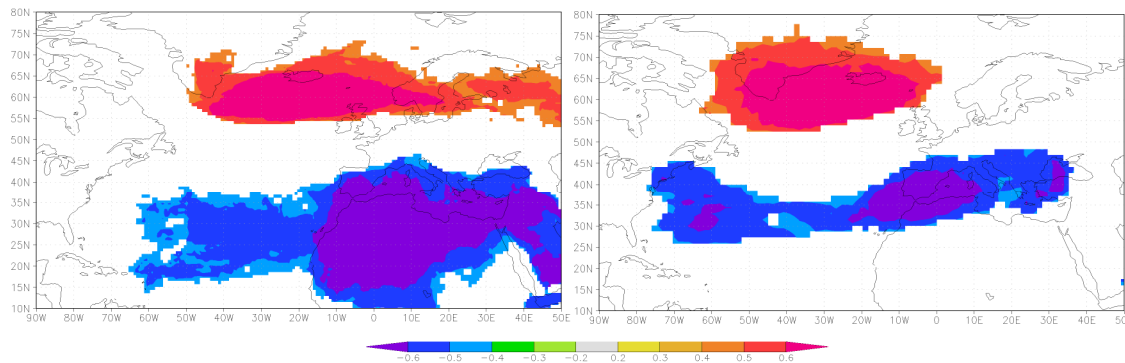
Figure 13 Spatial rank correlation of Grimsel Hospiz winter deuterium excess and ERA-INTERIM sea level pressure (left) and 500 hPa geopotential height (right) over the period 1993-2011. Analysis performed with the Climate Explorer tool (Trouet and Van Oldenborgh, 2013). Shaded areas indicate the correlation coefficient significant at a 5% level. Coherent patterns were found using other reanalysis (CFSR (Saha et al., 2010), Twentieth Century Reanalysis (Compo et al., 2011), MERRA (Rienecker et al., 2011), NCEP/NCAR (Kalnay et al., 1996)) with the core of the positive correlation extending over a region between 55°N and 70°N, approximately from Greenland to Scandinavia. The cores of the negative correlation with the Azores high were more limited to the Mediterranean region/North Africa in the CFSR and Twentieth Century Reanalysis, whereas MERRA and NCEP/NCAR showed a similar pattern as Figure 13 (not shown).

The summer signal is shown in Figure 14. In all the GNIP stations the deuterium excess presents increasing trends over the period 1993-2011 (varying between 0.2 and 0.3‰/year). Interestingly, the relative humidity decrease observed in winter at Meiringen persists also in summer with similar amplitude (0.3±0.1%/year). The summer temperature increase over 1993-2011 is significant only in Guttannen.
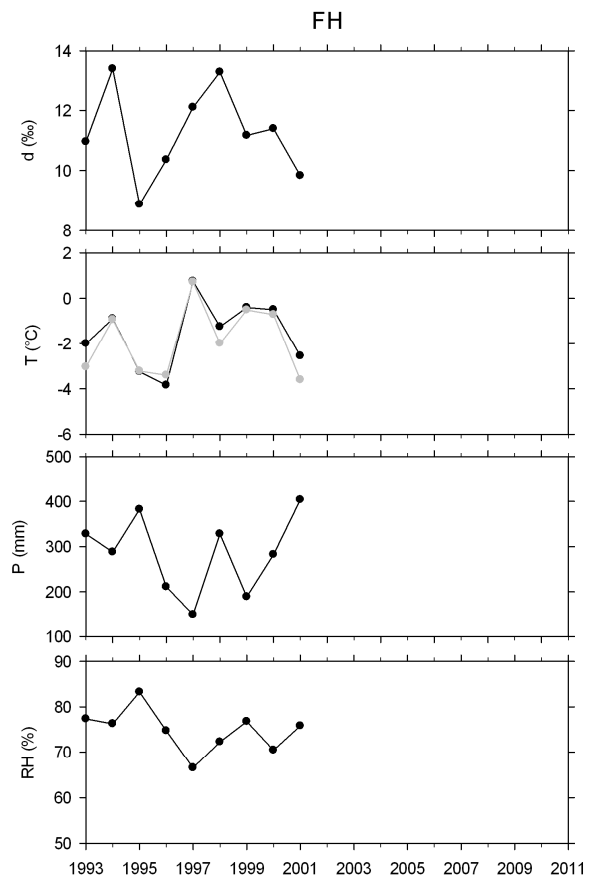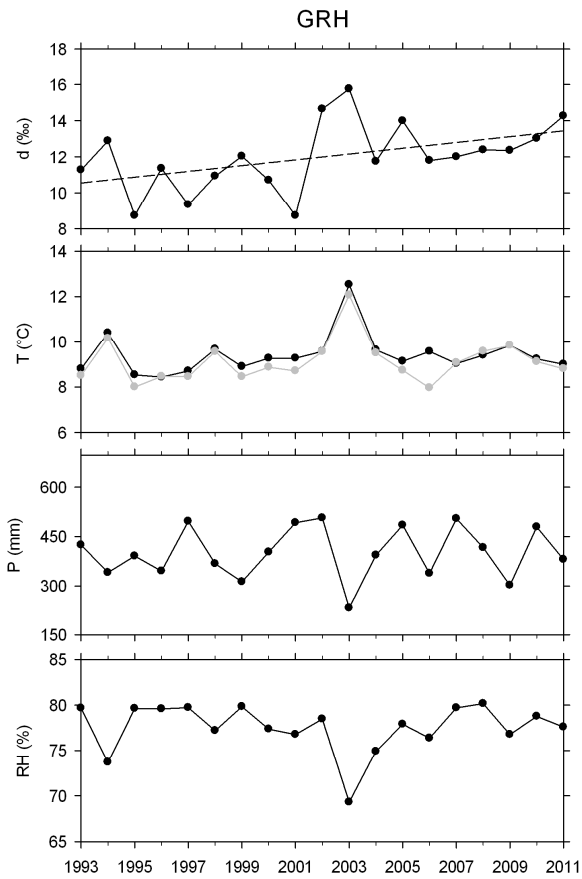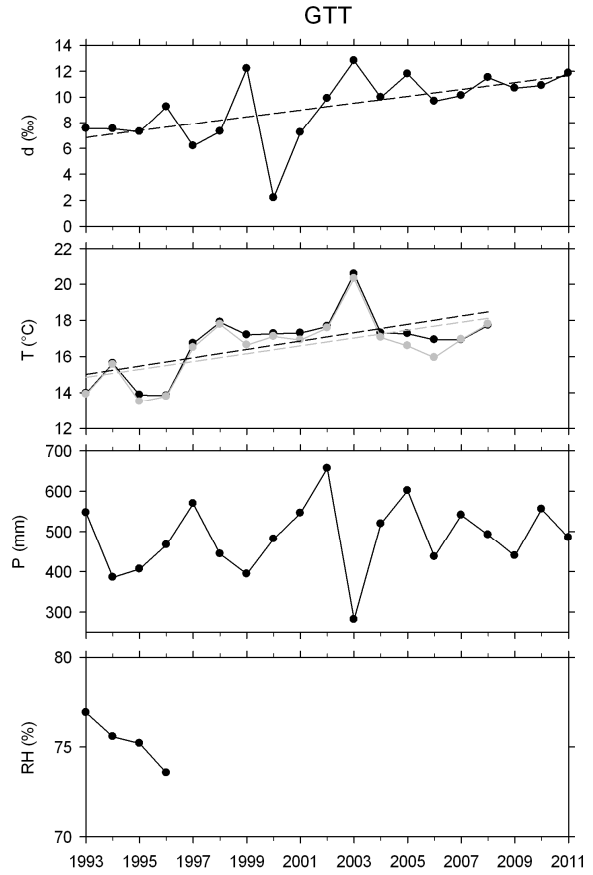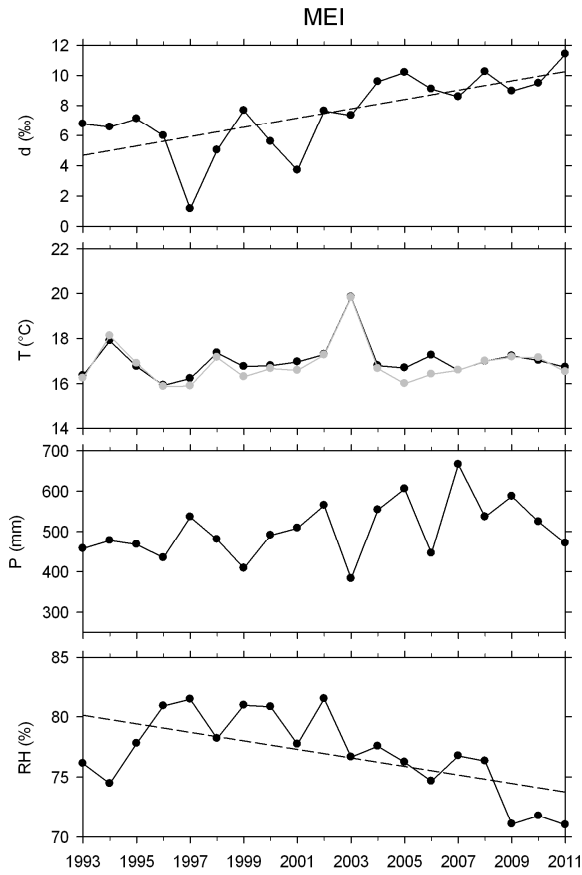
Figure 14 As Figure 12, but for summer. In gray the precipitation-weighted temperature. For the Fiescherhorn the temperature and relative humidity from the Jungfraujoch station was used according to the results shown in Table 5 (in black the AS mean temperature, in gray AS precipitation-weighted temperature using the Grimsel Hospiz precipitation data as weights. For precipitation and relative humidity AS mean values from Grimsel Hospiz and Jungfraujoch stations were used. Significant trends ($p<0.05$) are shown with a dashed line.

The hot summer 2003, clearly recognizable from the peak in temperature and $\delta^{18}O$ (not shown) and the drop in precipitation and relative humidity at all sites, is characterized by high deuterium excess indicating that it recorded the very dry conditions of that year (Schär et al., 2004). Such situations might potentially introduce a strong bias in the annual $\delta^{18}O$ in precipitation, as shown by Longinelli et al. (2006) using isotopic data from Italian stations. They indeed found that despite the extremely hot conditions of that summer, the strong reduction of precipitation during that season significantly biased the annual $\delta^{18}O$ toward more negative values due to the lower precipitation amounts compared to spring, fall and winter. The ice core does not show any particular link to the other parameters over the period 1971-2001.

In order to understand the possible atmospheric driver of such trends observed at the sites we analyzed the change in the summer weather types frequency over central Europe using the simple GWTWS classification scheme illustrated in Table 11 (Schiemann and Frei, 2010), provided by Meteoswiss. This scheme contains eight advective types and three convective types and is based on the 500 hPa height as input with the mean wind speed data used to discriminate between advective and convective types, see Weusthoff (2011) for details.

The high pressure situation is the most frequent, both in winter and summer (25-28%), followed by the westerly types (18-19%) and flat situation, ranging from 10% in winter up to 22% in summer. The flat situation is characterized by flat pressure gradients with development of local instabilities. Over the period 1993-2011 a decrease in both the high pressure situation (from 35% to 20%) and northwesterly type (from 12% to 5%) was observed and simultaneously an increase in the southwesterly type occurred (almost doubling from 10% to 20%). This might explain the increase of the summer deuterium excess, with more moisture carried from the Mediterranean that is a high-deuterium excess basin (Gat and Carmi, 1970).

	1993-2011	
	Winter	Summer
West	18	19
SouthWest	9	15 (4.4)
NorthWest	14	8 (-4.3)
North	11	3
NorthEast	5	1
East	2	0
SouthEast	1	0
South	2	1
Low Pressure	5	1
High Pressure	25	28 (-7.8)
Flat Pressure	10	22

Table 11 GWTWS weather types winter and summer frequencies (number of days per season) over the period 1993-2011. The numbers in parenthesis indicate the trends in terms of change of weather frequency/decade significant at a 10% level (Mann Kendall test).

5.1.5 Summary and concluding remarks

In this study we presented and analyzed the $\delta^{18}O$ and deuterium excess records from four sites <20 km distant each other in the Northern Swiss Alps (three GNIP stations and one high-altitude ice core). Such a high spatial resolution for the investigation of local processes in the isotopic records is hardly achievable in modeling studies. The scope was to investigate the spatial coherence of the isotopic signal. For the $\delta^{18}O$ an overall positive correlation with temperature and anticorrelation with relative humidity and precipitation in summer were found. The altitude effect follows the linear relationship with orographic-forced progressive distillation and slightly higher gradient in summer when sub-cloud re-evaporation and isotopic re-enrichment affect the lower sites.

The deuterium excess, characterized by high frequency fluctuations is correlated between the GNIP stations whereas the high-altitude ice core showed correlation only with the medium altitude GNIP station. The seasonality of the signal is not strongly pronounced; it shows higher values in fall and lower in spring and a general nonlinear increase with altitude, with comparable values at Grimsel Hospiz and Fiescherhorn. These results are in agreement with previous studies explaining that at higher altitudes the Bergeron-Findeisen process enhances

kinetic fractionation and leads to higher deuterium excess whereas at lower elevations sub-cloud re-evaporation partially decreases it (Liebminger et al., 2006).

We explain the increasing trend of the summer deuterium excess over 1993-2011 with an increased frequency in the SouthWesterly weather type, carrying moisture from the high-deuterium excess Mediterranean basin (Gat and Carmi, 1970). The winter NAO signal in the deuterium excess was recorded only at the Grimsel Hospiz site where a significant anticorrelation was found. The spatial correlation patterns show the NAO centers, although shifted eastward. A similar result was obtained by Field (2010) with the European $\delta^{18}O$ (positive correlation), suggesting that there could be a more general link to the Arctic Oscillation. The use of isotope-equipped GCMs might help in better understanding the influence of the atmospheric drivers on the isotopic variability in the Alpine region. Back trajectories capable to solve the complex Alpine topography might moreover identify the different distillation paths, but such high spatial resolution is not currently available to our knowledge.

In the ice core, despite the $\delta^{18}O$ shows a strong seasonal cycle, summer and winter signal seems to be not completely recorded. This might be due (i) seasonal values attribution and (ii) precipitation variability and post-depositional processes. The precipitation weighting of temperature did not improve the results because (i) the precipitation at the Grimsel Hospiz site might not be representative for the high-altitude glacier accumulation (ii) post-depositional processes might alter the accumulation destroying the relationship with the lower altitude sites.

Acknowledgements

5.2 Comparison with Grenzgletscher ice core

$\delta^{18}O$ and δD were measured in the Grenzgletscher ice core over the period 1961-1983 (Chapter 3). Here a comparison with the Northern Alpine Fiescherhorn ice core is discussed (for the Grenzgletscher the seasonal values were obtained in analogy to what was done for the Fiescherhorn, from linear interpolation and attribution of the season based assuming uniform distribution of precipitation throughout the year). The raw data of $\delta^{18}O$ and deuterium excess over the common period 1961-1983 are shown in Figure 15.
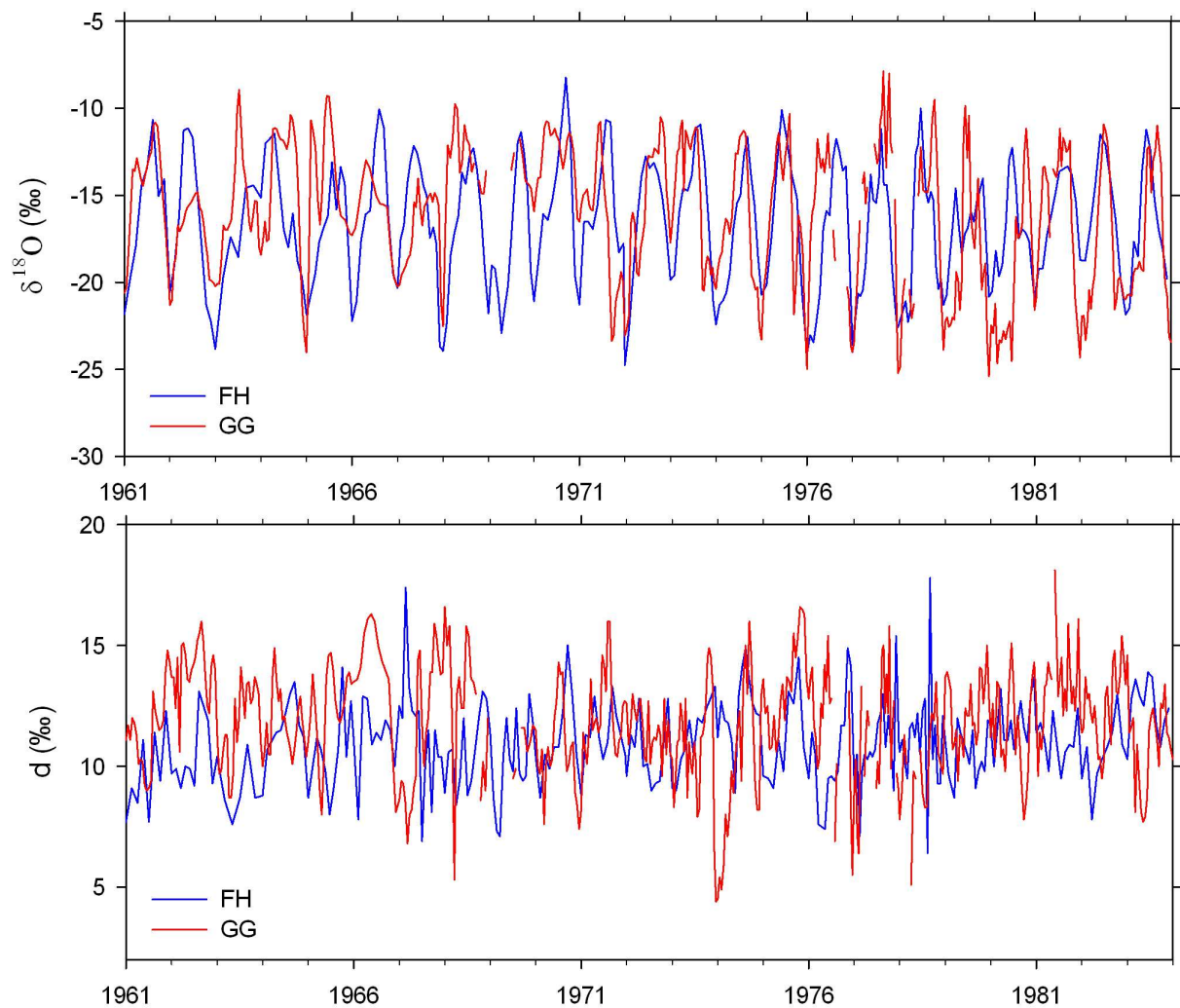
Figure 15 Data of Fiescherorn (FH, blue) and Grenzgletscher (GG, red) $\delta^{18}O$ (upper panel) and deuterium excess (lower panel) over the period 1961-1983, sampling resolution.

Both $\delta^{18}O$ series show a well pronounced seasonal cycle, as shown in Chapter 4 with the Jungfraujoch temperature for the Fiescherhorn and Grand Saint Bernard for the Grenzgletscher. The mean values are -16.62‰ at the Fiescherhorn and -16.22‰ at the Grenzgletscher. The deuterium excess is characterized by high frequency fluctuations, with

slightly higher mean values at the Grenzgletscher (11.8‰) than at the Fiescherhorn (10.9‰). In some periods the two sites show anticorrelated behavior (1966, 1967, 1974).

The LMWL of Fiescherhorn and Grenzgletscher data (sampling resolution) for the period 1961-1983 show very similar values in both, slope and deuterium excess (Figure 16).
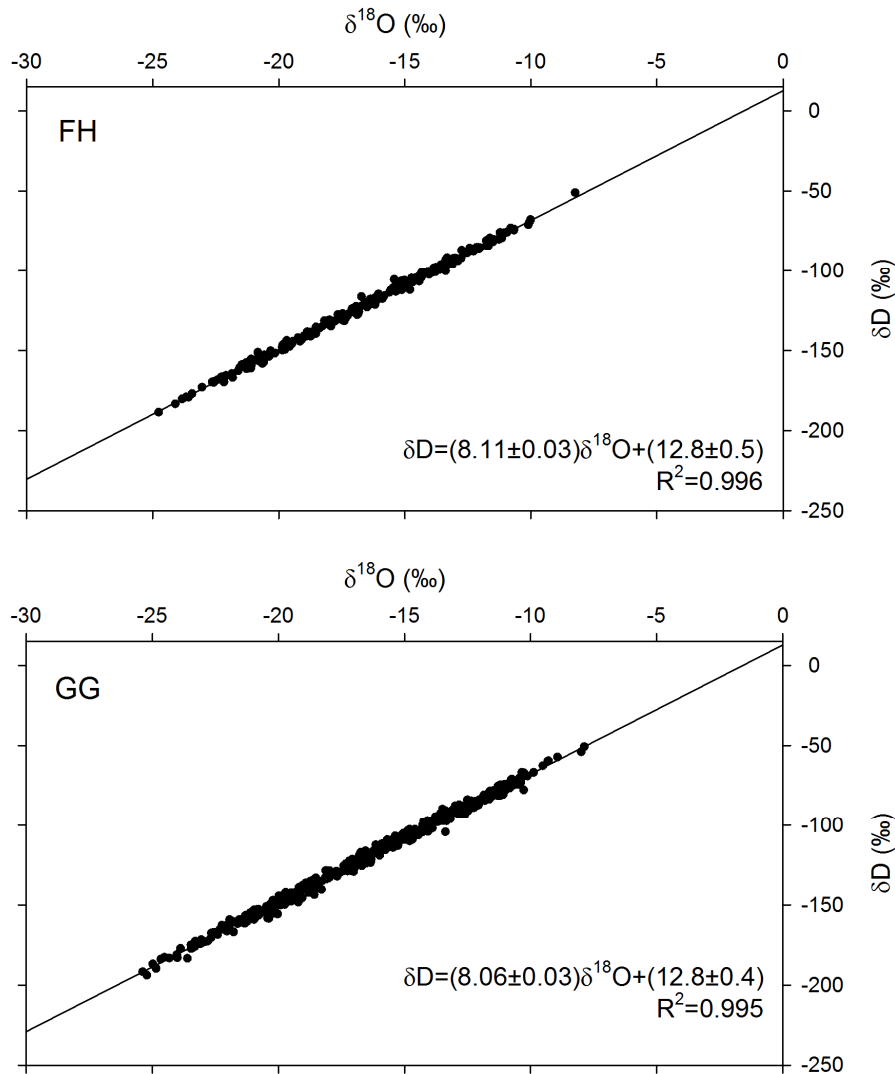

Figure 16 LMWL of Fiescherhorn (FH) and Grenzgletscher (GG) ice core data, sampling resolution over the period 1961-1983 (1968-1969 excluded). The slope and intercept (deuterium excess) of the regression line is shown together with the coefficient of determination R^2.

The ice cores $\delta^{18}O$ seasonality is similar in both, values and variability, whereas the deuterium excess is not distinguishable (Figures 17, 18 and Table 12). As observed previously, the Fiescherhorn tends to have slightly higher deuterium excess values in fall. Grenzgletscher shows higher values in both summer and fall, indicating possible enhanced contribution from the Mediterranean moisture source (Gat and Carmi, 1970).

168

	$\delta^{18}O$				Deuterium excess			
	GG		FH		GG		FH	
	Mean (‰)	1σ (‰)	Mean (‰)	1σ (‰)	Mean (‰)	1σ (‰)	Mean (‰)	1σ (‰)
Winter	-19.48	2.23	-19.73	1.97	11.6	2.1	10.7	0.9
Spring	-16.82	3.18	-16.63	2.03	11.3	2.0	11.0	1.4
Summer	-13.71	2.49	-13.94	1.87	12.6	1.6	10.9	1.3
Fall	-16.01	2.36	-15.47	1.77	12.7	1.4	11.6	1.1

Table 12 Mean seasonal values and standard deviation of $\delta^{18}O$ and deuterium excess from the Grenzgletscher and Fiescherhorn ice cores evaluated over the period 1962-1983 (1961 excluded because of not complete Grenzgletscher winter data in 1961). The years 1968-1970 were excluded because of gaps and the 1976-1978 due to suspected secondary fractionation of the samples in the Grenzgletscher record (Chapter 3).
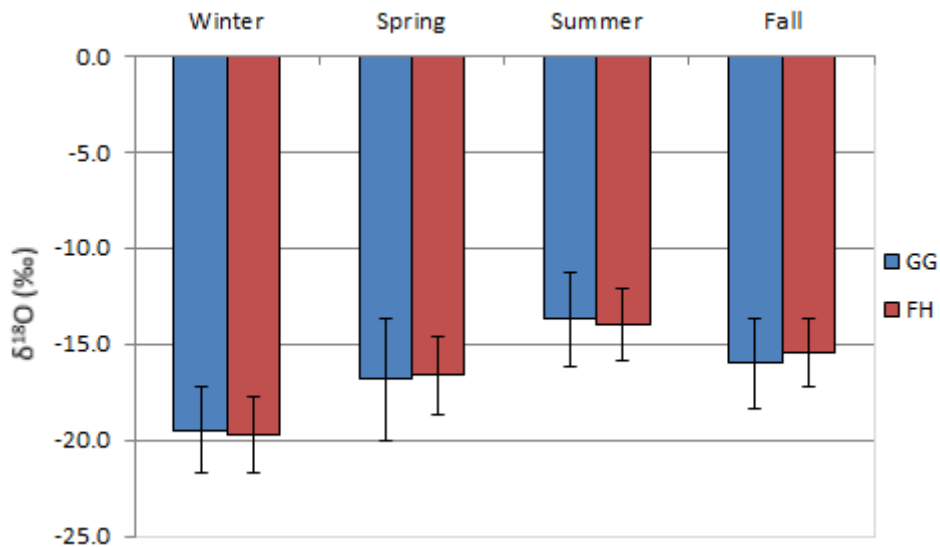

Figure 17 Seasonal means of the $\delta^{18}O$ over the period 1962-1983 at the Grenzgletscher (GG) and Fiescherhorn (FH). The bars indicate 1σ.
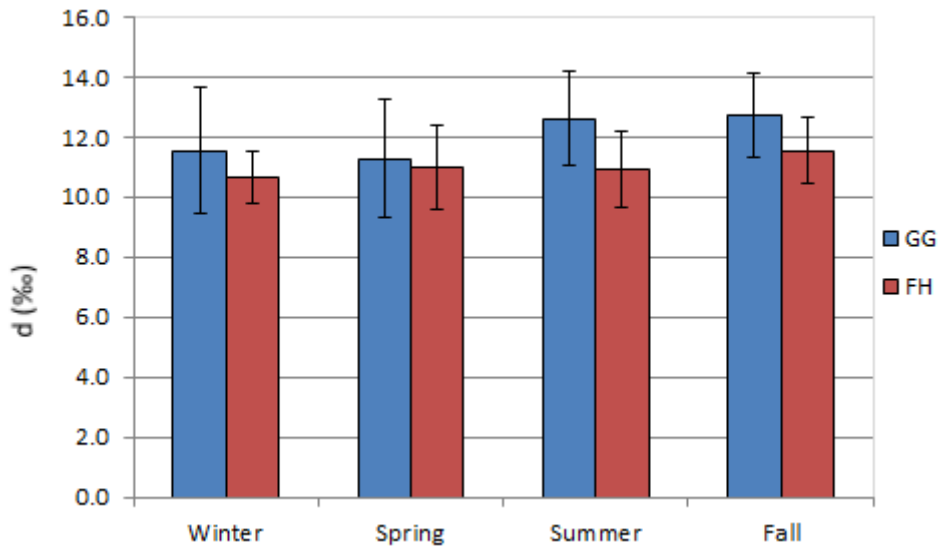
Figure 18 Seasonal means of the deuterium excess over the period 1962-1983 at the Grenzgletscher (GG) and Fiescherhorn (FH). The bars indicate 1σ.

The seasonal $\delta^{18}O$ does not show any correlation with the respective deuterium excess at the sites (Table 13). The $\delta^{18}O$ is well correlated between the two ice cores confirming that it is a good indicator of the regional temperature, whereas the deuterium excess does not show any relationship suggesting possible different moisture sources and secondary processes affecting the two glaciers. The slightly higher deuterium excess at the Grenzgletscher might be due to the contribution from the near Mediterranean moisture source, as stated previously.

FH	GG	FH/GG	FH/GG
$\delta^{18}O/d$	$\delta^{18}O/d$	$\delta^{18}O$	d
0.09	0.04	**0.48**	-0.08

Table 13 Spearman correlation coefficients of the $\delta^{18}O$ and deuterium excess (d) seasonal time series over 1961-1983. Values in bold indicate coefficients statistically significant at a 5% level.

References

Ambach, W., Dansgaard, W., Eisner, H. and Møller, J.: The altitude effect on the isotopic composition of precipitation and glacier ice in the Alps, Tellus, 20(4), 595–600, doi:10.1111/j.2153-3490.1968.tb00402.x, 1968.

Appenzeller, C., Begert, M., Zenklusen, E. and Scherrer, S. C.: Monitoring climate at Jungfraujoch in the high Swiss Alpine region, Sci. Total Environ., 391(2–3), 262–268, doi:10.1016/j.scitotenv.2007.10.005, 2008.

Baldini, L. M., McDermott, F., Foley, A. M. and Baldini, J. U. L.: Spatial variability in the European winter precipitation δ^{18}O-NAO relationship: Implications for reconstructing NAO-mode climate variability in the Holocene, Geophys. Res. Lett., 35(4), doi:10.1029/2007GL032027, 2008.

Barry, R. G.: Mountain Weather and Climate, 3rd ed., Cambridge University Press., 2008.

Brönnimann, S., Mariani, I., Schwikowski, M., Auchmann, R. and Eichler, A.: Simulating the temperature and precipitation signal in an Alpine ice core, Clim. Past, 9(4), 2013–2022, doi:10.5194/cp-9-2013-2013, 2013.

Clark, I. D. and Fritz, P.: Environmental Isotopes in Hydrogeology, CRC Press/Lewis Publishers, New York., 1997.

Compo, G. P., Whitaker, J. S., Sardeshmukh, P. D., Matsui, N., Allan, R. J., Yin, X., Gleason, B. E., Vose, R. S., Rutledge, G., Bessemoulin, P., Brönnimann, S., Brunet, M., Crouthamel, R. I., Grant, A. N., Groisman, P. Y., Jones, P. D., Kruk, M. C., Kruger, A. C., Marshall, G. J., Maugeri, M., Mok, H. Y., Nordli, Ø., Ross, T. F., Trigo, R. M., Wang, X. L., Woodruff, S. D. and Worley, S. J.: The Twentieth Century Reanalysis Project, Q. J. R. Meteorol. Soc., 137(654), 1–28, doi:10.1002/qj.776, 2011.

Craig, H.: Isotopic variations in meteoric waters, Science, 133, 1702–1703, doi:10.1126/science.133.3465.1702, 1961.

Dansgaard, W.: Stable isotopes in precipitation, Tellus, 16(4), 436–468, doi:10.1111/j.2153-3490.1964.tb00181.x, 1964.

Dee, D. P., Uppala, S. M., Simmons, A. J., Berrisford, P., Poli, P., Kobayashi, S., Andrae, U., Balmaseda, M. A., Balsamo, G., Bauer, P., Bechtold, P., Beljaars, A. C. M., van de Berg, L., Bidlot, J., Bormann, N., Delsol, C., Dragani, R., Fuentes, M., Geer, A. J., Haimberger, L., Healy, S. B., Hersbach, H., Hólm, E. V., Isaksen, L., Kållberg, P., Köhler, M., Matricardi, M., McNally, A. P., Monge-Sanz, B. M., Morcrette, J.-J., Park, B.-K., Peubey, C., de Rosnay, P., Tavolato, C., Thépaut, J.-N. and Vitart, F.: The ERA-Interim reanalysis: configuration and performance of the data assimilation system, Q. J. R. Meteorol. Soc., 137(656), 553–597, doi:10.1002/qj.828, 2011.

Eichler, A., Schwikowski, M. and Gäggeler, H. W.: Meltwater-induced relocation of chemical species in Alpine firn, Tellus B, 53(2), 192–203, 2001.

Eichler, A., Schwikowski, M., Furger, M., Schotterer, U., Gäggeler, H. W. and others: Sources and distribution of trace species in Alpine precipitation inferred from two 60-year ice core paleorecords, Atmos. Chem. Phys. Discuss., 4(1), 71–108, 2004.

Field, R. D.: Observed and modeled controls on precipitation δ^{18}O over Europe: From local temperature to the Northern Annular Mode, J. Geophys. Res. Atmos., 115(D12), D12101, doi:10.1029/2009JD013370, 2010.

Frei, C. and Schär, C.: A precipitation climatology of the Alps from high-resolution rain-gauge observations, Int. J. Clim., 18(8), 873–900, doi:10.1002/(SICI)1097-0088(19980630)18:8<873::AID-JOC255>3.0.CO;2-9, 1998.

Fröhlich, K., Kralik, M., Papesch, W., Rank, D., Scheifinger, H. and Stichler, W.: Deuterium excess in precipitation of Alpine regions – moisture recycling, Isot Env. Healt S., 44(1), 61–70, doi:10.1080/10256010801887208, 2008.

Gat, J. R. and Carmi, I.: Evolution of the Isotopic Composition of Atmospheric Waters in the Mediterranean Sea Area, Journ. Geophys. Res., 75(15), 3039–3048, doi:10.1029/JC075i015p03039, 1970.

Hurrell, J. and National Center for Atmospheric Research Staff (Eds): The Climate Data Guide: Hurrell North Atlantic Oscillation (NAO) Index (PC-based), Available from: http://climatedataguide.ucar.edu/guidance/hurrell-north-atlantic-oscillation-nao-index-pc-based, 2013.

Hurrell, J. W.: Decadal Trends in the North Atlantic Oscillation: Regional Temperatures and Precipitation, Science, 269(5224), 676–679, doi:10.1126/science.269.5224.676, 1995.

IAEA/WMO: Global Network of Isotopes in Precipitation. The GNIP Database. Accessible at: http://www.iaea.org/water, 2013.

Jenk, T. M.: Ice Core Based Reconstruction of Past Climate Conditions and Air Pollution in the Alps Using Radiocarbon, PhD thesis, Departement für Chemie und Biochemie, Univ. of Bern, Bern, Switzerland, 2006.

Jenk, T. M., Szidat, S., Schwikowski, M., Gäggeler, H. W., Brütsch, S., Wacker, L., Synal, H.-A. and Saurer, M.: Radiocarbon analysis in an Alpine ice core: record of anthropogenic and biogenic contributions to carbonaceous aerosols in the past (1650–1940), Atmos. Chem. Phys., 6(12), 5381–5390, 2006.

Johnsen, S. J.: Stable isotope homogenization of polar firn and ice, in Proc. Symp. on Isotopes and Impurities in Snow and Ice, I.U.G.G.XVI, General Assembly, Grenoble Aug. Sept. 1975, vol. 15, pp. 210–219, Washington, 1977.

Johnsen, S. J., Clausen, H. B., Cuffey, K. M., Hoffmann, G., Schwander, J. and Creyts, T.: Diffusion of stable isotopes in polar firn and ice: The isotope effect in firn diffusion, in Physics of Ice Core Records, pp. 121–140, Hondoh T., Sapporo, 2000.

Jouzel, J., Merlivat, L. and Lorius, C.: Deuterium excess in an East Antarctic ice core suggests higher relative humidity at the oceanic surface during the last glacial maximum, Nature, 299(5885), 688–691, doi:10.1038/299688a0, 1982.

Jouzel, J., Alley, R. B., Cuffey, K. M., Dansgaard, W., Grootes, P., Hoffmann, G., Johnsen, S. J., Koster, R. D., Peel, D., Shuman, C. A., Stievenard, M., Stuiver, M. and White, J.: Validity of the temperature reconstruction from water isotopes in ice cores, J. Geophys. Res. Oceans, 102(C12), 26471–26487, doi:10.1029/97JC01283, 1997a.

Jouzel, J., Fröhlich, K. and Schotterer, U.: Deuterium and oxygen-18 in present-day precipitation: data and modelling, Hydrol. Sci. J., 42(5), 747–763, doi:10.1080/02626669709492070, 1997b.

Kaiser, A., Scheifinger, H., Kralik, M., Papesch, W., Rank, D. and Stichler, W.: Links between meteorological conditions and spatial/temporal variations in long-term isotope records from the Austrian Precipitation Network, pp. 67–76, 2001.

Kalnay, E., Kanamitsu, M., Kistler, R., Collins, W., Deaven, D., Gandin, L., Iredell, M., Saha, S., White, G., Woollen, J., Zhu, Y., Leetmaa, A., Reynolds, R., Chelliah, M., Ebisuzaki, W., Higgins, W., Janowiak, J., Mo, K. C., Ropelewski, C., Wang, J., Jenne, R. and Joseph, D.: The NCEP/NCAR 40-Year Reanalysis Project, Bull. Am. Meteorol. Soc., 77(3), 437–471, doi:10.1175/1520-0477(1996)077<0437:TNYRP>2.0.CO;2, 1996.

Kern, Z., Kohán, B. and Leuenberger, M.: Monthly resolved biannual precipitation oxygen isoscape for Switzerland, Atmospheric Chem. Phys. Discuss., 13(4), 9895–9916, doi:10.5194/acpd-13-9895-2013, 2013.

Kohn, M. J. and Welker, J. M.: On the temperature correlation of $\delta^{18}O$ in modern precipitation, Earth Planet. Sci. Lett., 231(1–2), 87–96, doi:10.1016/j.epsl.2004.12.004, 2005.

Liebminger, A., Haberhauer, G., Papesch, W. and Heiss, G.: Correlation of the isotopic composition in precipitation with local conditions in alpine regions, J. Geophys. Res.-Atmos., 111(D5), D05104, doi:10.1029/2005JD006258, 2006.

Longinelli, A., Anglesio, E., Flora, O., Iacumin, P. and Selmo, E.: Isotopic composition of precipitation in Northern Italy: Reverse effect of anomalous climatic events, J. Hydrol., 329(3–4), 471–476, doi:10.1016/j.jhydrol.2006.03.002, 2006.

Masson-Delmotte, V., Jouzel, J., Landais, A., Stievenard, M., Johnsen, S. J., White, J. W. C., Werner, M., Sveinbjornsdottir, A. and Fuhrer, K.: GRIP Deuterium Excess Reveals Rapid and Orbital-Scale Changes in Greenland Moisture Origin, Science, 309(5731), 118–121, 2005.

Masson-Delmotte, V., Hou, S., Ekaykin, A., Jouzel, J., Aristarain, A., Bernardo, R. T., Bromwich, D., Cattani, O., Delmotte, M., Falourd, S., Frezzotti, M., Gallée, H., Genoni, L., Isaksson, E., Landais, A., Helsen, M. M., Hoffmann, G., Lopez, J., Morgan, V., Motoyama, H., Noone, D., Oerter, H., Petit, J. R., Royer, A., Uemura, R., Schmidt, G. A., Schlosser, E., Simões, J. C., Steig, E. J., Stenni, B., Stievenard, M., van den Broeke, M. R., van de Wal, R. S. W., van de Berg, W. J., Vimeux, F. and White, J. W. C.: A Review of Antarctic Surface Snow Isotopic Composition: Observations, Atmospheric Circulation, and Isotopic Modeling, J. Clim., 21(13), 3359–3387, doi:10.1175/2007JCLI2139.1, 2008.Merlivat, L. and Jouzel, J.: Global climatic interpretation of the deuterium-oxygen 18 relationship for precipitation, J. Geophys. Res. Oceans, 84(C8), 5029–5033, doi:10.1029/JC084iC08p05029, 1979.

Persson, A., Langen, P. L., Ditlevsen, P. and Vinther, B. M.: The influence of precipitation weighting on interannual variability of stable water isotopes in Greenland, J. Geophys. Res., 116(D20), D20120, doi:10.1029/2010JD015517, 2011.

Pfahl, S. and Wernli, H.: Air parcel trajectory analysis of stable isotopes in water vapor in the eastern Mediterranean, J. Geophys. Res.-Atmos., 113(D20), doi:10.1029/2008JD009839, 2008.

Pfahl, S. and Sodemann, H.: What controls deuterium excess in global precipitation?, Clim. Past Discuss., 9(4), 4745–4770, doi:10.5194/cpd-9-4745-2013, 2013.

Rank, D. and Papesch, W.: Isotopic composition of precipitation in Austria in relation to air circulation patterns and climate, in Isotopic composition of precipitation in the Mediterranean Basin in relation to air circulation patterns and climate: final report of a coordinated research project, 2000-2004, International Atomic Energy Agency, Vienna, 2005.

Rienecker, M. M., Suarez, M. J., Gelaro, R., Todling, R., Bacmeister, J., Liu, E., Bosilovich, M. G., Schubert, S. D., Takacs, L., Kim, G.-K., Bloom, S., Chen, J., Collins, D., Conaty, A., da Silva, A., Gu, W., Joiner, J., Koster, R. D., Lucchesi, R., Molod, A., Owens, T., Pawson, S., Pegion, P., Redder, C. R., Reichle, R., Robertson, F. R., Ruddick, A. G., Sienkiewicz, M. and Woollen, J.: MERRA: NASA's Modern-Era Retrospective Analysis for Research and Applications, J. Clim., 24(14), 3624–3648, doi:10.1175/JCLI-D-11-00015.1, 2011.

Risi, C., Bony, S. and Vimeux, F.: Influence of convective processes on the isotopic composition (δ^{18}O and δD) of precipitation and water vapor in the tropics: 2. Physical interpretation of the amount effect, J. Geophys. Res.-Atmos., 113(D19), doi:10.1029/2008JD009943, 2008.

Ropelewski, C. F.: The Climate of Summer 1983—A Season of Contrasts and Extremes, Mon. Weather Rev., 112, 591 1984.

Rozanski, K., Araguás-Araguás, L. and Gonfiantini, R.: Relation Between Long-Term Trends of Oxygen-18 Isotope Composition of Precipitation and Climate, Science, 258(5084), 981–985, doi:10.1126/science.258.5084.981, 1992.

Rozanski, K., Araguás-Araguás, L. and Gonfiantini, R.: Isotopic patterns in modern global precipitation, in Geophysical Monograph Series, vol. 78, edited by P. K. Swart, K. C. Lohmann, J. McKenzie, and S. Savin, pp. 1–36, American Geophysical Union, Washington, D. C., 1993.

Saha, S., Moorthi, S., Pan, H.-L., Wu, X., Wang, J., Nadiga, S., Tripp, P., Kistler, R., Woollen, J., Behringer, D., Liu, H., Stokes, D., Grumbine, R., Gayno, G., Wang, J., Hou, Y.-T., Chuang, H.-Y., Juang, H.-M. H., Sela, J., Iredell, M., Treadon, R., Kleist, D., Van Delst, P., Keyser, D., Derber, J., Ek, M., Meng, J., Wei, H., Yang, R., Lord, S., Van Den Dool, H., Kumar, A., Wang, W., Long, C., Chelliah, M., Xue, Y., Huang, B., Schemm, J.-K., Ebisuzaki, W., Lin, R., Xie, P., Chen, M., Zhou, S., Higgins, W., Zou, C.-Z., Liu, Q., Chen, Y., Han, Y., Cucurull, L., Reynolds, R. W., Rutledge, G. and Goldberg, M.: The NCEP Climate Forecast System Reanalysis, Bull. Am. Meteorol. Soc., 91(8), 1015–1057, doi:10.1175/2010BAMS3001.1, 2010.

Schär, C., Vidale, P. L., Lüthi, D., Frei, C., Häberli, C., Liniger, M. A. and Appenzeller, C.: The role of increasing temperature variability in European summer heatwaves, Nature, 427(6972), 332–336, doi:10.1038/nature02300, 2004.

Schiemann, R. and Frei, C.: How to quantify the resolution of surface climate by circulation types: An example for Alpine precipitation, Phys. Chem. Earth Parts ABC, 35(9–12), 403–410, doi:10.1016/j.pce.2009.09.005, 2010.

Schotterer, U., Fröhlich, K., Stichler, W. and Trimborn, P.: Temporal variations of oxygen-18 and deuterium excess in Alpine regions of Switzerland, in Isotope Techniques in the study of

Past and Current Environmental Changes in the Hydrosphere and the Atmosphere, pp. 53–64., 1993.

Schotterer, U., Fröhlich, K., Gäggeler, H. W., Sandjordj, S. and Stichler, W.: Isotope records from Mongolian and Alpine ice cores as climate indicators, Clim. Change, 36(3-4), 519–530, doi:10.1023/A:1005338427567, 1997.

Schotterer, U., Stichler, W., Graf, W., Bürki, H. U., Gourcy, L., Ginot, P. and Huber, T.: Stable isotopes in alpine ice cores: do they record climate variability, in Conference on isotope techniques in the study of past and current environmental changes in the hydrosphere and the atmosphere., 2001.

Schotterer, U., Stichler, W. and Ginot, P.: The influence of postdepositional effects on ice core studies: examples from the Alps, Andes, and Altai, Earth Paleoenviron. Rec. Preserv. - Low-Latit. Glaciers Ed. Wayne Ceciel Green JR Thompson LG Dev. Paleoenviron. Res. Ser. Kluwer Acad. Publ., 39–60, 2004.

Schürch, M., Kozel, R., Schotterer, U. and Tripet, J.-P.: Observation of isotopes in the water cycle—the Swiss National Network (NISOT), Environ. Geol., 45(1), 1–11, doi:10.1007/s00254-003-0843-9, 2003.

Schwikowski, M., Brütsch, S., Gäggeler, H. W. and Schotterer, U.: A high-resolution air chemistry record from an Alpine ice core: Fiescherhorn glacier, Swiss Alps, J. Geophys. Res., 104(D11), 13709–13,719, doi:10.1029/1998JD100112, 1999.

Siegenthaler, U. and Oeschger, H.: Correlation of ^{18}O in precipitation with temperature and altitude, Nature, 285, 314–317, doi:DOI: 10.1038/285314a0, 1980.

Sodemann, H. and Zubler, E.: Seasonal and inter–annual variability of the moisture sources for Alpine precipitation during 1995–2002, Int. J. Clim., 30(7), 947–961, doi:10.1002/joc.1932, 2009.

Stenni, B., Masson-Delmotte, V., Johnsen, S., Jouzel, J., Longinelli, A., Monnin, E., Röthlisberger, R. and Selmo, E.: An Oceanic Cold Reversal During the Last Deglaciation, Science, 293(5537), 2074–2077, doi:10.1126/science.1059702, 2001.

Stichler, W. and Schotterer, U.: From accumulation to discharge: modification of stable isotopes during glacial and post-glacial processes, Hydrol. Process., 14(8), 1423–1438, doi:10.1002/1099-1085(20000615)14:8<1423::AID-HYP991>3.0.CO;2-X, 2000.

Stichler, W., Schotterer, U., Fröhlich, K., Ginot, P., Kull, C., Gäggeler, H. and Pouyaud, B.: Influence of sublimation on stable isotope records recovered from high-altitude glaciers in the tropical Andes, J. Geophys. Res.-Atmos., 106(D19), 22613–22620, doi:10.1029/2001JD900179, 2001.

Trouet, V. and Van Oldenborgh, G. J.: KNMI Climate Explorer: A Web-Based Research Tool for High-Resolution Paleoclimatology, Tree-Ring Res., 69(1), 3–13, doi:10.3959/1536-1098-69.1.3, 2013.

Vimeux, F., Masson, V., Jouzel, J., Stievenard, M. and Petit, J. R.: Glacial–interglacial changes in ocean surface conditions in the Southern Hemisphere, Nature, 398(6726), 410–413, doi:10.1038/18860, 1999.

Wanner, H., Rickli, R., Salvisberg, E., Schmutz, C. and Schüepp, M.: Global climate change and variability and its influence on Alpine climate — concepts and observations, Theor. Appl. Clim., 58(3-4), 221–243, doi:10.1007/BF00865022, 1997.

Weusthoff, T.: Weather Type Classification at MeteoSwiss - Introduction of new automatic classification schemes, Arbeitsbericht MeteoSchweiz Nr. 235, 2011.

Outlook

In this study the suitability of the ice core parameters water stable isotope ratios and net snow accumulation as climate proxies was investigated over the recent time period by direct comparison with instrumental temperature, precipitation and other meteorological data over different time scales.

In Chapter 3 the setup and characterization of a WS-CRDS Picarro L2130-i laser spectrometer was described. Drift and memory effect were quantified and the analytical uncertainty was determined, resulting comparable with other techniques (<0.1‰ for δ^{18}O and <0.5‰ for δD). Internal laboratory standards were calibrated using international reference materials. A user-friendly measurement protocol for the calibration of the samples including memory and drift correction was developed and used for the measurement of the Grenzgletscher ice core samples, giving consistent results with what was obtained by previous measurements with IRMS technique.

The focus of Chapter 4 was on the analysis of temperature and precipitation proxies from the Fiescherhorn glacier, Northern Alps and Grenzgletscher, Southern Alps. From the low fraction of δ^{18}O variability explained by temperature (~20%) it is clear that the isotopic signal in this region is affected by additional processes, such as topographically-induced effects and changes of the moisture sources. Moreover, the relationship of annual δ^{18}O with temperature showed substantial differences in snow deposition and preservation at the two glaciers only 60 km distant, with the Grenzgletscher affected by high intraseasonal to interannual variability of precipitation and the Fiescherhorn characterized by more homogeneous conditions. The ice cores accumulation reconstructions showed the Northern and Southern Alpine glaciers to be influenced by different precipitation regimes, as expected from their location with respect to the orographic barrier.

Chapter 5 addressed the interpretation of the deuterium excess parameter in the Alpine region. Even over a limited area (<20 km) no homogeneous relationship with the meteorological parameters was found, with the deuterium excess generally lower in spring and higher in fall-winter. A nonlinear increase altitude was observed. The influence of the atmospheric circulation patterns was investigated, showing an anticorrelation between the deuterium excess and the NAO in winter at the Grimsel Hospiz site. In summer the common increasing trend of deuterium excess over the period 1993-2011 was explained with the increasing frequency of Southwesterly weather types, carrying moisture from the high deuterium excess Mediterranean basin.

In future studies it would be desirable to better identify the different contributions to the isotopic variability. With further development of the spatial resolution of isotope-equipped regional models and GCMs it might be possible to investigate the effects of different moisture sources even for Alpine subregions affected by distinct precipitation patterns. Another promising approach would be tracking of the water cycle over the Alpine region in the frame of a comprehensive monitoring network. This seems feasible with the recent development of laser spectrometers allowing continuous measurements of both the $\delta^{18}O$ and δD in water vapour and liquid water in the field.

Generally ice core records from Alpine glaciers offer the possibility to study climate proxies over longer time scales, even before the beginning of instrumental data. The Fiescherhorn ice core contains a 350 years record and the Colle Gnifetti spans with reasonably high time resolution the last two thousands years. Although it was not easy to interpret the isotopic signal at seasonal and interannual timescale, major changes in temperature, precipitation or atmospheric circulation patterns might be accessible on longer timescales. This is illustrated with the δD and deuterium excess records from Fiescherhorn and Colle Gnifetti ice core over the last 350 years in Figure 1.

Colle Gnifetti shows clearly a shift toward summer values, with a mean δD=-97.2‰ compared to Fiescherhorn (mean δD=-120.8‰), caused by the preferential erosion of winter snow. Due to the reduced number of points per year and diffusion effects, the Colle Gnifetti record appears smoothed, whereas the Fiescherhorn record preserves the seasonal cycle.

The deuterium excess signal is characterized at both sites by high frequency fluctuations and by higher values at the Colle Gnifetti (13.5‰) compared to Fiescherhorn (10.6‰). This probably indicates the influence of the high-deuterium excess Mediterranean moisture source at the Southern site. The most outstanding feature is the divergence of the two deuterium excess records over the period 1850-1890. In general this difference is 2-4‰ with lower values at the Fiescherhorn, but over the period 1850-1890 it increases to ~6‰. This discrepancy might indicate a strong change in the moisture sources and/or local processes affecting the parameter. This interesting feature requires further investigations. These might be conducted in parallel with other archives. The development of reanalysis data extended further back to the past and the use of modeling studies might help in understanding the processes governing such feature.
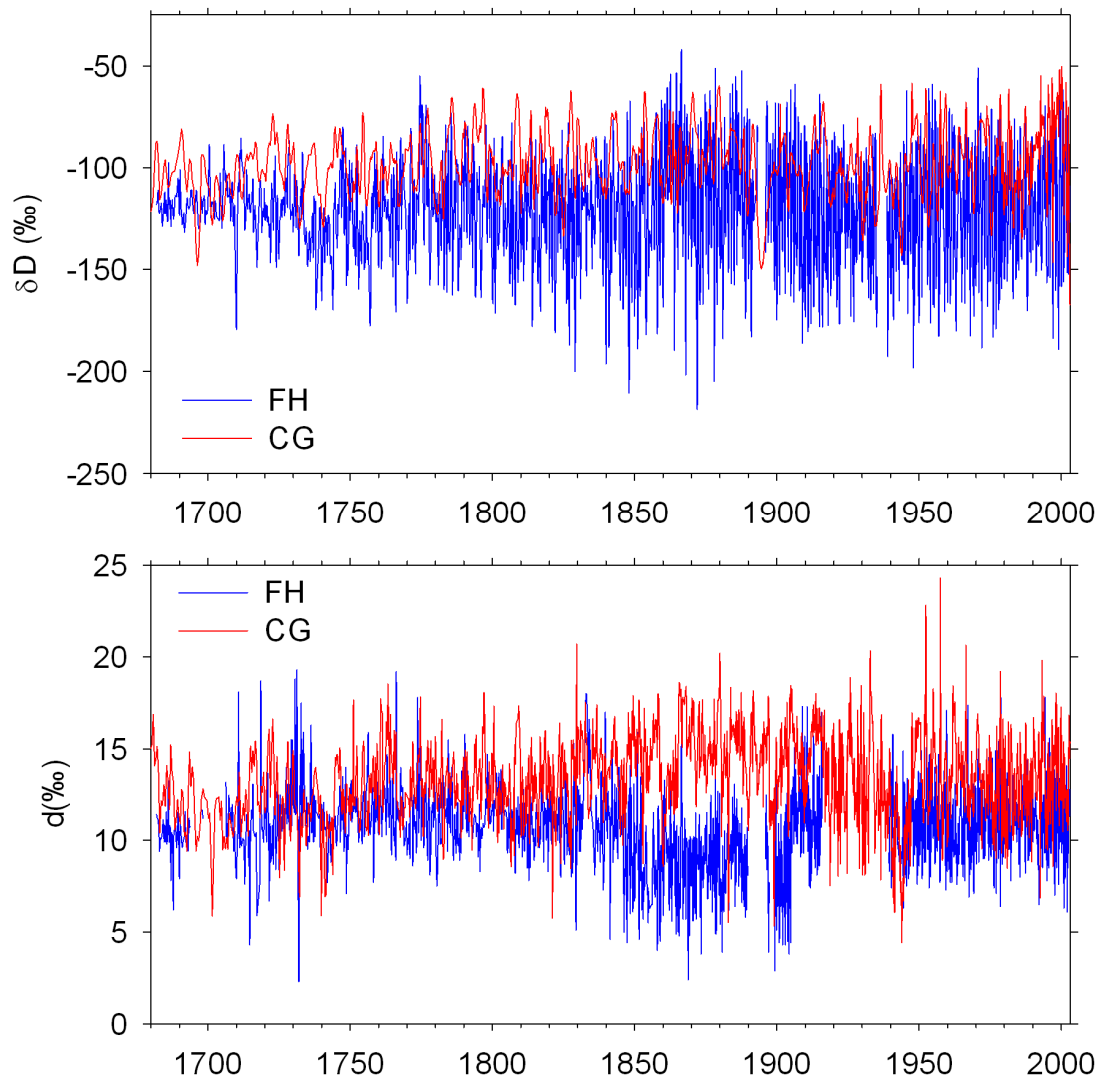
Figure 1 Raw data of Fiescherorn (FH, blue) and Colle Gnifetti (CG, red) δD (upper panel) and deuterium excess (lower panel) over the period 1680-2003.

Acknowledgements

Lara, Chuck, Tex, Cinzia, Little, Norton, Vince, because even if we meet once in a while, it seems that time has not passed.

Giovanni Angelo, for the conversations and the beautiful afternoons spent together wandering in the forests.

Richy and Sarah, for the many conversations we had during our travels on the week end.

Gemma, Davide Bertolotto, Davide Papini, Giancarlo, Ciro and Natalia, for the time we spent together on the way to PSI and not only.

Trupač, Sarah and Thomas, for the uncountable Friday evenings together.

Francesco Antani, for the sblinding moments spent together and for his great talent and tapiocity in analyzing posterdata.

Ilya Usoltsev and the PSI rock band, Norbert, Jacques, Daniel, Greg and Reto. It is not possible to describe how awesome was to play with you, I will always remember our great time in and outside the music room!

A special thought goes to Alexander Zapf, one of my officemates. I shared three years of my PhD with Alex, we had many Italian espressos, scientific discussions and funny moments. Unfortunately Alex is not here anymore. He passed away last January, in the mountains he loved.

I also had the chance to be in the field with Beat Rufibach. He was our mountain guide and he did a great job in motivating me, considering that it was the first time for me on the field. Also Beat is no longer with us, and I would like to remember him.

Finally, I want to thank the people that most shared with me the good and bad times during this PhD: my Mum, my Dad, my brother Claudio, who always supported, and Max, my love, who was always with me even if we had to spend most of our time apart. It would have not been possible without you. Thank you.

Erklärung

gemäss Art. 28 Abs. 2 RSL 05

Name, Vorname: Isabella Mariani

Matrikelnummer: 10-121-853

Studiengang: Climate Sciences

                     Bachelor ☐   Master ☐   Dissertation ☒

Titel der Arbeit: Water stable isotopes as proxies for temperature and atmospheric circulation

Leiterin der Arbeit: Prof. Dr. Margit Schwikowski

Ich erkläre hiermit, dass ich diese Arbeit selbständig verfasst und keine anderen als die angegebenen Quellen benutzt habe. Alle Stellen, die wörtlich oder sinngemäss aus Quellen entnommen wurden, habe ich als solche gekennzeichnet. Mir ist bekannt, dass andernfalls der Senat gemäss Artikel 36 Absatz 1 Buchstabe o des Gesetztes vom 5. September 1996 über die Universität zum Entzug des auf Grund dieser Arbeit verliehenen Titels berechtigt ist.

Villigen, 24.10.2013
Ort, Datum

                                      ....

                                              Unterschrift

Curriculum Vitae

Family name: Mariani

First name: Isabella

Date of birth: 28.05.1982

Place of birth: Torino, Italy

University Education

2009-2013:   PhD candidate at the University of Bern (Oeschger Center for Climate Change Research). Thesis title: "Water stable isotopes in Alpine ice cores as proxies for temperature and atmospheric circulation".
Supervisor: Prof. Dr. Margit Schwikowski.

2009: MSc in Environmental Physics (Magna Cum Laude) at the University of Torino (Italy). Thesis title ""Measurement of meteorites by gamma-spectrometry for the study of solar activity in the past". Supervisor: Prof. Dr. Carla Taricco.

2001-2009:   Studies of Physics at the University of Torino (Italy).

School Education

2001: High School Leaving Certificate (scientific background)

1996-2001: High school in Torino (Italy)

1988-1996: Primary and Secondary school in Torino (Italy)

Scientific publications

Brönnimann, S., Mariani, I., Schwikowski, M., Auchmann, R., Eichler, A.: Simulating the temperature and precipitation signal in an Alpine ice core, Clim. Past, 9(4), pp. 2013–2022, 2013.

Mariani, I., Eichler, A., Brönnimann, S., Auchmann, R., Jenk, T. M., Leuenberger, M. C., and Schwikowski, M.: Temperature and precipitation signal in two Alpine ice cores over the period 1961–2001, submitted to Clim. Past Discuss., 8, pp. 5867-5891, 2012.

Taricco, C., Bhandari, N., Colombetti, P., Mariani, I., Neeharika, V., Vivaldo, G.: A multiparametric HPGe-NaI acquisition system for low gamma activity measurements of meteorites, Mem. S. A. It. Suppl., 14, pp. 177–179, 2010.

Participation in conferences, workshops and scientific field work

2010　　　Conference "14th Alpine Glaciological Meeting", 25th-26th March, Milano, Italy, poster presentation.

Workshop "Weather and Climate Extremes During the Past 100 years", 7th-9th June, Diessenhofen, Switzerland, oral presentation.

9th International NCCR Climate Summer School "Adaptation and Mitigation: Responses to Climate Change", 29th August-3rd September, Grindelwald, Switzerland, poster presentation.

Participation in the ice core drilling campaign at the Aletschgletscher (Ewigschneefeld) in September.

2011　　　19th European Research Course on Atmospheres (ERCA), 10th January – 11th February, Grenoble, France, poster presentation.

2012　　　11th International NCCR Climate Summer School "The Water Cycle in a changing Climate: Observations, Scenarios, Impacts", 9th-14th September, Monte Verità, Switzerland, poster presentation.

Conference "Open Science Conference of the International Partnerships in Ice Core Sciences (IPICS) ", 1st-5th October, Presqu'île de Giens, France, poster presentation.

2013　　　Conference "Davos Atmosphere and Cryosphere Assembly (DACA)", 8th-12th July, Davos, Switzerland, oral presentation.